Replenishment of sediment downstream of dams: erosion and transport processes

THÈSE N^{O} 7239 (2016)

PRÉSENTÉE LE 9 DÉCEMBRE 2016

À LA FACULTÉ DE L'ENVIRONNEMENT NATUREL, ARCHITECTURAL ET CONSTRUIT
LABORATOIRE DE CONSTRUCTIONS HYDRAULIQUES
PROGRAMME DOCTORAL EN GÉNIE CIVIL ET ENVIRONNEMENT

ÉCOLE POLYTECHNIQUE FÉDÉRALE DE LAUSANNE

POUR L'OBTENTION DU GRADE DE DOCTEUR ÈS SCIENCES

PAR

Elena BATTISACCO

acceptée sur proposition du jury:

Prof. D. A. Barry, président du jury
Prof. A. Schleiss, Dr M. J. Rodrigues Pereira Da Franca, directeurs de thèse
Prof. Ph. Belleudy, rapporteur
Prof. B. Dewals, rapporteur
Dr C. Robinson, rapporteur

ÉCOLE POLYTECHNIQUE
FÉDÉRALE DE LAUSANNE
Suisse
2016

Come onda infrango
Come scoglio resisto
-Lagunari

Acknowledgements

Here is presented the output of four years spent at the Laboratory of Hydraulic Constructions at Ecole Polytechnique Fédérale de Lausanne. The study is funded by Swiss Federal Office for the Environment (FOEN-BAFU) in the framework of the Wasserbau und Ökologie – Geschiebe- und Habitatsdynamik project.

First of all, I would like to thank Professor Anton J. Schleiss, director of the laboratory and of my thesis, for the opportunity of being part of his team and Mário Franca, my thesis co-director, for his scientific support. I extend my gratitude to Professor Philippe Belleudy and Professor Benjamin Dewals and Dr. Christopher Robinson for accepting to be present as members of the jury that will access my work. My thanks to Professor Andrew D. Barry for being the president of this thesis jury.

My gratitude goes to the LCH workshop, who helped me every time in founding a solution for my facility. Thanks Cédric, I appreciated all our conversations and the Porches rides.

Thanks to Professor Virgilio Fiorotto, who trusted on me. A special thought goes to Dr. Giovanni De Cesare...Thanks Giovanni for your time, your patience, your trust and your support from the beginning of my experience at LCH until the last day. Your smile and your kindness made me feel at home.

I would like to thank all the LCH teams: the old generation, who welcomed me, and the new one that walked beside during good and bad times. Thanks to the master students, Adrien, Giovanni and Lena, that contributed to this project.

Tamara... I have learnt a lot from you, such as "where is Ticino" or "how to handle bad moments", till the point to consider you as a mentor... Devo dire che é stata una grande esperienza lavorare insieme a te, e son fiera di poter ancora sfogarmi con la stessa persona dopo quattro anni. Come pochi hai potuto capire i momenti di tensione, i momenti in cui la rabbia la fa da padrone e come pochi hai saputo darmi buoni consigli. Grazie infinite!

Un grazie di cuore ai miei genitori, Lorenzina e Pierantonio. Immagino non sia stato facile accompagnarmi fino a qui e lasciarmi andare, ancora una volta distante... Non credo sia stato facile nemmeno cercare di aiutarmi nei momenti di sconforto, ma siete sempre stati al mio fianco! Vi ringrazio ogni giorno per i sacrifici che avete fatto, per avermi insegnato che ci sono sempre delle prioritá e che dall'impegno si ottengono i risultati. Spero di rendervi fieri di me, come io lo sono di voi.

Lastly, my eternal gratitude to Severin, who listened, supported and encouraged me. Every day, you find a way to make me happy.

Abstract

Dams on rivers alter the sediment continuum, trapping water and sediment in the upstream reservoirs. River reaches downstream are affected by several negative effects, such as bed incision, reduction of the river morphological variability, development of an armoured layer and depletion of ecological habitat for fish. The replenishment of sediment technique has been used since the 1970s to mitigate the lack of sediment transport in the downstream reaches of dams. The method is mainly used to re-establish a sediment continuum, restore a natural bed morphology and to recover spawning grounds for fish. Even if both experimental and field tests have been performed in the past, there is still a lack of knowledge regarding the necessary flow released from the bottom outlet of the dam, the amount of sediment and the configuration of the replenished deposits.

This research aims at filling these gaps by means of experimental tests at the Laboratory of Hydraulic Constructions at Ecole Polytechnique Fédérale de Lausanne (EPFL). The main characteristics of an alpine stream were reproduced in a channel facility in terms of grain size distribution, slope and hydraulic conditions. The sediment replenishment technique was investigated as an influence to the geometrical configurations and volume of deposits, as well as applied discharge. The experiments showed that the bed morphological pattern created by the eroded replenishment material was linked to the initial geometrical arrangement of the replenishment volumes. When applying parallel configurations of replenishment volumes, a general bed fining was obtained with material spread over the entire channel width. Alternating replenishment positioning lead, in turn, to the creation of bed morphological patterns. The wavelength of these bed forms was seen to be related to the replenishment length.

Both constant discharge and transient flow were investigated. Three submergence conditions of the replenishment were tested: unsubmerged, completely submerged and over-submerged. A submergence equal to the replenishment volume height was optimal to obtain a complete erosion of the volumes with transport of the material along the channel and persistence of the material on the channel bed. Four slopes for the increasing and decreasing limb of triangular-shaped hydrographs, having the same maximum discharge, were tested and the results compared with the constant discharge cases. A discharge having a triangular distribution in time is similar to the operational condition of dams when releasing an artificial flood. Transient flows with steep rising limbs lead to a reduction of 70% of water consumption compared to a constant flow, although achieving the erosion of the replenished material. The application of the complete hydrographs showed to be counter-productive in terms of local

effect of the sediment replenishment. These hydrographs may be useful for reaching longer distance impacts in sediment replenishment.
Lastly, the effect of consecutive replenishment of sediments was investigated. A second replenishment can increase the deposition heights and volumes downstream. As expected, a second replenishment affects a longer downstream channel reach. Thus, consecutive replenishments are useful in field applications to have effects at longer downstream distances.

Key words: sediment continuum, flume experiments, sediment replenishment, sediment transport, hydrograph, river morphology, gravel augmentation

Résumé

Les barrages, retenant l'eau et les sédiments dans des réservoirs amonts, impacte la continuité sédimentaire. Les cours d'eau à l'aval sont affectés par une série d'effets négatifs, tels que l'incision du lit, la réduction de la variabilité morphologique de la rivière, le développement d'une couche de pavage et la diminution des habitats écologiques pour les poissons. Les techniques de réapprovisionnement en sédiments sont utilisées depuis les années 70 pour compenser l'insuffisance du transport sédimentaire à l'aval de barrages. Cette méthode est principalement utilisée pour rétablir une continuité sédimentaire, reconstruire une morphologie naturelle du lit et rétablir des lieux de reproduction pour les poissons. Même si des essais expérimentaux et in situ ont déjà été réalisés, il y a encore un manque de connaissance en ce qui concerne les débits devant être lâchés par les vidanges du fond des barrages, la quantité de sédiment et la configuration des dépôts de réapprovisionnement.

Ce projet de recherche vise à combler ces lacunes en réalisant des essais expérimentaux au Laboratoire de Constructions Hydrauliques de l'Ecole Polytechnique Fédérale de Lausanne (EPFL). Les principales caractéristiques d'un torrent alpin (distribution granulométrique, pente et conditions hydrauliques) ont été reproduites dans un canal. La technique de réapprovisionnement sédimentaire a été étudiée en terms d'influence de la configuration géométrique et volumes, en plus du débit. Les essais montrent que les schémas morphologiques du lit créés par l'érosion des matériaux de réapprovisionnement sont liés aux arrangements géométriques des volumes de réapprovisionnement. En appliquant des configurations parallèles de volumes de réapprovisionnement, un affinement général du lit est obtenu avec des matériaux distribués sur toute la largeur du canal. Alterner la position des réapprovisionnements permet de créer d'autres schémas morphologiques de lit. La longueur d'onde de ces formes de lit a pu être reliée à la longueur du réapprovisionnement.

Des débits constants et transitoires ont donc été examinés. Trois configurations de submersion des réapprovisionnements ont été testées : non-submergés, complètement submergés et sur-submergés. Il a été démontré que la submersion du volume de réapprovisionnement à 100% est la meilleure configuration pour obtenir : une érosion complète des volumes, un transport du matériau le long du canal et sa persistance sur le lit du canal.

Quatre pentes pour augmenter ou diminuer la branche montante de l'hydrographe, ayant un même débit de pointe, ont été testés et les résultats obtenus ont été comparés avec le cas du débit constant. Un débit suivant une variation temporelle triangulaire est comparable aux conditions opérationnelles d'un barrage relâchant une crue artificielle. Un écoulement transitoire avec une montée d'hydrographe raide permet une réduction de 70% du volume lâché par

rapport à un débit constant, en parvenant néanmoins à eroder les materiaux de réapprovisionnement. Un hydrographe complet relâché sur un tronçon fluvial surestime et réduit les effets positifs d'un réapprovisionnement sédimentaire. Ces hydrographes pourraient être utiles pour augmenter la distances d'impact du réapprovissionnement sédimentaire. Enfin, cette recherche étudie l'effet de la fréquence d'opération en réalisant des réapprovisionnements sédimentaires consécutifs. Cela a montré qu'un deuxième réapprovisionnement contribue à affecter le canal plus à l'aval. Des réapprovisionnements consécutifs peuvent être aussi utiles pour des applications in-situ pour toucher des tronçons plus à l'aval ou pour parvenir à des sites avec un accès limité.

Mots clefs : Expériences en canal, réapprovisionnement sédimentaire, transport sédimentaire, hydrographe, morphologie de rivière, augmentation de gravier

Contents

List of Figures

List of Tables

1 Introduction

1.1 Scope and motivation

In Switzerland, only few rivers are still in complete natural conditions. Hydropower plants, water diversions and anthropomorphic structures on rivers are the factors that affect the sediment transport balance. The sediment transport is reduced by more than 41% from a survey made by the DETEC (2012). The reduction of sediment supply has demonstrated to induce negative consequences to the linked ecosystem. Several studies highlighted the need for interventions to revitalize the watercourses. One of the main purposes of the Swiss Federal Office for the Environment (FOEN-BAFU) is the revitalization of the river basins in order to reactivate their natural functions or at least to preserve the existing ones, guaranteeing a suitable habitat for different species. The "Water protection law", originally introduced in 1991, was modified in 2011 based on the "Initiative Eaux vivantes", promoted by the Swiss Federation of Fishers (FSP). The revised law defines new parameters and methods that have to be taken into account for further river use. In particular, the following is required:

- Watercourses have to be revitalised in order to re-established natural conditions. Therefore, enough space for rivers has to be reserved
- Specific strategy have to be elaborated in order to accomplish the expected revitalizations which should consider rivers affected by water diversions or human interventions
- The negative effects due to hydroelectric energy production, namely on irregularity of the flow, deficit of solid transport by water and fish migration have to be reduced.

This research is funded by the Federal Office for the Environment (SFOEN-BAFU-OFEN), under the program "Wasserbau und Ökologie". It aims at giving a scientific answer for the revitalisation of the Swiss watercourses by using the replenishment of sediments technique. The SFOEN is responsible for ensuring sustainable use of natural resources, protection of citizens against natural hazards and protection of the environment from unacceptable adverse impacts. Figure 1.1 illustrates the different developed sub-project research. The present research corresponds to the second sediment transport task of the "Wasserbau und Ökologie" program (I.I.3, Figure 1.1).

1.2 Research questions

The replenishment of sediment revealed to be a useful tool in order to reduce the lack in sediment transport downstream of dams and to re-establish morphodynamics conditions close to nature. Several experimental and field works were so far performed on sediment replenishment. Nevertheless, this methods is still not fully understood in terms of sediment dynamics, deposit geometry and placement and required released discharge. These not well known parameters limit a wider applicability of the technique. The present study aims at filling these gaps of knowledge by means of laboratory experiments on a flume at the Laboratory

FOCUS I: Sediment rehabilitation by morphodynamics activation	
I.1	Sediment replenishment in lowland rivers
I.2	Re-establishment of the sediment continuum with bypass tunnel at alpine reservoirs
I.3	Replenishment of sediments downstream of dams in alpine rivers
I.4	Sediment trap design
I.5	Sediment composition and shore vegetation
I.6	Sediment rehabilitation and fish in alpine rivers
I.7	Sediment rehabilitation and zoobenthos in alpine rivers

FOCUS II: Rehabilitation of floodplains	
II.1	Dynamics of fine sediments in revitalised rivers
II.2	Habitat and species dynamics in hardwood floodplains
II.3	Monitoring concept
II.4	Montoring of species dynamics in floodplains

Figure 1.1 – Sub-project research development belonging to the "Wasserbau und Ökologie" program (Schleiss et al., 2014)

of Hydraulic Constructions (LCH) of Ecole Polytechnique Fédérale de Lausanne (EPFL). An armoured bed downstream of a dam was reproduced at a geometric scale of roughly 1:10, where replenished deposits were placed.

The replenishment of sediment is studied as a function of several parameters, such as the volume of sediments, the geometrical configurations, the frequency of the placement and the role of discharge. The discharge is artificially released by dam operations through bottom outlets. Normally, the discharge downstream of dams is regulated and limited to residual ecological flow. This study investigates the bed morphological changes induced by the replenished material, the shape of bed forms, their patterns on the channel bed and the implications for the environment. The objectives of this research may be synthesized in the following questions:

- Which geometry of sediment deposits are suitable for recreating morphological variability in the water reaches downstream sediment-retaining-structures?
- Where and how have replenishment deposits to be placed to be mobilized and conveyed in order to recreate bed morphological forms?
- Which controlled discharges are necessary for mobilizing the deposits downstream of the retaining structure? Which transport mechanism is related to the different cases?

1.3 Report structure

The present work is divided into ten chapters (Figure 1.2). Chapters 4, 7 and 8 are prepared in the form of scientific articles. Chapters 5 and 6 are parts of publications presented at scientific meetings. To avoid topic redundancy, their literature review has been removed and collected in Chapter 2. Chapter 2 includes a brief introduction on the topic of sediment transport, an overview on the morphological state of river reach downstream of dams, the description of the replenishment of sediment technique, previous laboratory studies and applications in the fields. Furthermore, a sight on the ecological aspect is given in this chapter.

The experimental method, including the experimental setup, the assessed parameters and the experimental procedure, is presented in Chapter 3.

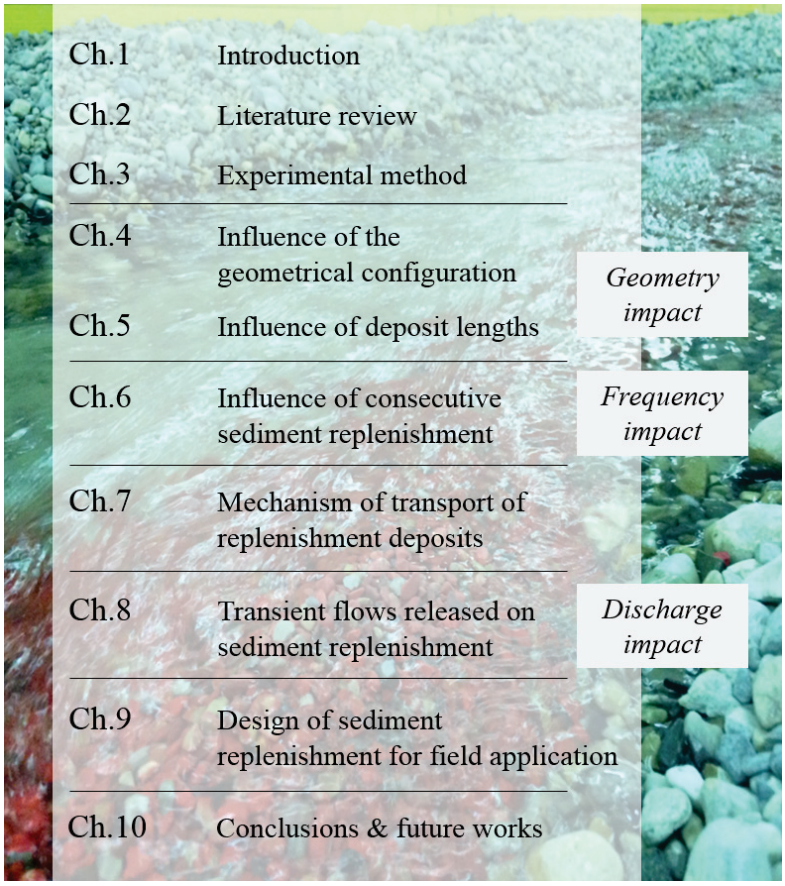

Figure 1.2 – Structure of the manuscript

Chapters 4 and 5 contain analysis and results related to the effects of geometrical parameters on the bed morphological response to sediment replenishment. Chapter 4 analyses in detail the influence of the geometrical configuration on bed morphology. Several geometrical configurations are tested and their response in terms of bed occupation by the replenished material, initiation of bed forms and morphological bed patterns are investigated. Evidences show that the parallel geometrical placement of the sediment deposits induces a wide spread

of material on the whole cross-section of the channel bed; whereas alternating placement leads to the creation of bed patterns. Chapter 5 investigates the role of the replenishment length on the development of morphological bed patterns.

The sediment replenishment technique is a method commonly repeated with a certain frequency over the year, therefore Chapter 6 analyses the effect of consecutive replenishment of sediments on the channel reach. Results shows that the sediments of the second replenishment contribute in increasing the size of the deposits created before. Therefore, an increment of deposit height due to the second replenishment is observed. This increase in deposit height is more evident for bed forms located further downstream along the channel.

Chapter 7 investigates the transport mechanisms link to sediment replenishment. The transport mechanism of replenished material results to be affected by the geometrical placement of deposits and the released discharge. Translation is induced by high submergence ratios, whereas a mixed transport is observed with lower submergences of the sediment replenishment volumes.

Chapter 8 compares bed morphological response to constant flow and transient regime released on the channel for the same geometrical configurations. It is shown that transient flows allows to reduce the necessary released water volume on the flume.

The design of sediment replenishment for a field application is presented in Chapter 9. The analysis of the case study results does not belong to this research. Conclusions and further developments are provided in Chapter 10. References are all given at the end of the manuscript. Tables and figures are numbered incrementally in each chapter and contain the reference to the chapter. Equations are numbered continuously through the document. In Appendix are collected the main results for every performed test.

2 Literature review

2.1 Sediment transport

The bedload transport is composed by sand, gravel, cobbles and boulders that are moved by rolling, sliding and bouncing along the river bed (Kondolf, 1997) (Figure 2.1).

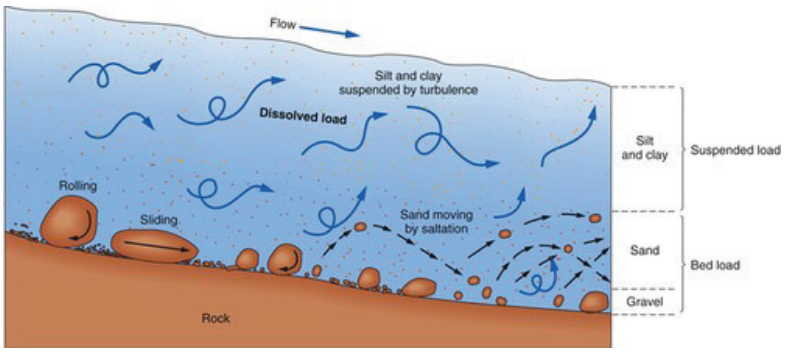

Figure 2.1 – Mechanism of bedload and suspended sediment transport, as proposed by Plummer et al. (1988)

The size of transported sediments changes along the river: larger gravels are carried by the flow in the steeper sections, while sands and silts present a large fractions in the downstream reaches (Kondolf, 1997). Sediment mobilisation depends on several material proprieties, such as the grain size, and on the fluid proprieties, namely the bed shear stress. Under uniform condition, the bed shear stress is proportional to the longitudinal slope S, the hydraulic radius R_h and it is defined as:

$$\tau = \rho * g * R_h * S \tag{2.1}$$

The bed load transport is a complex system and several threshold of movement were developed so far mainly based on laboratory experiments. Among others, the Shields diagram is commonly used to determine whether a certain sediment will be mobilise (Figure 2.2). Based on laboratory tests, Shields (1936) developed a criteria based on the dimensionless grain Reynolds number Re^*. The latter is defined as:

$$Re^* = \frac{u^* * d}{\nu} \tag{2.2}$$

where d is the grain size, u^* the shear velocity and ν the kinematic viscosity of the fluid. The plot shows that the dimensionless grain Reynolds number becomes constant for a turbulent flow (Re^*>400). The critical bed shear stress value fixed at 0.06 by Shields (1936) was lately corrected by Meyer-Peter and Müller (1948) to a value of 0.047. Basically, a critical bed shear stress value above 0.047 indicates that the grain will be transported by the flow. By

consequence, as soon as this value will decrease below the threshold of movement the grain will deposit on the channel bed.

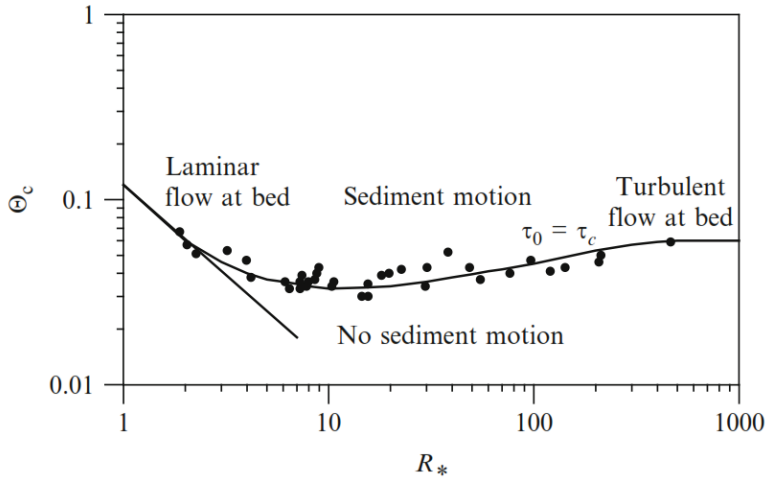

Figure 2.2 – Shield's diagram according to Dey (2011)

The above mentioned assumptions created the bases for developing formula on the potential sediment transport for certain given river characteristics. The most commonly applied formula for alpine channel for slopes varying between 0.5% and 2.0% was developed by Smart and Jäggi (1983). In this formula, the sediment load Q_s is related to the liquid discharge Q, the grain size in terms of d_{50} and d_{90}, and to the channel slope. Furthermore, a direct link to the bed shear stress is made by the critical slope S_c. Potential sediment transport and critical slope are defined respectively as:

$$Q_s = \left(\frac{4}{(s-1)}\frac{d_{90}}{d_{50}}\right)^{0.2} S^{0.6} Q(S - S_c) \tag{2.3}$$

$$S_c = \frac{\tau_c (S-1) d_{50}}{Re^*} \tag{2.4}$$

These moving sediments tend to create apparently stable bed forms, which are indeed composed by materials continuously replaced by the sediment transport from upstream (Kondolf, 1997). The river morphology can thus be seen as a result of transportation and deposition of bed material (Church, 2006).

Different approaches were proposed for classifying the river reach morphology. The Schumm (1977) method is a qualitatively approach based on sediment supply amounts, type of bed material, bed slope and channel stability. These parameters are related one to each other and the classification indicates how the river morphology will react to an increase or decrease of one of these variables (Figure 2.3).

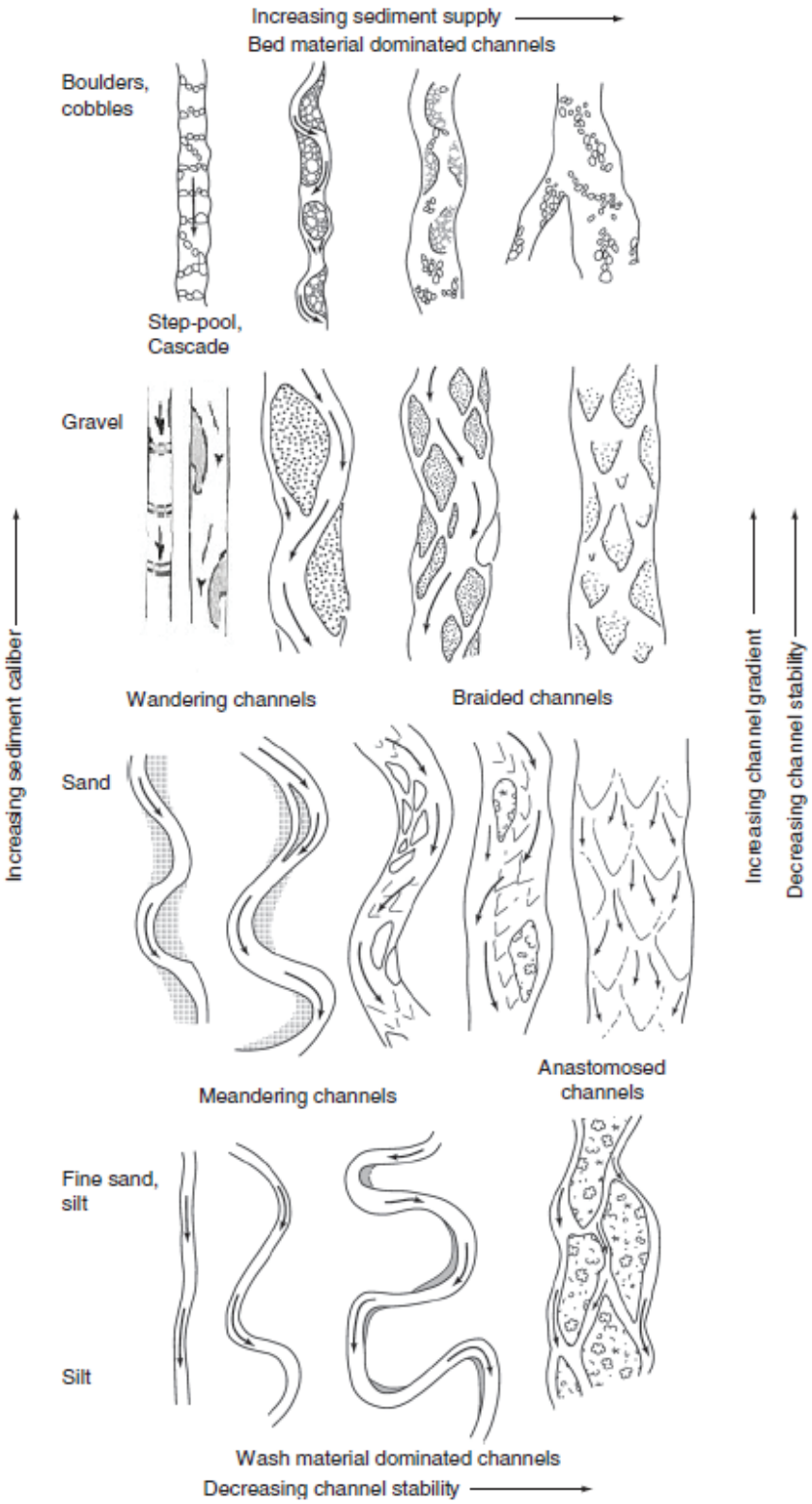

Figure 2.3 – Schumm classification of river morphological patterns, from Buffington and Montgomery (2013)

Rosgen (1994) provided a quantitative methodology based on dimensionless parameters. The approach identifies eight major river types based on river forms in terms of width, depth and sinuosity helping in characterising stream type and typical cross section. Finally, the channel bed morphology is found to be related to river width, water depth and typical grain size by Yalin and Da Silva (2001). This analysis is based on field observations. Data are plotted in relation to two dimensionless parameters: the ratio channel width and water depth (B/h) and the ratio water depth and median grain size (h/D) (Figure 2.4). This plot permits to foreseen further river development based on the river characteristics. Therefore, the characteristics of a river reach downstream of a dam can be introduced to visualise the morphological changes caused by the human infrastructure.

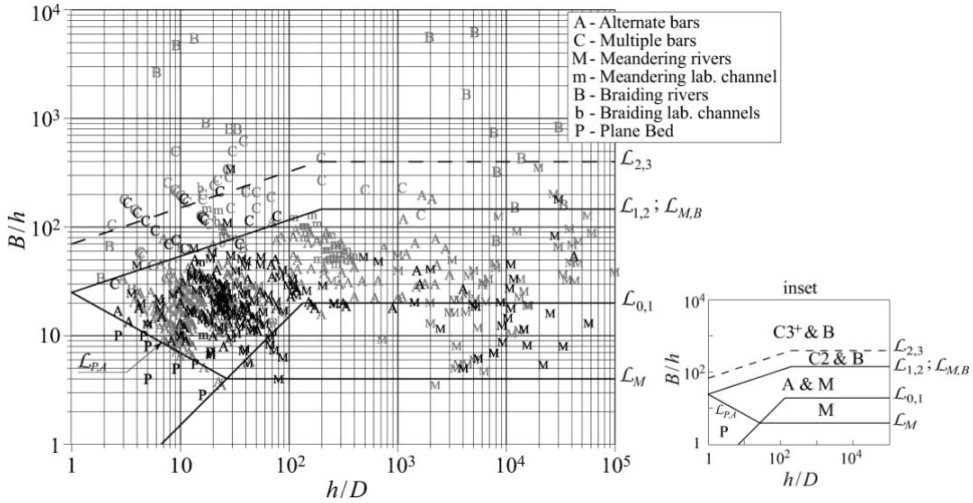

Figure 2.4 – Definition of bed forms regions by field observations, as proposed by Yalin and Da Silva (2001)

For maintaining and preserving aquatic and riparian ecosystems, continuous sediment transport and associated morphology diversity are understood as key processes (Kantoush et al., 2010b). A high sediment supply leads to a more complex river morphology (Church, 2006) and the two variables proofed to be strictly related (Venditti et al., 2012). This assumption is strengthened by field observations. A reduction in sediment supply, as occurred along the Sacramento river (California, USA) after Keswick dam construction, has modified the downstream river morphology from braided to single-thread channel (Kondolf, 1997).

To any change in sediment supply and discharge, rivers naturally respond by adjusting their width, depth, slope, bed morphology and channel features (Kondolf, 1997; Buffington and Montgomery, 1999). The nature of the change is strictly related to the original channel features in terms of flow regime and sediment loads (Kondolf, 1997). Several studies proofed a correlation between sediment supply and change in gravel-bed surface texture (Dietrich et al., 1989; Lisle and Hilton, 1992). The imbalance between the two of them leads to size-selective deposition or erosion, which may alter both the critical shear stress for moving sediment and

the effective bed shear stress (Naot, 1984; Buffington et al., 1992; Kondolf, 1997; Buffington and Montgomery, 1999). In particular, an increase in transport rate and higher bed stresses are observed when finer sediments are supplied into a coarser reach due to the creation of a smoother bed surface (Buffington and Montgomery, 1999). This is the typical occurrence when a sediment replenishment is applied in a river.

2.2 Bed morphology downstream of dams

A modification in terms of sediment supply and discharge along the river reach often occurs in proximity of human constructions, which represent one of the most grave interventions in the hydrological cycle (McCartney, 2009) (Figure 2.5). Human activities have drastically reduced the dynamics and the morphological variety of active rivers in the last decades (Pedroli and Dijkman, 1998).

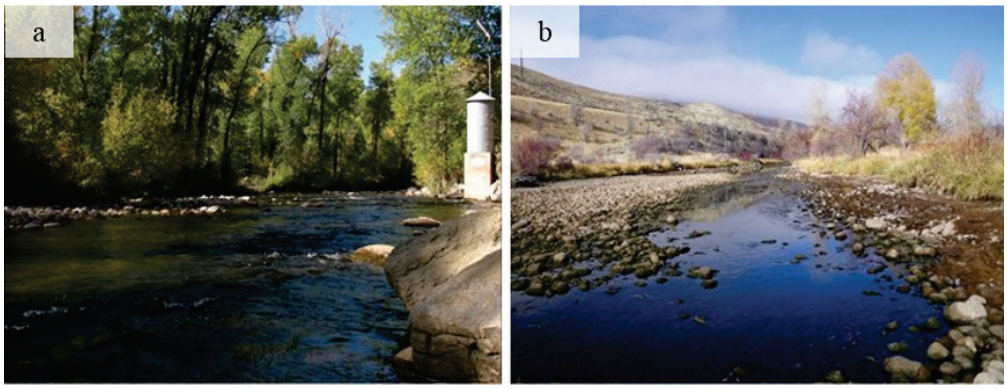

Figure 2.5 – (a) Natural flow of Weber River upstream of Echo Dam, (b) reduced flow downstream the Echo dam (Utah, USA). USGS photo: D. M. Carlisle

Dams, without flushing devices, trap sediment in the upstream reservoir, interrupting the natural sediment transport and creating a drastic reduction in sediment supply along the downstream reach (Kondolf, 1997; Brandt, 2000; Grant et al., 2003; Petts and Gurnell, 2005; Gaeuman, 2008). Williams and Wolman (1984) stated that almost all the sediments reaching large reservoirs are trapped, while the amount is slightly reduced for smaller basins. Some of the changes induced by dams involve both the upstream reservoir as well as the downstream reach. Dams reduce the seasonal fluctuations along the downstream reach and change the natural thermal variation, which are very important features for the ecological and biological point of view (Balland, 2004; Kondolf, 1997; Batalla et al., 2004).

In order to qualify the river changes linked to dam constructions, Kantoush et al. (2010b) categorized them considering three main aspects: ecology, hydrology and morphology (Figure 2.6). The main morphological changes in the downstream reach are related to riverbed incision, riverbank instability and failure, channel width reduction and bed coarsening (Kondolf and Wolman, 1993; Kondolf, 1997; Batalla et al., 2004). These negative effect are caused by the

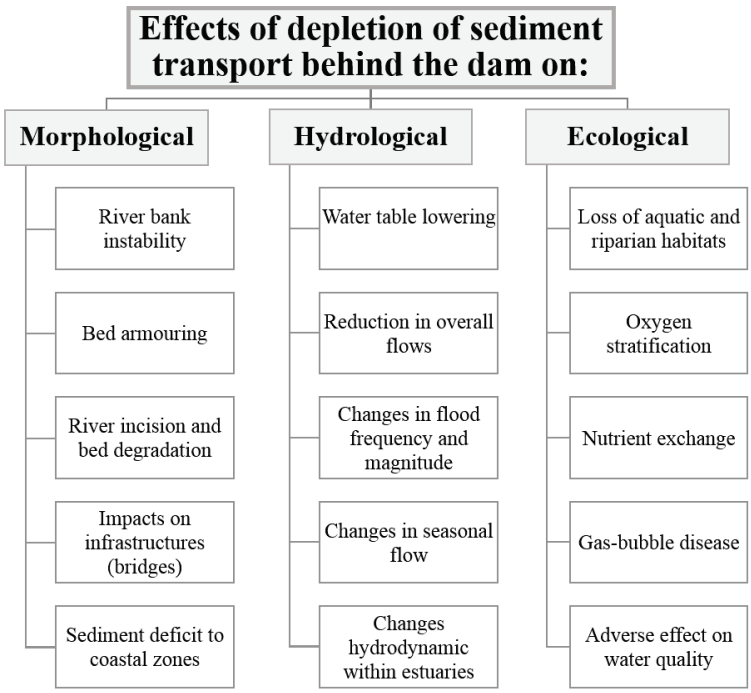

Figure 2.6 – Effects of dams on rivers downstream, from Kantoush et al. 2010

water transport capacity that exceeds the sediment supply. Fine sediments are eroded and transported without being replaced from upstream, therefore leading to the creation of an armour layer (Buffington and Montgomery, 1999). The armour layer is characterised by an increased d_{50}, thereby a higher magnitude of flow is necessary to mobilize the sediments (Batalla et al., 2006; Vericat et al., 2006). These reaches are generally highly regulated and flow variations are limited to natural flood. By consequence, a general reduction in amount of sediments transported downstream the dam is also observed (Brandt, 2000). On the other hand, in rivers where water has already created an armour layer, the most evident feature related to dam presence is channel erosion (Kondolf, 1997). According to Brandt (2000) and Petts and Gurnell (2005), the amount of trapped sediments is linked to reservoir storage capacity. Thus, the narrowing of the river reach downstream has been more evident for large reservoirs.

From the hydrological point of view, dams lead to a reduction in flood frequency and magnitude, reduction in overall flows and altered timing of releases (Kondolf and Matthews, 1991; Ligon et al., 1995; Batalla et al., 2004; Kondolf and Minear, 2004; Balland, 2004; Petts and Gurnell, 2005). Due to these changes in the flow regulation, the river loses its capability to recruit sediments from the riverbanks and terraces, with consequent decrease of the development of mid channel bars and islands (Ligon et al., 1995). This lack in sediment supply leads to the variation of braided rivers into more simplified single-thread channel along the reaches downstream of dams (Ligon et al., 1995). The Stony Creek river, a tributary of the Sacramento river (California, USA), is an example of these occurrences. After dam constructions, the river

moved from a braided pattern to a single-thread, incised and laterally migrating (Kondolf, 1997).

The reduction in water discharge and hydrological variability pauperise the riverine ecosystem in the reach downstream of a dam. A loss of the aquatic and riparian habitats and decrease water quality are observed in these affected rivers (Kondolf, 1997; Merz and Ochikubo Chan, 2005; Kantoush et al., 2010a; Grant et al., 2003; Ligon et al., 1995; Schmidt and Wilcock, 2008). The rivers are left dry, or too shallow, or the gravel bed areas have been replaced by fine sand and armoured bed (Barlaup et al., 2008). These conditions reduce the oxygen content in the river bed, thus the fish egg survival is compromised (Chapman, 1988). An overall reduction of suitable areas for pioneer species (i.e the riparian landscape) is proofed by the reduction of river lateral mobility (Salo et al., 1986; Kalliola and Puhakka, 1988; Florsheim et al., 2008; Karrenberg et al., 2003). The morphological disturbance regime was found to be a key criteria for the survival of these species.

Incision and coarsening of the bed, lack in sediment supply and loss in lateral river mobility are not necessarily linked to the distance from the dam, but derive from the intensity of the hydrological disturbance, the remaining amount of provided sediments and the local geomorphological constrains (Sherrard and Erskine, 1991; Grams and Schmidt, 2005). Thus, it may happen that these negative effects propagate further downstream depending on the hydrological change and stream type (Rollet et al., 2014; Williams and Wolman, 1984; Church, 1995), leading to an increased number of rivers not reaching the sea anymore (Kantoush and Sumi, 2010).

Beside the morphological aspects listed by Kantoush et al. (2010b), Brandt (2000) provided nine possible geomorphological changes occurring downstream of dams linked to distance from the dam, environment, substrate, released water and characteristics of sediment supply. At the same time, he provided also some guidelines to prevent serious damages for new human constructions in the river, whereas a less detailed categorisation is provided by Petts and Gurnell (2005). The latter divided the downstream river responses considering three kinds of adjustment:

- Passive response: both flows and channel dimensions are reduced, but without significant changes in bed elevations
- Degradation: bed and lateral banks are eroded while the river is moving toward a new equilibrium with a reduced sediment supply
- Aggradation: the reduction in discharge and the dam operations limit the channel capability to entrain and transport sediments, resulting in an increase in bed elevation when the sediment supply is not compromised.

As above mentioned, the issues related to human infrastructures concern both the upstream and downstream river reach. In the upstream reservoir, the sediments settle and a loss of

reservoir capacity is observed (Fan and Morris, 1992). The reduction of the storage capacity of reservoir may lead to a decline of flow regulation capacity (Graf, 1984; Schleiss et al., 2016) and, as a consequence, sediments may enter the waterway system and hydropower schemes (Schleiss et al., 1996). In worst case, the sediment may clog the gates (i.e bottom outlet) causing security problems (Schleiss et al., 1996). Therefore, a socio-economical issue can be addressed to the trapping of sediments by dams (Fan and Morris, 1992; Morris, 1994; Schleiss et al., 2016).

In this context, revitalisation of disturbed river reaches is becoming a core topic in river management. So far, several methods have been proposed for mitigating the negative effects of dams on the downstream river reach. Sediment sluicing and flushing are commonly practised (Brandt, 2000; Kondolf, 1997). By sediment sluicing the sediments are carried with the flow throughout the dam, either by the dam outlets or by density currents, before they can deposit in the reservoir. The flushing of sediments means the erosion and transportation of sediments already settled in the reservoir by dam outlets (Yoon, 1992). Flushing flows are used also for removing the fine sediments from the bed and for scouring the latter often enough to prevent encroachment of riparian vegetation (Kondolf, 1997; Reiser et al., 1989). Under these circumstances, the released amounts of material may be quite different from what would be naturally transported by the flow, thus altering even more the downstream conditions. This operation may cause an ecological drama when applied without precaution (Balland, 2004). Furthermore, the conveyance of bed load is not possible for dams with large reservoirs like in alpine catchment regions (Kondolf, 1997). In addition, for the river integrity and natural morphology maintenance Ligon et al. (1995); Hill et al. (1991) and Rosgen et al. (1986) recommends the bankfull discharge in the downstream reach of dams. Ligon et al. (1995) proposed a combination between high flood release from the dam and sediment augmentation for a concrete success.

Considering the above mentioned restrictions, the enrichment by sediment augmentation of rivers downstream of the retaining structure is the only practicable solution. Therefore, the sediment replenishment is obtaining worldwide more relevance and acceptance. Nevertheless, developing a general countermeasure is challenging and each single case should be treated properly, including for this the careful analysis of historical hydraulic and sediment supply data.

2.3 Sediment replenishment technique

Sediment replenishment is one of the proposed techniques to restore the natural morphological conditions in a river and the sediment supply along the reach downstream of a dam (Ock et al., 2013). This method aims at solving the deficit of sediments downstream of dams by artificial addition of them. Analysing several rivers, a common outcome is the necessity to increase the sediment transport in the downstream river (Balland, 2004).

The sediment replenishment technique aims at the recreation of a natural sediment transport regime and at promoting bed fining, in light of re-establishing bed morphology diversity (Bal-

land, 2004; Sklar et al., 2009; Pasternack et al., 2010). For these purposes, once the replenished material is placed along the reach, it relies on a natural or artificial flood, released from the dam, for being mobilized (Kantoush et al., 2010b). The replenished material may be excavated gravel from the reservoir or natural material taken from close sites (Kantoush et al., 2010b) (Figure 2.7).

Figure 2.7 – Schematic representation of replenishment of sediment method, from the excavation point to the delivery of material on the river (in Kantoush et al. (2010b)

A successfull replenishment of sediment is obtained by a good calibration of different parameters listed by Kantoush and Sumi (2010) (Figure 2.8). Both flow features and sediment characteristics play a key role. The flow is considered in terms of discharge, water depth and flow characteristics in order to obtain an adequate velocity distribution close to the replenishment deposits. The replenished material should be carefully chosen considering grain size distribution and grain features, such as permeability and cohesion.

The sediment replenishment may be used also for ecological restoration. Therefore, the sediment augmentation is made with a specific grain size distribution adequate for recreating spawning ground for fish normally finer than the exisitng channel bed (Wheaton et al., 2004; Pasternack et al., 2010; Gaeuman, 2008; Gaeuman and Krause, 2013). This leads to a strong limitations in the choice of replenished material. Furthermore, the sediment augmentation has to be done with particles which can be entrained for a given flow (Gaeuman and Krause, 2013). In light of this aim, Bunte (2004) distinguished between an active and a passive approach. By active replenishment, the material is placed at the location where the spawning grounds have to be improved, whereas the passive approach rely on released flow to mobilize the replenished material and create gravel deposits further downstream.

In previous studies and applications, the amount of gravel has been calculated as the product between the spawning habitat area to be restored and the gravel depth required for spawning

(Gaeuman and Krause, 2013). This kind of approach is reasonable for an immediate application, but it is not sufficient to satisfy a long-term geomorphic objective (Gaeuman and Krause, 2013). The augmentation rate has to be close to the quantity of sediments that the reach can transport considering the regulated flow by the dam without undergoing other changes in channel geometry (Gaeuman and Krause, 2013). Therefore, the amount of sediments to be added is different from the unregulated sediment load, since the transport capacity of river has been reduced. When considering sediment replenishment downstream of a dam, amplitude, time and period of the year for water releases should be defined accordingly. The spatial and temporal extension of the beneficial effects of the replenishment of sediment on the channel reach depend on the the transport capacity of the river and the environmental conditions, as well as on the amount of sediment, grain size distribution, released flow and method of placement (Okano et al., 2004; Kantoush et al., 2010b; Sumi et al., 2009; Sumi and Kantoush, 2010, 2011; Sklar et al., 2009). Commonly, the sediment volume is added along the bank at a certain elevation from the channel bed, thus avoiding a source of turbidity during the period of normal flow (Ock et al., 2013). In the so far tested method, the elevation of the replenishment was sufficient to be completely submerged when a high discharge occurs, typically several times a year (Sumi and Kantoush, 2010; Okano et al., 2004; Sumi and Kantoush, 2011). In field experiences, different replenishment injection methods were tested (Ock et al., 2013) (Figure 2.9). The in-channel bed stockpile method places directly the material on the channel bed (Figure 2.9*a*). The replenished material, immobile for low flow, would start to be eroded once the threshold of movement is exceeded. The main purpose is to create spawning forms in a short time (Ock et al., 2013). The weakness of this technique is in the in-channel work, which may increase the river turbidity. With the high-flow stockpile technique, commonly applied in Japan, the sediments are directly placed within the channel bank margin assuming that during peak flows the flow will be able to erode and transport these sediments, reshaping the reach (Figure 2.9*b*). This method performs well in case of short duration and high flow events, permitting to add a quite large amount of gravel. The major weakness of this approach lies in the restriction of available sites. With the point bar stockpile method, coarse sediment is introduced in order to create a point bar. It can be considered as a compromise between the above mentioned methods (Figure 2.9*c*). Gravels are placed in site-specific low flow and bankfull channel dimensions. Thus, this method is limited by the site features and it would be limited also to erosion and transport downstream. Finally, the high-flow direct injection was proposed by Gaeuman (2012) (Figure 2.9*d*). Thereby the material is directly added into the river using a conveyor belt while a high flow event is occurring. It is evident that the major weakness of this approach is related to the heavy working conditions and the costs involved (Ock et al., 2013).

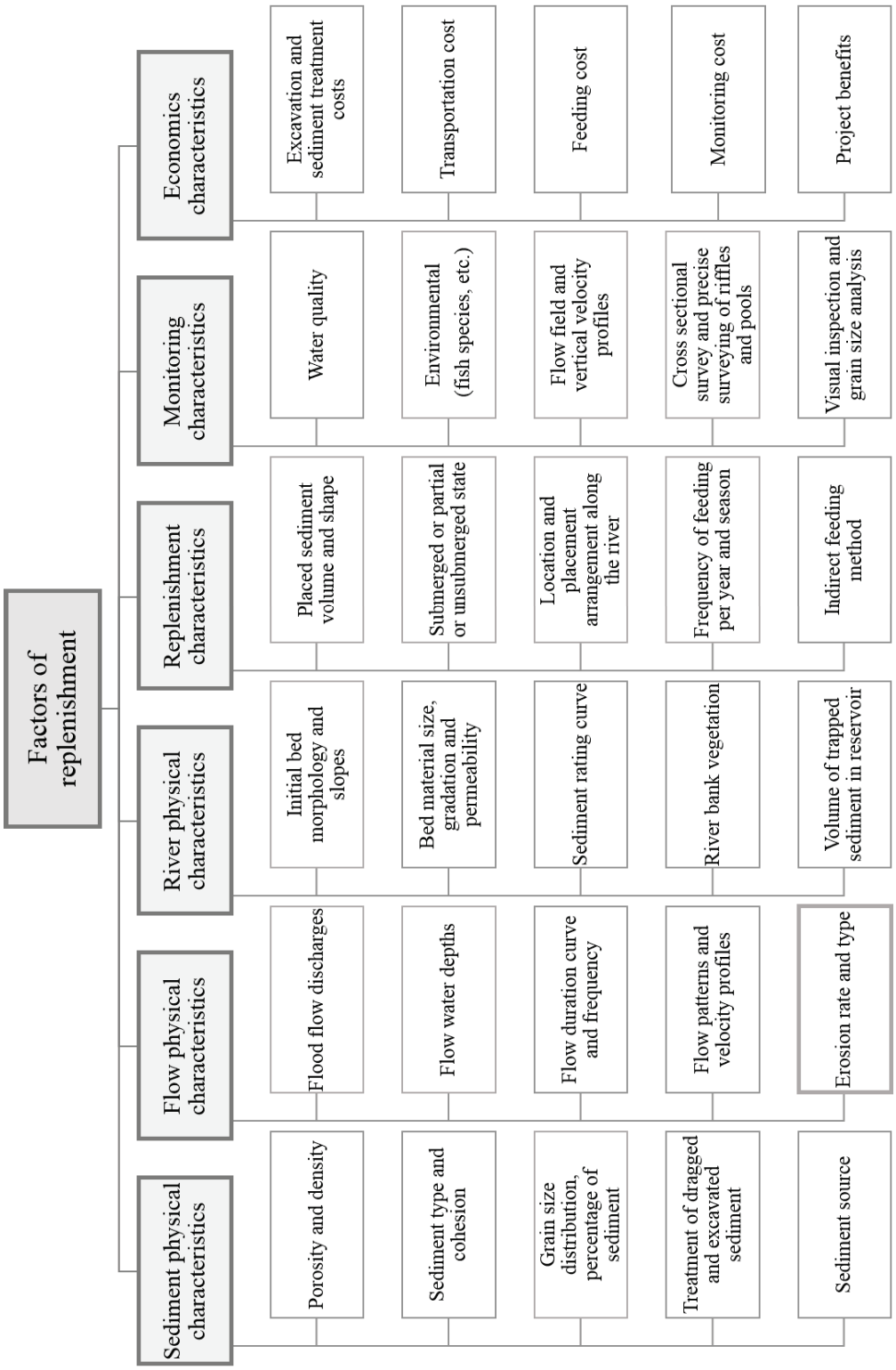

Figure 2.8 – Replenishment of sediments factors as mentioned by Kantoush et al. (2010b)

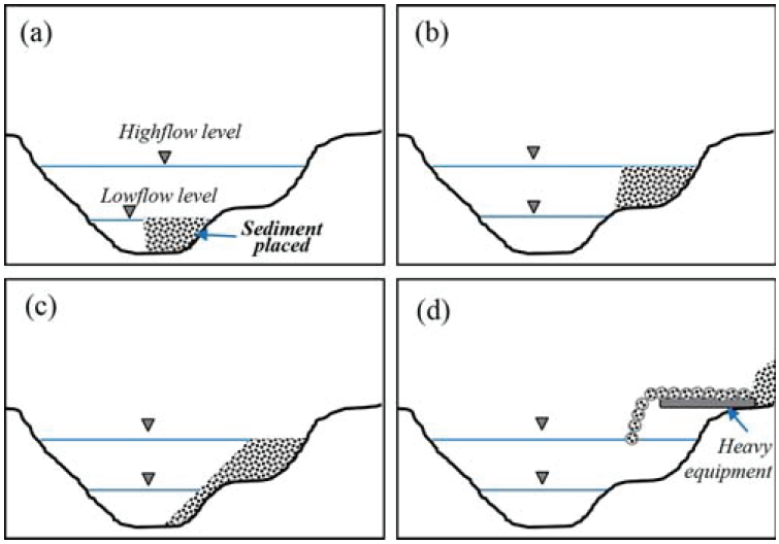

Figure 2.9 – Sediment replenishment injection methods, as proposed by Ock et al. (2013)

2.4 Ecological considerations

Most of the ecological processes on rivers are interrupted by dams (Ligon et al., 1995; Rollet et al., 2014; Sear, 1995; Grams and Schmidt, 2005), which limit the availability of gravel and cobbles, ecologically extremely important for creating spawning habitat for fishes (Kondolf, 1997).

As above mentioned, also the lateral migration of rivers is compromised by human interventions. Therefore, the presence of side channels and small islands, typical deposit areas for smaller cobbles and spawning grounds, are reduced (Ligon et al., 1995). By reductions of these areas, the present ecosystem is negatively affected with alteration of the food chain Ligon et al. (1995); Power et al. (1996); Sear (1995); Merz and Ochikubo Chan (2005); Pasternack et al. (2010).

The sediment transport reduction leads to the creation of an armoured bed. This limits the possibilities for fish spawning, since fishes are not able anymore to move the large surface gavels to incubate their eggs (Kondolf, 1997). In order to preserve the ecological habitats and the biodiversity of rivers, it is necessary to recreate a solid transport that persists in time. The sediments replenishment proofed to recreate artificial spawning riffles and also to improve salmonid spawning habitats (Kondolf and Matthews, 1991; Zeh and Dönni, 1994; Gaeuman, 2012). McManamay et al. (2010) found that, for more than 75% of the examined fished species, a gravel depth greater than 0.1 m measured above the top of the egg pocket assures their survival. Immediate benefit has been observed in terms of restoration of existing fish habitats downstream of the dams by sediment replenishment application (Sear, 1995; Gaeuman, 2008; Ock et al., 2013). Especially, profitable results in terms of new habitats for specific species and invertebrates were obtained in the United States (Fuselier and Edds, 1995; Gore et al.,

1998, 2001). Nevertheless, the in-situ experimentations revealed that the spawning grounds are not durable in time and it is necessary to add continuously additional material (Kondolf and Wolman, 1993; Kantoush et al., 2010b; Ock et al., 2013; Pulg et al., 2013; Barlaup et al., 2008). These results confirm that it is still necessary to improve the method of sediment replenishment (Kondolf, 1997; Kantoush et al., 2010b; Sumi and Kantoush, 2010).

2.5 Laboratory investigation and field observations

2.5.1 Laboratory investigations

The replenishment of sediment is a complex system involving different aspects, related to both the flow features and the replenishment material characteristics. Thus, a laboratory facility and systematic experiments are an efficient way to better understand these complexities (Lisle et al., 1997).

During the last years, several laboratory experiments were performed to assess the general erosion process of deposits (Kantoush and Sumi, 2010), the evolution of sediment waves (Lisle et al., 1997; Cui et al., 2003; Sklar et al., 2009) and the influence of sediment supply on river bed morphology (Ikeda, 1983; Venditti et al., 2010; Nelson et al., 2015; Venditti et al., 2012). In particular, the erosion process of sediment deposits was experimentally investigated by Kantoush and Sumi (2010). The erosion mechanism, especially for high-flow stockpile technique, is described as a combination between lateral erosion of the sediment deposit toe, by hydraulic forces, and mass failure, by gravitational mechanism due to over steepening of the banks. Field observations at Murou dam confirm these laboratory findings (Kantoush et al., 2010a). Furthermore, he observed that only the gravel with enough shear strengths to withstand the high shear stresses in the near bed region is deposited. The rate of erosion of the total added volume varied in function of the discharge: higher discharges higher the erosion of the replenishment of sediments (Kantoush et al., 2010a).

The role of sediment supply and sediment replenishment in contributing to river morphology diversity and alternate bar formation was investigated by Ikeda (1983) and (Venditti et al., 2012). Ikeda (1983) recreated alternated bars by sediment supply in a plane flume. These bed morphological changes occurred via small migrating bedforms, growing over time and stabilized as stationary alternate bars. Their wavelength was found equal to about 6 to 10 times channel width. Experimental finding by Venditti et al. (2012) evidenced that bar loss due to sediment deficit is reversible by adding sufficient sediment. He recreated sediment mounds after 3.5 hours testing with upstream sediment supply. These nascent bars resulted in the creation of alternate bars for constant flow and sediment feed (Venditti et al., 2012). Thus bar loss due to sediment deficit can be stated as reversible by adding sufficient sediment. Alternate bars are channel bed forms commonly indicating the beginning of meandering (Jäggi, 1984).

Recently, the sediment replenishment deposits have started to be analysed as artificial pulses

which increase locally the sediment supply (Sklar et al., 2009; Lisle et al., 1997; Madej, 2001; Cui et al., 2003). These studies contribute in understanding the main mechanisms of transport associated to sediment deposits. Pulses move by translation, by dispersion or by a mixed mechanism (Lisle et al., 1997, 2001) (Figure 2.10). The pulse of material moves by pure dispersion when the apex and the trailing edge do not migrate downstream and the corresponding center of mass only shifts downstream. It is assumed that the sediments do not propagate upstream the origin point. A pure pulse translation corresponds to a simultaneous and integral advancement downstream of the apex, trailing edge and center of mass of sediment longitudinal distribution. The volume moves like a solid body . Rare cases with mechanism different from mixed ones have been shown in literature (Lisle et al., 2001).

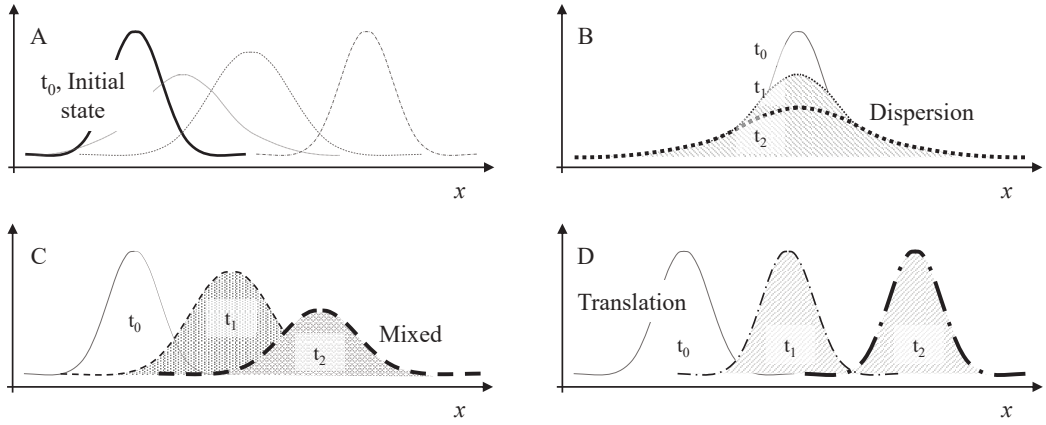

Figure 2.10 – Temporal theoretical behaviour of sediment pulse evolution along the longitudinal direction, x, for (a) Initial state, t_0, of the pulse and global overview on transport mechanisms, (b) Dispersion, (c) Translation and (d) Mixed transport at two consecutive time steps (t_1 and t_2)

Lisle et al. (2001) demonstrated that dispersive pulses attenuate but have longer impact on downstream reach, whereas translation pulses maintain the same intensity but in a more limited impact area. Dispersion was observed by Lisle et al. (2001) while performing tests with different grain size distributions for both the channel bed and the pulse. Translation was observed for gravel bed and pulse material finer than the pre-existing bed surface. Furthermore, former experiences indicate that translation of sediments should be expected for low Froude numbers (Sklar et al., 2009; Humphries et al., 2012). For an ideal replenishment of sediment, Sklar et al. (2009) stated that the grains may reach the target point by translation, and then they should move to dispersion. While performing tests on a 0.5% slope flume and immobile bed, Sklar et al. (2009) found that sediment replenishment are mainly transported by a mixed mechanism between translation and dispersion. Whereas, more clear tendency to translation was observed with smaller amounts of fine sediment (Sklar et al., 2009). The experimental work performed by Cui et al. (2003) basically confirmed the observations by Lisle et al. (1997): augmentations of finer sediment than the pre-existing bed lead to translation mechanism, whereas dispersion mechanism is predominant for mixed replenishment

material. Thus, translation is expected downstream of dams where the replenishment are commonly composed by finer grains (Sklar et al., 2009).

The role of the discharge in the success of sediment replenishment has started to be investigated by both constant and transient flow. Humphries et al. (2012) and Mao (2012) gave an important contribution in the understanding of the channel reach response to a hydrograph. Humphries et al. (2012) compared the effect of a sediment replenishment impacted by a constant discharge with the effects due to a hydrograph. In those experiments, sediment replenishment and channel bed have the same grain size distributions. Hydrographs with different peak discharges were released on a flume facility. The hydrograph induces a clockwise hysteresis in sediment transport. The intensity of the hydrograph defines whether translation or dispersion of sediment may occur. Large hydrograph (peak much larger than the threshold of movement for sediment) with steep limbs cause translation, whereas smaller hydrographs lead to dispersion of the sediment replenishment. These tests were performed on a bed with fixed stationary bars on the bottom. The sediment supply together with the hydrograph leads to the creation of bed patches of replenished material. Mao (2012) investigated the sediment transport rate and grain size for a continuous feed channel and different hydrograph. The sediment transport is less important during the falling limb of the hydrograph showing clockwise hysteresis of sediments. Furthermore, the size of the transported material increases after the discharge peak, but the material is less mobile and the rate of entrainment decreases (Mao, 2012). The above mentioned laboratory tests investigated the role of an hydrograph in terms of influence on the sediment movement and mechanism of transport. The morphological bed aspect played a marginal role in these studies. Finally, (Nelson et al., 2015) resumed that transient flows and wide grain size distribution are necessary in order to obtain success in the sedimetn replenishment.

2.5.2 Field applications

The replenishment of sediments technique has been used since the 1970s in the United States in more than 17 rivers below dams, like the Sacramento-San Joaquin River basin in California, the Carmel River below San Clemente Dam and the Lagunitas Creek below Kent Dam (Kondolf and Matthews, 1991; Gaeuman, 2012). The initial program was increased to a wider scale from 1992 (Bunte, 2004). The sediments were added in order to recreate artificial spawning riffles intended to keep the spawning zone in place and also to improve salmonid spawning habitats. Unfortunately, the data about all the river sediment augmentation projects were not well collected and much information was lost. On the Trinity river, below Lewiston dam, the Draft Coarse Sediment Management Plan (CSMP) specifies 0.15 m as a maximum size for grain diameter, based on empirical observations of bed movement and flow regime. As noted by Wilcock (2004), addition of finer sediment to a coarse bed can be expected to change the threshold of bed mobility and bedload transport relation (Kondolf and Minear, 2004).

Nevertheless, the volumes of added gravel were too small compared with the sediment deficit

and they were washed away by floods with return periods between 1.5 and 4 years (Kondolf, 1997). Thus, the material addition is continuously required. The added material within the Trinity River Restoration program had a grain size varying from 25 to 102 mm and the amounts were estimated based on budgets calculations (Gaeuman, 2008). In dependence from the "water type year", the released amount of replenished material were chosen (Gaeuman and Krause, 2013). The material was added by high-flow injections during high flow periods. The field observations proofed that the replenishment lead to increased bed elevation changes and to the creation of morphological bed forms as medial bars and riffle-like structures.

Figure 2.11 – (a) Englebright dam (California, USA), (b) Injection of sediment along the Yuba river (California, USA), (c) material excavation (Pictures by G. B. Pasternack)

Sediments were supplied along the Yuba river for promoting spawning grounds for fish in the framework of a joint project between The United States Army Corps of Engineers (The Corps), the Pasternack Lab at UC Davis and USFWS. Washed gravels were injected below Englebright Dam in November 2007, during low flow period, to find out if replenishing cobbles is a profitable tool for spawning ground enhancement (Figure 2.11). The study aimed at monitoring if the material would be eroded and where it would deposit. The material (500 tons) was purchased from a nearby quarry downstream. Then, a high flow (250 m^3/s) was released into the river below Englebright Dam in order to mobilise the replenished volume. Despite high flows occurred during two years, much of the injected sediment was still in the original injection location (Pasternack et al., 2004). Nevertheless, the Yuba Accord RMT observed

an increase in redds population despite the limited eroded material from the deposit. This response leads to the conclusion that a higher portion of material would have accommodated even more redds (Pasternack et al., 2004).

Recent applications were undertaken in several Japanese rivers, where the sediment replenishment is used as a tool to restore the reservoir capacity of dams. The common practice in Japan is to remove the sediments trapped in the reservoir and then transport and place them on the channel immediately downstream of the dam. One of the most important application of the method in Japan took place 150 m downstream the Muron dam in 2006 (Kantoush et al., 2010b). These field application were useful for investigating the response of the river in terms of morphological changes. Kantoush et al. (2010a); Sumi and Kantoush (2010) provided a wide investigation on the morphological evolution of the river bed and flow fields during the experiments. The volume of added sediments was equal to 0.6% of the annual deposited volume of sediments in the reservoirs (Kantoush et al., 2010a; Sumi and Kantoush, 2010). It is suggested to add at least the 30% or 40% of the annual deposited volume upstream the dam. Several tests were performed using both artificial and natural flood. The artificial flushing lasted for about 10 hours during only one day and the remaining grains were moved by natural flood that have longer period and discharge. The results show a complete erosion of the replenished volume and, through a monitoring campaign, effects of improvement were observed in riverbed formations and materials, benthic organisms and algae (Kantoush et al., 2010a; Sumi and Kantoush, 2010). Furthermore, the results indicate that it is necessary to increase annually the total amount of sediments.

Since 2004, experiments were undertaken also downstream the Nunome Dam (Japan) (Figure 2.12). Several hundreds cubic meter of material were placed 300 m downstream the Nunome dam for each experiment, relying on high flow to be eroded (Kantoush et al., 2010a). The added material was a mixture between sand and gravel, with median grain size diameter d_{50} equal to 0.38 mm. During the flood, most of the deposit material was eroded allowing restoration of the sediment transport. Furthermore, the eroded material was deposited on the top of existing bars and new sand bars was also created. Nevertheless, the major depositions were found only 300 m downstream the deposit placement and few floods were not completely successful since the material was not mobilized or transported by the flow (Kantoush et al., 2010a; Sumi and Kantoush, 2010). Thus, the study points out the necessity to extend the peak flow duration in order to obtain a complete erosion of the deposit and a longer impact distance (Ock et al., 2013).

From the morphological point of view, the greatest changes in channel structure was the disappearance of bars and islands in the reach immediately downstream the dam (Kantoush et al., 2010a). At 300 m from the dam, the bed morphology changed again demonstrating the capability of the replenishment technique to restore bed load transport and associated habitats (Kantoush et al., 2010a). Nevertheless, the newly deposited fine material does not seem stable and they may be washed away by natural floods (Kantoush et al., 2010a).

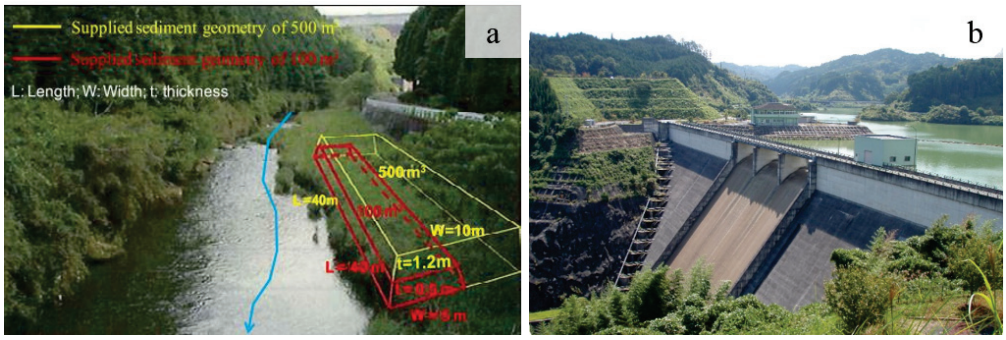

Figure 2.12 – (a) Replenishment downstream the Nunome dam (Japan) (Picture by S. Kantoush), (b) Nunome dam (Picture by Hi, A.)

Several other experiences have been carried out also in Alpines rivers in Germany and in Switzerland. On the Rhine River downstream of Iffezheim dam (Germany) another example of sediments replenishment took place (Figure 2.13*b*). In this river, an average of 170,000 tons of gravel and sand are added annually along the banks (Kondolf and Minear, 2004). The approach has resulted successful in reducing further incision of the riverbed (Kuhnle, 1992). Furthermore, along the High-Rhine river, 500 m downstream of the hydropower plant of Eglisau (Switzerland) about 10 m^3 of washed gravel were introduced to test the potential of gravels as spawning ground in 1990 (Zeh and Dönni, 1994). The used grain size distribution for the sediment augmentation varied from 16 to 50 mm while the grain size dimension of riverbed varies from 50 to 300 mm. The main differences of this application are the irregular shape used for the replenishment distributed along the river with a thickness of 0.2 m and the loss of bedload transport. The sediment augmentation has demonstrated to be able to recreate stable spawning grounds (Zeh and Dönni, 1994).

Figure 2.13 – (a) Replenishment of sediment along the Sacramento river downstream the Keswick dam (USA, Picture by Kondolf, G. M.), (b) Replenishment of sediment along the Rhine river downstream the Iffezheim dam (Germany, Picture by Kondolf, G. M.)

These field applications have permitted to improve the knowledge on the complex geomorphological processes occurring in rivers while applying sediment replenishment (Bunte, 2004; Kantoush et al., 2010b; Kantoush and Sumi, 2010). Furthermore, they proofed that a successful replenishment requires of an appropriate combination between available discharge, flood duration and adapt placement of the sediment replenishment (Ock et al., 2013). Nevertheless, he stated that the so far achieved knowledge about sediment replenishment is not sufficient to draw general guidelines for river management downstream of dams. Especially the influence of discharge, the sediment load on the river geometry and the time scales of changes due to sediment replenishment are core topics for a better understanding (Kantoush et al., 2010b; Ock et al., 2013). Without more precise knowledge about these factors sediment replenishment cannot be adapted appropriately, which may result in undesirable ecological consequences or even in failure of the restoration project itself (Kantoush et al., 2010b).

2.6 Summary

The replenishment of sediment is becoming a common method to restore morphological diversity along disturbed and pauperised reaches downstream of dams. The increase of bed morphology diversity has demonstrated to be efficient in creating spawning grounds for fishes. Thus, the method helps in restoring both ecological and morphological aspect of rivers. Nevertheless, the gap of knowledge about the link between sediment supply and channel bed morphology still requires research (Lisle et al., 1997; Venditti et al., 2012).

More detailed studies are necessary on the factors influencing the success of the gravel augmentation projects, since many of the restoration projects are still only conceptually designed based on past experiences (Kondolf, 1997; Sklar et al., 2009; Kantoush et al., 2010a). Namely, the role of the discharge and the frequency of its release (i.e. artificial flood), the required amount of sediment, their geometrical placement and the mechanism of sediment propagation through the channel are core topics to develop (Kantoush et al., 2010a; Venditti et al., 2012).

In light of these missing points, this research aims at exploring new aspect related to the geometrical configuration of deposits. For this reason, for the first time, deposits are placed on both banks and several geometrical configurations of the sediment replenishment are proposed. Several geometrical aspects of the replenishment deposit are investigated: placement, length and consecutive augmentations. Thereby, several volumes of grains are tested.

The role of discharge is considered by investigating both constant and transient regimes. Three submergence ratios link the flow depth with the replenishment height are performed. Then, the role of transient flows is investigated by means of triangular-shaped hydrographs.

3 Experimental method

3.1 Experimental Setup

3.1.1 Experimental channel

The experiments were performed at the Laboratory of Hydraulic Constructions (LCH) of the Ecole Polytechnique Fédérale de Lausanne (EPFL), in Switzerland. The tests were run in a 15 m long, 2.5 m wide and 0.7 m high channel. The side-walls consist of a steel frame with glass windows (Figure 3.1). At the upstream end of the channel, a basin ensured a regular inflow into the flume. The water flowing into the channel was provided by a constant-level reservoir. At the downstream end of the flume, the water flowed through a weir and freely fell into a basin where it was collected into the laboratory recirculation system. The discharge was imposed by a pumping system, controlled by a flow-meter, aiming at the envisaged water depths. The water depths in the channel are measured with a water gauge at the deposit positions, before these are placed.

When scaling from prototype dimension to a reduced model, it is necessary to be aware of scale effects. Scale effects arise from the inability to keep force ratios constant between model and prototype. Open-channel hydraulic models are normally scaled using the Froude similarity criteria. By this criteria, a constant ratio between inertia and gravity force is guaranteed. Scale effects and viscous forces are stated to be negligible (Heller, 2011). Therefore, Froude similarity is applied to these experiments. Considering Froude values for the tested submerged conditions, the experimental facility well simulates a mountain stream reach, where Froude varies from 0.3 to 1 (Cui et al., 2003; Weichert, 2006). A reference geometric scale factor λ_L of about 10 was used to define the main channel dimensions. The scale factor of 1:10 is considered adequate for modelling bed morphology of Swiss mountain rivers downstream of dams (Parker and Toro Escobar, 2002; Cui et al., 2003; Rickenmann, 1997). The longitudinal slope of the channel, equals to 1.5%, well corresponds to a typical gravel bed stream (Parker and Toro Escobar, 2002). The model intends to reproduce a river stretch of roughly 150 m in length and 4 m in width in prototype.

The flume was divided in two geomorphological identical channels (Figure 3.1). This allows to have a study area where the length-to-width-ratio is more adequate to a reference reach. With the two channels, two different geometrical configurations of replenishment deposits were tested simultaneously (Figure 3.5). Each channel had a trapezoidal cross section, with a channel bed width of 0.4 m and a bank slope of 2:3 (height : length). The channel cross section is constant along its entire length (Figure 3.2).

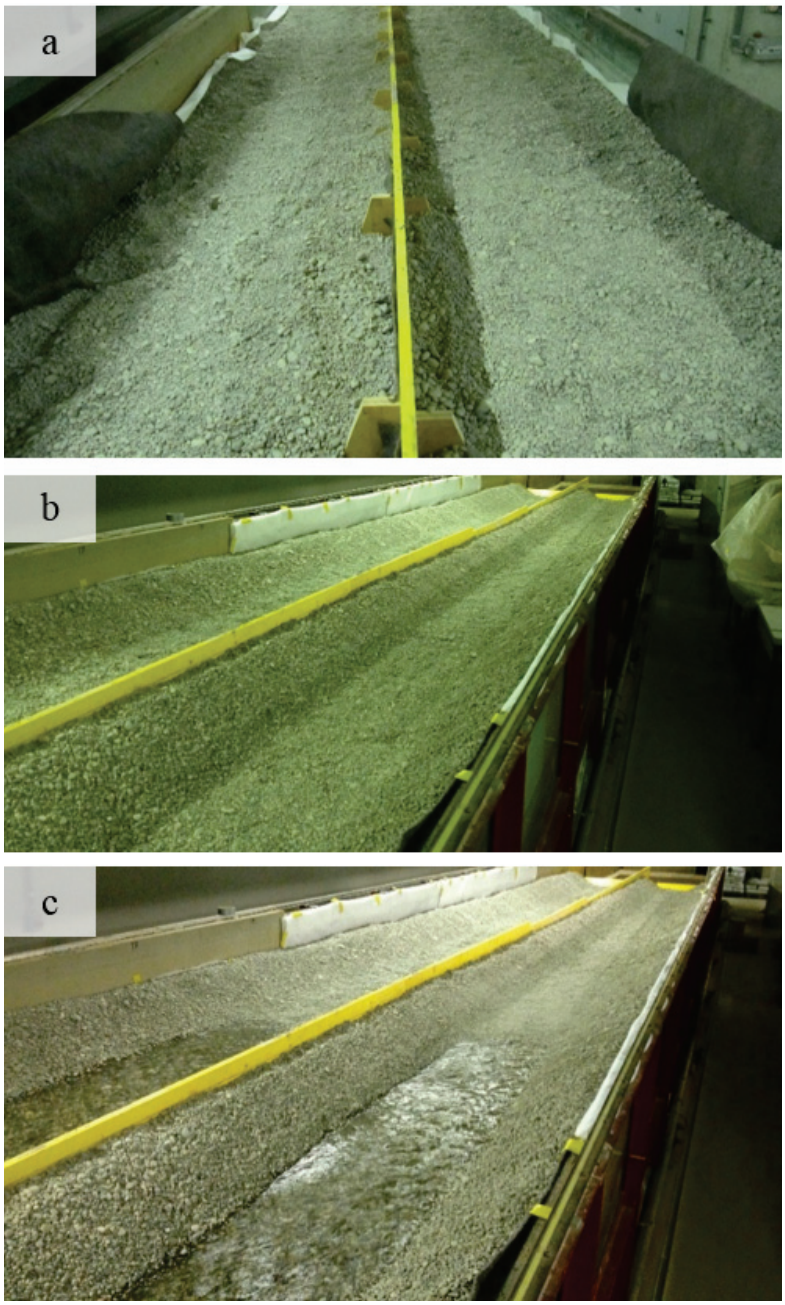

Figure 3.1 – Construction phase of the experimental channel: (a) preparation of the two channels, (b) view of the two morphological identical channels after modelling of the trapezoidal cross section and (c) preliminary test with water

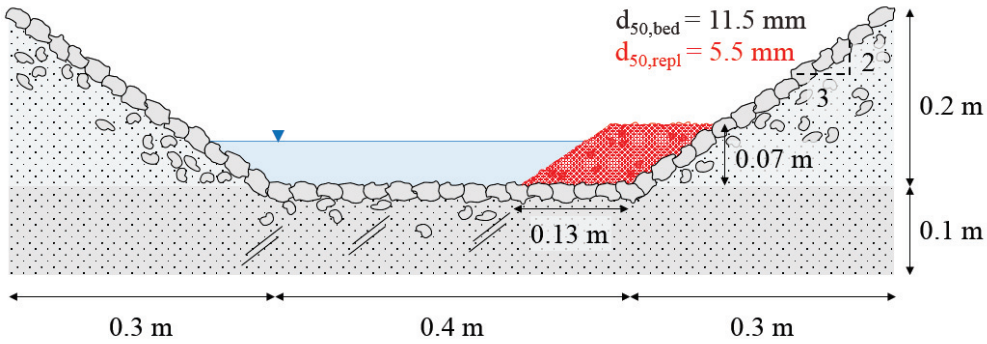

Figure 3.2 – Schematic cross section of the experimental channel at LCH. The characteristic diameter d_{50} of both bed and replenishment material are indicated. The replenishment deposit occupies about one third of the channel width (in red)

3.1.2 Replenishment characteristics

Sediments

Accounting for bed armoring, typical of downstream dam reaches, the channel bed is formed by gravel larger than 7 mm with a median diameter, $d_{50,b}$, of 11.5 mm (Figure 3.3). A reduced part of the dimensionless bed grain size distribution proposed by Hersberger et al. (2015) is used, which well reproduces the conditions of Alpine streams. The same material used for the bed was used for the banks, which are immobile for the performed discharges. The channel bed is composed by concrete slabs upon which the gravel bed is placed; the sediments are kept fixed by placing them in a cement mortar. The replenishment volumes are composed by a finer grains varying from 3 to 8 mm with a $d_{50,r}$ of 5.5 mm. Considering the geometrical scale factor, the chosen grain size distribution for the replenishment volume lies in the upper range of possible values for fish spawning habitat (Kondolf and Wolman, 1993; Ock et al., 2013). The geometric standard deviation of grain size distribution, σ, is equal to 1.30 for the bed and bank material and to 1.13 for the replenished material. The parameter σ is defined as the ratio between d_{84} and d_{50} of the material. The selected channel and replenishment material are in the right constant area of the Shields diagram as proposed by Ahmari and Da Silva (2011). Therefore, the scale effects induced by the different material behaviour after scaling from prototype to model can be minimised. Indeed, this would occurs for grain dimension smaller than $\pm 3-4$ mm. In Table 3.1 the dimensionless bed shear stress is above the threshold of movement of 0.047 only for the replenishment material.

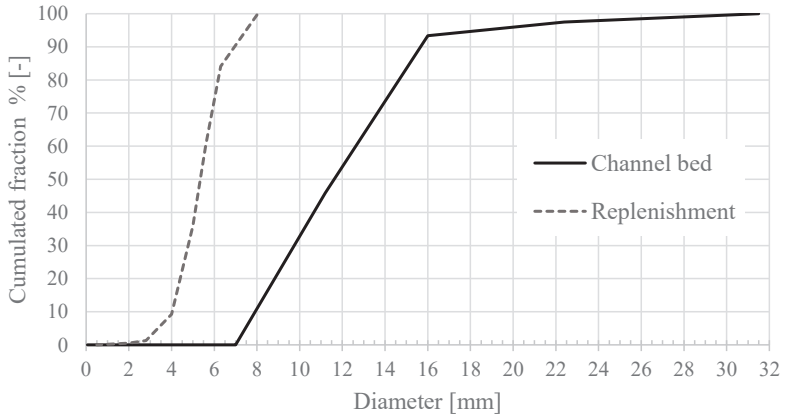

Figure 3.3 – Grain size distribution of replenishment and bed material

Replenishment configurations

The volumes are implemented on the dry channel before the test start and considered to be eroded and transported by an artificial flood. Considering the methods proposed by Ock et al. (2013), the sediment replenishment is placed with the in-channel stockpile technique. The replenishment height is kept constant, equal to 0.07 m (corresponding to 17.5% of channel width), for all the performed experiments. The total weight of placed gravel and the amount of washed out from the channel length grains are weighted for each experiment. The replenishment volume is placed in four deposits on both channel banks. Each one with the same shape and the same volume (around 0.007 m^3 on model). Each deposit has a length of 0.75 m a width of 0.13 m. An exception is made for the tests with shorter and longer deposits, where they are created with a length of respectively 0.5 and 1.0 m.

Six different geometrical configurations were tested (Figure 7.1). Configurations A, D and F are defined as parallel with downstream shift of volumes equal respectively to zero, two and one quarter of replenishment length. The remaining geometrical configurations (B, C and E) belong to the alternating placement, where the downstream shift of the volumes varying respectively between half, one and three quarter of replenishment length. To avoid any influence from the upstream boundary, the first deposit is placed 2.5 m downstream from the upstream section. For the same reasons, the last 2.5 m channel length before the downstream section of the channel are not considered for data analysis. Thus, the final observation length is 10 m.

The grains are coloured red in order to be distinguishable from the channel bed and banks allowing image tracking of the evolution of the channel morphology (Figure 3.5).

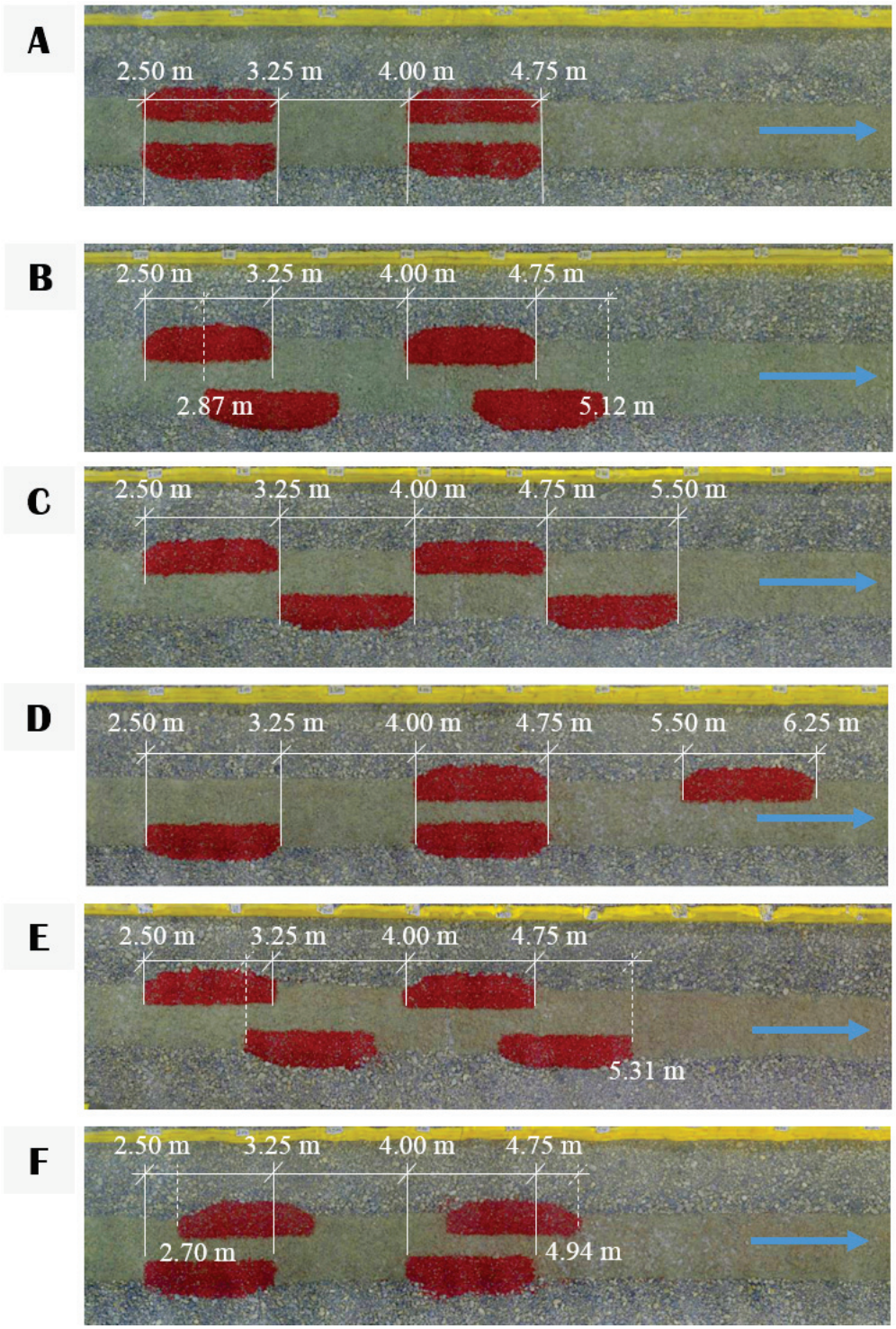

Figure 3.4 – The six tested geometrical configurations for the replenishment. Detailed: (A) parallel volumes, (B) volumes shifted half the replenishment length, (C) volumes one replenishment length shifted downstream, (D) single volume and parallel volumes placed on both banks, (E) volumes 3/4 replenishment length shifted downstream, (F) volumes 1/4 replenishment length shifted downstream. Flow direction from left to right, indicated by arrows. Distances are indicated along the flow direction

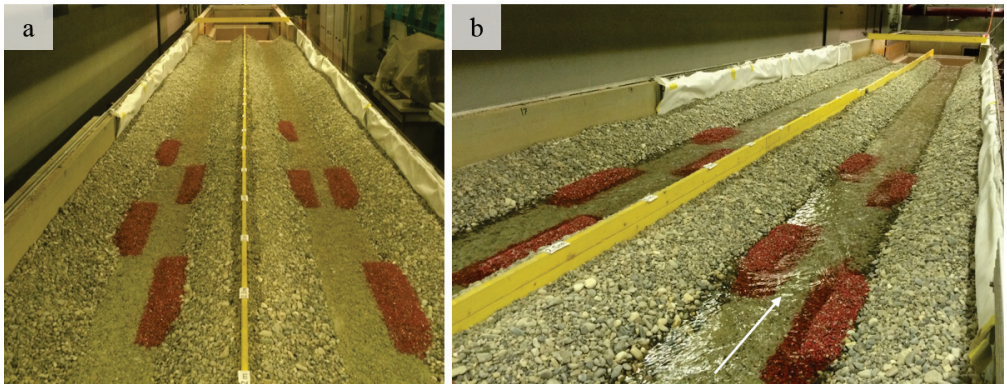

Figure 3.5 – (a) Configuration C (left) and configuration D (right) on dry channels, (b) Configuration C (left) and configuration B (right) during a test with 100% submergence ratio

3.1.3 Hydraulic conditions

The discharge is indirectly determined by the submergence of the replenishment volumes. Furthermore, the discharges were chosen in a way that the bed shear stress is large enough to mobilize the replenishment, but low enough not to erode the bank material. By a trial and error optimization, the water depth for a submergence ratio of 100% was chosen equal to 0.07 m. Three submergence ratios are tested: non-submerged (water depth equal to 70% of the volume height, Figure 3.6*a*), just submerged (water depth equal to 100% of the volume height, Figure 3.6*b*) and over submerged (water depth equal to 130% of the volume height, Figure 3.6*c*). These three water depths correspond respectively to 0.007 m^3/s, 0.019 m^3/s and 0.031 m^3/s in the experimental channel. A submergence ratio of 100% with a model discharge of 0.019 m^3/s equals 6.0 m^3/s in prototype dimension.

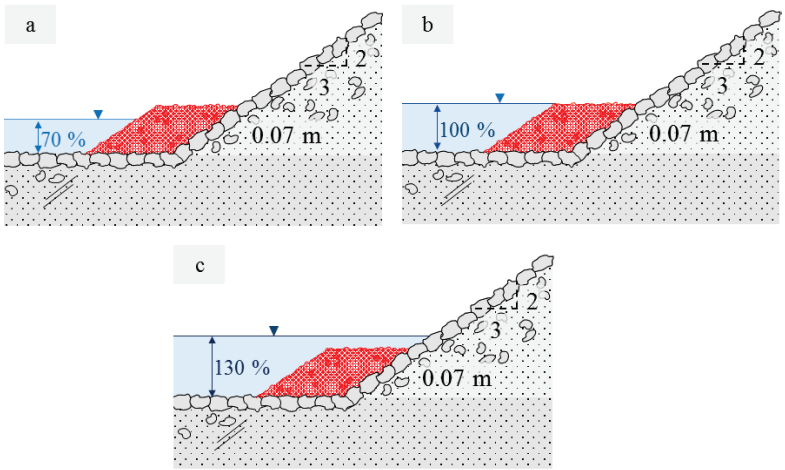

Figure 3.6 – Submergence ratios tested on the experimental flume: (a) not submerged, (b) completely submerged and (c) over submerged

The initial hydraulic conditions for the tested submergence ratios are listed in Table 3.1. The

hydraulic radius R_h is calculated as the ratio between the cross-sectional flow area and the wet perimeter for each submergence ratio. The cross sectional averaged flow velocity, taking into account the imposed discharge, is used to compute the Froude number when divided by $(g * R_h)^{(1/2)}$, where g is the gravitational acceleration. The Reynolds numbers Re is respectively calculated with d_{50} for both replenishment and bank material, and calculated as follows:

$$Re = \frac{(g * R_h * S)^{1/2} * d_{50}}{\nu} \tag{3.1}$$

where S is the longitudinal slope and ν is the kinematic viscosity of the water. For both materials, the dimensionless bed shear stress τ^* is calculated as follow:

$$\tau^* = \frac{\tau_0}{(\rho - \rho_s) * g * d_{50}} \tag{3.2}$$

where τ_0 is the bed shear stress defined as ρ*g*S*R_h, and ρ and ρ_s are respectively the water and sediment density.

The flows are all sub-critical (Fr<1), with the Froude number varying from 0.44 to 0.67 and fully turbulent (Re>>2000).

Table 3.1 – Initial hydraulic characteristics for different tested submergence conditions, Reynolds and Shields shear stress are estimated considering $d_{50,repl}$=5.5 mm and $d_{50,bed}$=11.5 mm, for the replenishment and the bed material respectively

Submergence		70%	100%	130%
Discharge	m^3/s	0.007	0.019	0.031
Flow depth	m	0.05	0.07	0.09
Hydraulic radius	m	0.04	0.05	0.07
Flow mean velocity	m/s	0.30	0.54	0.64
Froude number	-	0.44	0.65	0.67
Repl: Grain Reynolds number	-	384	446	496
Repl: Shields shear stress	-	0.07	0.09	0.11
Bed: Grain Reynolds number	-	804	932	1037
Bed: Shields shear stress	-	0.03	0.04	0.05

3.2 Measurement, equipment and data acquisition

3.2.1 Instrumentation

Two types of measurements are made: pictures and laser scanner. The instrumentation (camera and laser) is mounted on a carriage riding on two rails along the channel at a fixed height. It is manually driven and moveable along both the longitudinal and cross sectional directions (Figure 3.7).

Figure 3.7 – (a) Laser scanner, (b) camera: GoPro Hero 3+, (c) acquisition system, (d) moveable instrumentation installed on carriage and (e) laser scanner on the support

Camera

Image data (2D) are acquired with a GoPro Hero 3+ black edition camera (Figure 3.7*b*). The pictures are taken at 12 Mega-Pixel with a focal length of 2.77 mm. The resolution of each picture is 4000x3000 pixels. Pictures are collected each 0.5 m along the channel length, resulting in 22 pictures per channel per time step, with a superimposition of 25% (Figure 3.7*d*). During the first test hour, five picture series are taken at 5, 15, 30, 45 and 60 minutes. Then pictures are taken every 30 minutes for the remaining two hours testing. Two other picture series are taken at the beginning and at the end of the test, in dry condition, to document the initial and final channel morphology. More detailed information on the picture acquisition time steps are provided in Figures 3.13 and 3.14.

To obtain an undistorted image of the entire channel length, a calibration of the camera was done with the software Agisoft Lens. The latter allows to sort the image residues and to correct the camera parameters. These parameters are related to normal and tangential distortion. The software Agisoft Photoscan Professional was used to eliminate the fisheye effect from each picture and for merging together all the picture recorded for the single channel. Therefore, a panoramic view of the single channel was built for each recorded time step. Furthermore, the software creates a panoramic 3D view using the calibration parameters (Figure 3.8).

Laser scanner

The bed morphology (3D) is recorded at the beginning and at the end of each test in dry conditions by means of a laser scanner (Baumer, model OADM 13I7480/S35A), which measures distances (Figure 3.7*a*). The tool is a photoelectric sensor, punctual emitter of light, at a wavelength of 650 nm. The accuracy of the laser in the vertical direction is ± 0.8 mm. The laser was calibrated for then converting measurements in Volt to distances in meters. The laser profiles are laterally spaced by 20 mm, whereas longitudinally the profile is recorded every 1 mm. In total 25 longitudinal profiles are recorded for each channel.

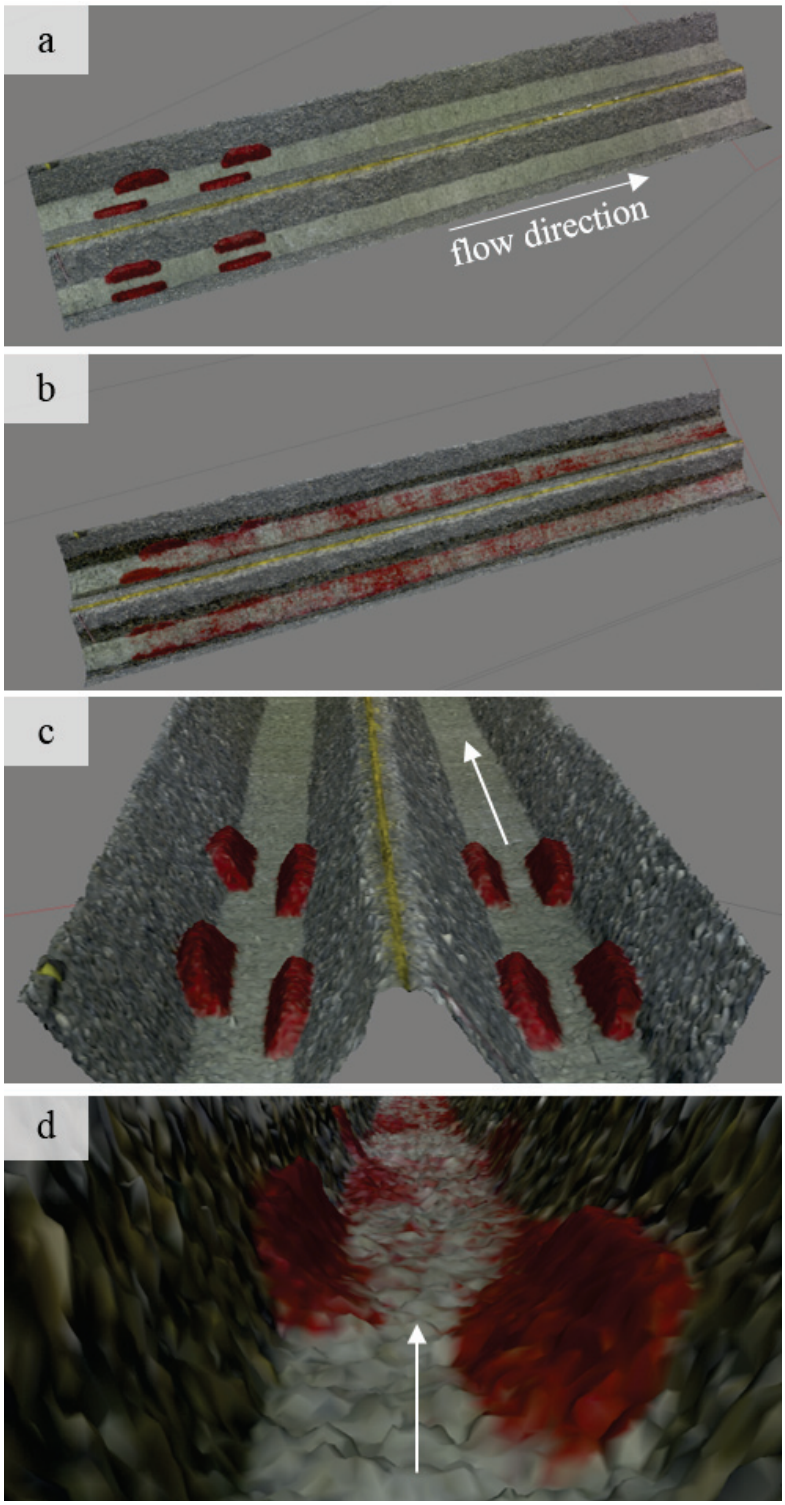

Figure 3.8 – (a) Reconstructed picture of the initial state for configuration A on the right channel and configuration B on the left channel, (b) reconstructed picture of the final state for the same configurations, (c) cross sectional picture of the reconstructed channel, (d) insight of configuration B for the final state. Arrows indicate the flow direction

3.2.2 Data acquisition

To perform both image and laser analysis, the area of interest (A_{oi}) was defined. It corresponds to the channel bed width, without the banks (0.4 m), and longitudinally to the observation lengthof the channel (10 m). The A_{oi} is the same for each image. The picture were converted into a binary metrics by applying an RGB-threshold value based on the Otsu's method. This procedure includes the selection of a threshold to minimize the intraclass variance of the black or white pixels (Otsu, 1979) (Figure 3.9). This method associates a value of 1 to pixel containing red gravels and 0 to all the remaining pixels. The pixel size is equal to 2.7x2.7 mm^2.

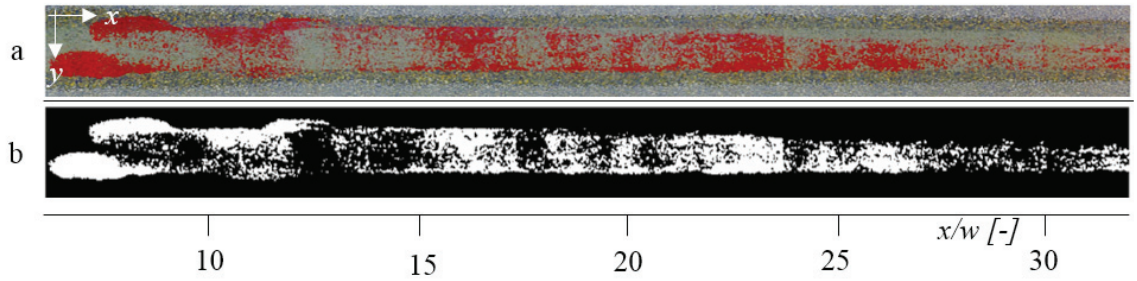

Figure 3.9 – (a) Original plane picture for Configuration B at the test end with a submergence ratio of 100%; (b) Binary conversion of the original picture

3.3 Assessed parameters

For giving a complete overview on the channel bed morphology development and on the time influence, a set of parameters was defined which are related to the measured variables. These parameters describe the channel response to sediment replenishment in view of morphological changes, time needed for erosion, required flow and influence distance downstream of the initial replenishment volumes.

1. Persistence of sediment replenishment, (PD, %), which indicates the amount of gravel which was transported out of the flume based on weight measurements. An efficient replenishment should have a high persistence value in the reach to be restored. The persistence, PD, is calculated as:

$$PD = \left(1 - \frac{M\,washed\,out}{M\,placed\,sediment}\right) * 100 \tag{3.3}$$

2. Covered Surface, (CS,%), which is the ratio between the area covered by the replenished sediments (red pixel , A_{or}) and the total area of interest (A_{oi}). It is based on 2D images.

This parameter indicates the grain distribution downstream. CS is calculated as:

$$CS = \frac{\sum A_{or}}{\sum A_{oi}} * 100 \tag{3.4}$$

3. Compactness of covered surface, (NCD) which allows for evaluating if the mobilized gravel tends to aggregate forming clusters. The bed forms looking like cluster are more likely seen as spawning habitats for fishes (Geist and Dauble, 1998). In literature the most common approach of assessing compactness of a shape is done by comparing its perimeter to the perimeter of a circle, containing the same area. The images taken at the end of each experiment show the irregularity and the presence of holes in the covered surface. Using the compactness theories presented by Li et al. (2013) and Bribiesca (1997), the normalized discrete compactness (NDC, %) is defined as:

$$NDC = \frac{C_b - C_{b,min}}{C_{b,max} - C_{b,min}} * 100 \tag{3.5}$$

where C_b is the sum of all boundaries (in the sense of perimeters) that connect two cells of covered surface, $C_{b,min}$ represents the minimal amount of connecting boundaries for a shape of the same area and $C_{b,max}$ the maximal amount correspondingly. Thus $C_{b,min}$ would be obtained for a line, while $C_{b,max}$ results for a contour most close to a circle. The values of NDC ranges from 0 to 1, where 1 indicates the most compact shape (Bribiesca, 1997). The advantage of this method is that it can be applied directly on raster data sets. Furthermore, it is independent from scale and it can account for holes (Li et al., 2013).

4. Transport distance of center of mass (TD_{50}, m) and sediment front (TD_{99}, m): determined using the 2D binary images. The center of mass and the front are defined at the location where 50% and 99% of the covered surface is located upstream, respectively. The analysis of the transport distances over time allows to estimate the bulk velocity of the transport of the replenished sediments. This analysis is only meaningful as long as no sediment is washed out of the channel. This instant (t_{end}) is defined as the moment at which the front reaches the lower channel length.

5. Occupation Ratio along the channel, (OCR, %), which represents the portion of replenished sediments covering the bed surface calculated for every cross section. The OCR along the channel is calculated as follows:

$$OCR_x = \frac{\sum(red\ pixels\ at\ cross\ section)}{\sum(pixels\ at\ cross\ section)} \tag{3.6}$$

The Power Spectral Distribution (PSD) of the signal of OCR is used to find periodicity in

the analysed data (Stoica and Moses, 2005). The PSD is estimated only for the portion of the channel downstream of the replenishment, in order to avoid an influence of the original configuration of the latter. As all parameters tend to reach a quasi equilibrium value after the three hours of experiment, the OCR and corresponding PSD are analysed only for this final equilibrium state. The entire downstream length is used as data input for the PSD estimation. Window size is set to half of data length with an overlapping of 50%, for applying Welch's method. The PSD of the OCR signal is of practical relevance since it indicates how the replenishment may impact the downstream reach.

6. Topographic Differences. The laser measurement records for the channel bed are used to evaluate the changes on bed elevation due to the replenishment. The deposit heights are obtained by subtracting the final elevation from the initial one. The differences are then averaged in cross sectional direction, which allows a comparison with the OCR. The resulting cross sectional mean differences are further analysed by interpreting their PSD in the downstream reach, which is estimated as described for OCR.

7. Bed roughness. The standard deviation of the bed elevation is used as an estimation of the bed roughness scale, as proposed by Coleman et al. (2011). Standard deviation is calculated for the initial and final topography of the channel bed. Among others, one of the main aims of replenishment is to enhance bed morphological changes. The replenishment may affect the bed roughness by filling the pools with the gravels deposit (decreasing the global roughness), or by developing bed forms (increasing roughness) (Madej, 2001).

8. Volume of deposition and erosion: (based on laser measurements) the volumes of deposition and erosion are calculated from the integration of the differences in bed elevation over the entire channel length. These values are than further compared with the persistence (PD).

9. Velocity of center of mass and sediment front: the velocity is calculated as the distance run by the respectively the TD_{50} and the TD_{99}, considering from the beginning of the test, divided by the time required for reaching this distance.

10. Transport mechanism: assessed as Sklar et al. (2009) by comparing the interquartile length (IQL) with the position of the center of mass (TD_{50}) of the covered surface. The interquartile length is defined as the length of the central 50% of covered surface, without considering the upper and lower 25% of the area (Figure 7.2). A large increase of the IQL with a small change of the TD_{50} corresponds to a transport of dispersion type. Whereas a movement of the TD_{50} associated to a quasi-constant IQL value is related to a translation mechanism of transport. The slope (IQL/TD_{50}) indicates whether sediment is transported by dispersion or translation. When the ratio between IQL and TD_{50} tends to infinite, the transport mechanism is defined as pure dispersion type, while a ratio equals to 0 represents pure translation type. A mixed mechanism, between pure translation and pure dispersion correspond to a slope of 0.5, in agreement with Nelson et al. (2015).

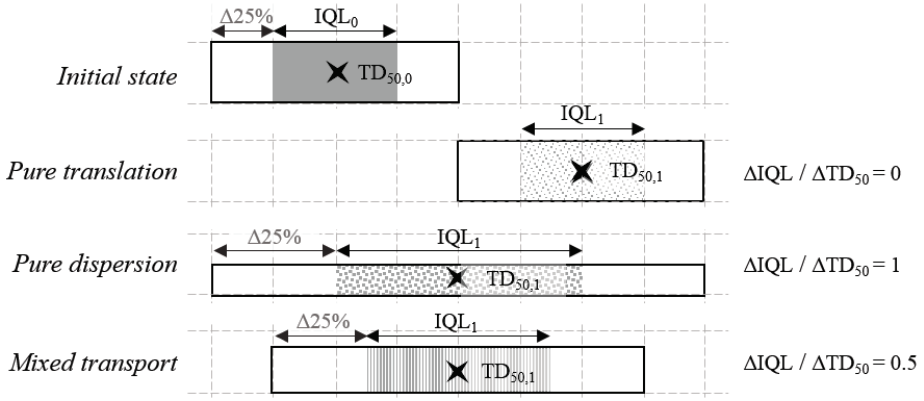

Figure 3.10 – Schematic representation of the temporal evolution of the longitudinal distribution of the replenished volume of sediments. Example of dispersion, translation and mixed transport

3.4 Performed experiments

3.4.1 Preliminary tests

An armoured bed was created by adding the desired material and shaping the two channels. Then, a constant flow was released in order to wash out the fine particles until the sediment transport was almost zero. The preliminary tests were performed on this flume conditions (Figure 3.11), but few problems were immediately highlighted. The replenished material was percolating into the armoured bed enhancing the bed mobilization. Thus, the traceability and the quantification of the eroded and transported material was compromised. Therefore, the armoured bed was replaced by mortar slab assuring a fixed armoured bed.

During preliminary tests, different amounts of replenishment material and configurations of the deposits were tested. Alternating and parallel placement of the deposits, on one or both banks, were used . One single volume was not completely eroded nor for 100%, nor 130% submergence ratio (Figure 3.12). Nevertheless it was considered that this amount of replenished sediments was not enough for creating any morphological variation on the whole downstream reach. Therefore, the quantity was progressively increased from one single volume to two (Figure 3.12). The narrowing of the cross section created by the two deposits placed along the same bank enhances higher transport capacity and therefore the volumes were eroded and transported. However, the distance travelled by the grains was not longer than twice the replenishment length, nor morphological relevant changes were observed on the study reach. The eroded material tended to accumulate close to the channel bank without affecting the whole bed cross section (Figure 3.12). Finally, the final amount of replenished material was chosen following also the investigations by Venditti et al. (2010), which indicates the maximum volume for a replenishment as the amount necessary to cover with a layer of 1 or 2 times d_{50} the entire bed surface of the channel reach. A total amount of 0.027 m^3 was

thus considered suitable for the replenishment testing.

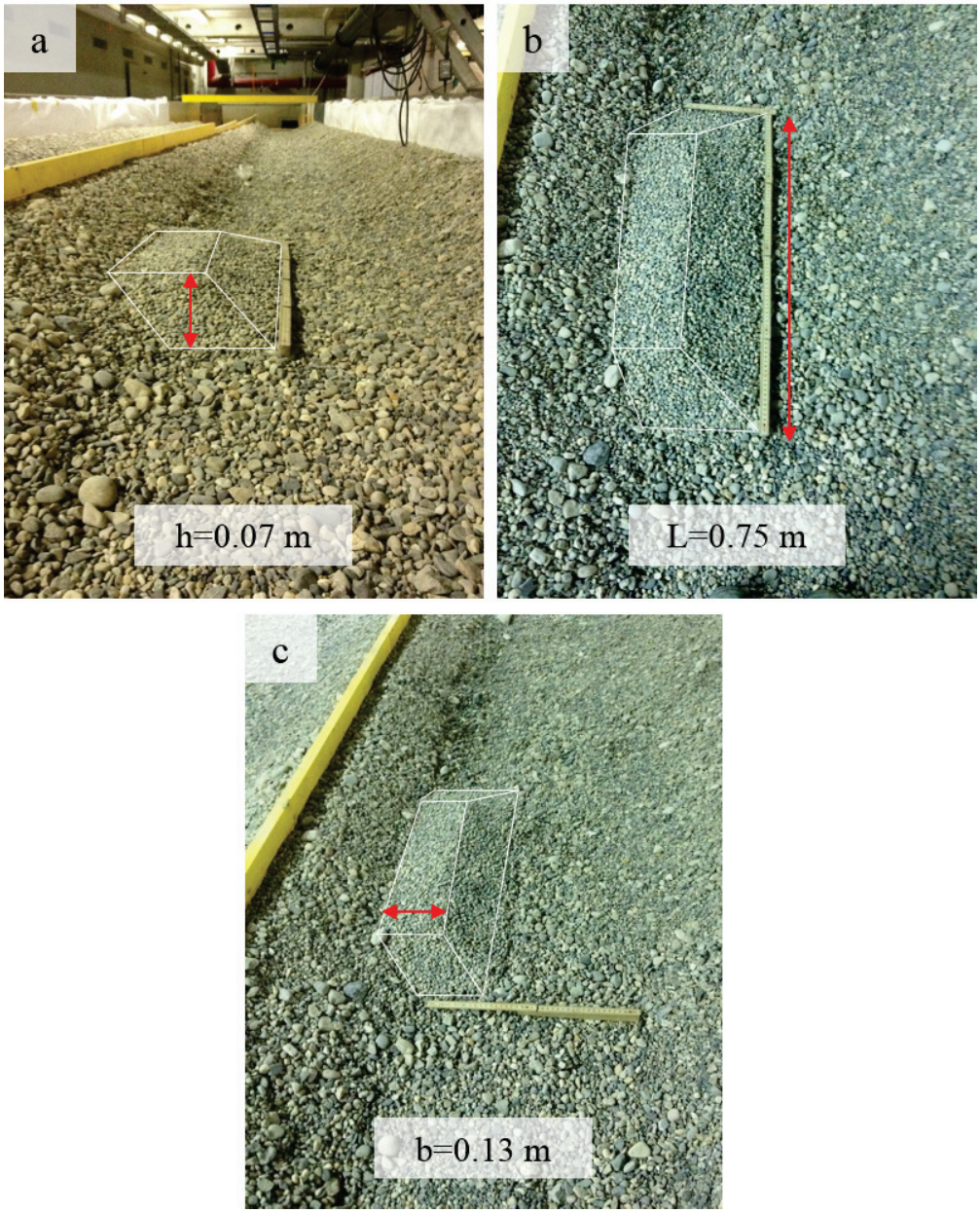

Figure 3.11 – Preliminary test with single replenishment deposit: (a) height of 0.07 m,(b) length of 0.75 m and (c) width of 0.13 m, (d) deposit erosion during a preliminary test, (e) channel at the end of the test showing partial erosion of the replenishment deposit

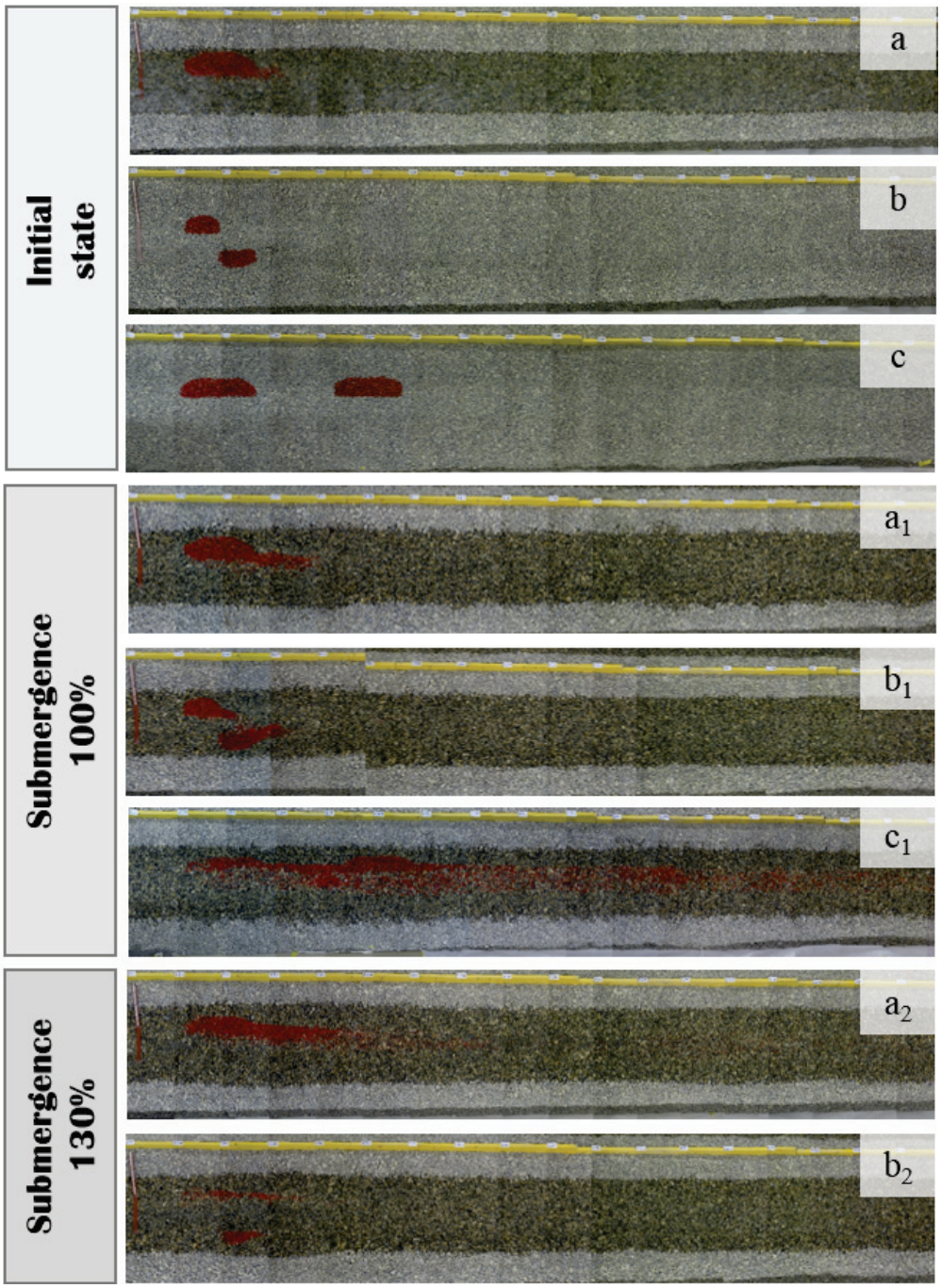

Figure 3.12 – Initial state for respectively: (a_1) single deposit and (a_2) double alternated half deposits. Final state for 100% submergence for respectively: (b_1) single deposit and (b_2) double alternated half deposits

3.4.2 Performed experiments

Figures 3.13 and 3.14 present an overview of all experiments performed during the whole study. Tests from 1 to 7 were performed on moveable bed indicated as M, whereas all the remaining experiments were run on fixed bed, indicated with F. The submergence ratios listed as 070, 100 and 130 correspond respectively to a water depth of 70%, 100% and 130% the deposit height. L indicates the replenishment length. Furthermore, the tests are divided in eight groups, indicated by a letter. To a and b correspond the preliminary tests on moveable and fixed bed, to c the experiments run with not-submerged condition, d with completely submerged and e over submerged tests. In groups f and g are respectively included tests with consecutive replenishment and experiments with different replenishment length. The group h indicates the tests undertaken with transient flows. In the following chapters, reference to tests from 11 to 46 will be done.

	Test	Submer	Conf	Bed	Duration	Q	L	Placed	Camera: Time series	Laser	Reple series	
						[m^3/s]	[m]	[m^3]	[min]		1st	2nd
a	1	100	SV	M	4h30	0.019	0.74	0.007	(0' 15' 30' 45' 60' 75' 105' 120' 135' 150' 180' 210' 240' 2	-	Y	-
	2	130	SV	M	1h45	0.035	0.74	0.007	(0' 5' 10' 15' 20' 25' 30' 45' 60' 75' 90' 105' ww)	-	Y	-
	3	100	DAlt	M	4h30	0.019	0.37	0.007	(0' 15' 30' 45' 60' 75' 90' 120' 135' 150' 165' 180' 195' 21(	-	Y	-
	4	130	DAlt	M	1h45	0.035	0.37	0.007	(0' 5' 10' 15' 20' 25' 30' 45' 60' 75' 90' 105' ww)	-	Y	-
	5	100	DAli	M	4h30	0.019	0.37	0.007	(0' 15' 30' 45' 60' 75' 90' 105' 120' 135' 150' 165' 180' 19	-	Y	-
	6	130	DAli	M	1h45	0.035	0.37	0.007	(0' 5' 10' 15' 20' 25' 30' 45' 60' 75' 90' 105' ww)	-	Y	-
	7	100	DV	M	4h30	0.019	0.74	0.014	(0' 150' 30' 45' 60' 75' 90' 105' 120' 135' 150' 180' 210' 2	-	Y	-
b	8	070	SV	F	2h30	0.007	0.74	0.007	15' first hour, 30' until end	-	Y	-
	1	100	SV	F	4h30	0.019	0.74	0.007	(0' 15' 30' 60' 90' 120' ww)	-	Y	-
	2	130	SV	F	1h30	0.035	0.74	0.007	(0' 10' 20' 30' 60' 90' 120' 150' ww)	-	Y	-
	3	100	DAlt	F	4h00	0.019	0.37	0.007	(0' 10' 20' 30' 45' 60' 75' 90' 105' 120' 135' 165' 195' 225'	-	Y	-
	4	130	DAlt	F	1h30	0.032	0.37	0.007	(0' 10' 20' 30' 45' 60' 75' 90' ww)	-	Y	-
	5	100	DAli	F	4h00	0.019	0.37	0.007	(0' 10' 20' 30' 45' 60' 75' 90' 105' 120' 135' 165' 195' 225'	-	Y	-
	6	130	DAli	F	1h30	0.032	0.37	0.007	(0' 10' 20' 30' 60' 90' 120' 150' ww)	-	Y	-
	7	100	DV	F	2h30	0.019	0.74	0.014	(0' 10' 20' 30' 60' 90' 120' 150' ww)	-	Y	-
	9	130	DV	F	1h30	0.035	0.74	0.014	(0' 10' 20' 30' 60' 90' 120' 150' ww)	-	Y	-
c	11	070	C	F	3h00	0.008	0.74	0.027	(0' 15' 30' 45' 60' 90' 120' 150' 180' ww) 9t	Y	Y	-
	12	070	D	F	3h00	0.008	0.74	0.027	(0' 15' 30' 45' 60' 90' 120' 150' 180' ww) 9t	Y	Y	-
d	1	100	A	F	3h00	0.019	0.74	0.027	(0' 15' 30' 45' 60' 90' 120' 150' 180' ww) 9t	-	Y	-
	3	100	A	F	3h00	0.019	0.74	0.027	(0' 15' 30' 45' 60' 90' 120' 150' 180' ww) 9t	-	Y	-
	2	100	B	F	3h00	0.019	0.74	0.027	(0' 15' 30' 45' 60' 90' 120' 150' 180' ww) 9t	-	Y	-
	4	100	B	F	3h00	0.019	0.74	0.027	(0' 15' 30' 45' 60' 90' 120' 150' 180' ww) 9t	-	Y	-
	7	100	C	F	3h00	0.019	0.74	0.027	(0' 15' 30' 45' 60' 90' 120' 150' 180' ww) 9t	-	Y	-
	15	100	C	F	3h00	0.019	0.74	0.027	(0' 5' 15' 30' 45' 60' 90' 120' 150' 180' ww) 10t	Y	Y	-
	8	100	D	F	3h00	0.019	0.74	0.027	(0' 15' 30' 45' 60' 90' 120' 150' 180' ww) 9t	-	Y	-
	16	100	D	F	3h00	0.019	0.74	0.027	(0' 5' 15' 30' 45' 60' 90' 120' 150' 180' ww) 10t	Y	Y	-
	27	100	E	F	3h00	0.020	0.74	0.027	(0' 5' 15' 30' 45' 60' 90' 120' 150' 180' ww) 10t	Y	Y	-
	28	100	F	F	3h00	0.020	0.74	0.027	(0' 5' 15' 30' 45' 60' 90' 120' 150' 180' ww) 10t	Y	Y	-
e	5	130	A	F	3h00	0.031	0.74	0.027	(0' 15' 30' 45' 60' 90' 120' 150' 180' ww) 9t	-	Y	-
	6	130	B	F	3h00	0.031	0.74	0.027	(0' 15' 30' 45' 60' 90' 120' 150' 180' ww) 9t	-	Y	-
	9	130	C	F	3h00	0.031	0.74	0.027	(0' 15' 30' 45' 60' 90' 120' 150' 180' ww) 9t	-	Y	-

Figure 3.13 – Performed tests in the experimental flume. T=test duration, Q=discharge, Y indicates that data set are available for the specific test. SV=single deposit, $DAlt$=alternating double half deposits, $DAli$=parallel double half deposits, DV=two deposits, $A2, B2, C2$ and $D2$=consecutive replenishment configurations. The list is not in chronological order

	Test	Submer	Conf	Bed	Duration	Q	L	Placed	Camera: Time series	Laser	Reple series	
						[m^3/s]	[m]	[m^3]	[min]		1st	2nd
e	10	130	D	F	3h00	0.031	0.74	0.027	(0' 15' 30' 45' 60' 90' 120' 150' 180' ww) 9t	-	Y	-
	31	130	E	F	3h00	0.031	0.74	0.027	(0' 5' 15' 30' 45' 60' 90' 120' 150' 180' ww) 10t	Y	Y	-
	32	130	F	F	3h00	0.031	0.74	0.027	(0' 5' 15' 30' 45' 60' 90' 120' 150' 180' ww) 10t	Y	Y	-
f	13	100	A	F	3h00	0.019	0.74	0.027	(0' 5' 15' 30' 45' 60' 90' 120' 150' 180' ww) 10t	Y	Y	-
	14	100	B	F	3h00	0.019	0.74	0.027	(0' 5' 15' 30' 45' 60' 90' 120' 150' 180' ww) 10t	Y	Y	-
	17	100	A_2	F	3h00-6h00	0.019	0.74	0.027	(0' 5' 15' 30' 45' 60' 90' 120' 150' 180' ww) 10t	Y	-	Y
	18	100	B_2	F	3h00-6h00	0.019	0.74	0.027	(0' 5' 15' 30' 45' 60' 90' 120' 150' 180' ww) 10t	Y	-	Y
	19	100	C	F	3h00	0.020	0.74	0.027	(0' 5' 15' 30' 45' 60' 90' 120' 150' 180' ww) 10t	Y	Y	-
	20	100	D	F	3h00	0.020	0.74	0.027	(0' 5' 15' 30' 45' 60' 90' 120' 150' 180' ww) 10t	Y	Y	-
	21	100	C_2	F	3h00-4h30	0.019	0.74	0.027	(0' 5' 15' 30' 45' 60' 90') 7t	Y	-	Y
	22	100	D_2	F	3h00-4h30	0.019	0.74	0.027	(0' 5' 15' 30' 45' 60' 90') 7t	Y	-	Y
	23	100	C	F	3h00	0.019	0.74	0.027	(0' 5' 15' 30' 45' 60' 90' 120' 150' 180' ww) 10t	Y	Y	-
	24	100	D	F	3h00	0.019	0.74	0.027	(0' 5' 15' 30' 45' 60' 90' 120' 150' 180' ww) 10t	Y	Y	-
	25	100	C_2	F	3h00-6h00	0.019	0.74	0.027	(0' 5' 15' 30' 45' 60' 90' 120' 150' 180' ww) 10t	Y	-	Y
	26	100	D_2	F	3h00-6h00	0.019	0.74	0.027	(0' 5' 15' 30' 45' 60' 90' 120' 150' 180' ww) 10t	Y	-	Y
g	33	100	B	F	3h00	0.019	0.50	0.018	(0' 5' 15' 30' 45' 60' 90' 120' 150' 180' ww) 10t	Y	Y	-
	34	100	C	F	3h00	0.019	0.50	0.018	(0' 5' 15' 30' 45' 60' 90' 120' 150' 180' ww) 10t	Y	Y	-
	35	100	B	F	3h00	0.020	1.00	0.036	(0' 5' 15' 30' 45' 60' 90' 120' 150' 180' ww) 10t	Y	Y	-
	36	100	C	F	3h00	0.020	1.00	0.036	(0' 5' 15' 30' 45' 60' 90' 120' 150' 180' ww) 10t	Y	Y	-
h	37	H	B	F	1h30	0.042	0.74	0.027	(0' 10' 20' 30' 45' 60' 90' ww) 7t	Y	Y	-
	38	H	C	F	1h30	0.042	0.74	0.027	(0' 10' 20' 30' 45' 60' 90' ww) 7t	Y	Y	-
	39	H_1	B	F	3h00	0.031	0.74	0.027	(0' 10' 20' 30' 45' 60' 90' 120' 150' 180' ww) 11t	Y	Y	-
	40	H_1	C	F	3h00	0.031	0.74	0.027	(0' 10' 20' 30' 45' 60' 90' 120' 150' 180' ww) 11t	Y	Y	-
	41	H_2	B	F	3h00	0.031	0.74	0.027	(0' 10' 20' 30' 45' 60' 90' 120' 150' 180' ww) 11t	Y	Y	-
	42	H_2	C	F	3h00	0.031	0.74	0.027	(0' 10' 20' 30' 45' 60' 90' 120' 150' 180' ww) 11t	Y	Y	-
	43	H_3	B	F	3h00	0.031	0.74	0.027	(0' 10' 20' 45' 60' 70' 90' 105' 120' 150' 180' ww) 12t	Y	Y	-
	44	H_3	C	F	3h00	0.031	0.74	0.027	(0' 10' 20' 45' 60' 70' 90' 105' 120' 150' 180' ww) 12t	Y	Y	-
	45	H_4	B	F	3h00	0.031	0.74	0.027	(0' 30' 60' 90' 105' 120' 135' 150' 165' 180' ww) 11t	Y	Y	-
	46	H_4	C	F	3h00	0.031	0.74	0.027	(0' 30' 60' 90' 105' 120' 135' 150' 165' 180' ww) 11t	Y	Y	-

Figure 3.14 – Performed tests in the experimental flume. T=test duration, Q=discharge, Y indicates that data set are available for the specific test. SV=single deposit, $DAlt$=alternating double half deposits, $DAli$=parallel double half deposits, DV=two deposits, $A2, B2, C2$ and $D2$=consecutive replenishment configurations. The list is not in chronological order

4 Influence of geometrical configuration of sediment deposits

This chapter is based on the scientific article "Sediment replenishment: Influence of the geometrical configuration on the morphological evolution of channel-bed" by E. Battisacco, M.J. Franca and A.J. Schleiss, accepted for publication in "Water Resources Research", DOI: 10.1002/2016WR019157

4.1 Introduction

The replenishment of sediment proofed to be an efficient measure to restore morphological diversity in disturbed river reaches downstream of dams (Ock et al., 2013). In Section 2.3 several examples of successful applications of the method on the field are cited. Previously performed field experiments always used one single volume of sediment replenishment. To explore different alternatives, the replenished volume was here divided in four deposits with the motivation to influence also the morphological evolution downstream. Six different geometrical configurations of sediment replenishment were tested for the first time in a laboratory experiment and are herein discussed. Furthermore, as mentioned by Kantoush and Sumi (2010), the choice of the released discharge is fundamental for a successful replenishment in terms of erosion and distribution of grains. Thus, the geometrical replenishment configurations were run with three submergence ratios of the deposit. The results of the sediment replenishment mitigation technique are described in terms of occupied surface of the flume bed and the temporal evolution of erosion and transport of introduced sediments.

4.2 Method

A complete overview on the experimental installation is given in Section 3.1.1. The total amount of sediment replenishment is divided in four deposits, having the same dimensions. The deposits are placed on both channel banks creating six different geometries (Figure 4.1). A complete list of tested cases is provided in Table 4.1. Two data set are available: photos and laser scanner. The acquisition procedure is detailed in Section 3.2.

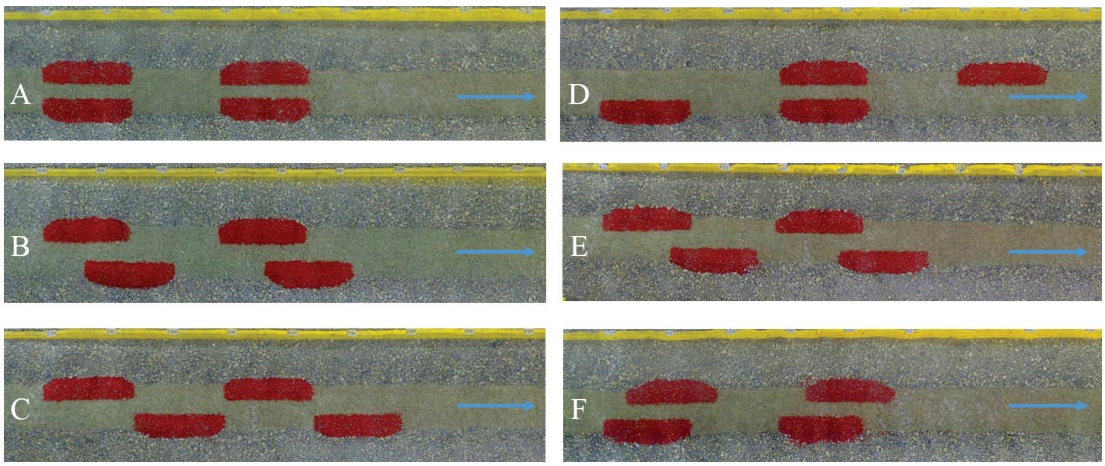

Figure 4.1 – Experimental channel with replenished sediment (red) for all tested configurations. Flow direction from left to right, indicated by the arrow

Table 4.1 – Analysed tests. Conf = configuration type, Subm = submergence ratio, Tot = total number of time step, Shift downstream = distance between deposits along the same bank

Test	Conf	Subm	Time steps		Data set	Shift downstream
			Tot	Time		
		%		min		m
11	C	70	10	0,5,15,30,45,60,90,120,150,180	Photo, Laser	0.75
12	D	70	10	0,5,15,30,45,60,90,120,150,180	Photo, Laser	1.50
1	A1	100	9	0,15,30,45,60,90,120,150,180	Photo	0.00
13	A2	100	10	0,5,15,30,45,60,90,120,150,180	Photo, Laser	0.00
4	B1	100	9	0,15,30,45,60,90,120,150,180	Photo	0.37
14	B2	100	10	0,5,15,30,45,60,90,120,150,180	Photo, Laser	0.37
7	C1	100	9	0,15,30,45,60,90,120,150,180	Photo	0.75
15	C2	100	10	0,5,15,30,45,60,90,120,150,180	Photo, Laser	0.75
19	C3	100	10	0,5,15,30,45,60,90,120,150,180	Photo, Laser	0.75
8	D1	100	9	0,15,30,45,60,90,120,150,180	Photo	1.50
16	D2	100	10	0,5,15,30,45,60,90,120,150,180	Photo, Laser	1.50
20	D3	100	10	0,5,15,30,45,60,90,120,150,180	Photo, Laser	1.50
27	E	100	10	0,5,15,30,45,60,90,120,150,180	Photo, Laser	0.19
28	F	100	10	0,5,15,30,45,60,90,120,150,180	Photo, Laser	0.56
5	A	130	9	0,15,30,45,60,90,120,150,180	Photo	0.00
6	B	130	9	0,15,30,45,60,90,120,150,180	Photo	0.37
9	C	130	9	0,15,30,45,60,90,120,150,180	Photo	0.75
10	D	130	9	0,15,30,45,60,90,120,150,180	Photo	1.50
31	E	130	10	0,15,30,45,60,90,120,150,180	Photo, Laser	0.19
32	F	130	10	0,15,30,45,60,90,120,150,180	Photo, Laser	0.56

4.2.1 Analysed parameter

The channel bed morphology development and the time influence are analysed by a series of parameters based on measured variables. A complete description of the parameters is available in Section 3.3. Those used for this analysis are listed below.

Persistence	PD	%
Covered surface	CS	%
Compactness of covered surface	NDC	%
Travel distance of center of mass of sediment	TD_{50}	m
Travel distance of the front of sediment	TD_{99}	m
Occupation rate	OCR	%
Power Spectrum Density of OCR-signal	PSD	db
Bed roughness		m

4.3 Results

4.3.1 Reproducibility of the tests and channel reach variables

To assess the reproducibility of the results, the tests for configurations from A to D were performed two or three times for 100% of submergence. The reproducibility of test is in a first step assessed visually and later by regarding the equilibrium values of CS and NDC after three hours, as well as PD (Table 4.2). The maximum difference in term of PD is recorded for configuration A, equal to 17.6%. The difference might be explained by the variation on the initial amount of placed sediments. For the other configurations the average difference drops to less than 10%. In terms of CS and NDC the differences among the different geometrical configurations are negligible.

To assess the reproducibility of final OCR-signal, the (zero-lag) correlation coefficients between the different experiments are calculated (Table 4.3). Among similar configurations the cross-correlation coefficient is high, which confirms the reproducibility of the experiments.

Table 4.2 – Main results in terms of persistence (PD), covered surface (CS) and compactness of covered surface (NDC) for all configurations, for the three submergence conditions and for the replicated tests. The subscript $zero$ indicates the values at the initial state and $3h$ stays for the value at the end of the test. Tests listed in terms of performed configurations. Configurations from A to D are repeated at least two times for 100% submergence. The two highest values for each parameter and each submergence are in bold.

Conf	Subm	Placed sediment	Washed sediment	PD	CS_0 initial	CS_{3h} 3h	NDC_0 initial	NDC_{3h} 3h
	%	Kg	Kg	%	%	%	%	%
C	70	27.3	0.0	100.0	8.8	10.0	0.92	0.88
D	70	28.5	0.0	100.0	9.4	10.5	0.92	0.86
A1	100	27.0	3.0	88.9	9.6	37.4	0.97	0.84
A2	100	30.0	8.6	71.3	10.1	**42.7**	0.97	0.83
B1	100	29.7	1.0	96.6	10.4	37.5	0.95	0.85
B2	100	27.0	0.1	**99.6**	9.4	35.7	0.97	**0.86**
C1	100	25.9	1.6	93.8	10.2	36.6	0.96	0.83
C2	100	26.2	1.0	96.2	10.0	34.4	0.95	0.84
C3	100	27.0	0.2	**99.3**	9.2	36.2	0.97	**0.86**
D1	100	27.9	7.0	74.9	10.1	31.6	0.96	0.79
D2	100	29.4	8.6	70.7	10.2	**38.7**	0.97	0.83
D3	100	27.0	4.4	83.7	9.7	28.8	0.97	0.83
E	100	24.4	4.1	83.0	8.3	35.3	0.95	0.83
F	100	24.6	8.2	66.6	9.6	34.0	0.94	0.77
A	130	27.0	16.3	39.8	9.9	**26.7**	0.97	0.79
B	130	27.0	11.7	56.8	9.9	18.8	0.97	**0.80**
C	130	27.0	10.9	**59.6**	10.3	24.5	0.97	**0.83**
D	130	27.0	11.4	**57.8**	9.7	21.1	0.97	**0.80**
E	130	21.4	11.0	48.7	8.2	13.2	0.87	0.71
F	130	22.9	15.1	34.3	9.6	**29.2**	0.94	0.75

Table 4.3 – Cross-correlation coefficients of the OCR-signals for all the experiments performed with 100% submergence ratio. The correlation coefficient for similar configuration are in bold

	A1	A2	B1	B2	C1	C2	C3	D1	D2	D3	E1	F1
A1	1.00	**0.79**	0.48	0.48	0.35	0.41	0.48	0.69	0.70	0.63	0.31	0.47
A2		1.00	0.22	0.25	0.09	0.16	0.30	0.59	0.67	0.62	0.03	0.50
B1			1.00	**0.91**	0.67	0.78	0.66	0.52	0.35	0.38	0.36	0.29
B2				1.00	0.62	0.76	0.79	0.56	0.32	0.39	0.34	0.32
C1					1.00	**1.0**	**0.86**	0.52	0.38	0.13	0.17	0.67
C2						1.00	**0.63**	0.42	0.15	0.24	0.62	0.22
C3							1.00	0.39	0.28	0.40	0.24	0.30
D1								1.00	**1.00**	0.59	0.49	0.30
D2									1.00	**0.88**	0.04	0.64
D3										1.00	0.10	0.76
E1											1.00	0.15

4.3.2 Adequate replenishment submergence

Kantoush et al. (2010a) and Kondolf and Matthews (1991) mentioned the relevance of the flow discharge, seen as an artificial flood, in the mobilization and further deposition of the sediment replenishment. Therefore, three submergence conditions of the replenishment volume are tested for two configurations (configurations C and D, Figure 4.1) in order to assess the most efficient discharge and to confirm former preliminary results. Previous tests showed low erosion for a non-submergence condition (Bösch et al., 2016).

The efficiency of the submergence is evaluated taking into account the CS, the PD, the travel distance of the sediment front and by visual observations. Table 4.2 contains the results in terms of persistence PD, covered surface CS and compactness NDC for all the tested configurations.

The CS and the travel distance for configuration C and D are almost constant in time for 70% submergence. After a slight increment of CS in the first 15 minutes of the test, the erosion process stops and no further changes are observed for both tested configurations (Figure 4.2 and Figure 4.3). In detail, the CS for 70% submergence is always below 20% which together with the visual observations confirm a low capacity of the flow to erode the replenishment volumes. Thus, not enough sediment is available to be transported downstream. The difference between the results with 70% submergence and the two higher submergence conditions in terms of CS and travel distance, is evident as shown in Figures 4.2 and 4.3.

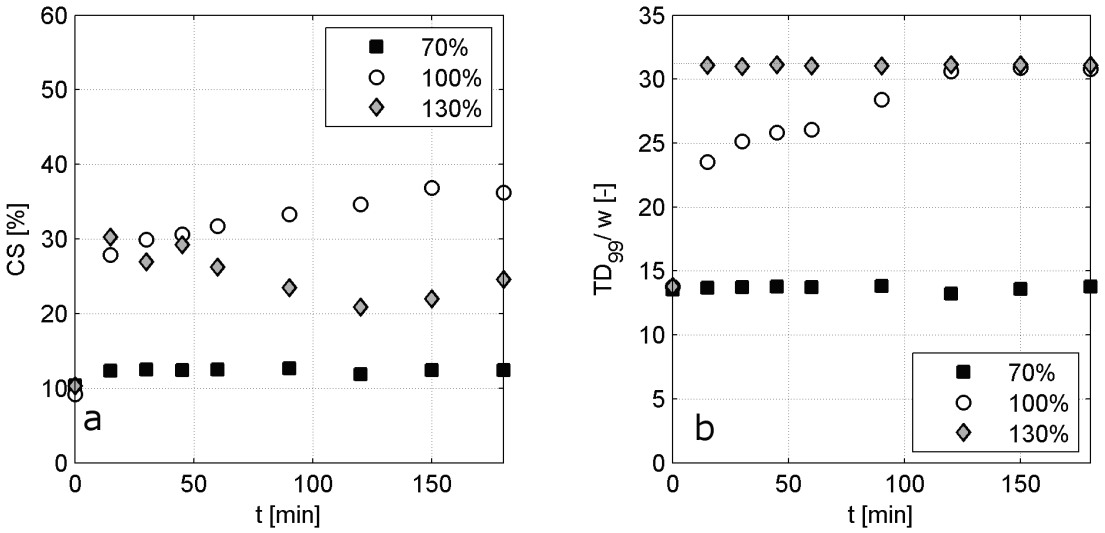

Figure 4.2 – (a) Covered surface CS and (b) travel distance of the front TD_{99} normalized by the channel width for configuration C as a function of time for different submergence ratio

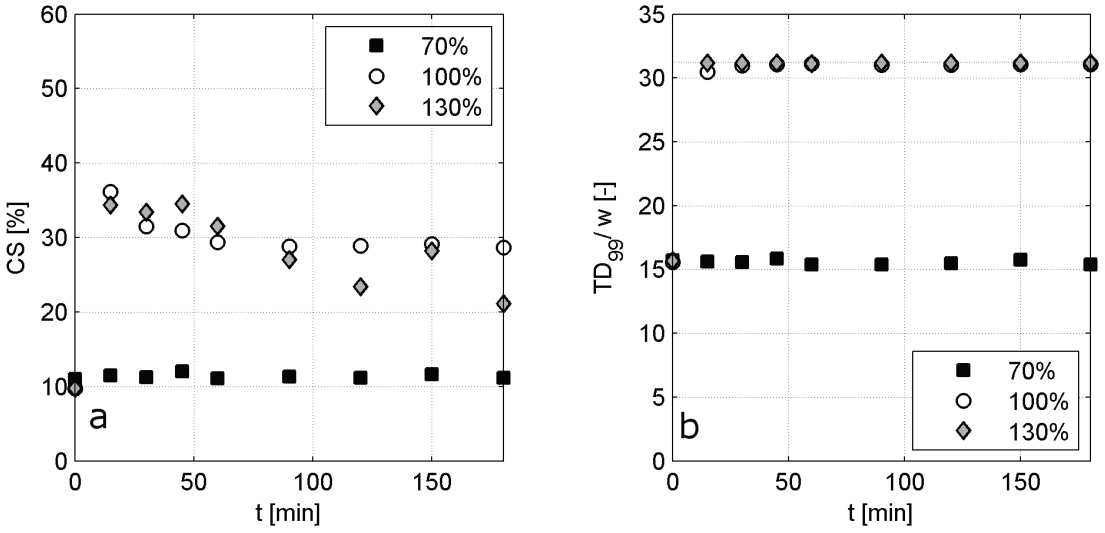

Figure 4.3 – (a) Covered surface CS and (b) travel distance of the front TD_{99} normalized by the channel width for configuration D as a function of time for different submergence ratio

For submergence of 100% and 130%, the CS and the travel distance of the front continuously vary in time and their values range from 20% to 40% of the bed surface for both configurations. For configuration C and a submergence ratio of 100%, the CS increases constantly in time attaining an equilibrium value of about 36% after two hours of testing. This stabilization of CS value for 100% of submergence occurs roughly when the sediments reach the channel downstream section (Figures 4.2b and 4.3b.) With a submergence of 130%, for the same

configuration C, the spread of the sediment along the channel increases rapidly in the first hour, with a maximum in the first 15 minutes, before reducing to an almost constant value of about 25%. The sediments rapidly reach the end of the channel for these tests (Figures 4.2*b* and 4.3*b*).

When looking at the travel distance of the replenishment front for the submergence ratio of 130%, the first grains reach the end of the channel (x/w = 31.25, channel end) in less than half an hour as shown in Figures 4.2 and 4.3. This process continues constantly until the end of the test, which corresponds to a progressive reduction of replenishment material remaining in the flume. The highest submergence condition of 130% does not allow for the creation of stable morphological bed forms downstream, since most of placed material is washed out and the remaining quantity is not enough to re-establish these bed forms. The PD is also a good indicator of the behaviour of the replenishment sediment in the observed channel reach since it indicates the final portion of replenishment material affecting the channel bed. For 70% and 100% submergences, almost all the total initial amount of supplied replenishment sediment remains in the channel bed, while for the 130% submergence just a small portion is still present at the end of the tests.

For 100% submergence, the CS increases continuously during the test confirming that the placed material is eroded and transported along the channel, where it settles and remains. After two hours of testing, a morphological equilibrium is reached on the channel bed and it is visually observed that the grain clusters stop developing. Only after two hours of testing do the first grains of replenishment reach the end of the channel, strengthening the observation that the erosional processes are not too fast, and that these flow conditions enhance the recreation of bed forms. Consequently, the submergence of 100% is chosen as the most adequate submergence condition to be analysed.

4.3.3 Time analysis of sediment replenishment development along the channel

Considering the channel response, the geometrical configurations can be categorized in two groups. Configurations B, C and E, having volumes shifted downstream more than 1/4 of the replenishment length (Figure 4.1), produced similar results among each other in terms of PD, providing values fluctuating between 83% and 99%. Thus, for these cases, almost all the placed material remained in the study reach. Configurations A and F have lower persistence in the channel since the almost parallel placement of volumes induces a strong narrowing of the cross section and the resulting flow concentration increases the flow velocity, and consequently, the transport capacity. As a result, a larger portion of material is transported out of the channel. Finally, configuration D behaves in an intermediate fashion between configurations A and C in terms of flow behaviour and persistence of the placed sediments.

The time evolution of CS is similar for all configurations, with final values after stabilization ranging typically between 30% and 45% (Figure 4.4). Configuration A has the highest value of CS and configuration D the lowest. The time evolution of the NDC parameter is similar for all

configurations ranging from 1, at the beginning of the test, to value as low as 0.77 (Figure 4.5).

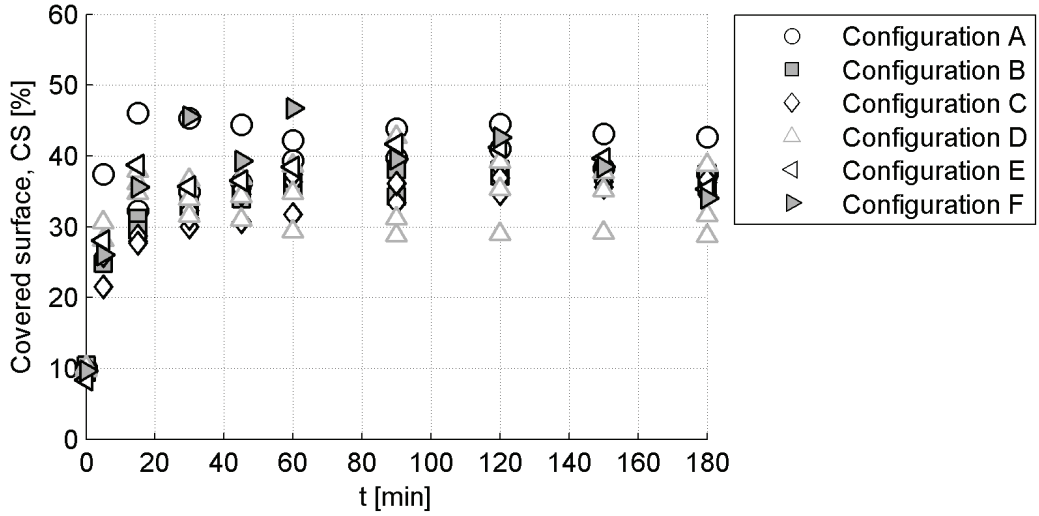

Figure 4.4 – Temporal evolution of the covered surface, CS, for all configurations, for 100% of submergence

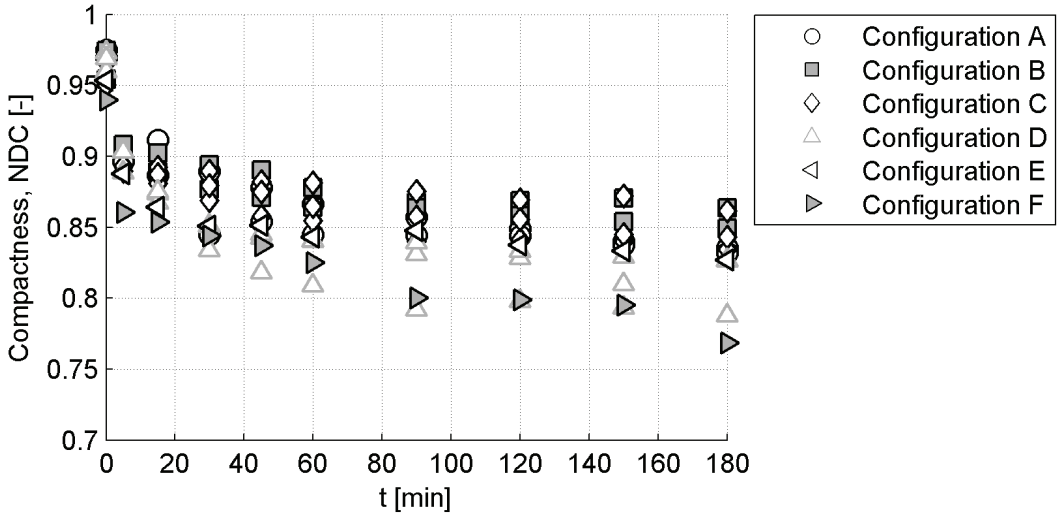

Figure 4.5 – Temporal evolution of the compactness, NDC, for all configurations, for 100% of submergence

For both variables, CS and NDC, the main evolution (increasing for CS and decreasing for NDC) is observed in the first 30 minutes of the test, stabilizing after roughly one hour. Cross-analysing PD, CS and NDC of the replenishment material within the channel reach reveals that the eroded material is spread bi-dimensionally for configuration A and F and no three dimensional bed forms (gravel bars) are created. For configuration D, the smaller increase of

CS compared to the other configurations indicates that the replenishment volumes are not totally eroded which was confirmed by visual observation. The longitudinal distribution of the sediment occupation of the channel for all tested configurations at the end of the tests is shown in Figure 4.6. In Table 4.3, the values of the normalized correlation coefficient between the longitudinal distribution of *OCR* are given.

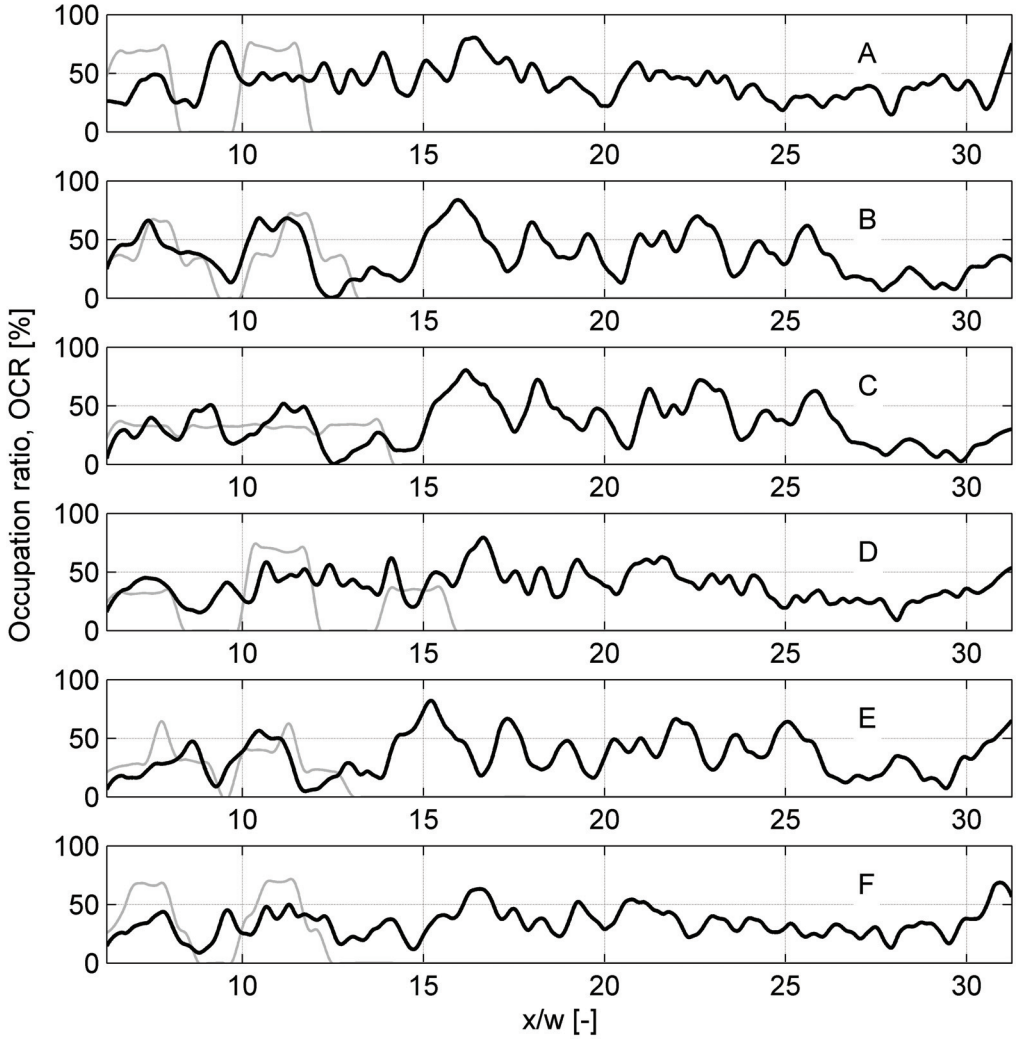

Figure 4.6 – Occupation ratio distribution (*OCR*) for all configurations: gray line for initial state , black line after 3 hours, for submergence ratio of 100%. From the top, configurations: A, B, C, D, E, F

By analysing Table 4.3, some pairs of configurations have a high cross-correlation, with values reaching 0.76. Thus, similar morphological response can be associated with different configurations. Low cross-correlation values stand for different bed channel response to replenishment in terms of *OCR*. Configuration B, C and E can be associated to an alternating

configuration of replenishment volumes. Configurations A, D and E are clearly distinguishable as parallel geometries. The similar behaviour of certain configurations is visible also in terms of OCR. In Figure 4.6, more pronounced peaks of OCR are evident for the alternating configurations. Parallel geometries of initial sediment replenishment volumes result in a more uniform distribution of replenishment gravel in the channel bed. Thus the OCR does not present peaks of distribution on the channel bed.

4.3.4 Sediment patterns at equilibrium

The initial and final bed topography was recorded by a laser scanner which highlights the creation of the morphological bed forms and the erosion of the replenishment volumes (Figure 4.7). The replenishment volumes which are more downstream situated are completely eroded at the end of the experiment for all configurations. On the other hand, the most upstream volume is not always completely eroded by the flow. The bed forms created by the eroded grains have maximum heights of 30 mm for configuration B, which is almost five times the $d_{50,r}$ of the replenishment material. Furthermore, the volumes downstream may impose two effects: trap the upstream eroded sediments in between them and, by imposing a backwater effect, reduce the transport capacity of the flow. These effects limit the longitudinal transport of sediments.

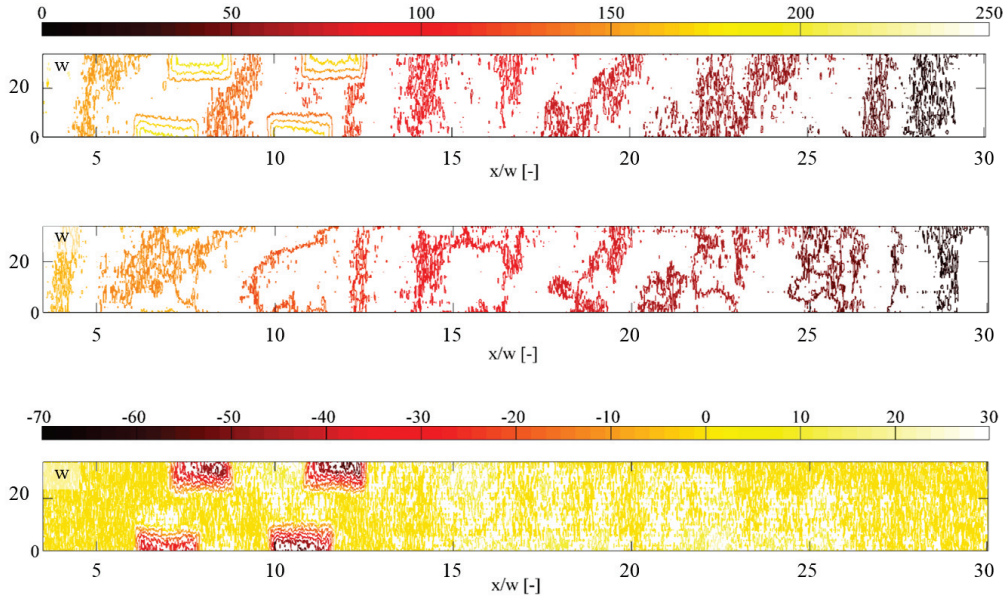

Figure 4.7 – Bed topography of the A_{oi} obtained for (top) initial state, (middle) final state and elevation differences in mm (bottom), for configuration B and a submergence ratio of 100%. Colour bar in mm. Channel width, w, equals to 0.4 m

The Power Spectrum density, PSD, of the channel depositions is analysed together with the PSD of the OCR-signal based on 2D images. The PSD results in a wavelength for grain deposition on channel bed. To avoid the influence of the initial placement of the replenishment volumes, the portion of channel occupied by them is not considered. In Figure 4.8, the PSD of the OCR-signal for the configurations B, C and E have a pronounced peak at a distance of about 1.5 and 1.6 times the channel width (w), respectively. Such pronounced morphological pattern is not visible for the remaining configurations. The same result is evident within the OCR distribution (Figure 4.6).

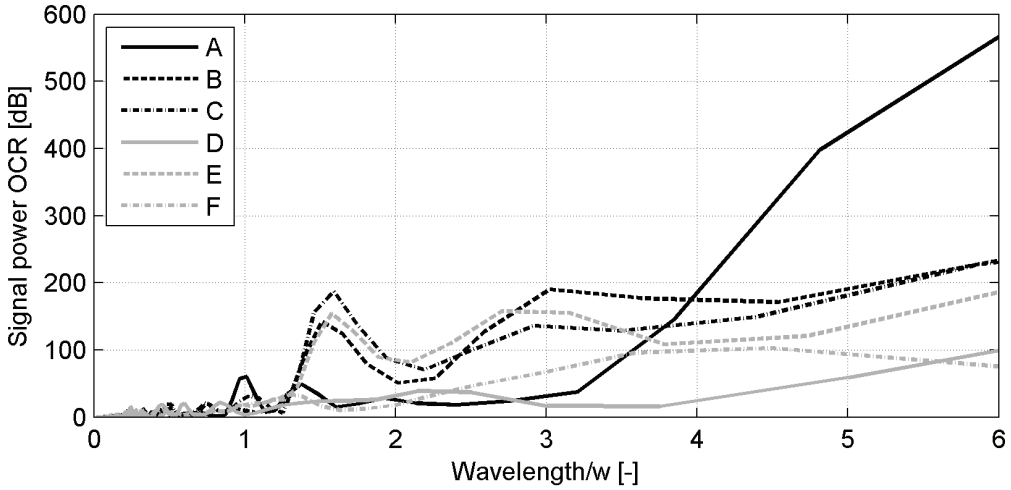

Figure 4.8 – Signal power of bed elevation changes, PSD, along the downstream reach for all configurations, by means of 2D images

For configurations A, D and F, the material is spread throughout channel width without creating clusters. The second peak observed for geometry B and C at a distance of 2.8 times the channel width seems to be a harmonic of the first one. Another artefact is related to the continuous increase of the signal power which can be explained by the channel length being too short in order to observe periodicity.

Figure 4.9 shows the PSD of the mean deposition changes of the OCR-signal for the laser scanner data set. The highest deposits occur in areas where OCR reaches bigger values with a morphological bed pattern of 1.7 times the channel width. In agreement with Figure 4.8, the wavelength of morphological bed forms is more evident for alternating configurations (B, C and E), while the parallel geometries do not highlight periodicity.

4.4 Discussion

The effect of different submergence ratio on the replenishment of sediment erosion and transport was evaluated. Six geometrical configurations were tested.

A ratio of 100% submergence regime produces the most adequate spread of the material along

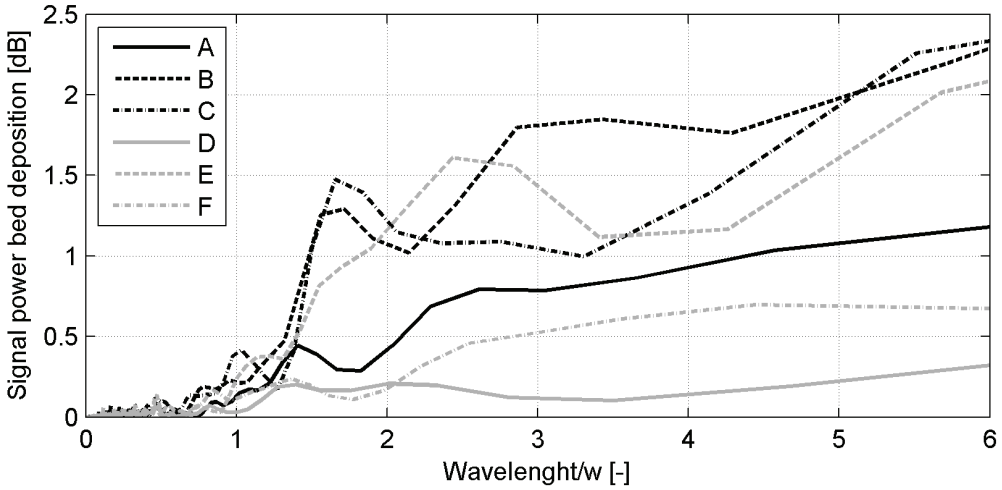

Figure 4.9 – Signal power of mean bed deposition changes, PSD, along the downstream reach for all configurations, by means of laser data

the channel bed and within the study reach, with high persistence of the placed material locally, and a complete erosion of the replenishment volumes. Visual observations confirm the erosional process described by Kantoush et al. (2010b), assuming to be valid for all tested configurations.

The covered surface (CS) and the compactness (NDC) have a logarithmic-type behaviour, composed by a rapid initial increase lasting less than one hour, attending an equilibrium state within two hours of testing. Thus, the test duration was sufficient to completely study the process of erosion and transport of sediment replenishment. The behaviour is the same for all the geometrical configurations. Nevertheless, some differences are remarkable in terms of covered surface CS, compactness NDC and persistence PD. Configurations A and D have high initial flow velocity inducing fast erosion of volumes. Thus, a wider spread of material is achieved during the first hour with consequent covered surface values, CS, close to 50%. However, the covered surface values for the remaining configurations do not reach 40%. The higher values are due to the initial parallel geometry.

Considering both the covered surface CS and the cluster compactness NDC, for parallel configurations high values of CS are linked with low NDC. Indeed, alternating geometries have high values for both above-mentioned variables.

The channel responds differently to parallel and alternating configurations. Parallel configurations create a narrowed cross section resulting in higher flow velocity and transport capacity. The replenishment volumes are thus easily eroded by the flow. Additionally, the material is mainly spread over the whole channel width as confirmed by the lower NDC results. For alternating configurations, the upper volumes behave like a fixed obstacle, deviating the flow toward the opposite bank, facilitating erosion. Consequently, the downstream replenishment

volumes are firstly eroded. Alternating geometries are more efficient in terms of CS and present higher NDC values. These configurations facilitate the creation of bed clusters as gravel bars.

The OCR analysis reveals a grain pattern distribution along the downstream reach, with peaks of depositions occurring in a repeating distance. By PSD analysis of the OCR-signal a wavelength equal to around 1.7 times the channel width is observed for certain geometrical configurations. The wavelength of such depositions is close to the replenishment length. Consequently, it can be assumed that the replenishment dimension plays a key role in determining the downstream bed morphology. In agreement with Venditti et al. (2012), it is demonstrated how the replenishment of sediment can help restore the bed morphology in sediment depleted reaches. Thus, the presence of a periodicity for certain geometrical configurations, highlighted by the PSD of the OCR-signal, helps in the choice of a geometrical configuration for field application in relation to the expected results. By using an alternating geometry, a more diversified morphological pattern may be imposed close to the injection point of the material for a downstream length of about 10 times the channel width. On the other hand, parallel configurations produce a wider spread of replenished grains on a longer impact area downstream.

The deposits created downstream by the eroded grains have a maximum height of about five times the median grain size diameter of the replenishment material. Thus, the bed elevation changes produced by the replenishment are not pronounced. This might be explained by these reasons. Firstly, the width of channel is not allowed to vary thus avoiding flow velocity changes and the deposition and erosion of bank material at different locations as mentioned by Nelson et al. (2015). Secondly, considering the results in Babaeyan-Koopaei (2012), the laboratory setup is close to the limit between plane bed and alternate bar regime such that the deposition of eroded material in alternate patterns is not strongly facilitated. Thirdly, the fixed armored bed does not allow the small grains to penetrate into the armored bed layer. In Venditti et al. (2012) it is demonstrated that the fine sediments of replenishment, percolating into the armoured bed layer, increase the mobilization of bed material. The same behaviour was observed during the preliminary tests performed with an armored bed but not fixed in mortar. This setup was later abandoned since it was not possible to precisely quantify the amount of replenished material percolated and to monitor the material movement. The influence of the geometrical configuration of replenishment volumes is still poorly investigated. Thus, the use of a fixed bed allows for an easier identification of the movement of the replenishment material throughout the channel, which was the main goal of the study. Furthermore, the imposed water depth and related bed shear stress were not high enough to produce the complete destruction of the armour layer. In those conditions, the use of a fixed bed is a good approximation of the river reach state downstream of dams where frequent morphological floods are missing. The bed forms obtained in the present research could be seen as mounds forming the initial condition for alternating bars development as remarked by Venditti et al. (2012).

4.5 Conclusions

By using systematic laboratory experiments the relation between the released discharge, the amount of gravels and the geometrical configuration for a successful replenishment of sediment downstream of dams could be obtained. These variables are assessed by testing six geometrical configurations on a flume facility reproducing a typical alpine gravel-bed stream. The sediment replenishment performed in the flume facility reproduces the high-flow stock pile method. The erosion process of sediment replenishment includes two phases: first, toe erosion, second, mass failure and downstream transport of the sediments. Thus using a replenishment slope close to the internal friction angle of the material may facilitate the process.

The experiments showed that a complete submergence of the replenishment volumes by supplied discharge (i.e. artificial flood) is suitable for providing sediments on a considerable length downstream. The persistence of the added material is observed in a channel reach of roughly ten times the replenishment length. Parallel geometrical configurations of the sediment replenishment produce a larger spread of the eroded material on the entire channel bed. However, these geometries do not enhance the formation of clear defined bed-forms along the channel bed. Alternating geometrical replenishment configurations promote bed morphological cyclic patterns having a scaling wavelength corresponding to the replenishment length. The parallel configurations should be preferred for re-establishing a longer impact distance of the replenishment.

Since the replenishment of sediment method can serve different purposes, it may be suggested to choose parallel configurations for a bed fining, while alternating geometries are more favourable for increasing the complexity of bed morphology. This helps in recreating a natural sediment transport along the disturbed reach downstream a dam. Applying multiple sediment replenishment volumes with an alternating geometries is successful in creating downstream bed morphology patterns. The obtained bed forms can be used as spawning grounds by fish, thus re-establishing former ecological habitats. Furthermore, the results show for the first time that adding multiple replenishment volumes at the same time facilitates the volume erosion and increases the delay before the following replenishment campaign.

5 Influence of sediment deposit length

5.1 Introduction

By replenishment of sediment it is possible to re-establish morphological bed forms, fining the bed and recreate gravel bars (Sklar et al., 2009). Furthermore, experiment works demonstrated the reversibility of bar formation by supplying again enough sediment on the reach (Venditti et al., 2012). Ock et al. (2013) stated a lack of knowledge for defining guidelines for river restoration by replenishment based on previous experiences. A insufficient knowledge on these factor might derive to replenishment failure or even to undesirable ecological effects (Kantoush et al., 2010b). This chapter investigates the response of the channel bed to different replenishment length. Three different lengths were tested with a submergence ratio of 100% on two geometrical configurations. The results show that the discharge, together with the geometrical placement of volumes, have a dominant influence on the erosion process. The pattern of the obtained morphological forms, created on the channel bed and related to the replenishment length, is presented and discussed.

This chapter is part of the proceeding of the ISRS 2016 Conference, in Stuttgart (Germany). The submitted paper is titled "Laboratory experiments on the influence of the length of a sediment replenishment applied with alternated geometrical configuration", by E. Battisacco, M.J. Franca and A.J. Schleiss.

5.2 Method

5.2.1 Experimental setup

The experiments were performed in the flume which is detailed in Section 3.1.1. Preliminary tests have demonstrated that alternating configurations provide a more robust bed morphological pattern on channel bed. Thus, those configuration, B and C, are herein considered for the evaluation. Three replenishment lengths are tested (Figure 5.1).

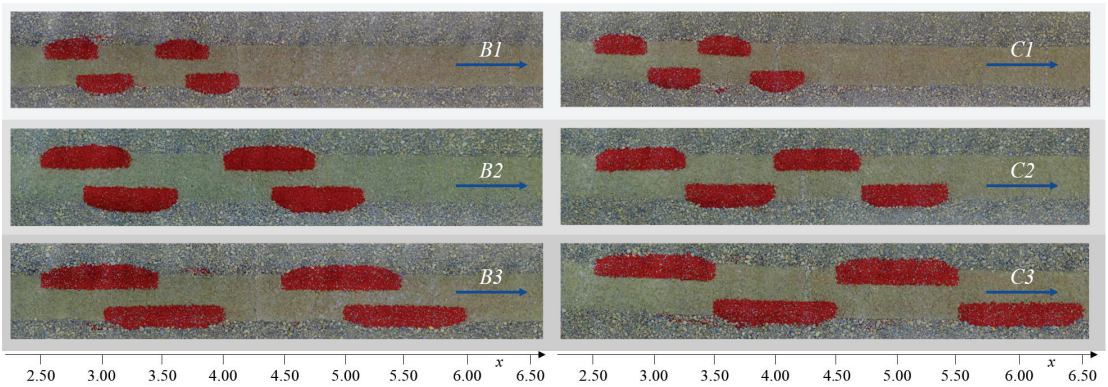

Figure 5.1 – Experimental channel with replenished sediment (dark) for configuration B (left column) and C (right column). Replenishment sediment with different length: 0.5, 0.75 and 1.0 m (rows from top). On the bottom, distances along the flow direction in meter

In configuration B the volumes are shifted downstream by half a deposition length, while for configuration C they are shifted by one deposit length. The non-dimension replenishment lengths, defined as the ratio between deposit length (L) and channel width (w=0.4 m), result in respectively 1.25, 1.87 and 2.5. The replenishment material is placed in four deposits on the channel bed following the in-channel stockpile method (Ock et al., 2013). Due to the different deposit length, the total amounts are respectively: 0.018, 0.027 and 0.036 m^3. The efficiency of the replenishment is discussed in terms of persistence of placed material, compactness of channel bed forms and more or less pronounced capacity to restore bed form periodicity. Former results demonstrated the core role played by the submergence conditions of the replenishment volume (Bösch et al., 2016). A submergence of 100% is the most adequate for obtaining a complete volume erosion, a high persistence of placed material and a large area of impact on the channel bed. This submergence condition assures a bed shear stress large enough to erode the replenished sediment and small enough to let the channel bed and banks immobile. The discharge on the experimental facility is equal to 0.019 m^3/s corresponding to a flow depth of 0.07 m. The discharge is kept constant over the entire experiment duration.

5.2.2 Experimental procedure

To evaluate the impact of the sediment replenishment in the downstream channel bed morphology nine series of pictures are taken during the tests by a GoPro Hero 3+ Camera. Channel bed topography is measured with the laser scanner for initial and final condition of each replenishment experiment. A pumping system controls the flow which is fixed for a submergence ratio of 100%. More detail information on the experimental procedure and on the measurement installation are provided in Section 3.2.

5.2.3 Data analysis

The analysis is computed on the area of interest (A_oi), defined as the channel bed surface ($L * w = 4\ m^2$). The temporal evolution of the morphological changes on the area of interest A_oi is evaluated by means of several parameters on the binary images. A complete description of the parameters is available in Section 3.3. Those used for this analysis are listed below. Each parameter is calculated for each phase of test. The experiments analysed in this chapter are listed in Table 5.1.

Persistence	PD	%
Covered surface	CS	%
Compactness of covered surface	NDC	%
Occupation rate	OCR	%
Power Spectrum Density of OCR-signal	PSD	db
Difference in channel elevation	Δz_b	mm

Table 5.1 – Analysed tests. Tot = total number of recorded time steps, Length = replenishment longitudinal dimension

Test	Conf	Subm %	Tot	Time steps min	Data set	Length m
33	B1	100	10	0,5,15,30,45,60,90,120,150,180	Photo, Laser	0.50
19	B2	100	10	0,5,15,30,45,60,90,120,150,180	Photo, Laser	0.75
35	B3	100	10	0,5,15,30,45,60,90,120,150,180	Photo, Laser	1.00
34	C1	100	10	0,5,15,30,45,60,90,120,150,180	Photo, Laser	0.50
20	C2	100	10	0,5,15,30,45,60,90,120,150,180	Photo, Laser	0.75
36	C3	100	10	0,5,15,30,45,60,90,120,150,180	Photo, Laser	1.00

5.3 Results

Former experiments have demonstrated the efficiency of these replenishment configurations in terms of eroded material, persistence on the channel bed and restoration of bed forms (see Chapter 4). The present study aims at evaluating the influence of the replenishment length on the above-mentioned parameters. A clear alignment is remarkable on the CS behaviour in terms of L/w ratio (L= replenishment length, w= channel width). The temporal evolution of the covered surface follows a logarithmic function, approaching an equilibrium state after two hours for all the performed experiments (Figure 5.2). Thus the *CS* values are constantly increasing in time with consequently spreading of replenishment grain. Nevertheless, this value does not overcome the 30% of the channel width for the lower L/w whereas higher values are reached for the other configurations. For both configurations, the maximum CS value corresponds to 0.37 for a L/w ratio equal to 1.87 (Figure 5.2). A difference is remarkable for the same L/w between configuration B and C. Higher CS values are obtained with the longer replenishment during the first hour, for then approaching an equilibrium state. Different is the case for the NDC. The compactness of the bed forms reaches its maximum for L/w equal to 1.87 (Figure5.3).

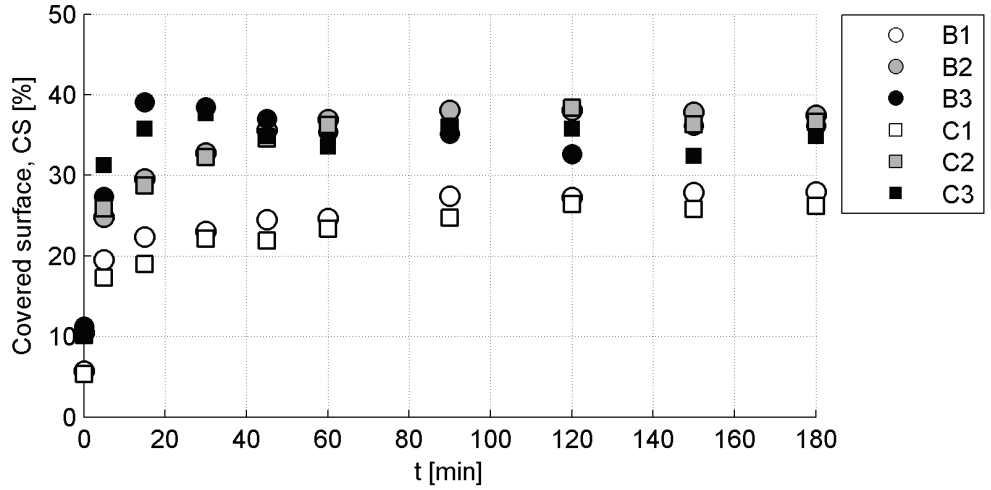

Figure 5.2 – Temporal evolution of covered surface CS for all the experiments

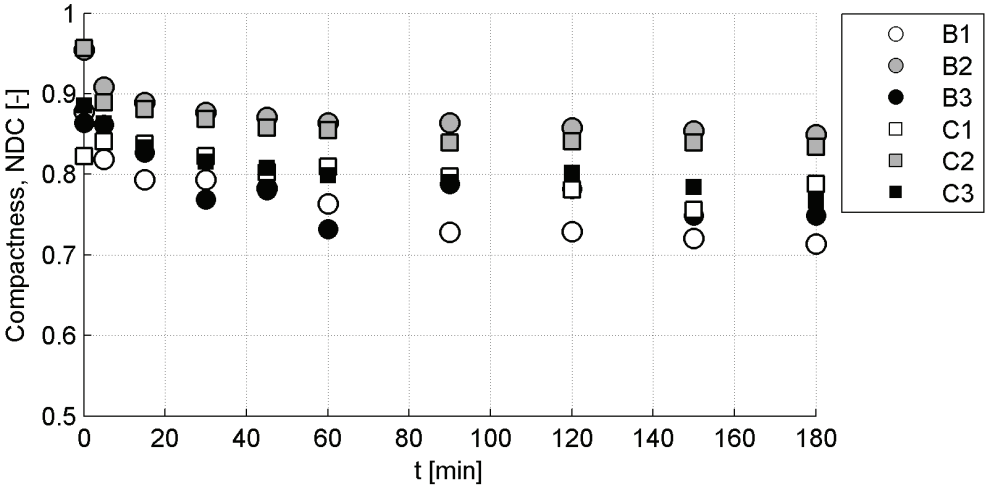

Figure 5.3 – Temporal evolution of compactness NDC for all the experiments

The other configurations, presenting lower values of NDC, indicate that the replenished material is spread on the entire channel bed without creating clusters. The persistence after the replenishment is generally high (Table 5.2). No remarkable differences are visible between the geometrical configurations. For the lower tested L/w ratios, the persistence is 100% for both geometrical cases. The PD decreases to 69% and 73% respectively for configuration B and C for a replenishment length of 1 m. In agreement with what shown by the CS temporal evolution, the fast initial erosion corresponds to a high rate of washed out material, thus the lower persistence (Table 5.2).

Table 5.2 – Covered surface CS: initial, final and relative increase; persistence PD for tested configurations and compactness NDC: initial, final and relative decrease. N = total number of time steps. *(final-initial)/initial

Configuration	CS		Relative	PD	NDC		Relative
	initial	final	increase*		initial	final	increase*
	-	-	%	%	-	-	%
B1	5.69	27.97	392	94	0.88	0.71	-19
B2	10.44	37.48	259	96	0.95	0.85	-11
B3	11.22	36.14	222	69	0.86	0.75	-13
C1	5.34	26.19	390	100	0.82	0.79	-4
C2	10.18	36.61	260	100	0.96	0.83	-13
C3	10.18	34.88	243	73	0.89	0.77	-13

The spread of material on channel bed leads to a bed fining. The initial standard deviation of the bed elevation reduces from around the average diameter of the bed, $d_{50,b}$ (11.5 mm), at the test beginning to the average diameter of the replenished material, $d_{50,r}$ (5.5 mm), after three hours. The fining effect is more prominent for configuration B, where the maximum value reach the 50% of the initial state (Table 5.3).

Table 5.3 – Standard deviation (STDV) of bed elevation along the channel reach downstream of the replenishments for initial and final condition. *(final-initial)/initial

Configuration	STDV		Relative increase*
	initial	final	increase*
	mm	mm	%
B1	8.71	5.25	40
B2	12.59	6.89	45
B3	10.81	5.31	50
C1	9.98	6.42	35
C2	12.22	7.01	43
C3	12.01	6.79	43

The occupational ratio, OCR, is an index of the grain distribution along the downstream reach of the channel. In Figure 5.4, the OCR and the deposition heights are shown for both configurations. The distances along the channel length, x, were normalised using the channel width, w. Furthermore, the initial replenishment positions were excluded from the data analysis. Clusters of high and low CS section are established. For configuration B the peak

cluster is placed at x/w=16, thus around 0.4 m far the most downstream volume.

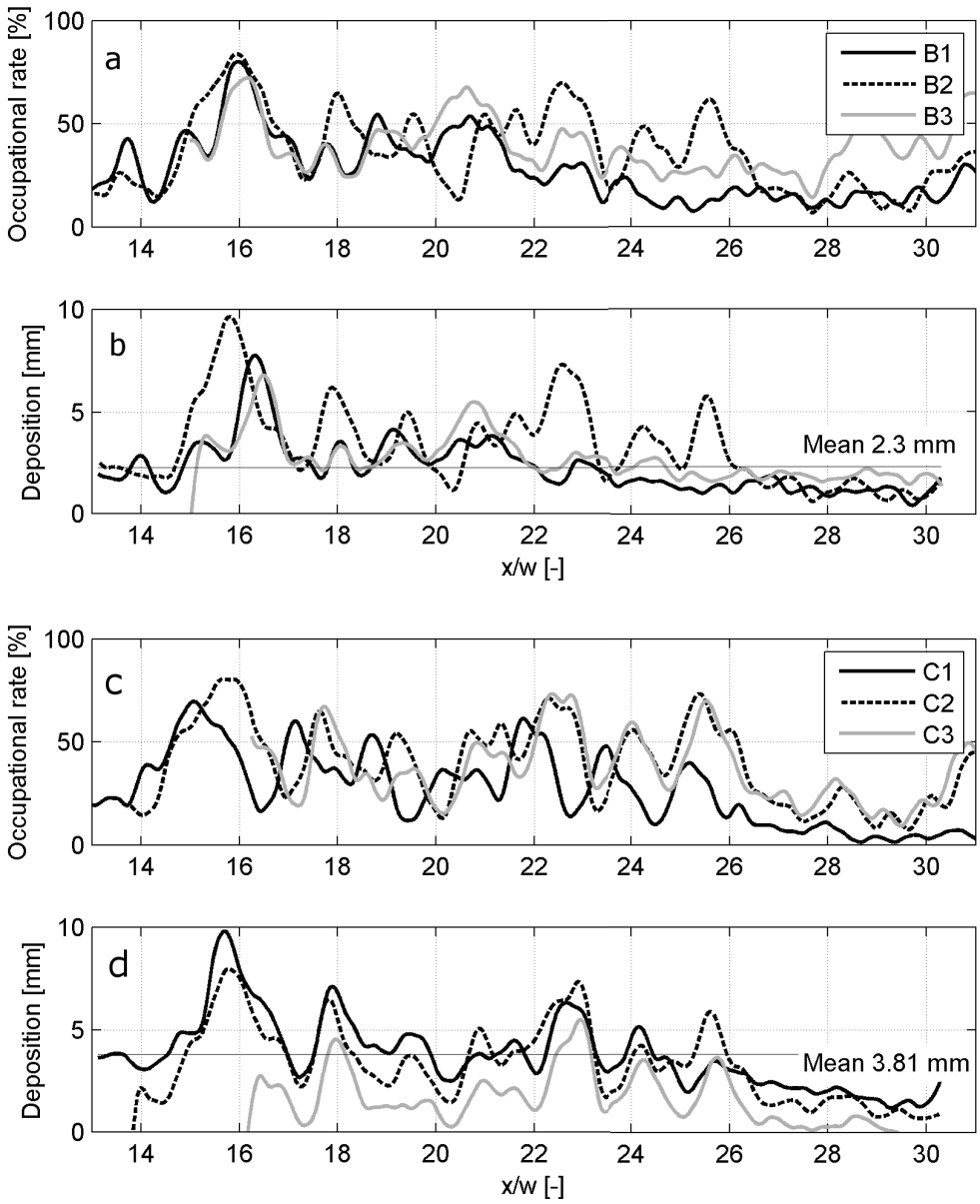

Figure 5.4 – (a,c) Occupational ratio distribution, OCR, and (b,d) deposition height averaged in cross sectional direction along the downstream reach after 3 hours, for configurations B and C

The pattern created by the replenishment is regular and the same distribution of peaks for the OCR and deposition are obtained in both cases. However, configuration C shows better accordance for all the replenishment lengths. The OCR decreases along the flow direction since the material is not enough for equally cover all the A_{oi}. However, for both configuration cases, a slight OCR increase is present close to the channel end. In agreement with the CS,

it is not surprising that the OCR and the deposition height distribution for the longer L/w replenishment are not pronounced. Indeed, the reduce amount of placed material reduces the final deposition height. The PSD of the OCR signal revels a clear peak for both configuration B and C. Generally, these alternated configurations lead to a periodicity of bed forms occurring with a periodicity of 1.6 channel width (Figures 5.5 and 5.6). The periodicity is more relevant for configuration C than B. Where the L/w equal to 1.87 shows a periodicity for configuration B in line with the results for configuration C. Shorter and longer replenishment volume of configuration B does not show periodicity as clear as for 1.87 L/w ratio. The bed pattern becomes more consistent when compared with the OCR distribution. Peaks of distributions can be visually located on channel bed (Figure 5.7). Like for the analysis of the PSD, the photo analysis show a difference from the configuration B to C comparing the L/w equal to 2.5. The clear bed pattern of configuration C is not present in B for the same replenishment length. Recalling the PD values, configuration B has suffered from a higher material wash out (69%, 73% respectively for configuration B and C) that may explain the lack in bed forms in the downstream part of the channel. Furthermore, the influence of the initial geometry appears in Figure 5.7. Configuration B, with volumes shifted half the replenishment length downstream, induces a stronger section narrowing with consequent flow acceleration. The upstream replenishment directs the flow to the opposite bank working initially like a fix obstacle. Thus, at the last time step a considerable portion of the volume has not been eroded.

Different flow behaviour occurs for configuration C, whereas for the same discharge and replenishment length, the flow is not diverged by the upstream volume and the erosion process appears more uniform.

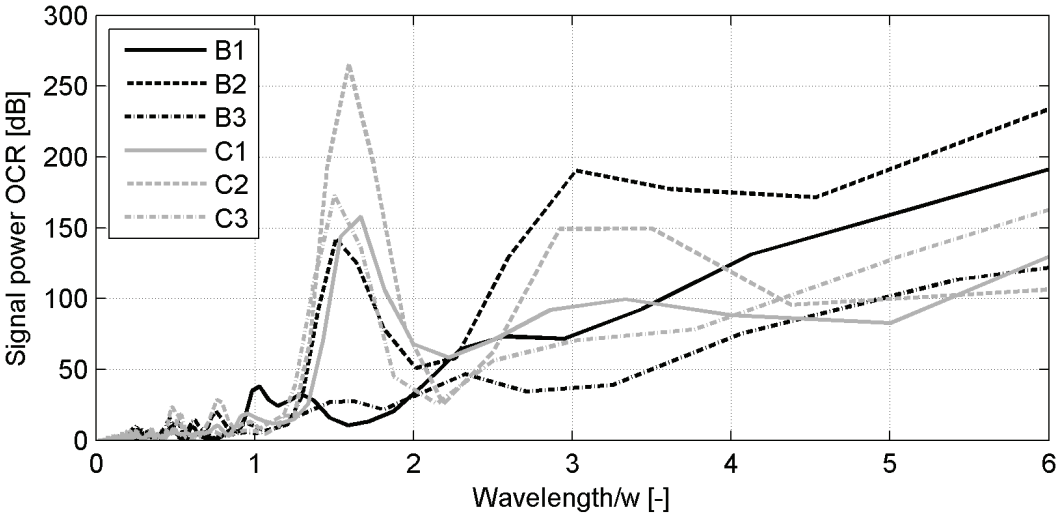

Figure 5.5 – Power Spectral Density (PSD) of the OCR-signal (laser data) for all the experiments, in the downstream reach

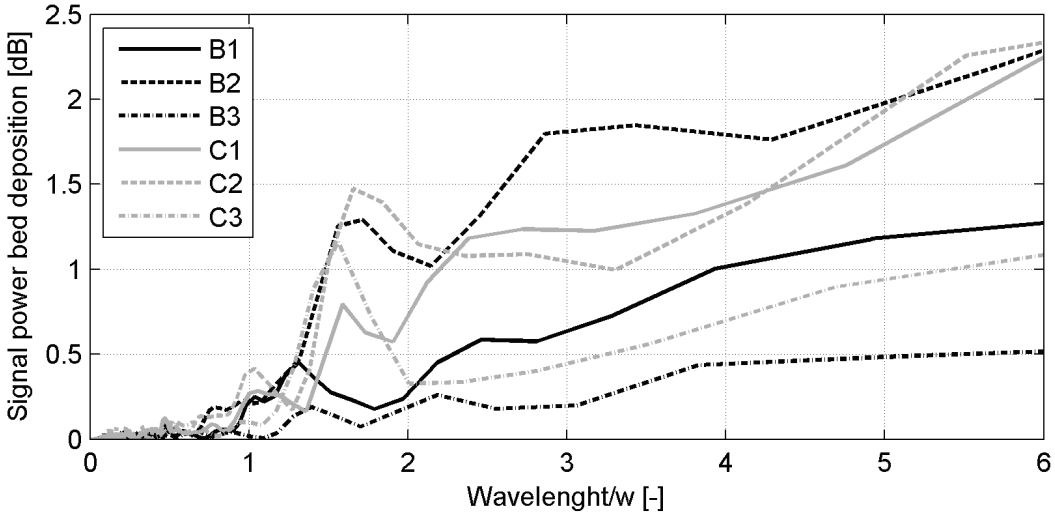

Figure 5.6 – Power Spectral Density (PSD) of the deposition heights (image data) for all the experiments, in the downstream reach

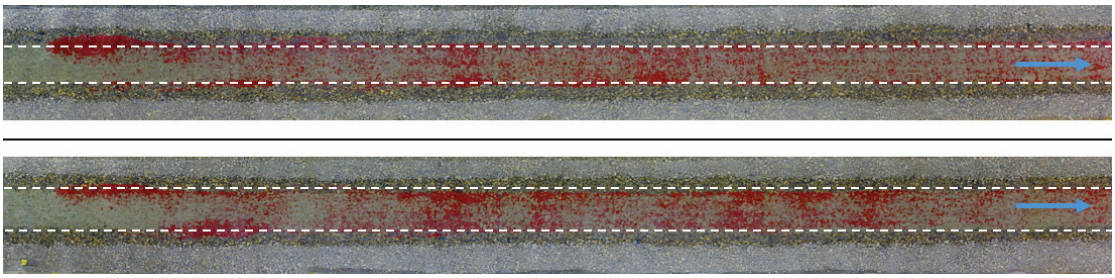

Figure 5.7 – Panoramic view after 3 hours for L/w=2.5: configuration B (top) and configuration C. Flow direction indicated by blue arrow. Replenishment grains represented by the darker areas between dash lines

5.4 Discussion

For obtaining a complete erosion of volumes, persistence of placed material and bed forms, former experiments demonstrated the adequateness of 100% submergence of replenishment volumes. The present results show high persistence of material for the performed configurations in agreement with Bösch et al. (2016) for the shorter replenishment deposit. Due to the consistent wash out of placed material for the replenishment of 1.0 m length, the persistence of such deposits is consistently lower. Consequently, the remaining portion of placed material is not enough for affecting the entire channel length.

Different hydraulic behaviours can be assumed analysing the proposed geometrical configurations. For short replenishment, the cross sectional narrowing contributes just locally to increase flow velocity and diverging flow direction, thus the erosion is diffused on all the replenishment volumes. Otherwise, the diverged flow by the upstream volume is lead toward

a reduced cross section where flow velocity and transport capacity are higher. Thus, bigger amount of placed material exit the channel end with a lower final persistence. This effect is more prominent for configuration B where the volumes are closer one each other.

Replenishing sediment on an experimental flume leads to a bed fining. In general this observation is in agreement with the reaction of steep mountain gravel streams to sediment pulse input described by Madej (2001) which observed a roughness decrease due to sediment pulse. Furthermore, recent morphodynamic modelling performed by Ferguson et al. (2015) predicted a bed fining related to increased sediment supply.

A clear bed pattern is observed for the alternated configurations, especially when volumes are shifted one length downstream from the first. Laser and pictures are able to capture the development of a periodic deposition, that may indicate the initiation of a more pronounced morphological change. As it was already observed by Venditti et al. (2012) the periodic depositions and alternated bars are reversible process and they can be re-established when sediment supply is restored. Nevertheless, the peaks of deposition height are not very pronounced and, often, the grains tend to fill the void between large sediments on the channel bed. The limited deposit height may also be explained by the constraints of experimental setup. The fixed bed does not allow the fine grain to filter in the armour layer, thus avoiding mobilisation of bed material like already confirmed in the literature Venditti et al. (2010). Likewise, it can be expected that deposits height may be increased with a moveable bed.

Venditti et al. (2012) highlighted that distance between bars is equal to their length. Herein results show a periodicity ranging from 1.5 to 1.7 channel width independent from the replenishment length. The bed form pattern, more pronounced for configuration C and lower L/w, allows to the assumption that an optimum replenishment length to channel width exist. Indeed, it can be assumed that high L/w allow higher wash out of material with corresponding reduction of available placed grains. Thus, the channel bed would be less influenced by the positive effects of the replenishment. However, the obtained periodicity is below the periodicity of alternate bars of 6 to 10 channel width (Ikeda, 1983; Whiting and Dietrich, 1993). The difference from the results herein to literature observations might be corrected by a longer observation length for the PSD analysis. The PSD analysis is performed only on 7 m of experimental channel, corresponding to a maximum observable wavelength of 3.5 m ($\pm 9w$).

5.5 Conclusions

The replenishment of sediment is a suitable technique to reduce negative effects downstream of dams. Laboratory experiments were performed aiming at determining the impact of several sediment replenishment lengths on the downstream morphological bed forms development in a laboratory flume. Tests are run applying three different lengths to channel width ratios and two geometrical configurations. The results show the efficiency of sediment replenishment in re-establishing bed form periodicity on an experimental flume.

The proposed geometrical configurations present very similar results in terms of persistence of placed material, spreading of replenished grains on the channel bed and wavelength of bed forms. The channel is affected on its entire length by the replenishment in terms of surface occupied by the placed material. Alternated configurations leads to re-establishing a bed form periodicity despite the length of the replenishment deposit.

Longer replenishments tend to enhance higher flow velocities and higher transport capacity. When cross sectional narrowing is extended for a longer distance along the channel, more sediments exit the downstream section and the replenishment is less effective in creating bed forms. The configurations with volumes shifted by one length downstream are more efficient for re-establishing morphological bed variety: higher persistence of material on channel bed, big channel bed surface affected by transported grains and development of bed channel form for the three length variants. The obtained pattern is stable in time and reaches an equilibrium state before the test end. A smaller amount of grains per time are less prone to be transported far away and the reaches suffer for a more diffuse effect. When the volumes have a length to channel width ratio lower than 2.5, then the portion of material remaining on place is bigger, allowing to higher deposits on longer distances. Volumes with length to width ratio equal to one re-established periodicity for twenty times the channel width.

This outcome is of essential importance in case of scarce availability of material. It can be assumed that an optimum length to channel width ratio exists in sediment replenishment method. Thus lower amount of material are enough in creating bed form periodicity on channel bed. Since the amount of material can be reduced, it helps in lowering problem of transport distance and excavation cost. Overall the costs of sediment replenishment may be decrease, rising the restoration project feasibility.

6 Influence of consecutive sediment replenishment

6.1 Introduction

The proposed literature review about sediment replenishment in Section 2.3 points out gaps of knowledge on the frequency of replenishment operation. The so far field applications of sediment replenishment show the need of repeating the procedure almost one time per year. In the present study the influence on channel bed morphology of consecutive gravel augmentation is assessed by means of systematically laboratory experiments using multiple replenishment deposits. This allows to determine three characteristics: the effect of sediment replenishment on channel bed morphology, the persistence of formed depositions and if a larger amount of sediment enhances higher changes in bed topography.

This chapter is part of an extended paper available in the River Flow 2016 conference proceedings, titled "Influence of consecutive sediment replenishment on channel bed morphology" by L. Bösch, E. Battisacco, M.J. Franca and A. J. Schleiss, based on a Master Project performed at the Laboratory of Hydraulic Construction (LCH) in collaboration with L. Bösch.

6.2 Methods

6.2.1 Experimental setup

The experiments were performed in the tilting flume presented at Section 3.1.1. The replenishment material is placed in four deposits, of equal shape and volume ($\pm$ 0.007 m^3 each) following four different configurations. Configurations A, B, C and D are tested (Figure 6.1). From configuration A to D, deposits are placed parallel and then they are shifted downstream of half a deposition length to two deposition lengths. Preliminary investigations found optimal constant equal to 100% of submergence of the replenishment. This corresponds to a flow depth 0.07 m and a discharge of 0.019 m^3/s, kept constant over the entire experiment. This discharge allows effective erosion of the replenishment and the largest area of impact was observed (Bösch et al., 2016). Initial hydraulic conditions in the experimental channel are listed in Table 6.1.

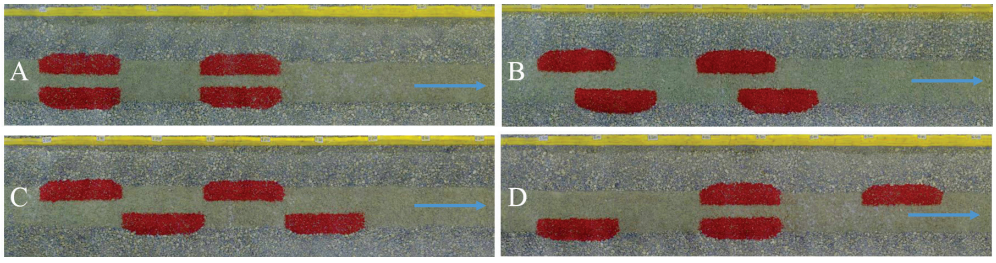

Figure 6.1 – Experimental channel with replenished sediment (red) for all tested configurations. Flow direction from left to right, indicated by the arrow

Table 6.1 – Initial hydraulic conditions in the experimental channel. For the flow: Discharge Q, velocity V and Froude number Fr_f. Respectively for replenishment material and channel bed material are listed: Dimensionless bed shear stress θ_c and Reynolds number Re

Q	h	V	Fr_f	Re_f	Replenishment		Channel bed	
					θ_r	Re_r	θ_b	Re_b
m^3/s	m	m/s	-	-	-	-	-	-
0.019	0.07	0.54	0.65	34203	0.09	446	0.04	932

6.2.2 Experimental Procedure

Each test is performed in two phases. After placing the first replenishment into the dry channel, discharge is applied continuously over three hours with a submergence ratio of 100%. Then the test is interrupted in order to undertake the laser measurements, to weight the washed out sediments and to refill the eroded replenishment. Thus, the same initial geometry as for the first replenishment is built. The test is restarted with the same discharge for another three hours. The total test duration is 6 hours.

To analyse the influence of consecutive sediment replenishment two different data sets are acquired: picture (2D) and laser (3D-Topography). Detailed information about the measurement installation and data acquisition procedure are provided at Section 3.2.

6.2.3 Data analysis

The channel bed morphology development and the time influence are analysed by a series of parameters based on measured variables. A complete description of the parameters is available in Section 3.3. Those used for this analysis are listed below. Each parameter is calculated for each phase of test. The list of tests analysed in this study are provided in Table 6.2. The same kind of analysis is performed for both first and second replenishment.

Persistence	PD	%
Covered surface	CS	%
Compactness of covered surface	NDC	%
Travel distance of center of mass of sediment	TD_{50}	m
Travel distance of the front of sediment	TD_{99}	m
Occupation rate	OCR	%
Power Spectrum Density of OCR-signal	PSD	db
Bed roughness		m
Volume of deposition		mm^3
Difference in channel elevation	Δz_b	mm

Table 6.2 – Analysed tests. Subm = submergence ratio, Shift = distance from the first deposit to the second, N = number of recorded time steps

Test	Conf	Subm	Time steps		Data set	Shift
			N	Time		downstream
		%		min		*m*
13	A	100	10	0,5,15,30,45,60,90,120,150,180	Photo, Laser	0.00
14	B	100	10	0,5,15,30,45,60,90,120,150,180	Photo, Laser	0.37
17	A2	100	10	0,5,15,30,45,60,90,120,150,180	Photo, Laser	0.00
18	B2	100	10	0,5,15,30,45,60,90,120,150,180	Photo, Laser	0.37
15	C	100	10	0,5,15,30,45,60,90,120,150,180	Photo, Laser	0.75
16	D	100	10	0,5,15,30,45,60,90,120,150,180	Photo, Laser	1.50
19	C	100	10	0,5,15,30,45,60,90,120,150,180	Photo, Laser	0.75
20	D	100	10	0,5,15,30,45,60,90,120,150,180	Photo, Laser	1.50
21	C2	100	7	0,5,15,30,45,60,90	Photo, Laser	0.75
22	D2	100	7	0,5,15,30,45,60,90	Photo, Laser	1.50
23	C	100	10	0,5,15,30,45,60,90,120,150,180	Photo, Laser	0.75
24	D	100	10	0,5,15,30,45,60,90,120,150,180	Photo, Laser	1.50
25	C2	100	10	0,5,15,30,45,60,90,120,150,180	Photo, Laser	0.75
26	D2	100	10	0,5,15,30,45,60,90,120,150,180	Photo, Laser	1.50

6.3 Results

Hereinafter, only the results for configuration A and B are discussed. The plots for configurations C and D are available in Appendix B.7.

6.3.1 Reproducibility of test

Visual observations during the experiments show that erosion of the deposits occurs as a combination of fluvial erosion at the deposit toe and mass failure of the above placed sediment due to over-steepening. The collapsed mass is than further eroded and transported downstream by fluvial forces. Deposits are eroded in each configuration similarly. For all the tested configurations, the most upstream deposit is less eroded than the others at the test end. The highest erosion of the most upstream deposit is achieved for configuration A. This difference is related to the higher transport capacity induced by the geometrical configuration and strong cross sectional narrowing. Some reproducible differences between the four configurations can be observed. For at least two experimental runs available for all configurations, configuration A leads to the highest CS, whereas the lowest value of CS after three hours testing is shown by configuration D. For configuration C and B after three hours testing, only minor differences in CS can be observed. The relative increase of CS strengthens

that configuration D has the lowest resulting CS. The reproducibility of tests is confirmed by the persistence PD. Configurations A and D lead to a PD between 71.3% and 88.9%, while configurations B and C show remarkably higher values of PD ranging between 93.8% to 99.6% (Table 6.3).

Table 6.3 – Comparison of persistence PD after 3 h, covered surface CS of initial condition and after 3 h for all experiments. STDV = standard deviation of covered surface CS increase

Conf	PD 3 h %	CS initial %	CS 3 h %	Relative increase %	Mean CS 3 h %
A	88.9	9.6	37.4	291	40.0
	71.3	10.1	42.7	322	
B	99.6	9.4	35.7	280	36.6
	96.6	10.4	37.5	259	
C	99.3	9.2	36.2	294	35.8
	93.8	10.2	36.6	260	
	96.2	10.0	34.4	245	
D	83.7	9.7	28.8	195	33.0
	74.9	10.1	31.6	213	
	70.7	10.2	38.7	279	

Figures 6.2 and 6.3 show the initial and final occupational ratio distribution, OCR, for both experiments with configurations A and B. The corresponding figures for configurations C and D can be found in Appendix B. In Figure 6.3, it can be seen that the OCR-signal after three hours follows a very similar pattern for both experiments with configurations A and B. The same reproducibility of OCR distribution occurs for all the other configurations. The analysis of the OCR distribution for these configurations is detailed in Chapter 4.

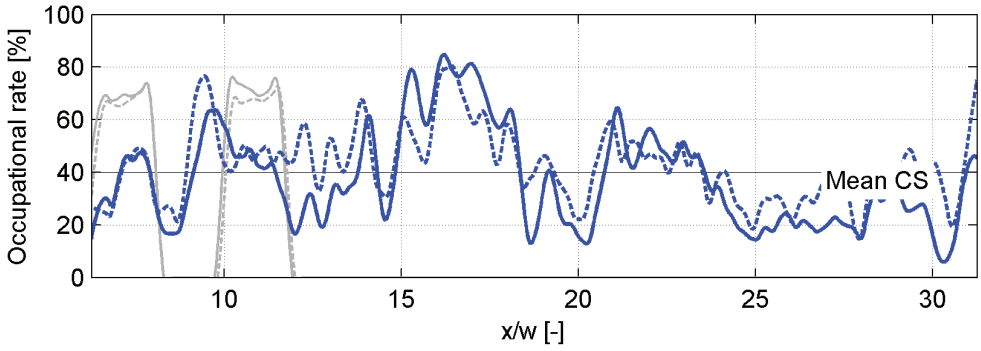

Figure 6.2 – Occupation ratio for configuration A. Initial state in gray and final state in blue

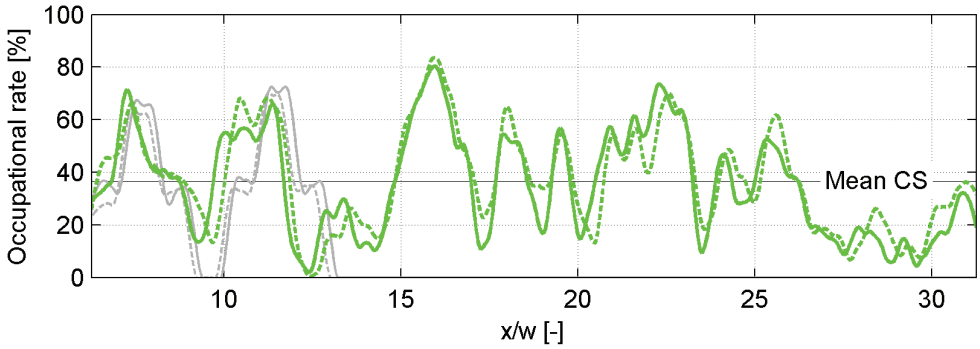

Figure 6.3 – Occupation ratio for configuration B. Initial state in gray and final state in blue

The power spectrum density PSD of the OCR-signal for all the tested configurations is shown in Figure 6.4. As already mention in Section 4.3, both alternating configurations B and C show a pronounced peak in their OCR-signal for a wavelength of about 1.5 and 1.6 times channel width (w) respectively. Configurations A and D do not show so pronounced peak in their PSD. In all experiments the resulting PSD of the final OCR-signal is similar for each replicate configurations, thus also reproducibility in the periodicity can be assumed. The second peak observed, at the double wavelength for configurations B and C, seems to be an artefact of the first one. Thus, it is not further described.

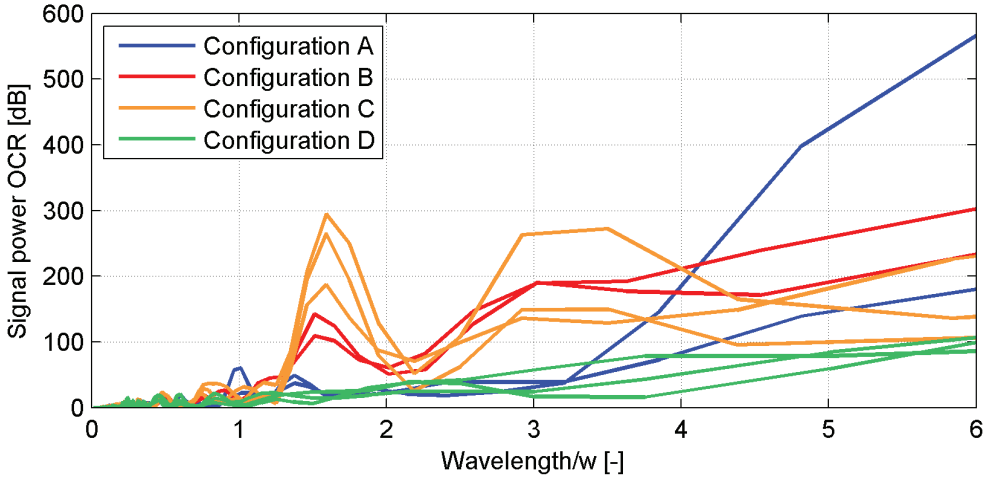

Figure 6.4 – Power spectrum density PSD of the OCR-signal for the first replenishment and all the tested configurations

6.3.2 Influence of second replenishment

Figures 6.5 and 6.6 show the initial and final state for both the replenishment phases for configurations A and B. The same plots for remaining configurations C and d are provided in Appendix B. These figures evidence that deposition areas are not changed by the second

replenishment. As occurred for the first replenishment test, the most upstream deposit suffers from a less complete erosion. Nevertheless, this deposit is almost completely eroded for configuration A after 6 hours testing.

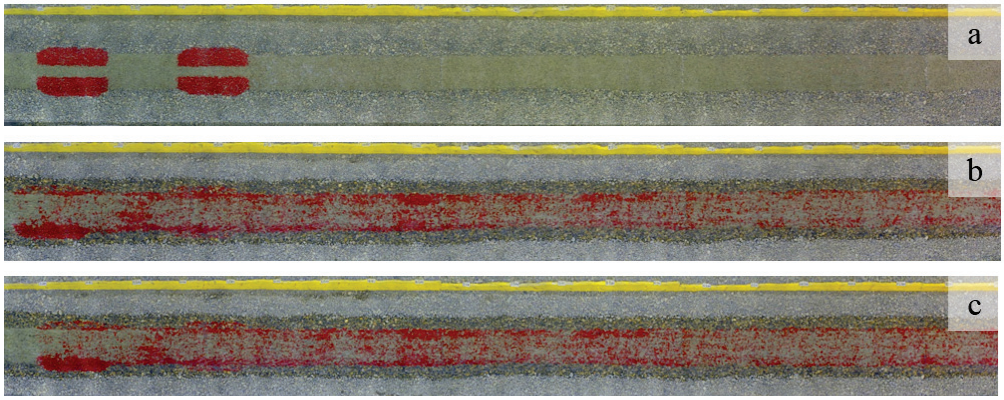

Figure 6.5 – Experimental channel for configuration A with replenished sediment (red): (a) initial state, (b) end of first replenishment test, (c)end of the second replenishment test

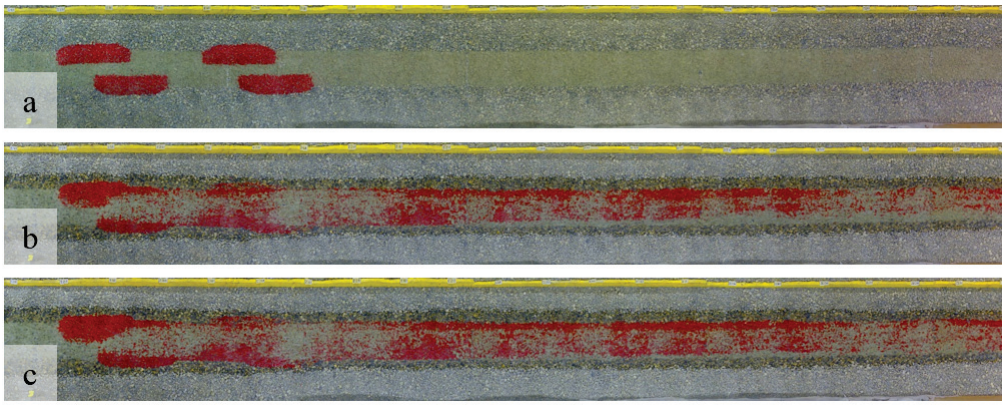

Figure 6.6 – Experimental channel for configuration B with replenished sediment (red): (a) initial state, (b) end of first replenishment test, (c)end of the second replenishment test

Figure 6.7 shows the temporal evolution of covered surface CS over the entire six hours of experiment. It can be seen that after the second gravel augmentation CS increases slightly at the beginning, although this increase is less pronounced than for the first replenishment. After the initial increase, the CS tends toward an equilibrium state. The final value lies slightly above the value attained at the end of the first replenishment. This equilibrium is reached for both replenishment phases around after 1.5 hour testing. The final values of persistence PD and covered surface CS are listed in Table 6.4. For all configurations the second replenishment leads to a slight increase in final CS. The increase is smaller for configurations A and D than for configurations B and C.

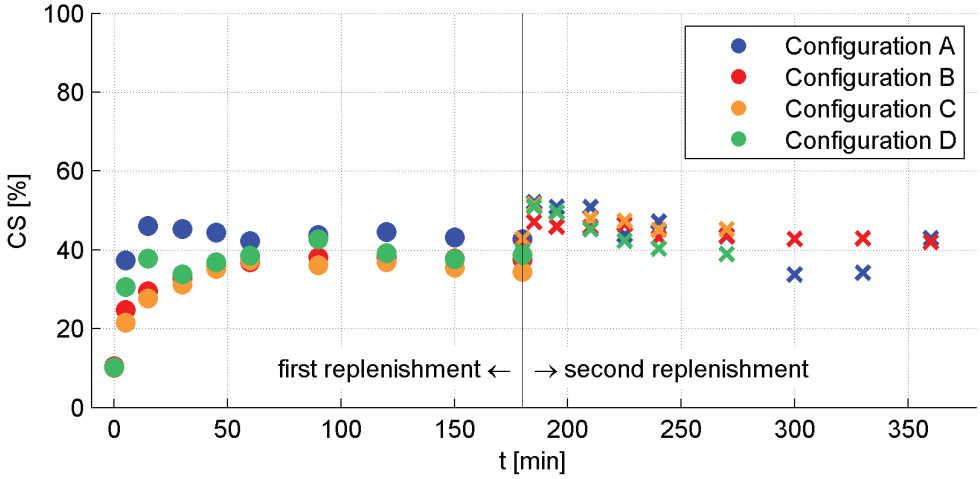

Figure 6.7 – Temporal evolution of the covered surface CS for first (dot) and second replenishment (cross), for all tested configurations

Table 6.4 – Comparison of CS and PD after 1st and 2nd replenishment

Conf	1^{st} PD 3 h %	2^{nd} PD 6 h %	1^{st} CS 3 h %	2^{nd} CS 6 h %	Difference %
A	71.3	13.9	42.6	42.9	0.3
B	96.6	40.8	37.5	42.0	4.5
C	96.2	-0.03	34.4	38.0	6.7
D	70.7	-0.06	38.7	38.4	0.5

For both configurations A and B, the PD of second replenishment is around 56% smaller than after first replenishment (Table 6.4). This finding is further confirmed by the volumes of the deposition, where the increase due to the second replenishment is smaller (Table 6.5). Nevertheless, for configuration B a relative increase by 20% is observed in deposited volume. Unfortunately, the current installation does not allow to distinguish between material belonging to the first or second replenishment. Therefore, it is not possible to establish if the consecutive replenishment enhances the transport of first bed depositions.

For both configurations, A and B, the first replenishment leads to a remarkable bed fining, reducing initial standard deviation from around the average diameter of the bed material, ($d_{50,b}$ = 11.5 mm) to the replenishment average diameter ($d_{50,r}$ = 5.5 mm). The second replenishment slightly increased the bed roughness, while the effect is again more pronounced for the alternating configuration (B and C) (Table 6.6).

The temporal evolution of compactness NDC over six hours is shown in Figure 6.7. The compactness NDC tends to increase in the first 30 minutes after the second replenishment.

Table 6.5 – Volume of deposition along entire channel after 1^{st} (3 h) and 2^{nd} (6 h) replenishment. *=(2^{nd}-1^{st})/1^{nd}

	Deposition 3 h mm^3	Deposition 6 h mm^3	Relative increase* %
A	9.24E+06	9.60E+06	4
B	1.10E+07	1.31E+07	20

Table 6.6 – Standard deviation ($STDV$) along the channel reach downstream of the replenishment for initial condition, after 1^{st} (3 h) and after 2^{nd} (6 h) replenishment. *=(2^{nd}-1^{st})/1^{nd}

	STDV initial mm	STDV 3 h mm	STDV 6 h mm	Relative increase* %
A	11.09	5.31	5.49	3
B	12.59	6.89	7.24	5

After this initial increase, NDC approaches again the equilibrium value reached after first gravel augmentation. The influence of the second replenishment on the equilibrium value of NDC is thus small (Table 6.7). After the second replenishment, alternating configurations (B and C) show more compact covered surface than the parallel configurations.

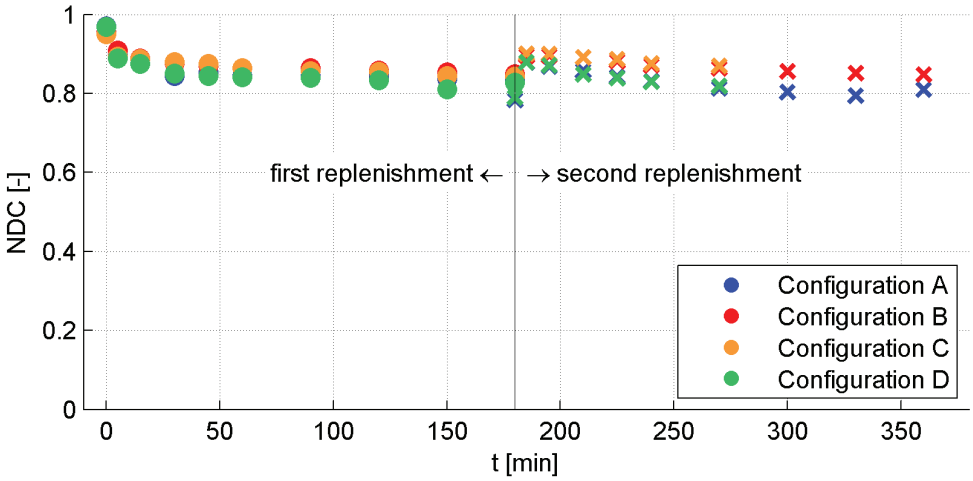

Figure 6.8 – Temporal evolution of the compactness of bed forms NDC for first (dot) and second replenishment (cross), for all tested configurationsB

Table 6.7 – Comparison of CS and PD after 1st and 2nd replenishment

Conf	1^{st} NDC 3 h -	2^{nd} NDC -	Difference 6 h -
A	0.83	0.81	-0.02
B	0.85	0.85	0.00

Figures 6.9 and 6.10 show the *OCR* and its cumulative sum for both configurations A and B, for the first (solid line) and the second replenishment (dashed line) in the channel reach downstream of the initial replenishment deposits.

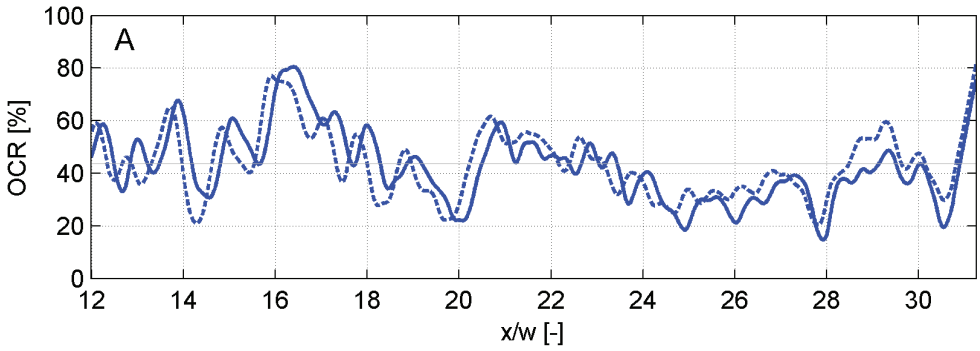

(a) *OCR* configuration A

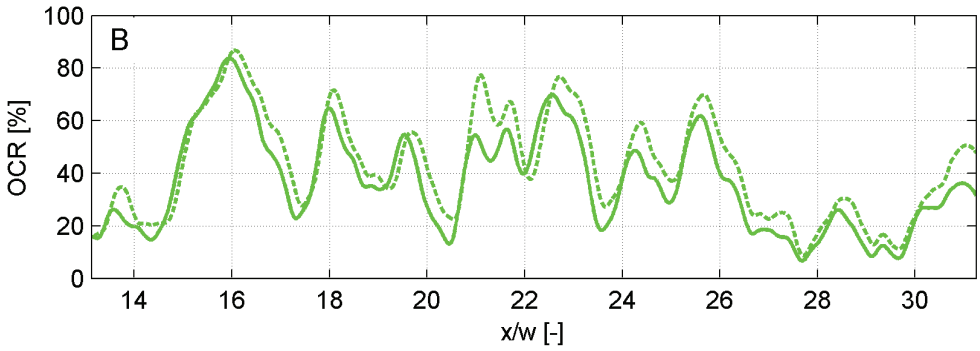

(b) *OCR* configuration B

Figure 6.9 – Occupational rate (OCR) along channel reach downstream of the replenishments for configuration A and B. First replenishment=solid line, second replenishment=dashed line

In these figures the distance along the channel length, x, is normalized by the channel width, w. Clusters of replenished material are created after the first replenishment. For both configurations A and B, the second replenishment does not change the spatial pattern of *OCR*

established after the first replenishment. In case of the alternating configuration B, the OCR is slightly increased by the second replenishment mainly after $x/w = 17$. This observation is confirmed by the cumulative sum of OCR, where a difference between first and second replenishment can only be observed after this distance. For the parallel configuration A, no such trend can be identified. Thus, for this configuration the effect of the second replenishment is small over the entire channel length.

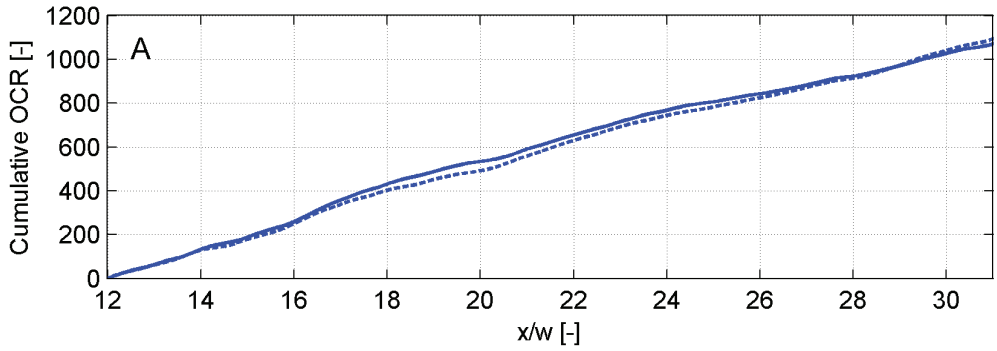

(a) Cumulative sum of OCR, for configuration A

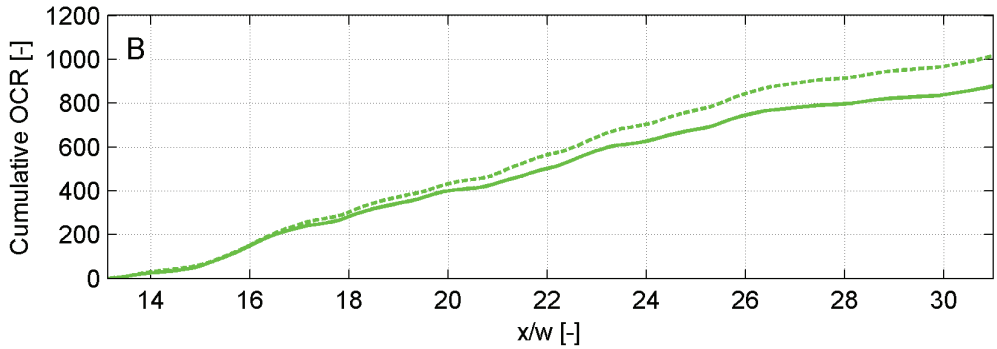

(b) Cumulative sum of OCR, for configuration B

Figure 6.10 – Cumulative sum of the occupational rate (OCR) along channel reach downstream of the replenishments for configuration A and B. First replenishment=solid line, second replenishment=dashed line

These observations are confirmed by analysis of the bed topography changes, Δz_b, obtained by the laser scanner (Figure 6.11). Generally peaks in the Δz_b are consistent for the first and second replenishment, thus pattern established after the first augmentation remains. For configuration B, mean deposition height is remarkable increased to 4.12 mm. For alternating configurations (B and C), the increase in deposition height due to the second replenishment mainly occurs after $x/w = 17$ as it was already the case for the OCR (Figure 6.12). For the parallel configurations (A and D), only a minor effect of the second replenishment can be observed. In latter case, mean deposition height is only increased by 0.2 mm and no large difference in the cumulative sum can be observed.

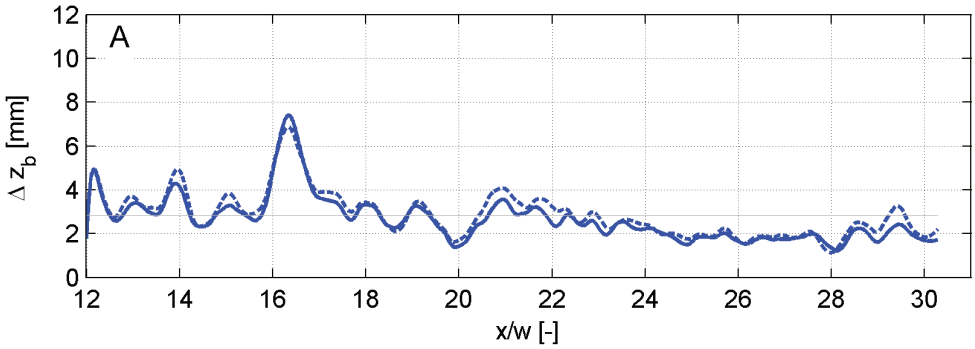

(a) *OCR* configuration A

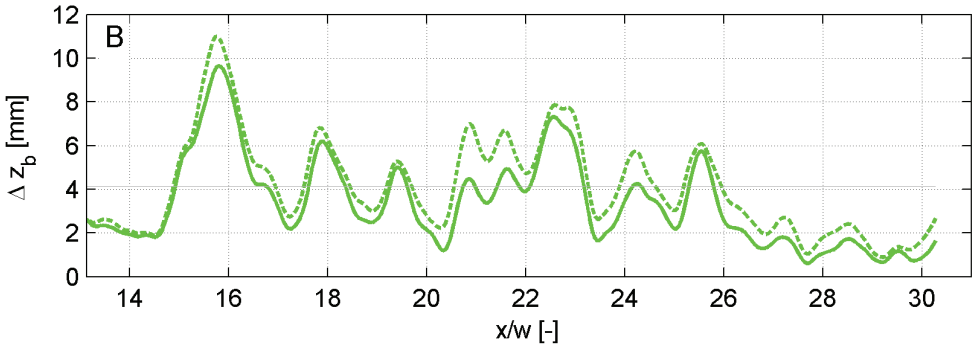

(b) *OCR* configuration B

Figure 6.11 – Elevation difference (Δz_b) of the morphological bed changes (bottom) for configuration A (green) and configuration B (blue), after first (solid line) and second replenishment (dashed line) downstream of replenishments

The analysis of the laser and the image data leads to the assumption that the patterns of *OCR* and Δz_b are highly correlated. This observation is proved by the correlation coefficients shown in Table 6.8. The highest correlation is obtained for configuration B (0.94), while configuration D shows the lowest correlation (0.78) between image in terms of *OCR* and laser data (measured deposit heights). This high agreement between laser and image data strengthens the soundness of the results and supports the method of monitoring effects of sediment replenishment by means of images.

Table 6.8 – Correlation coefficients between OCR-signal and deposition height along the channel reach downstream of the replenishment for all the configurations

Configuration	A	B	C	D
Correlation coefficient	0.88	0.94	0.79	0.78

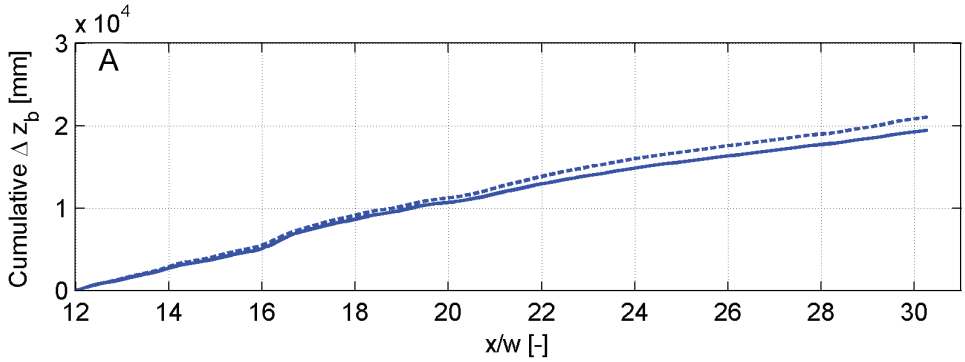

(a) Cumulative sum of OCR, for configuration A

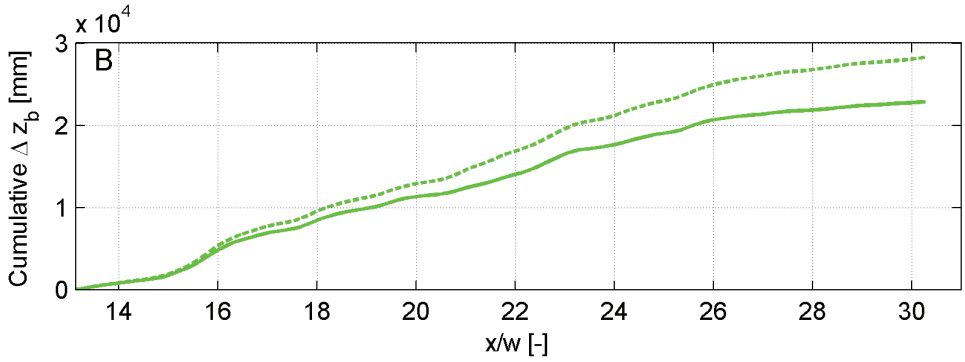

(b) Cumulative sum of OCR, for configuration B

Figure 6.12 – Cumulative sum of the elevation difference (Δz_b) for configuration A (green) and configuration B (blue), after first (solid line) and second replenishment (dashed line) downstream of replenishments

A periodicity in the distribution of bed forms is observed by the PSD of the first replenishment OCR-signal and of the bed elevation changes Δz_b (Figure 6.13, solid line). The depositions of replenished material along the downstream channel reach have a wavelength of $1.5w$. This result is confirmed when observing the OCR pattern for configuration B (Figure 4.6). Peaks in the OCR can be located visually at a smaller distance than twice channel width. For the parallel configuration A, no pronounced peaks in the OCR can be observed. Consequently, the PSD does not show relevant wavelength for this configuration for both data sets.

The PSD of the second replenishment is shown in Figure 6.13 (dash line) for both OCR-signal and bed elevation changes Δz_b. The wavelength of bed forms created by the first replenishment is not changed by the second augmentation of sediments. Nevertheless, the PSD amplitude is increased by the consecutive replenishment, in agreement with OCR and deposition volume analysis.

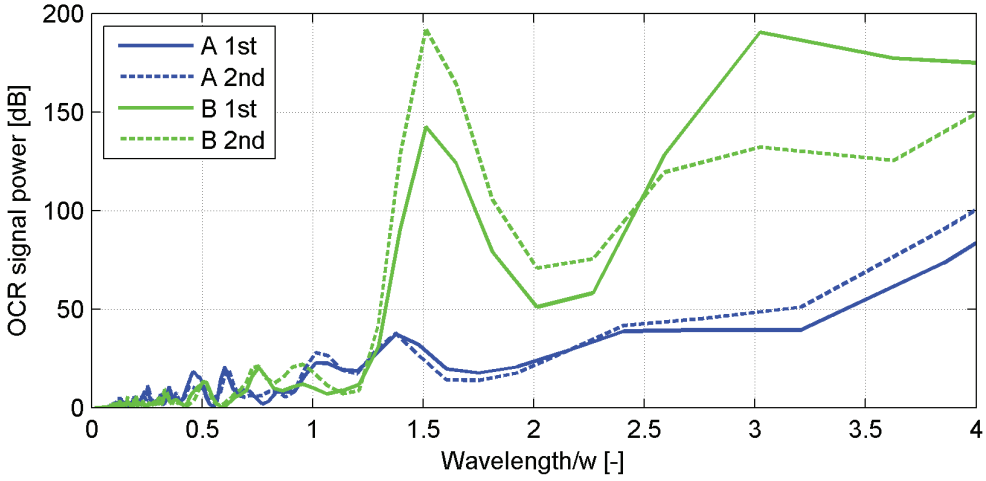

(a) *PSD* of *OCR*-signal

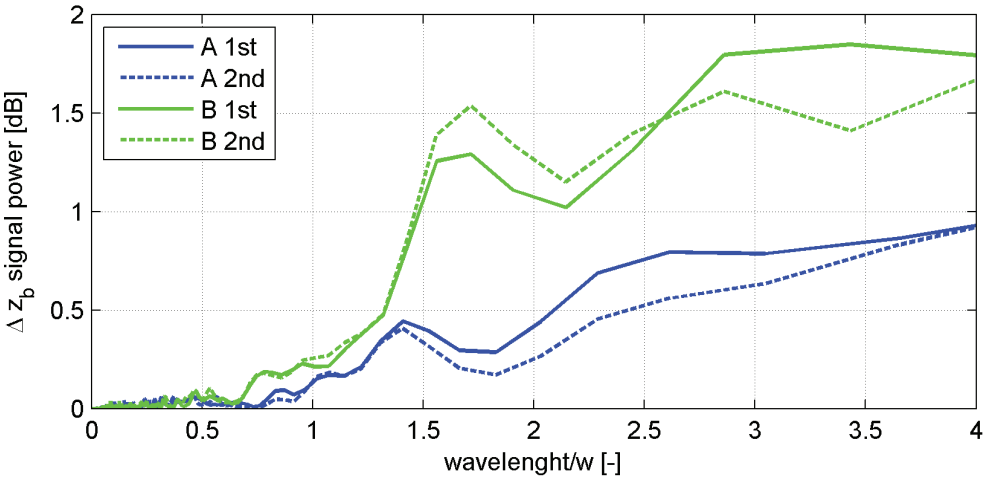

(b) *PSD* of deposition heights

Figure 6.13 – Power spectral density PSD of the changes in bed elevation Δz_b downstream of the replenishments

6.4 Discussion

6.4.1 Bed channel morphological variations

The comparison between the analysed parameters, such as persistence PD, covered surface CS and compactness of bed forms NDC, show a high reproducibility of the final values for all the tested configurations. The longitudinal distribution of replenished material described in terms of occupational ratio OCR is almost the same between replicate tests, confirming the reproducibility. This is one more time strengthened by the consistent periodicity observed in the PSD.

6.4.2 Influence of second replenishment

The second replenishment has only a minor effect on channel morphology in terms of covered surface CS and compactness of bed forms NDC. The second replenishment reached the same equilibrium values of CS and NDC obtained after the first replenishment. Nevertheless, a slight increase in CS is observed for the alternating configurations (B and C). A remarkably smaller portion of replenished material remains on the channel bed after the second replenishment, leading to a lower value of persistence PD. The occupational ratio OCR of the second replenishment is similar to the first, and the same peak of replenished material concentrations are observed. The only minor influence of the second replenishment indicates that the volume of the first gravel augmentation was enough to create an equilibrium condition in the channel. Nevertheless, a slight increase in the deposition heights is observed after the second replenishment for the alternating configurations. The analysis of the cumulative OCR and Δz_b shows that this increase is most likely to occur in the very downstream channel reach. Thus it can be assumed that for configuration B an equilibrium state was not reached over the entire channel reach after the first replenishment. A second replenishment could thus increase the impact length. For the parallel configurations, no general increase in the OCR and Δz_b signal can be detected after the second replenishment meaning that an equilibrium situation was achieved after the first augmentation. The periodicity of depositions developed during the first replenishment remains constant after the second replenishment as observed by the PSD analysis. Thus, it can be assumed that the pattern of deposition created after the first replenishment is stable in time and the second replenishment has less impact than the first augmentation on the channel bed morphology. This periodic depositions can be understood as mounds, forming the initial condition of alternating bars, as it was already observed by Venditti et al. (2012). Nevertheless, the deposition heights are not very pronounced. Former studies highlighted that channel width variations are core condition for the formation of topographic variations (Nelson et al., 2015). Width variations lead to changes in flow velocity and consequently allow deposition in wider channel section and erosion in the narrower, respectively. These diversities in flow velocity cannot occur on this flume, therefore the deposit heights are limited. In addition, the present experimental conditions are close to the plane bed occurrence for alternated bar formation, as proposed by Ahmari and Da Silva (2011). No enhanced bed elevation variations can thus be expected, but the zone limits from Ahmari and Da Silva (2011) are based on field observations and their validity are not assured for laboratory experiments. Finally, the fixed bed does not allow small replenished grains to percolate into the armored channel bed. Venditti et al. (2010) stated that augmentation of fine grains, which could percolate, may increase the mobilization of bed material. It can be assumed that changes in channel bed topography and deposition heights would be higher in the case of a mobile bed. In addition, the minor effects of the second replenishment can be explained by the change in initial roughness condition. The first replenishment decreases roughness of the channel bed. This consequently results in higher bed shear stress, which leads to increased transport capacity. In order to increase the effect of the first replenishment on the upper river reach by means of a second replenishment the applied discharges should be

decreased accounting for the established roughness conditions. Thereby, a higher persistence value may be reached. This conclusions are strengthened by the results from Ferguson et al. (2015), who showed that bed fining and consequently increased bed shear stress raised the transport capacity by an order of magnitude. With increased transport capacity the augmented sediment is transported further downstream, where the first replenishment had no impact and deposited there with a similar pattern. When applying consecutive replenishment without accounting for reduced roughness, the impact distance of replenishment material along the downstream reach may be increased. In light of these observations, only one input point for sediment replenishment may be needed. This is an advantage in case of limited access for sediment replenishment in the more downstream river reach. By using only one upstream implementation point, the distance between excavation and deposition site is reduced, notably reducing the costs of restoration projects. Regardless the configuration, roughness of channel bed is decreased by the replenishment from initial standard deviation corresponding to the $d_{50,b}$ to the $d_{50,r}$. This result is in agreement with the reaction of steep mountain gravel streams to a first sediment pulse input, observed by Madej (2001).

6.5 Conclusion

Sediment replenishment can be applied for different goals, such as the fining of armoured channel bed downstream a dam or the enhancement of channel bed elevation variations. In the present study different geometrical configuration of replenishments and the effects of consecutive gravel augmentation were experimentally investigated. The channel bed is influenced in different ways depending on the geometrical configuration. The alternated configuration is found to be more effective: persistence of material in the channel is higher and the development of periodic bed elevation changes can be observed only for this configuration. The periodic bed patterns follow a wavelength which correspond to the length of replenishments. Although a remarkable bed fining is observed for both configurations, configuration A leads to the largest covered surface value and corresponding bed fining. The decrease in roughness induced by the first replenishment leads to higher transport capacities as initial condition for the second replenishment. An increase in replenishment volume by means of a second replenishment did not remarkably enhance elevation changes. It is assumed that channel bed variation may be enhanced by decreasing the discharge. This would would help in keeping more material on the channel bed, by matching the roughness conditions established after the first replenishment. The pattern of deposition established after the first replenishment is very stable. The volume of the first replenishment was enough to establish an equilibrium condition along the channel. In case of the alternating configuration this equilibrium condition was not reached over the entire channel length after first replenishment, and the second replenishment did remarkably influence the very downstream reach of the channel. Consecutive sediment replenishment is stated to be an effective measure in order to increase the impact length of river restoration projects. This is of essential importance in case of limited access for sediment replenishment along more downstream river reaches.

7 Mechanisms of transport of sediment deposits

7.1 Introduction

The technique of sediment replenishment has demonstrated to be successful in re-establishing morphological bed forms and reactivating the natural sediment dynamics in sediment depleted river reaches. In order to perform a successful river restoration by sediment replenishment technique, the transport mechanism responsible of the grain erosion and transport should be clarified.

So far, the main mechanism responsible of the erosion and transport of sediment replenishment in an open-channel have been studied in the field or in laboratory, with either one single replenishment volume or with continuous feeding on a moveable bed. These conditions do not fit completely with the river state downstream of a dam.

In agreement with former studies, sediment replenishment deposits can be assumed and analysed as artificial pulses which increase locally the sediment supply. It was demonstrated that pulses may move by a translation, by dispersion or by a mixed mechanism (Lisle et al., 1997, 2001). The same kind of analysis is performed on the multiple replenishment of sediment.

Former experiences were performed is the same range of Froude number by Sklar et al. (2009) and the sediments were mainly moved by a translation-type mechanism. For practical applications of sediments replenishment, translation-type mechanism is of particular interest mainly where the access points for delivering the material are limited. In these cases, a longer portion of channel reach is affected by the replenishment effects (Sklar et al., 2009). In this research, for the first time, the mechanisms of transport are investigated in laboratory with multiple sediment volumes replenished in the channel on a fixed armour bed. Six geometrical replenishment configurations with alternated and parallel volumes are tested in the laboratory. In addition, two submergence ratios of the volumes of sediments are tested: complete submergence and over-submergence of the replenishment volume.

7.2 Method

A complete overview on the experimental installation is given in Section 3.1.1. Preliminary series of tests confirmed that three hours of test duration are enough for achieving an equilibrium state in terms of erosion and transport. The total amount of sediment replenishment is dived in four deposits, having the same dimensions. The deposits are placed on both channel banks creating different geometries (Figure 7.1). The complete submergence ratio (water depth=deposit height, 100%) and over submergence ratio (water depth= 1.3 deposit height, 130%) are tested. A complete list of tested cases is provided in Table 7.1.

The temporal evolution of the erosion and transport processes are recorded by means of photos as described in 3.2. The initial and final bed topography are registered by a laser scanner. During the first hour of test five series of photos are acquired at 0, 5, 15, 30, 45 and 60 minutes (t_1, t_2, t_3, t_4, t_5, t_6). The following two test hours, the interval between photos is

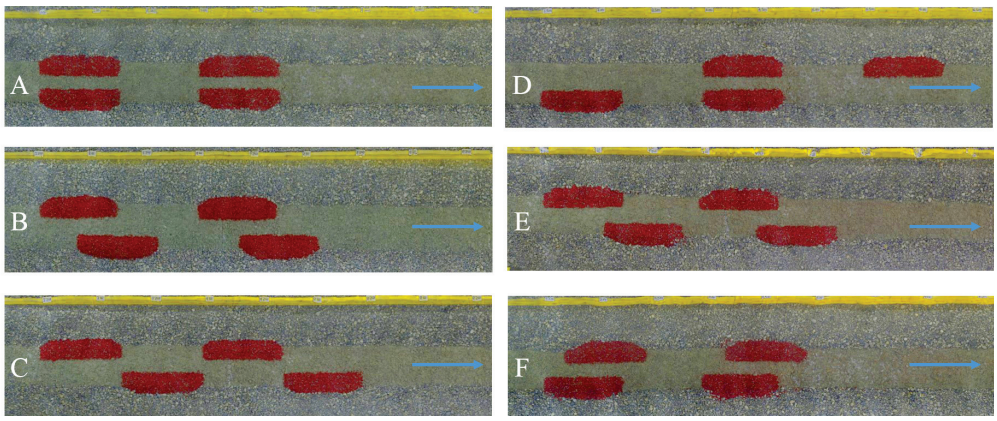

Figure 7.1 – Experimental channel with replenished sediment (red) for all tested configurations. Flow direction from left to right, indicated by the arrow

extended to 30 minutes (t_7, t_8, t_9, t_{10}). For the submergence condition of 130%, the time series at 5 minutes has not been recorded. According to these intervals, in all graphs showing the test results, times are listed from t_1 to t_{10}, with t_1 corresponding to the initial state and t_{10} to the channel configurations at the end of the test.

Table 7.1 – Hydraulic characteristics for the two tested submergence conditions (100% and 130%), Froude and Reynolds numbers are estimated considering $d_{50,repl}$=5.5 mm and $d_{50,bed}$=11.5 mm

Submergence		100%	130%
Discharge	m^3/s	0.019	0.031
Flow depth	m	0.07	0.09
Hydraulic radius	m	0.05	0.07
Velocity	m/s	0.54	0.64
Fr, Froude number	-	0.65	0.67
Re, Repl: Particle Reynolds number	-	446	496
θ_r, Repl: Shields number	-	0.09	0.11
Bed: Particle Reynolds number	-	932	1037
θ_b, Bed: Shields number	-	0.04	0.05

7.2.1 Analysed parameters

The effects of the replenishment on the bed morphology in the channel reach is analysed in terms of persistence, occupation surface, spatial and temporal distribution of replenished material as presented in (Battisacco et al., 2016; Juez et al., 2016). Following, the parameters used for determining the transport mechanisms which drives the replenished material along the channel reach during the test duration are listed. These parameters describe the channel

Table 7.2 – Analyzed tests

Conf	Subm	Time steps		Data set	Shift downstream
		Tot	Time		
	%		min		m
C	70	10	0,5,15,30,45,60,90,120,150,180	Photo, Laser	0.75
D	70	10	0,5,15,30,45,60,90,120,150,180	Photo, Laser	1.50
A1	100	9	0,15,30,45,60,90,120,150,180	Photo	0.00
A2	100	10	0,5,15,30,45,60,90,120,150,180	Photo, Laser	0.00
B1	100	9	0,15,30,45,60,90,120,150,180	Photo	0.37
B2	100	10	0,5,15,30,45,60,90,120,150,180	Photo, Laser	0.37
C1	100	9	0,15,30,45,60,90,120,150,180	Photo	0.75
C2	100	10	0,5,15,30,45,60,90,120,150,180	Photo, Laser	0.75
C3	100	10	0,5,15,30,45,60,90,120,150,180	Photo, Laser	0.75
D1	100	9	0,15,30,45,60,90,120,150,180	Photo	1.50
D2	100	10	0,5,15,30,45,60,90,120,150,180	Photo, Laser	1.50
D3	100	10	0,5,15,30,45,60,90,120,150,180	Photo, Laser	1.50
E	100	10	0,5,15,30,45,60,90,120,150,180	Photo, Laser	0.19
F	100	10	0,5,15,30,45,60,90,120,150,180	Photo, Laser	0.56
A	130	9	0,15,30,45,60,90,120,150,180	Photo	0.00
B	130	9	0,15,30,45,60,90,120,150,180	Photo	0.37
C	130	9	0,15,30,45,60,90,120,150,180	Photo	0.75
D	130	9	0,15,30,45,60,90,120,150,180	Photo	1.50
E	130	10	0,15,30,45,60,90,120,150,180	Photo, Laser	0.19
F	130	10	0,15,30,45,60,90,120,150,180	Photo, Laser	0.56

response to sediment replenishment in view of morphological changes, needed time for erosion, required released flow and affected distance downstream of the initial replenishment volumes. The above mentioned parameters are presented in a more complete way in Section 3.3.

The transport mechanism is assessed as by Sklar et al. (2009) comparing the interquartile length (IQL) with the position of the center of mass (TD_{50}) of the covered surface. The interquartile length is defined as the length of the central 50% of covered surface, without considering the upper and lower 25% of the area (Figure 7.2). A large increase of the IQL with a small change of the TD_{50} corresponds to dispersion transport. Whereas a movement of the TD_{50} associated to a constant IQL value is related to a translation mechanism. The slope (IQL/TD_{50}) indicates whether the sediment are transported by dispersion or translation. For the herein setup, a slope of 1 corresponds to pure dispersion, while 0 represents pure translation. A mixed mechanism, between pure translation and pure dispersion correspond to a slope of 0.5, in agreement with Nelson et al. (2015).

Persistence	PD	%
Covered surface	CS	%
Compactness of covered surface	NDC	%
Travel distance of center of mass of sediment	TD_{50}	m
Travel distance of the front of sediment	TD_{99}	m
Velocity of center of mass	Velocity TD_{50}	m/s
Velocity of center of sediment front	Velocity TD_{99}	m/s
Occupation rate	OCR	%
Transport mechanism		

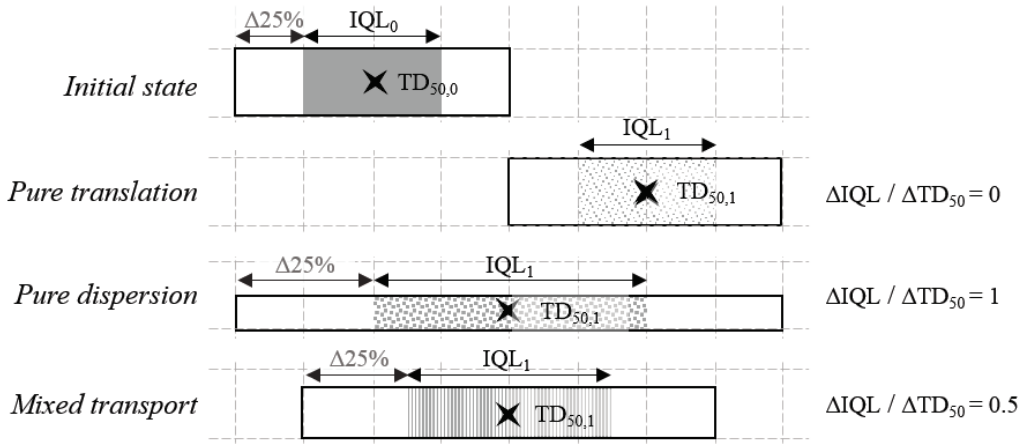

Figure 7.2 – Schematic representation of the temporal evolution of the longitudinal distribution of the replenished volume of sediments. Example of dispersion, translation and mixed transport

7.3 Results

7.3.1 Transport distance of the front and the center of mass

The temporal evolution of the front and of the center of mass of the replenished material for a submergence ratio of 100% is shown in Figure 7.3 and Table 7.3. In Figure 7.3 it can be seen that the for all the tested configurations the front of the moving grains reaches the end of the channel. However, the time when this happens varies in relation with the initial conditions.

For parallel configurations (A, D and F), the front of the moving mass, TD_{99}, reaches the channel end between 30 and 45 minutes after the beginning of the test. For configuration D, the first grains reach the final section in 15 minutes. For the parallel geometries (A, D and F), the erosion and transport processes are mainly occurring during the first 45 minutes. For these cases, the flow is concentrated over roughly one third of the channel cross section, thus flow velocity and transport capacity are higher.

With alternated configurations (B, C and E), the water flows over about two third of the channel

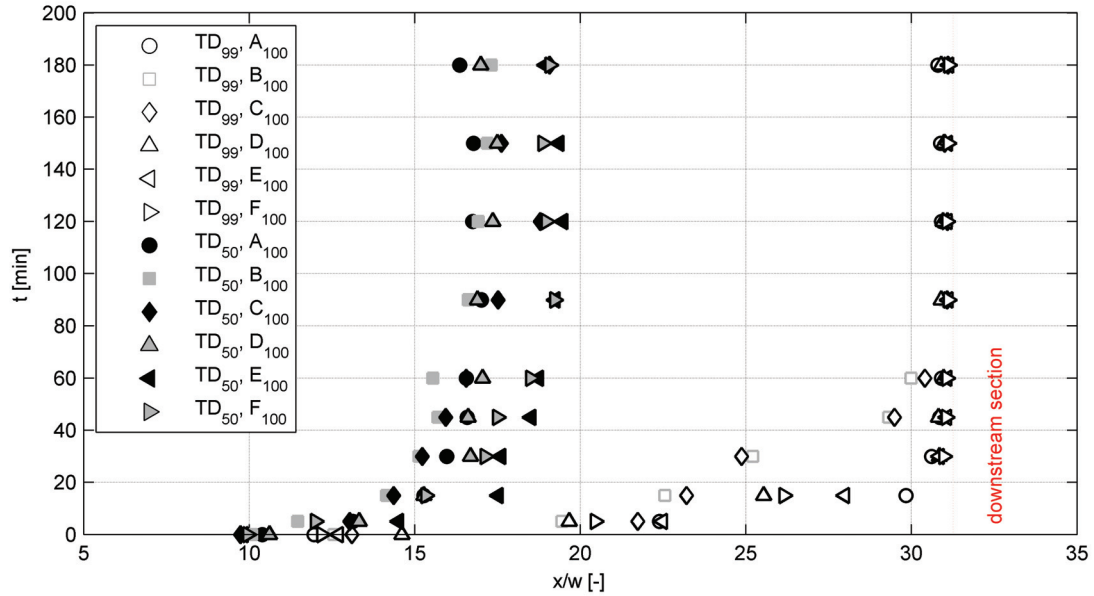

Figure 7.3 – Temporal evolution t of the transport distances x/w of TD_{99} (empty symbols) and TD_{50} (filled symbols), for all configurations (from A to F) and for a submergence ratio of 100%

width. Consequently, the erosion process develops more progressively. The slope between the normalized distance (x/w) and the time, indicating the velocity, is less steep for alternated configurations, thus the transport process needs more time as can be seen in Figure 7.3. The TD_{99} of the moving mass may reach the last channel section in two hours. The position of the mass center, TD_{50}, of the replenishment grains moves downstream mainly in the first two hours of test. Then, the TD_{50} tends to an equilibrium slightly downstream the first half of the channel length from x/w=15.8 to 18.6. The temporal evolution of TD_{99} and TD_{50} for a submergence ratio of 130% are shown in Figure 7.4 and Table 7.3. It is visible that the erosion process becomes faster compare with a submergence ratio of 100%. Furthermore, no clear difference on the behaviour of the different geometrical configurations is visible. The most downstream channel section is reached (position of TD_{99}) in approximately 30 minutes for all the configurations. For the remaining test duration a part of the replenishment material is transported out from the observation reach. Thus, a continuous decrease of the total volume of replenishment sediments is observed in the channel reach. The position of TD_{50} evolves quickly in the first test hour and stabilizes in the position corresponding to x/w=20.

Table 7.3 gives the distances run by the TD_{50} and TD_{99} for all the performed replenishment configurations and the two submergence ratios. The velocities are calculated as the ratio between travel distance, for both TD_{50} and TD_{99}, and needed time to reach the distance (i.e. V [m/s] = $TD_{50,120min}$ [m] / 5*60 [s]). Independently from the submergence ratio, a decrease of the velocity is observed between the first and the second test hour. This confirms the previous observations on the erosion process occurring in the first hour of experiment. From the second hour until the end of the test the velocity decreases to values close to zero. Thus,

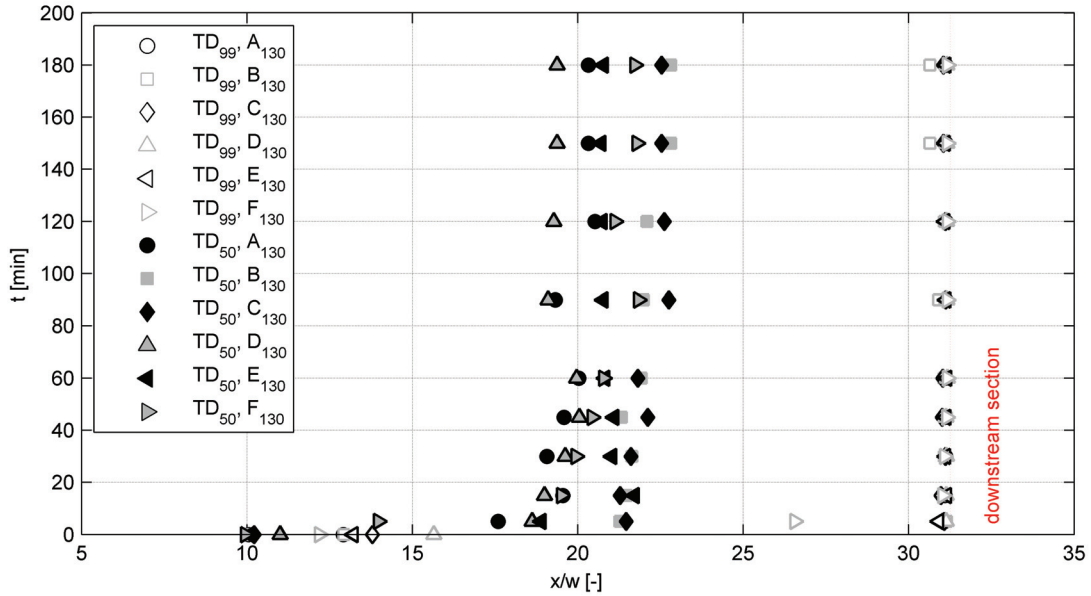

Figure 7.4 – Temporal evolution of the transport distances of TD_{99} (empty symbols) and TD_{50} (filled symbols), for all configurations (from A to F) and for a submergence ratio of 130%

the transport process has reached an equilibrium state and no further remarkable changes occurred.

7.3.2 Temporal distribution of sediment along the channel length

The success of the application of the artificial replenishment of sediments can be evaluated by the extension of the area affected by the mobilized sediments, as mentioned by Sklar et al. (2009). In the first column (a) of Figure 7.5 and 7.6, the time evolution of the occupation ratio (OCR) for a submergence ratio of 100% is shown. Areas of channel bed covered by replenished material alternate with others almost not affected by the replenishment grains. This distribution of replenished material throughout the channel bed is established in only about 15 minutes from the test beginning. Some peaks of sediment concentration are observed along the channel. Their positions are the same for all the remaining test duration. This trend of OCR distribution is similar for all the different geometrical configurations. Nevertheless, the temporal analysis points out a variation in the intensity of the OCR peaks in time, column (a) from Figure 7.5 to 7.8.

In these figures it is visible that, during the first 1.5 hour, more intense peaks of OCR are located in the upstream half of the channel, with values sometimes higher than 80%, whereas the peaks downstream are not higher than 50%. In the second half of the duration of the tests, the peaks of OCR decrease, whereas an increase of OCR is visible downstream. This different evolution between the upstream ($x/w < 18$) and the downstream regions ($x/w > 18$) indicates that a transfer of sediments is occurring from a region to the following. The OCR follows a

clear pattern, with a wavelength corresponding to the length of the replenishment volume as already observed in preliminary tests (Battisacco et al., 2016). It can be also noted that, for the parallel configurations (A, D and F), the pattern observed downstream shows the imprint of the initial form of the replenishment. On the other hand, for alternating configurations, a shorter and more varied wavelength of the downstream pattern is observed.

The temporal evolution of OCR for a submergence of 130% is presented in the first column (a) of Figures 7.7 and 7.8. For parallel configurations, especially A and F, the peaks of OCR are as high as 80% for the initial time steps in the upstream half of the channel, and lower than 40% in the downstream channel reach. These higher initial values of OCR for parallel configurations correspond to a wider spread of material over the channel width. The peaks in OCR sediment distribution are less intense for a submergence ratio of 100% than 130% for parallel replenishment geometries (A, D and F). The comparison in OCR distribution between a submergence ratio of 100% and 130% shows that, for alternating configurations (B, C and E), the peaks of sediment concentration are located slightly more downstream with a higher submergence. This longer distance is due to the higher transport capacity for the 130% submergence, which leads to a higher initial deposit erosion and transport. For the same reason, the depositions are more intense for higher discharge, since the flow erodes more grains. In addition, the geometrical configuration contributes to strengthen the effect of submergence. Parallel configurations confine the flow in one third of the cross section, notably increasing the transport capacity.

In Figures 7.5 and 7.6, second column (b), the correlation function between the OCR distributions of consecutive time steps is presented for each configuration and a submergence ratio of 100%. Correlation functions were determined for the instantaneous signals of OCR paired by consecutive time steps. The peak of correlation function corresponds to the distance between similar patterns of the longitudinal distribution of the replenishment sediment through the channel. The spatial lag (corresponding to the peak of correlation) divided by the time step between the OCR signals corresponds to a travelling velocity of the sediment patches.

The main movement of replenished material occurs mainly during the first 5 to 15 minutes from the test beginning (t_2 and t_3). The part of channel bed occupied by the transported grains in the interval t_2-t_3 remain constant for the rest of the test, despite the variation of the OCR values. Thus, the lags between OCR distributions tend to zero since no further significant movements of the bed forms occurred in the channel bed. The alternated configurations (B, C and E) require more time compared to parallel geometries to reach an equilibrium state in terms of covered surface as already observed by (Battisacco et al., 2016). For alternated configurations, the correlation function presents a somehow flatter distribution around the peak. This effect is related with a higher variety of bed forms in the channel.

The correlation functions for the submergence ratio of 130% are shown in Figures 7.7 and 7.8, second column (b). The main movement of sediment patterns occurs in the first 15 test minutes of testing. No significant differences can be seen between the geometrical

configurations. Thus, the transport dynamics of parallel (A, D and F) and alternated (B, C and E) configurations are similar for 130% submergence ratio.

The temporal evolution of the normalized cumulative sum of the OCR distribution is presented in Figures 7.5 and 7.6, third column (c), for a submergence ratio of 100%. The cumulative sum of the OCR signals, along the longitudinal direction, allows to infer the time the replenished sediments require to be active on the whole channel, complementary the previous analysis. The cumulative sum also illustrates the temporal evolution of the process of filling and depletion of the sediment replenishment. The cumulative of OCR is normalized by the area of interest in these figures.

In alternated configurations (B and C mainly), it clearly takes longer (45 minutes) until the replenished sediments can be observed along the whole channel. This happens when a flat region is not longer observed in the longitudinal distribution of the cumulative sum of OCR (i.e. Figure 7.5, configuration B, from t_5 to t_6). For the parallel (A and D) and nearly parallel configurations (E and F), the replenished sediments are present throughout the entire channel before 15 minutes. Later, with more evidence for parallel configurations (A and F), the cumulative area decreases in the downstream half of channel reach, corresponding to a channel depletion. For alternated configuration B and C, the depletion of sediments from the channel is lower than for parallel configurations (A, D and F). The persistence of bed morphological forms seems to last longer for the alternated configurations.

For a submergence ratio of 130% (see Figure 7.7 and 7.8, third column (c)), the replenished volumes for all the geometrical configurations have suffered for a complete erosion in the upstream half of the channel after 15 minutes. The maximum occupation of bed surface occurs in less than half an hour of testing corresponding to the initial spread of material. For the remaining test duration, the flow continues to transport the sediments and the bed morphology is washed away. No clear differences are evident between alternated and parallel configurations of replenishment volumes.

Submergence ratio 100%												
Time, [min]	Normalised distance TD_{50}, x/w [-]						Velocity TD_{50}, [m/s] * 10^{-2}					
	conf. A	conf. B	conf. C	conf. D	conf. E	conf. F	conf. A	conf. B	conf. C	conf. D	conf. E	conf. F
0.1	10.40	10.08	9.74	10.62	9.82	9.96						
5	13.13	11.46	13.04	13.32	14.52	12.00	1.750	1.528	1.738	1.776	1.935	1.600
15	15.27	14.15	14.37	15.27	17.52	15.34	0.679	0.629	0.638	0.679	0.779	0.682
30	15.96	15.13	15.23	16.68	17.60	17.13	0.355	0.336	0.338	0.371	0.391	0.381
45	16.59	15.70	15.94	16.61	18.51	17.50	0.246	0.233	0.236	0.246	0.274	0.259
60	16.56	15.55	16.56	17.04	18.74	18.50	0.184	0.173	0.184	0.189	0.208	0.206
90	17.01	16.62	17.52	16.89	19.24	19.23	0.126	0.123	0.130	0.125	0.143	0.142
120	16.74	16.92	18.79	17.36	19.47	18.98	0.093	0.094	0.104	0.096	0.108	0.105
150	16.77	17.19	17.62	17.49	19.35	18.87	0.075	0.076	0.078	0.078	0.086	0.084
180	16.36	17.31	19.08	16.99	18.95	19.08	0.061	0.064	0.071	0.063	0.070	0.071
Time, [min]	Normalised distance TD_{99}, x/w [-]						Velocity TD99, [m/s] * 10^{-2}					
	conf. A	conf. B	conf. C	conf. D	conf. E	conf. F	conf. A	conf. B	conf. C	conf. D	conf. E	conf. F
0.1	11.96	12.56	13.11	14.61	12.69	12.19						
5	22.39	19.44	21.74	19.67	22.48	20.46	2.985	2.592	2.898	2.622	2.997	2.727
15	29.84	22.56	23.21	25.53	27.98	26.16	1.326	1.002	1.031	1.135	1.243	1.162
30	30.61	25.21	24.87	30.84	30.84	30.98	0.680	0.560	0.553	0.685	0.685	0.688
45	30.85	29.31	29.49	30.81	31.06	31.05	0.457	0.434	0.437	0.456	0.460	0.460
60	30.90	29.99	30.41	30.97	31.07	31.07	0.343	0.333	0.338	0.344	0.345	0.345
90	31.02	30.99	31.08	30.90	31.11	31.11	0.230	0.230	0.230	0.229	0.230	0.230
120	30.90	31.08	31.09	30.96	31.08	31.07	0.172	0.173	0.173	0.172	0.173	0.173
150	30.88	31.07	31.01	30.98	31.09	31.11	0.137	0.138	0.138	0.138	0.138	0.138
180	30.80	31.10	31.11	30.90	31.12	31.12	0.114	0.115	0.115	0.114	0.115	0.115
Submergence ratio 130%												
Time, [min]	Normalised distance TD_{50}, x/w [-]						Velocity TD50, [m/s] * 10^{-2}					
	conf. A	conf. B	conf. C	conf. D	conf. E	conf. F	conf. A	conf. B	conf. C	conf. D	conf. E	conf. F
0.1	10.05	10.07	10.22	11.01	10.08	9.96						
5	17.59	21.27	21.46	18.62	18.90	13.98	2.345	2.836	2.861	2.482	2.519	1.863
15	19.55	21.48	21.28	18.99	21.71	19.51	0.869	0.954	0.946	0.844	0.965	0.867
30	19.06	21.64	21.61	19.62	21.03	19.95	0.424	0.481	0.480	0.436	0.467	0.443
45	19.59	21.32	22.12	20.04	21.09	20.44	0.290	0.316	0.328	0.297	0.312	0.303
60	20.03	21.92	21.82	19.96	20.82	20.79	0.223	0.244	0.242	0.222	0.231	0.231
90	19.32	21.98	22.75	19.10	20.76	21.84	0.143	0.163	0.169	0.141	0.154	0.162
120	20.52	22.09	22.62	19.27	20.73	21.12	0.114	0.123	0.126	0.107	0.115	0.117
150	20.32	22.81	22.53	19.38	20.70	21.79	0.090	0.101	0.100	0.086	0.092	0.097
180	20.32	22.81	22.53	19.38	20.77	21.72	0.075	0.084	0.083	0.072	0.077	0.080
Time, [min]	Normalised distance TD_{99}, x/w [-]						Velocity TD_{99}, [m/s] * 10^{-2}					
	conf. A	conf. B	conf. C	conf. D	conf. E	conf. F	conf. A	conf. B	conf. C	conf. D	conf. E	conf. F
0.1	12.91	12.93	13.80	15.65	13.21	12.19						
5	31.09	31.14	31.08	31.14	30.90	26.56	4.145	4.152	4.143	4.151	4.120	3.541
15	31.10	31.05	30.98	31.14	31.14	31.03	1.382	1.380	1.377	1.384	1.384	1.379
30	31.11	31.08	31.11	31.14	31.11	31.09	0.691	0.691	0.691	0.692	0.691	0.691
45	31.09	31.14	31.02	31.13	31.13	31.15	0.461	0.461	0.459	0.461	0.461	0.461
60	31.09	31.07	31.03	31.17	31.15	31.17	0.345	0.345	0.345	0.346	0.346	0.346
90	31.12	30.91	31.13	31.15	31.13	31.17	0.231	0.229	0.231	0.231	0.231	0.231
120	31.12	31.08	31.11	31.14	31.10	31.17	0.173	0.173	0.173	0.173	0.173	0.173
150	31.12	30.64	31.05	31.15	31.11	31.17	0.138	0.136	0.138	0.138	0.138	0.139
180	31.12	30.64	31.05	31.15	31.12	31.17	0.115	0.113	0.115	0.115	0.115	0.115

Table 7.3 – Normalized distances and velocities of travel distance of the center of mass TD_{50} and travel distance of the sediment front TD_{99}, for all the configurations and for a submergence ratio of 100% and 130%. Parallel configurations (A,D,F) are highlighted in gray

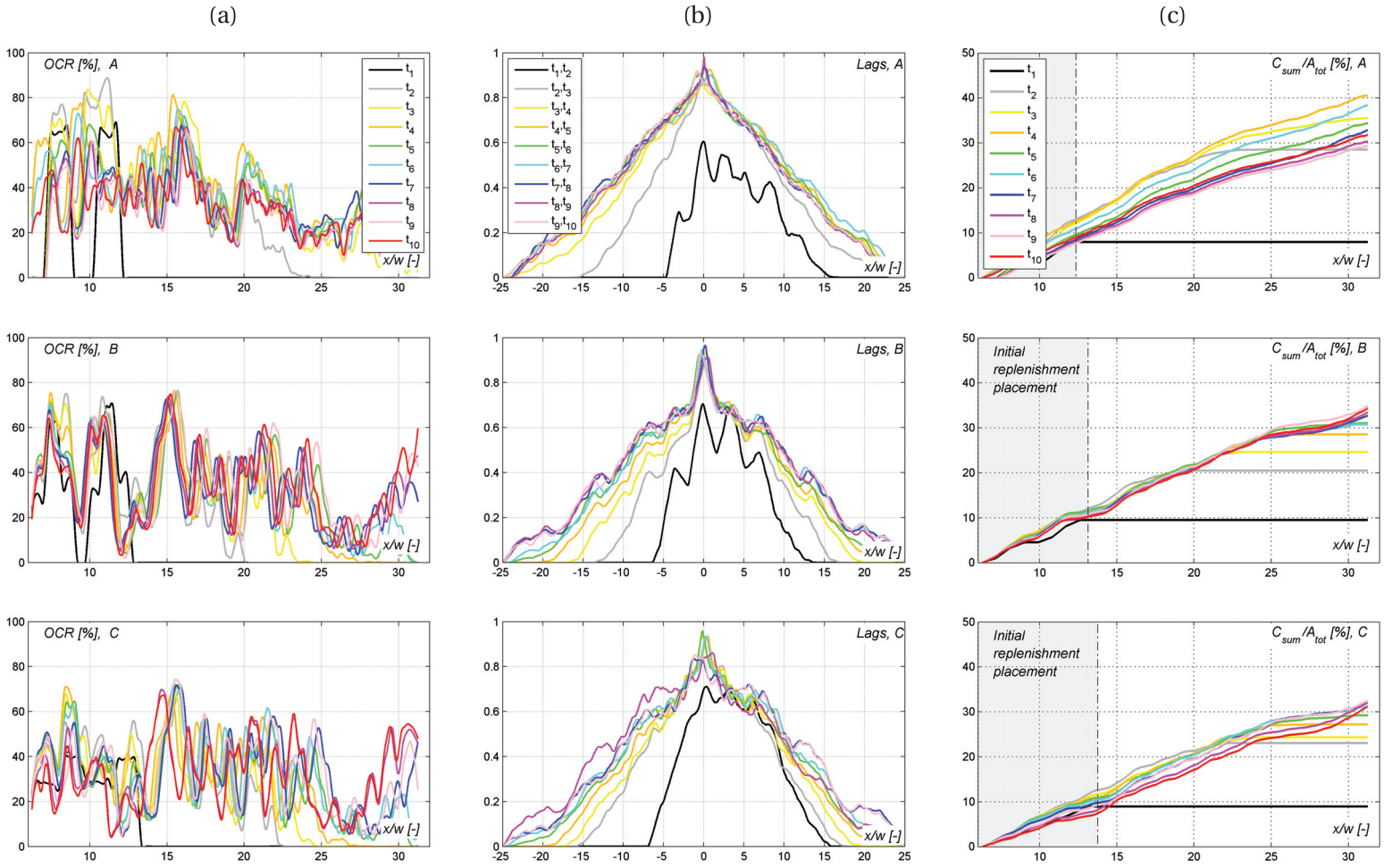

Figure 7.5 – First column (a) Occupation ratio distribution (OCR), Second column (b) temporal evolution of the OCR-distribution correlations, Third column (c) cumulative sum of the OCR-distribution, for configurations A, B and C, and 100% of submergence. Area initially occupied by the replenished deposits in gray

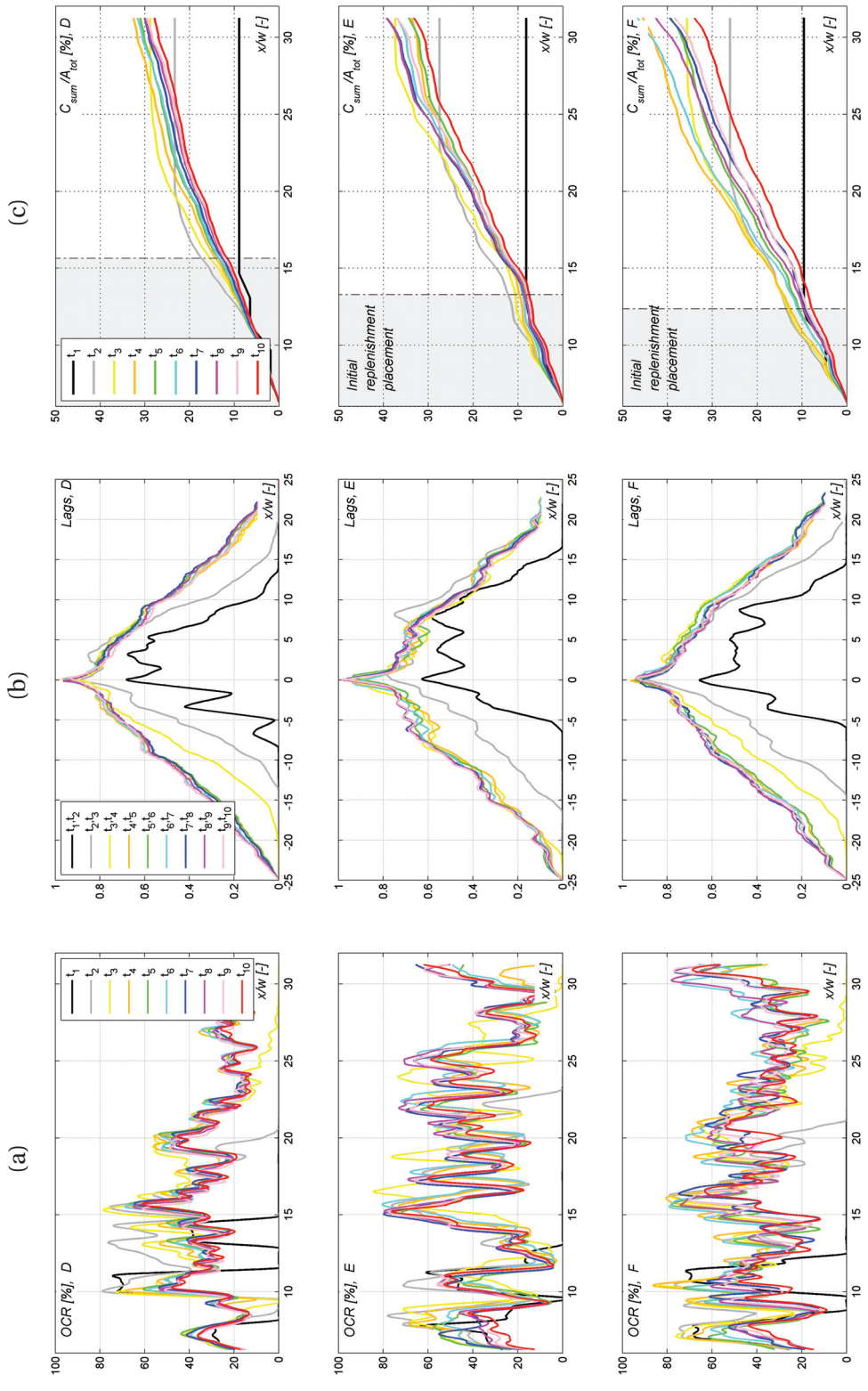

Figure 7.6 – First column (a) Occupation ratio distribution (OCR), Second column (b) temporal evolution of the OCR-distribution correlations, Third column (c) cumulative sum of the OCR-distribution, for configurations D, E and F, and 100% of submergence. Area initially occupied by the replenished deposits in gray

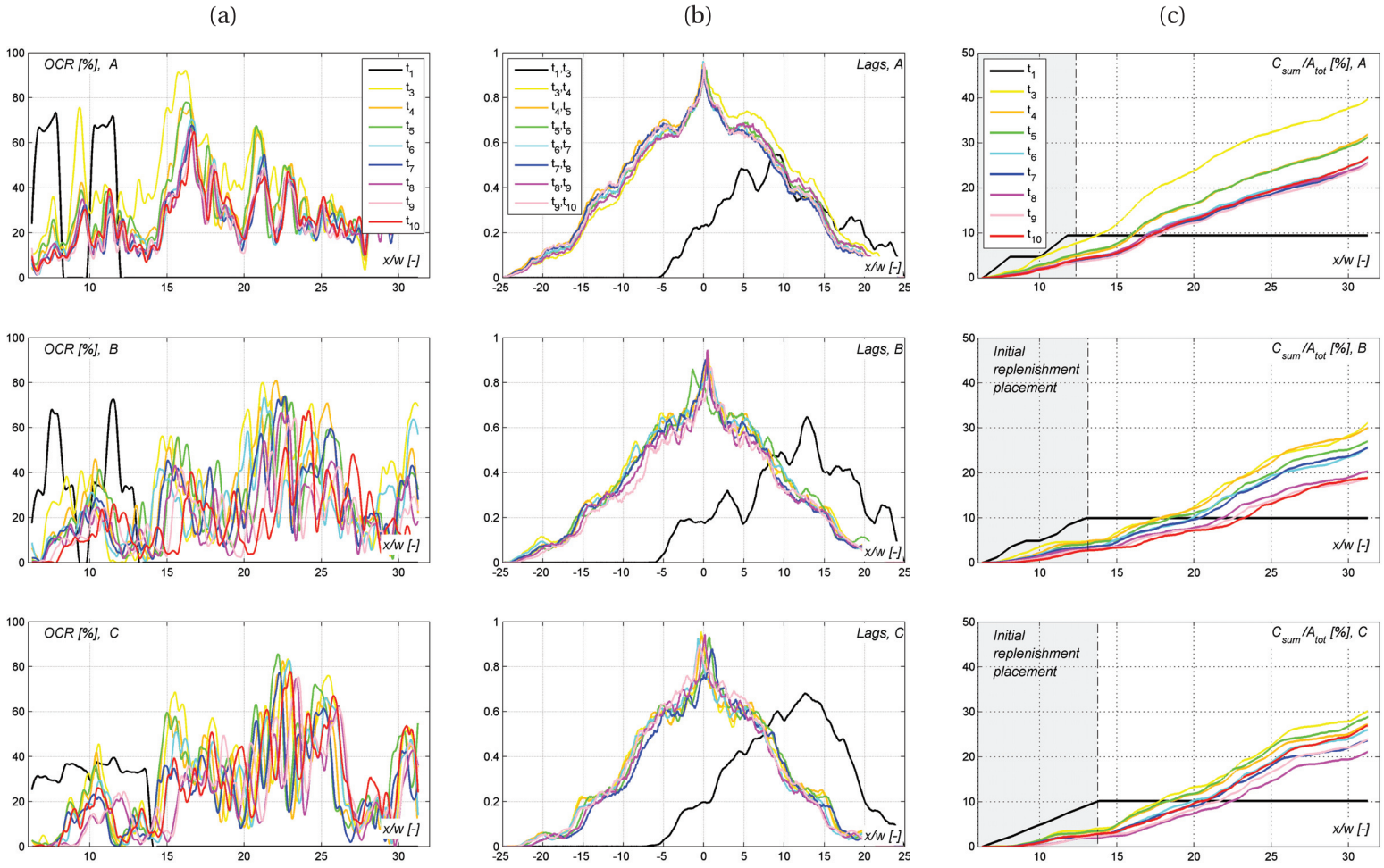

Figure 7.7 – First column (a) Occupation ratio distribution (OCR), Second column (b) temporal evolution of the OCR-distribution correlations, Third column (c) cumulative sum of the OCR-distribution, for configurations A, B and C, and 130% of submergence. Area initially occupied by the replenished deposits in gray

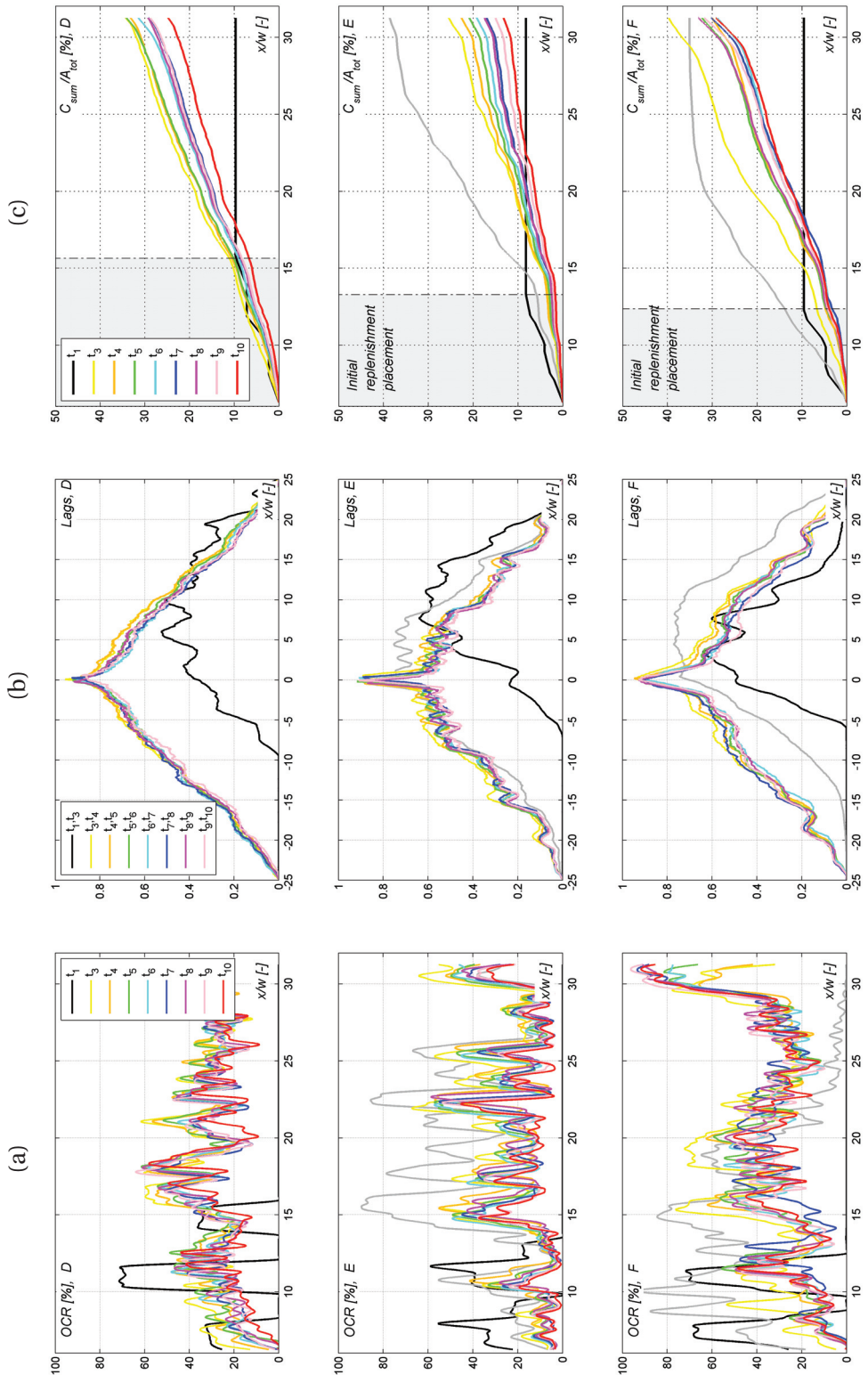

Figure 7.8 – First column (a) Occupation ratio distribution (OCR), Second column (b) temporal evolution of the OCR-distribution correlations, Third column (c) cumulative sum of the OCR-distribution, for configurations D, E and F, and 130% of submergence. Area initially occupied by the replenished deposits in gray

7.3.3 Dispersion and translation

Figure 7.9*a* shows, for a submergence ratio of 100%, the evolution of the location of the center of mass, TD_{50}, against the interquartile length, IQL, both normalized by the channel width. This method was proposed by Sklar et al. (2009). It can be seen that transport is slightly dominated by dispersion in all the experiments. The alternated configurations, B, C and E, move downstream mainly by dispersion. By time, the transport mechanism for alternated configurations evolves from mixed to dispersive dominated. Nevertheless, for configurations B, C and E a component of translation (slope < 0.5) is observed in the last time steps. The remaining configurations, with parallel replenishment volumes, are governed by an intermediate mechanism between translation and dispersion, with a slight preference for translation.

The transport mechanism for a submergence ratio of 130% is shown in Figure 7.9*b*. The erosion process is speed up by the increased flow velocity and the mechanism is purely translation independently of the performed configurations. Nevertheless, parallel configurations (A, D and F) are more close to a mixed transport mechanism.

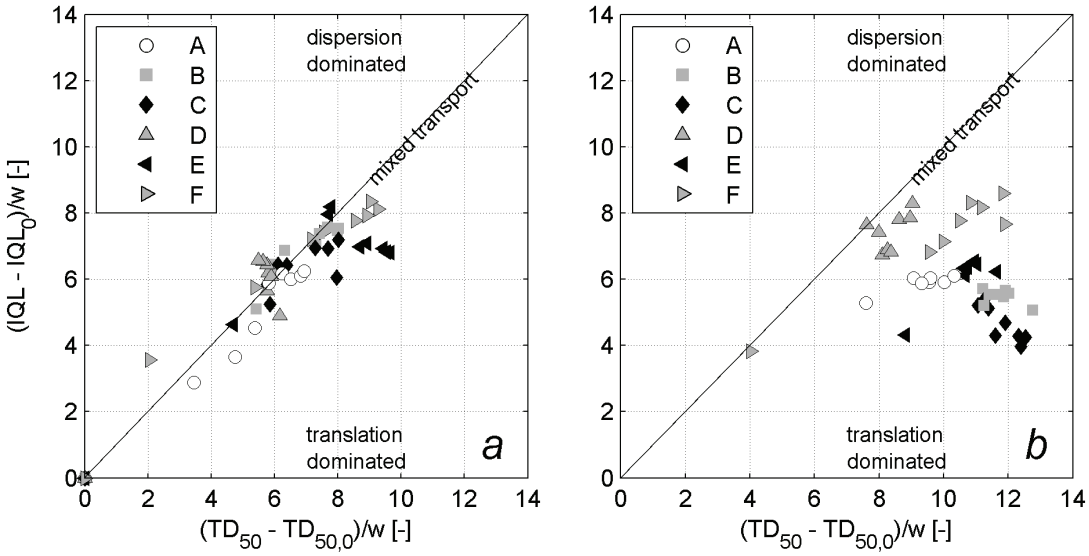

Figure 7.9 – Location of the center of mass (TD_{50}) against the interquantile length (IQL), both normalized by the channel width (w), for a submergence ratio of 100% (a) and 130% (b)

7.4 Discussion

7.4.1 Influence of the submergence ratio in the transport mechanism

The performed replenishment of sediments evolves downstream both by translation and dispersion mechanism of transport. The temporal evolution of the occupation ratio for a submergence ratio of 100% shows all the components of dispersion: attenuation of the peak intensity

in the fix locations, movement downstream of the leading edge and, by consequence, spread of the sediments along the channel. For a submergence ratio of 100%, the erosion occurs at the beginning of the test, while the transport process develops more progressively in time. The transport mechanism changes from dispersion-dominated to translation-dominated in the last phases of test.

Translation is observed for a submergence ratio of 130%. Alternating configurations, especially B and C, lead to a lower spread of the material on channel bed. On the other hand, for the same displacement of center of mass, parallel configurations (D and F) show a bigger spread of grains. The different behaviour is due to the higher flow velocity and transport capacity.

The OCR signals and the correlation functions for both submergence ratios underline two main sediment movement in terms of displaced amount of sediments. A large sediment displacement runs out in the first minutes and it is responsible of the high sediment erosion upstream and the creation of bed form pattern further downstream. The second sediment movement lasts during the whole the test duration, and correspond to the displacement of smaller amount of sediments as shown in the temporal evolution of OCR (see Figures from 7.5 to 7.8). This movement is responsible of depletion of upstream bed forms in favor of increase of the downstream ones in the later states of the test. Nevertheless, the deposition pattern of the replenishment is unaltered during the test duration.

Furthermore, for a constant discharge, a small amount of sediments is continuously moved downstream to fill the less densely covered areas. In agreement with McManamay et al. (2010), flows without high flow variations do not provide changes in the bed shear stress. The herein performed discharges do not allows these bed shear stress variations. Therefore, streambed mobilization is not possible. A constant flow allows only the shift of sediments at areas that have already deposits. Also when applying consecutive replenishments, it was obsreved that the eroded sediments tend to deposit in the same downstream areas occupied by the first replenishment Bösch et al. (2016).

7.4.2 Relation between transport mechanisms and the objectives of river restoration projects

Whether translation- or dispersion-type of transport processes should be favoured, when performing artificial replenishment of sediments into a river reach, depends on the objectives of the restoration project. Our results show that translation transport is associated mainly to high submergence of the replenishment. This situation is more suitable when a longer impact distance is wanted. This may be the case of a restoration project aiming at restore sediment supply at great distances. A submergence ratio of 100% of the replenishment favours a shorter distance effect but more persistent in time.

The bed form pattern created by either parallel or alternated configurations of the replenishment deposits may also be a criteria of choice in the aim of the project. Parallel configurations

of replenishment volume behave like a single mass moving downstream, with a more chaotic distribution of grains on the channel bed. The movement downstream for alternated configurations enhances the formation of more pronounced alternate bars, leading to a more natural morphological aspect. Alternated configurations might be preferred instead of parallel in order to obtain a clearer bed pattern and slower diffusion of the grains towards downstream. Nevertheless, the geometrical configuration of the replenishment volumes plays a marginal role compared to the submergence ratio.

Sediment replenishment volumes, finer than the pre-existing bed, lead to a wide bed surface fining and to a re-mobilization of part of the armoured bed since they are able to percolate through (Frey and Church, 2009; Venditti et al., 2010). This bed refinement also conditions the downstream transport of sediment by the creation of flow corridors with higher transport capacity (Juez et al., 2016).

The use of a constant discharge corresponds to a single flood event of a duration of nine hours in prototype, considering Froude scale transformation and a geometrical scale factor of 1:10. This single event might be quite far from a real application. Nevertheless, as mentioned in Battisacco et al. (2016), the test duration guarantees the achievement of an equilibrium state for the morphological bed forms.

For a submergence ratio of 130%, the length of the experimental channel may be a limitation for the present study, especially considering the distance travelled by the grains. For these flow conditions, a portion of the replenishment material went out of the channel. Therefore, it was not possible to observe if the grain deposition patterns followed the same trend further downstream.

7.5 Conclusions

The transport mechanisms of multiple sediment replenishment volumes are studied by a series of laboratory experiments for two submergence ratios and six geometrical configurations of the deposits.

The replenishment volumes are eroded rapidly in the first minutes and the grains distribution along the downstream reach is maintained stable for the remaining test duration with small changes. Two velocities of movement can, thus, being seen. The first is responsible of the initial sediment movement, while the second sediment displacement is responsible of the depletion of the bed forms upstream for the increase of those more downstream.

Regardless the geometrical configuration of the replenishment volumes, the mechanism is mainly dispersive when the replenished deposits are subjected to a complete submergence. By the spatial and temporal analysis of sediments distribution, it is observed that the grains, when transported downstream, deposit following a clear pattern. These patterns keep their positions along the channel, but reduce their amplitude with time due to sediment depletion.

With higher submergence ratio, the flow velocity and transport capacity are higher, and in these flow conditions the transport mechanism is more of the translational type. The main erosion phase and the longest movement of grains occur in the first minutes, while then the distribution of grains attains an equilibrium in terms of occupied areas.

The dispersive mechanism leads to more stable bed forms and more important morphological changes. The aquatic fauna and flora may find benefits by the restoration of a stable bed pattern, where spawning habitats can be created by fishes since different flow conditions, in terms of velocity and bed shear stress, are enhanced. The thickness of these bed forms is equal to three to five times the median diameter of the replenished material. Thus, considering the applied geometrical scale factor, enough for being new spawning ground areas for fishes.

A translation-type transport mechanism of sediment replenishment requires a shorter flow release, i.e. artificial flood, and the effects are distributed farer downstream the river reach. These conditions are suitable for the operational and economical points of view. Indeed, minimizing the released amount of water and the time required for the operation are aspects to be considered in field applications. Furthermore, the translation behaviour permits to affect longer distances, thus, allowing to overcome problems of reaches difficult to be affected by the replenishment deposits.

8 Transient flows released on sediment deposits

8.1 Introduction

Previous tests showed that when placing multiple replenishment deposits on both banks of the flume in alternating configuration, a complete material erosion is achieved. The succession of narrower and larger sections due to the geometrical configuration establishes hydraulic forces able to erode and transport all the material, as described in Chapter 4. These results were obtained using a constant discharge on the flume, corresponding to a complete volume submergence (water depth = replenishment height). These may not be really representative of the hydraulic conditions during an artificial flood release. Thus, a series of experiments was run using a triangular shaped hydrographs. Recently, Humphries et al. (2012) and Mao (2012) studied the morphological response of a channel reach to a hydrograph with constant sediment feeding from upstream. Therefore, both studies cannot be directly related to sediment replenishment in armoured bed. Mao (2012) investigated the sediment transport rate and grain size for a continuous feed channel and different hydrograph, whereas Humphries et al. (2012) compared the effect of a sediment replenishment impacted by a constant discharge with the effects due to a hydrograph. In line with these studies, this Chapter aims at investigating the influence of hydrographs with different rising and falling limb slopes applied on alternated replenishment configurations. The hydrographs are comparable to the complete submergence case by the same total bed shear stress performed on the entire test duration. The results in Chapter 4 indicate that sediment replenishment deposits placed in an alternating configurations are completely eroded by a complete submergence and they develop morphological bed forms on the downstream reach. In light of the use of sediment replenishment as a tool for restoring morphological variability in dam affected reach, these configurations are here considered for evaluating the influence of the hydrograph.

8.2 Methods

8.2.1 Experimental setup and data acquisition

Detailed information on the flume facility are available in Section 3.1.1. Two alternating configurations, B and C, are tested with the transient flows. Figure 8.1 shows the flume installation with the replenished volumes forming the two alternating configurations.

The available data set are pictures and laser scanner. The instrumentation is mounted on a moveable structure on longitudinal and cross sectional directions (Figure 8.2). All the information related to experimental facility and data acquisition procedure are presented in Chapter 3. A summary of the data available for all the performed tests are provided in Table 8.1. The analysis is undertaken on the area of interest (A_{oi}) defined as the channel bed surface (channel width, 0.4 m, times observation length, 10.0 m). The Otsu's method (Otsu, 1979) is used to converted the image into binary metrics. The data analysis is performed on the binary picture.

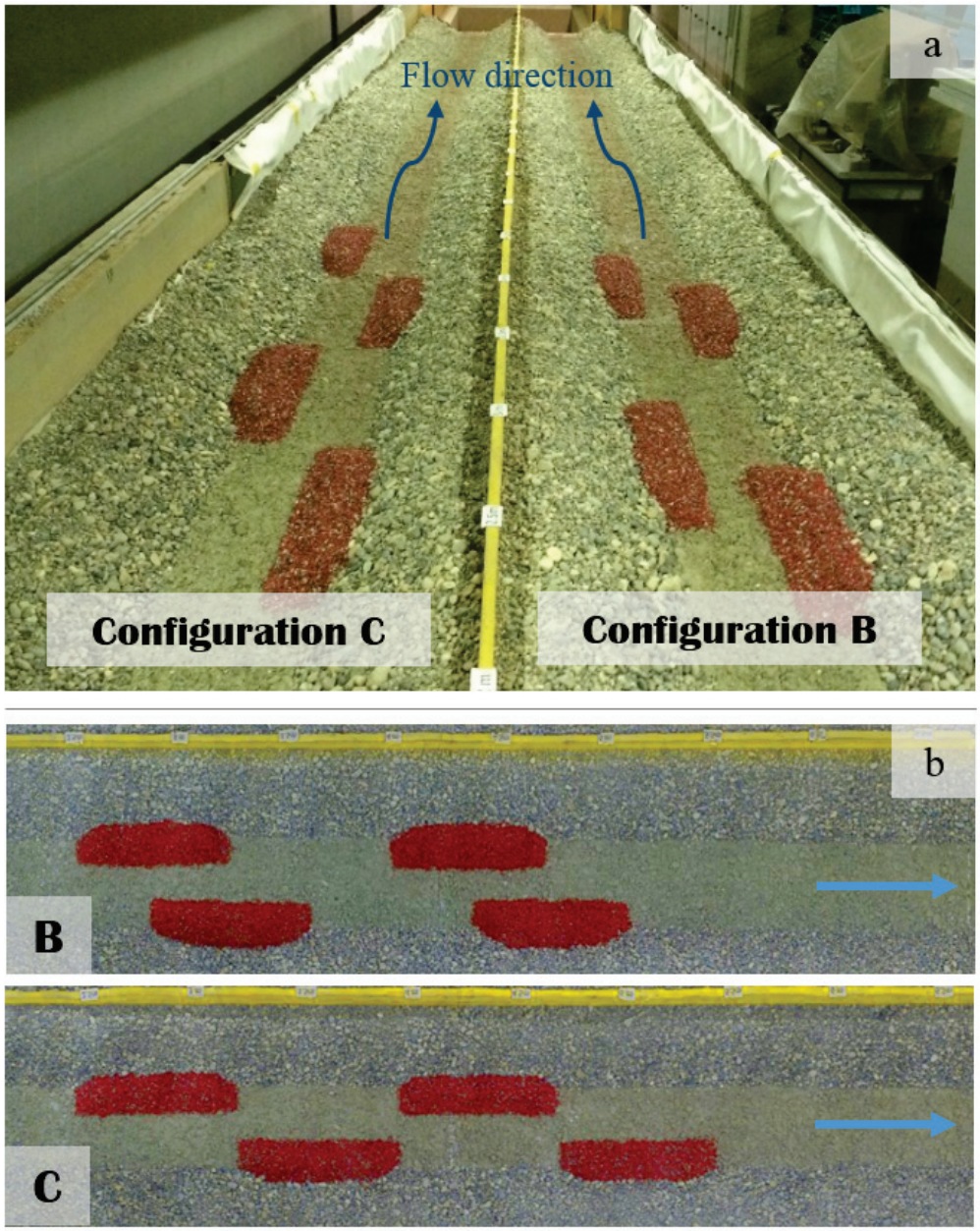

Figure 8.1 – (a) Flume channel with implemented sediment replenishment, (b) Sediment replenishment configurations (B and C) and their dimensions

Figure 8.2 – Flume installation: (a) instrumentation mounted on carriage and (b) view of the channel from the downstream end

8.2.2 Tested configurations and hydrographs

The channel response to the sediment replenishment is tested with both constant and transient discharge. A constant discharge with complete submergence of the replenishment volumes proofed to be an adequate condition for the erosion of the volumes and the creation of morphological bed forms downstream (see Chapter 4).

In addition, four triangular-shaped hydrographs were tested. The hydrographs have the same peak discharge, but different rising and falling limb slopes (Figure 8.3*a*).

The test duration is equal to 180 minutes for all the performed tests. The peaks of discharge occur respectively at 20, 45, 90 and 160 minutes from the beginning of the experiment. Different time steps are shown for each performed cases, with higher frequency close to the passage of the discharge peak. In the following data analysis the above mentioned hydrographs are recalled: H_1, H_2, H_3, H_4 and H_c (Table 8.1).

Table 8.1 – Conditions of the tests for configuration B and C. The discharge is indicated as Q in $[m^3/s]$. Peak indicates the time needed for reaching the discharge peak. Time step indicates the timing of pictures

Discharge	Name	Peak [min]	Max Q $[m^3/s]$	Time step [min]
Variable	H_1	20	30	0, 10, 20, 30, 45, 60, 90, 120, 150, 180
Variable	H_2	45	30	0, 10, 20, 30, 45, 60, 90, 120, 150, 180
Variable	H_3	90	30	0, 10, 20, 45, 60, 70, 90, 105, 120, 150, 180
Variable	H_4	160	30	0, 30, 60, 90, 105, 120, 135, 150, 165, 180
Constant	H_c	-	19	0, 5, 15, 30, 45, 60, 90, 120, 150, 180

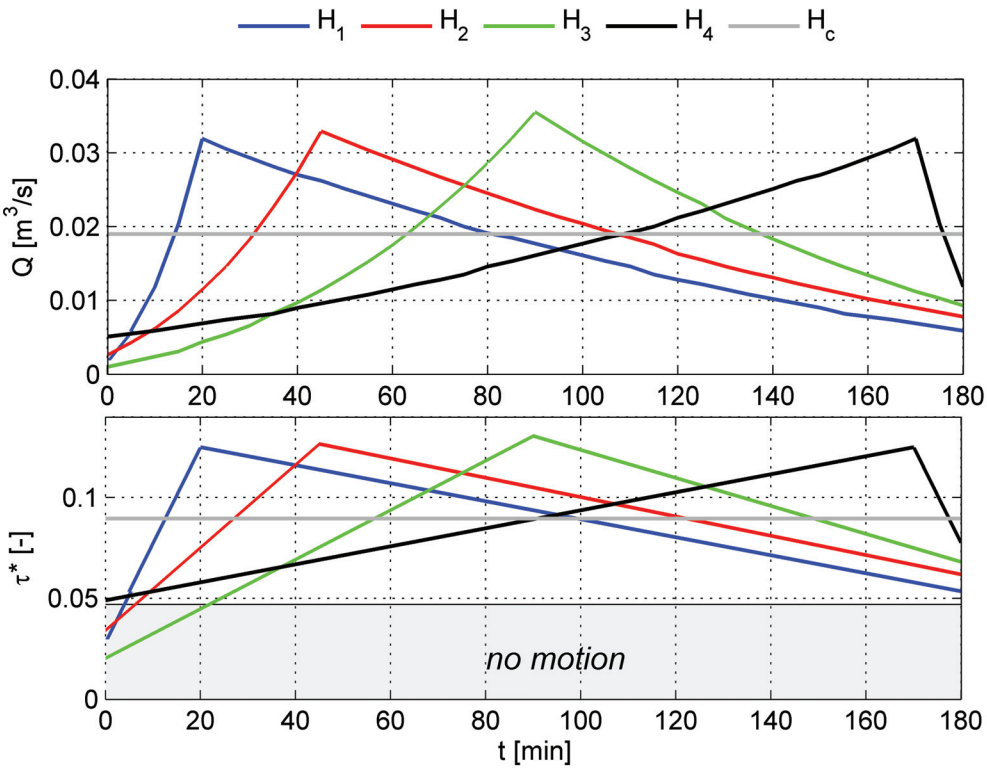

Figure 8.3 – (a) Designed discharge: constant discharge and hydrographs, (b) Dimensionless bed shear stress for the designed discharges and threshold of movement

These hydrographs are divided in steep and mild configuration. H_1 and H_2 belong to the first group, which have steeper rising limb than falling one. Following the same criteria, H_3 and H_4 are defined as mild hydrographs. The hydrographs have been defined in a way that the constant discharge and transient flow create the same total bed shear stress integrated in three hours testing (Figure 8.3*b*).

The definition of bed shear stress, τ_0, and dimensionless bed shear stress, τ^*, are provided in Section 2.1. A dimensionless time is used in the following plots considering the constant discharge case with complete submergence as reference. The dimensionless time, $Time^*$, is defined as the time needed by the uniform flow (at the uniform flow velocity, $v_{m,100}$ for 100% submergence) to run throughout the observation length, L (equal to 10 m) (see Section 3.1.3).

$$Time^*[-] = \frac{t}{L/v_{m,100}} \tag{8.1}$$

8.2.3 Analysed indicators

The indicators listed below describe the channel response to both a constant and a transient flow in terms of morphological bed forms, bed fining and transport distance. A complete description of the analysed parameters is provided in Section 3.3. The herein computed parameters are listed:

Persistence	PD	%
Covered surface	CS	%
Compactness of covered surface	NDC	%
Occupation rate	OCR	%
Power Spectrum Density of OCR signal	PSD	db
Bed roughness	Ks	$m^{1/3}/s$
Volume of deposition		mm^3

8.3 Results

8.3.1 Visual analysis of the response of bed morphology on transient and constant flow

Figures 8.4 and 8.5 show the replenished material distribution for configuration B at 30, 60, 120 and 180 minutes from the test beginning (20 minutes for H_3) for transient and constant discharge tests. At 30 minutes from the test begin the discharge peak has already passed for the test with hydrograph H_1, whereas for all the remaining case the discharge is still increasing. In the case of H_1, the replenishment volumes are almost completely eroded at this time step and only a few grains remain in the original positions. The replenishment material has already reached the channel end section and a continuous reduction of the initial replenishment volume is occurring. For the other transient flows, the more upstream volumes are almost unaltered by the flow, while the downstream deposits have suffered from erosion.

The erosion process has started from the downstream tail of the replenishment deposits where the transport capacity is higher due to the section narrowing. On the other hand, a constant discharge, with a submergence ratio of 100%, after 30 minutes from the test begin has eroded and transported the most downstream deposits almost 10 times their lengths toward the channel. Furthermore, a bed morphological pattern has already started to develop on the channel bed. The material is deposited with a clear pattern on the whole channel bed. The bed morphology is slightly modified between the two time steps at 120 and 180 minutes, meaning that an equilibrium state in terms of erosion and transport of replenished material is reached in the meanwhile.

For the transient flows, at the test end, the deposits are completely eroded and the material is spread on the whole channel bed. Part of the replenished material went out from the observation reach and the available material on channel is, thus, reduced. Nevertheless, a bed

morphological pattern is created on the channel bed.

In Figures 8.6 and 8.7, the temporal evolution for configuration C for the same time steps are plotted. For the transient flows, after 30 minutes from the beginning of the test, the initial volume shapes are slightly modified. It can be seen that the erosion starts from the more downstream deposits, while the more upstream do not suffer from any erosion. For the constant flow, three over four deposits are almost completely eroded and the process is taking place on the most upstream replenishment. Nevertheless, the bed morphology presents slight differences between this time step and the final state.

At the test end, the replenished volumes are totally eroded for all the cases. The amount of sediment remaining in the channel reach varies depending on the applied hydrograph. The portion of replenished material going out from the channel reach increases as the duration of the hydrograph rising limb becomes longer. For H_4, when the discharge peak occurs most of the replenished material has already exited the observation channel. As mentioned in Chapter 3, the observation length is defined as the undisturbed length on channel, thus excluding the upstream and downstream 2.5 m.

The erosion and transport processes behave similarly for configurations B and C. For both configurations morphological bed forms are created.

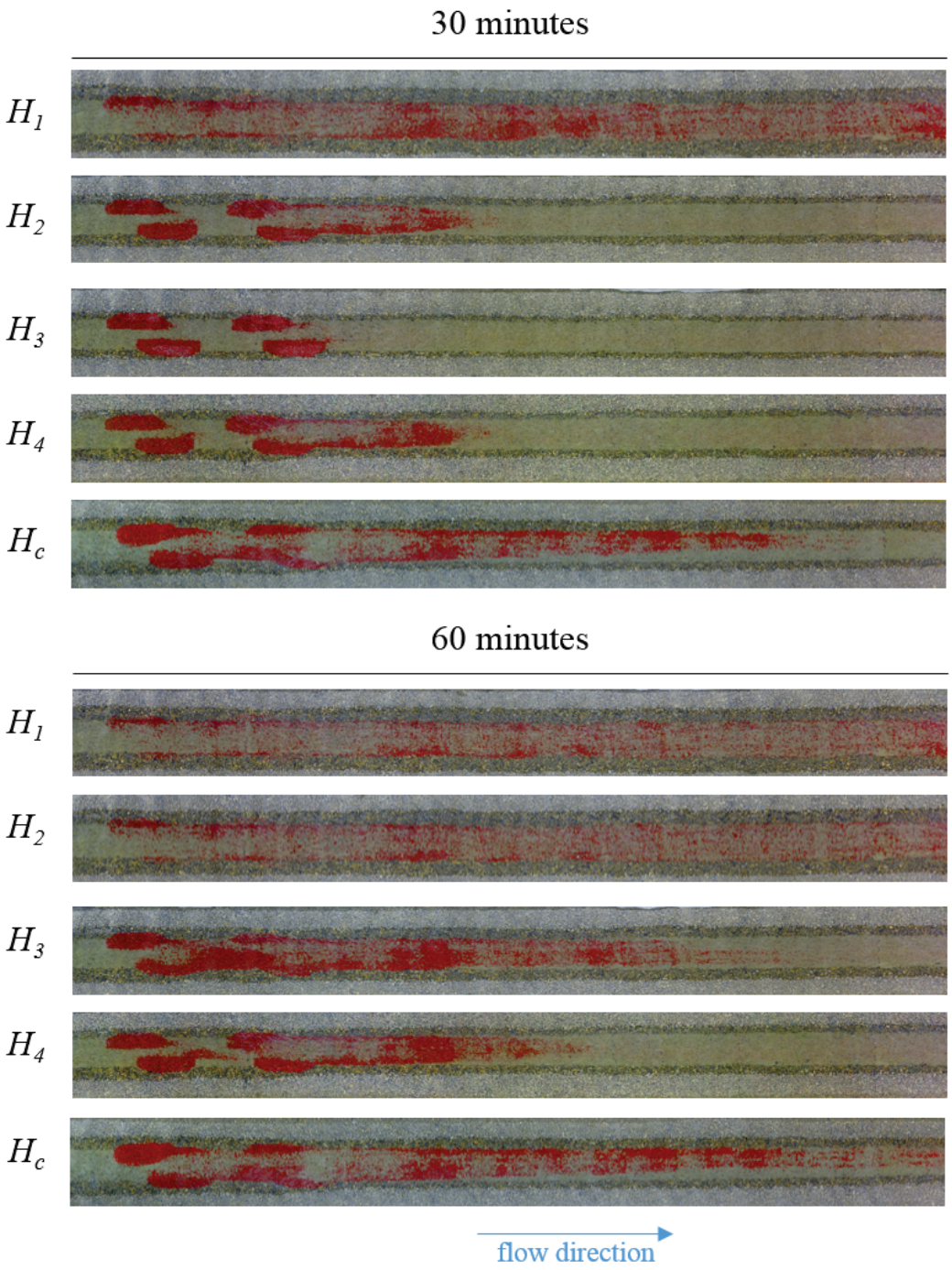

Figure 8.4 – Temporal evolution of the erosion and transport of replenished material by picture records for configuration B, for all tested flow conditions at 30 and 60 minutes from the test begin

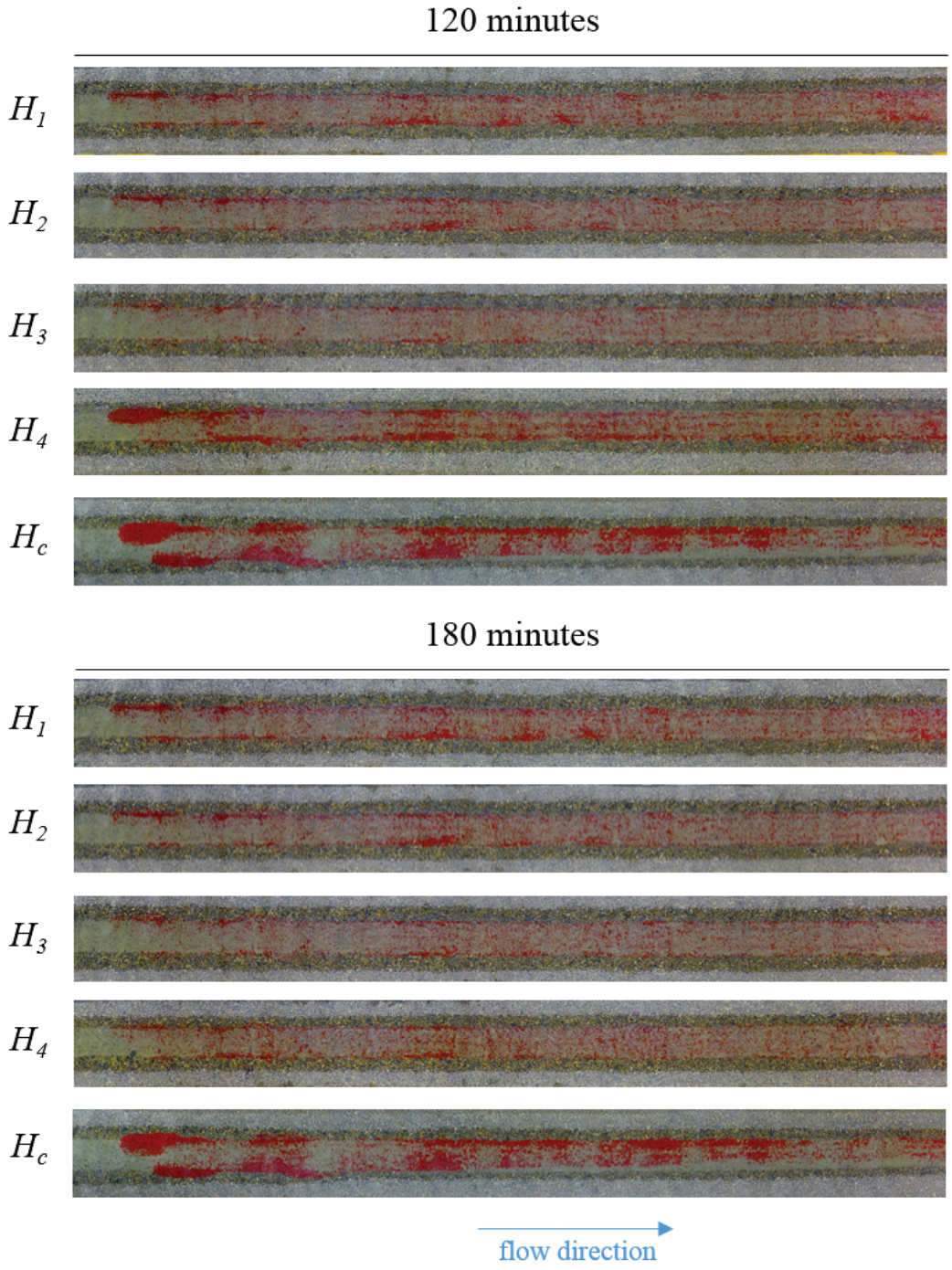

Figure 8.5 – Temporal evolution of the erosion and transport of replenished material by picture records for configuration B, for all tested flow conditions at 120 and 180 minutes from the test begin

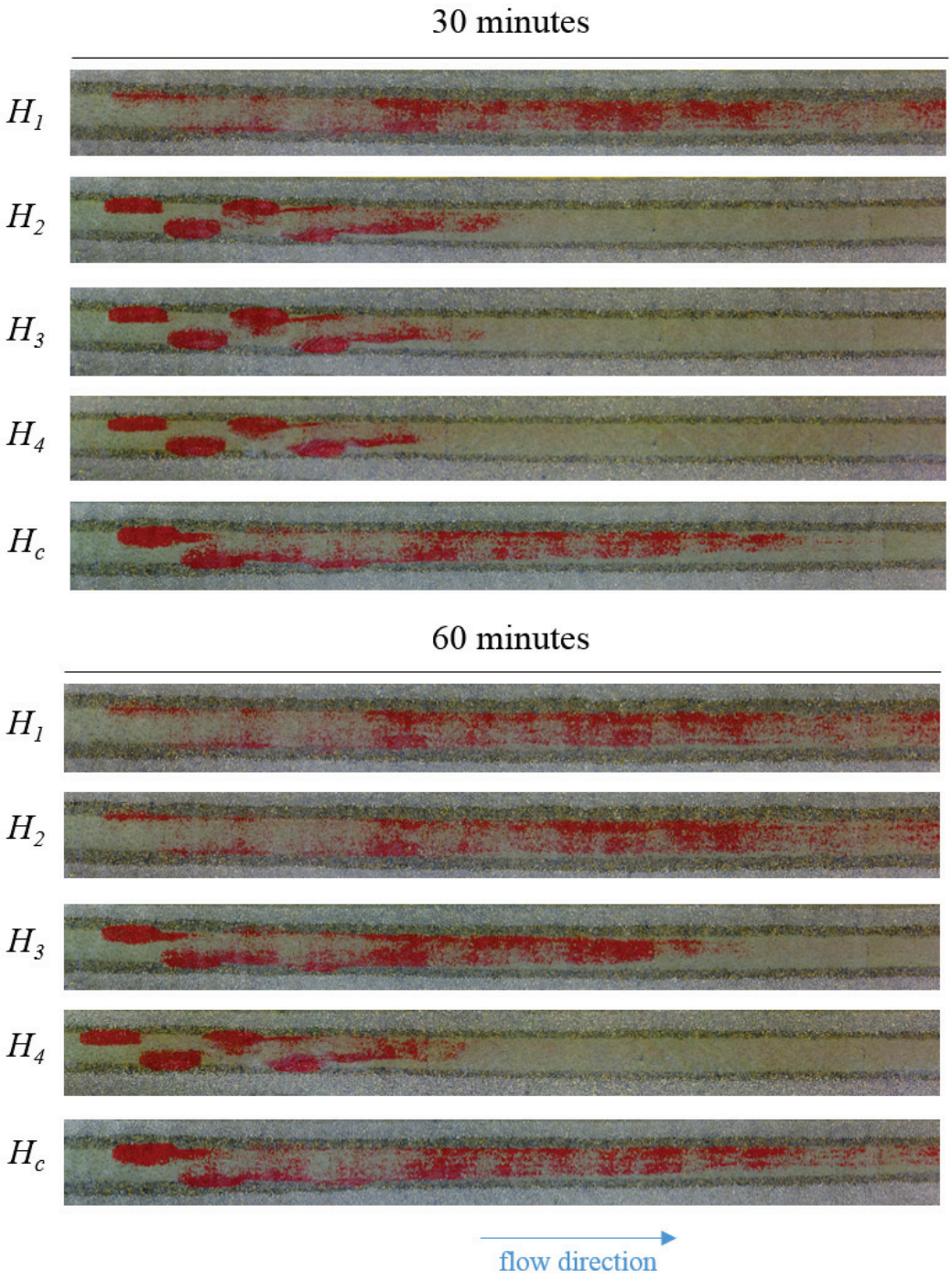

Figure 8.6 – Temporal evolution of the erosion and transport of replenished material by picture records for configuration C, for all tested flow conditions at 30 and 60 minutes from the test begin

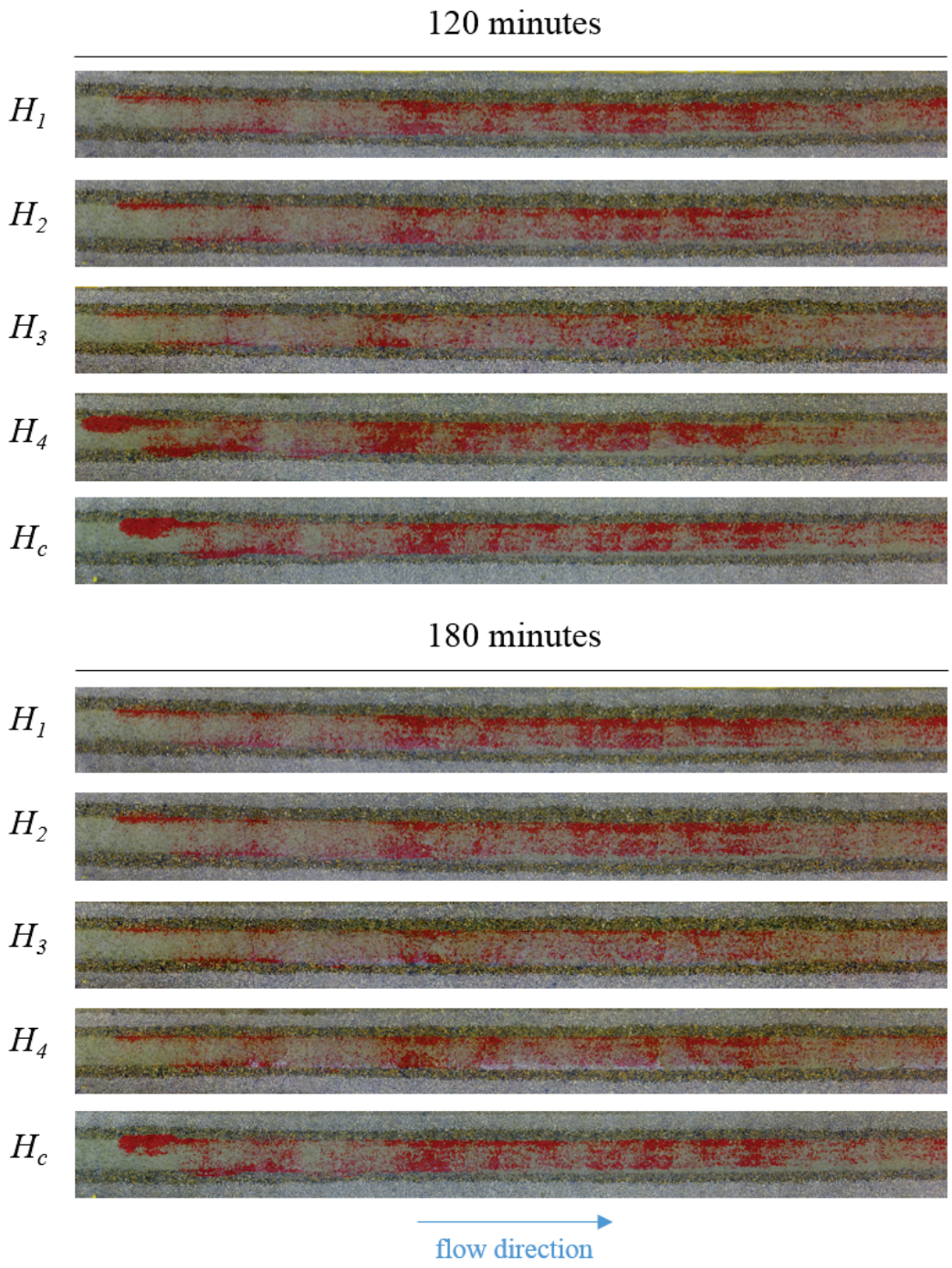

Figure 8.7 – Temporal evolution of the erosion and transport of replenished material by picture records for configuration C, for all tested flow conditions at 120 and 180 minutes from the test begin

8.3.2 Temporal distribution of sediment replenishment material on channel bed

In Figure 8.8 the temporal evolution of the covered surface CS for the transient flow cases is plotted as a function of the dimensionless time, $Time^*$, and the dimensionless bed shear stress τ^*.

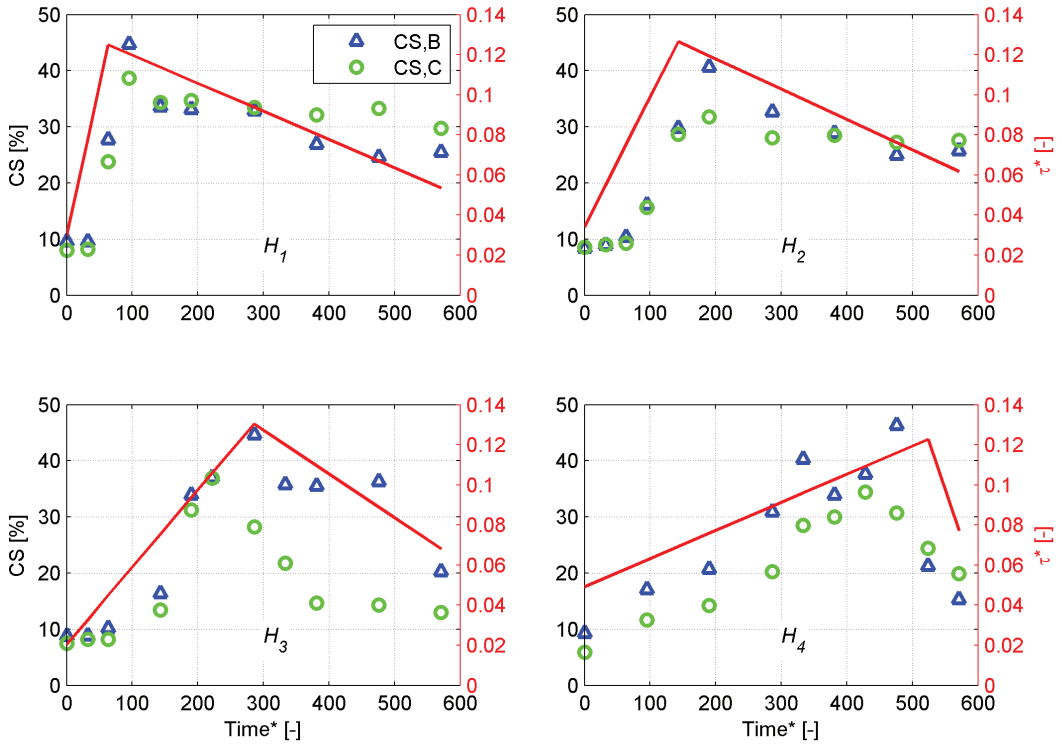

Figure 8.8 – Temporal evolution of covered surface CS as function of the dimensionless time $Time^*$ and the dimensionless bed shear stress $\tau*$

The CS distribution varies with the steepness of the rising limb. For steep rising limbs, as H_1 and H_2, the CS has a peak between 100 and 200 $Time^*$ after the discharge peak. For H_4, considered as a mild hydrograph, the CS maximum is attained before the discharge peak (corresponding to the maximum value of τ^*), whereas H_3 reaches the maximum of CS almost in correspondence with the discharge peak. In all the performed cases, configuration B shows higher maximum values of CS than configuration C, reaching 47% for H_4. After the discharge peak, the CS tends to an equilibrium state with smaller variations in time for both configurations H_1 and H_4. For a steep rising limb (H_1 and H_2), the maximum CS value drops respectively about 20% and 10% for configurations B and C at the test end. For H_3 and H_4, the CS diminishes of 30% for configuration B and 20% for configuration C. Most of the replenished material is washed out from the observation length once the discharge decreases, especially for steep hydrographs when a parallel volume geometry (configuration B) is placed in the channel. The remaining material in the observation stretch for configuration C is bigger (Table

8.2).

Table 8.2 – Main results in terms of persistence (PD), covered surface (CS) and compactness of covered surface (NDC) for all configurations. The subscript $zero$ indicates the values at the initial state and $3h$ stays for the value at the end of the test

Test	Conf	Peak	Placed	Washed sediment	PD	CS_0 initial	CS_{3h} 3h	NDC_0 initial	NDC_{3h} 3h
		min	Kg	Kg	%	%	%	%	%
39	B, H_1	20	23.2	15.3	34.1	9.6	25.5	0.93	0.59
41	B, H_2	45	23.0	9.6	58	8.4	25.7	0.89	0.66
43	B, H_3	90	29.9	11.7	60.8	8.7	20.2	0.90	0.62
45	B, H_4	160	23.8	14.7	38.2	9.3	15.3	0.90	0.53
19	B, H_c	-	27.0	0.1	99.8	9.4	37.5	0.97	0.86
40	C, H_1	20	24.6	3.6	98.5	8.0	29.7	0.90	0.73
42	C, H_2	45	23.2	4.1	82.2	8.5	27.6	0.87	0.74
44	C, H_3	90	23.9	9.0	62.2	7.5	13.0	0.89	0.57
46	C, H_4	160	22.0	9.8	55.6	5.9	19.9	0.87	0.67
20	C, H_c	-	27.0	0.2	99.3	9.2	36.2	0.97	0.86

The hydrographs lead to a higher spread and transport of the replenished material compared to the constant discharge case, as described in Chapter 4. For a submergence ratio of 100%, constant during the test duration, the erosion of the replenished material occurs in the first 50 $Time^*$ of testing, for later approaching an equilibrium state. The CS for configurations B and C are about 35% at the equilibrium state.

The occupation of the channel bed by the replenished material is evaluated also in terms of compactness NDC of the covered surface. Table 8.2 presents the initial and final values of CS and NDC for all the performed cases. As highlighted from Figures 8.4 to 8.7, the bed forms at the test end are more evident for cases performed with a constant discharge than with any transient flows. Nevertheless, configuration C leads to more compact bed morphological shapes with maximum values obtained for steep rising hydrographs (H_1 and H_2). For configuration B, the lowest NDC corresponds to the longest rising limb H_4. In this case, a high portion of replenished material was transported out from the observation reach.

Figure 8.9 presents a phase plot with the covered surface CS against the dimensionless bed shear stress τ^*. For each transient flow case, configurations B and C behave similarly. For steep rising limb, H_1 and H_2, the final CS value is higher than the initial state. This corresponds to a global bed fining on the channel bed. For these cases, a counterclockwise behaviour can be seen for the covered surface CS.

On the other hand, the CS for H_3 attends the maximum value almost simultaneously to the discharge peak. The final CS value for H_3 is close to the initial condition for both configura-

tions, with a slight better performance of configuration B. Therefore, it can be assumed that the sediment replenishment has a minor effect on the channel bed (Figure 8.9). Differently from the other cases, the maximum CS is achieved before the bed shear stress peak for the mildest hydrograph H_4.

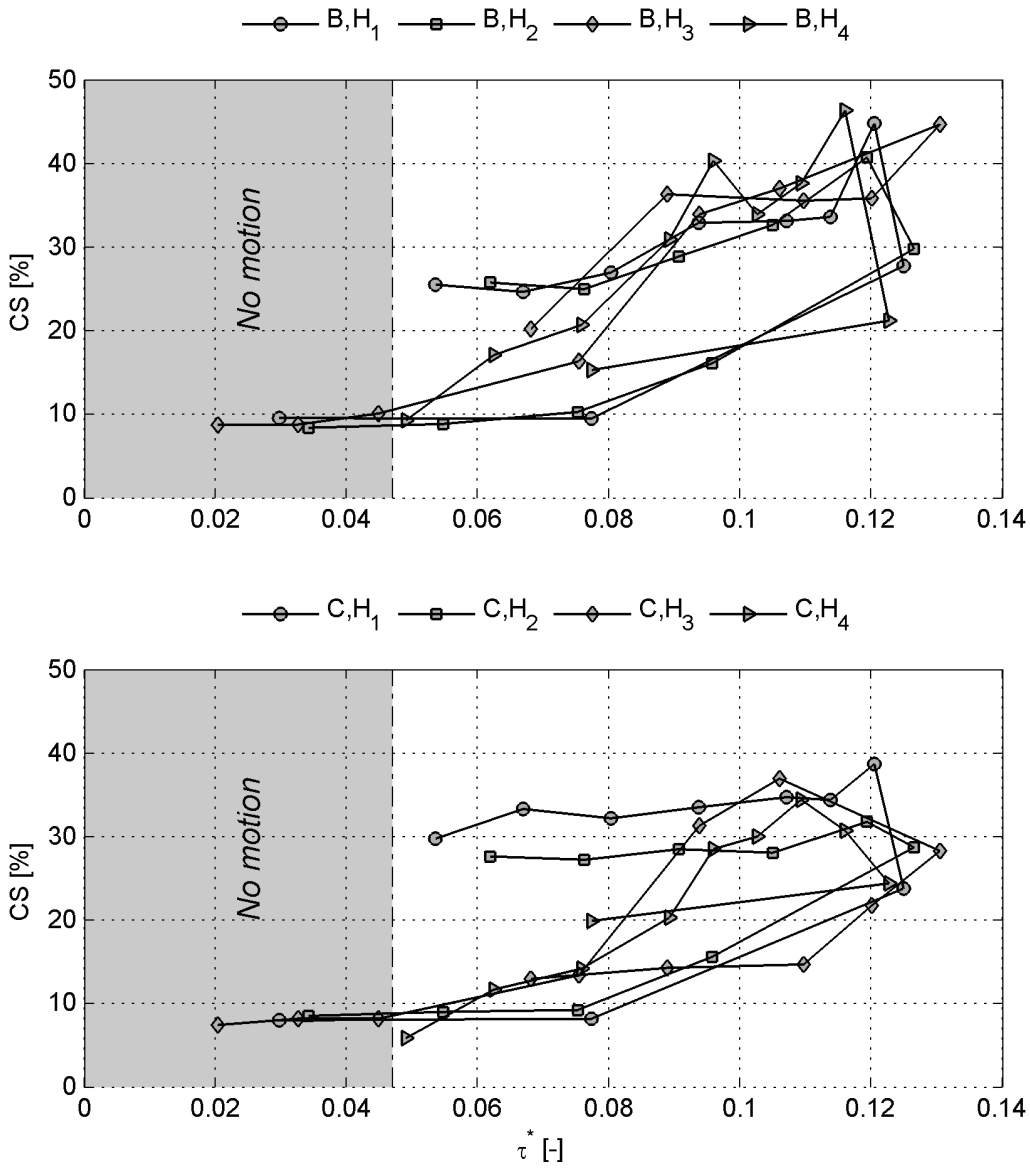

Figure 8.9 – Covered surface (CS) plotted versus the dimensionless bed shear stress ($\tau*$) for configuration B (a) and C (b), and all the flow conditions

8.3.3 Bed roughness and deposition depth

The standard deviation $STDV$ of bed elevation variations can be used to state the morphological changes occurred on the bed channel (Coleman et al., 2011). Table 8.3 plots the values of $STDV$ before and after the replenishment for the performed experiments.

Table 8.3 – Standard deviation of bed elevation changes for configuration B and C. The data are provided by the laser measurements. * = (final- initial)/initial

Test	Configuration	STDV		Relative
		initial	final	increase*
		[mm]	[mm]	[%]
B	H_1	11.98	6.44	-46
B	H_2	11.62	5.92	-49
B	H_3	11.65	5.69	-51
B	H_4	11.65	6.37	-45
B	H_c	12.59	6.89	-45
C	H_1	12.00	7.19	-40
C	H_2	12.21	7.24	-41
C	H_3	12.14	7.13	-41
C	H_4	12.07	6.80	-44
C	H_c	12.22	7.01	-43

The bed fining provided by configuration B is slightly higher than configuration C. Configuration B leads to a wide spread of the material on the channel bed, due to the geometrical placement of volumes. On the other hand, the flow is initially guided towards the replenishment volumes for configuration C. Thus, the transported material has a bigger tendency to group in bed forms.

The general reduction of channel bed surface roughness reaches the 51% for H_3 for configuration B. However, it should be remembered that a consistent portion of replenished material went out from the observation reach for the long rising limb test (H_4).

8.3.4 Comparison of volumes between constant discharge and hydrograph

The needed water volumes for obtaining the maximum values of covered surface CS are illustrated in Figures 8.10 and 8.11. The maximum volume is required by the constant discharge. In Chapter 4 it is stated that after two hours of test, an equilibrium state in terms of CS. This released volume is used as reference case against the hydrograph volumes. The H_1 requires the 21% of the flow volume needed for the constant discharge case, while for H_2, H_3 and H_4 respectively the 39%, 47% and 74% are necessary for configuration B.

Table 8.4 – Maximum covered surface CS values and required time for achieving it with related released water volume. The ratio is calculated between constant discharge and transient flow volumes

Test	Conf	CS		Volume	Ratio
		max	time		
		[%]	[min]	$[m^3]$	[%]
B	H_1	45	30	35.4	21
B	H_2	41	60	66.2	39
B	H_3	45	90	81.0	47
B	H_4	46	150	126.6	74
B	H_c	35	150	171	100
C	H_1	39	30	35.4	26
C	H_2	32	60	66.2	48
C	H_3	37	70	48.5	35
C	H_4	34	135	102.5	75
C	H_c	34	120	137	100

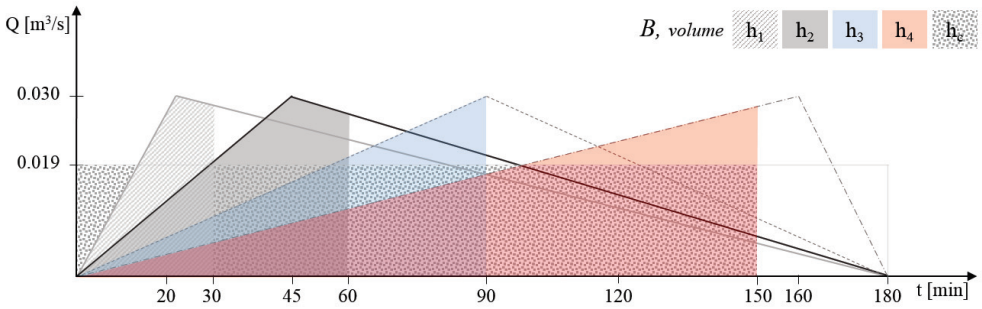

Figure 8.10 – Schematic representation of the required flow volume for achieving the maximum of covered surface (CS) for configuration B, for all the flow conditions

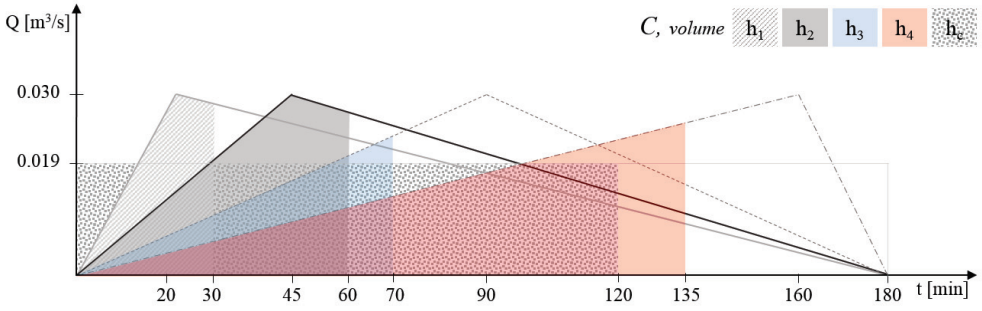

Figure 8.11 – Schematic representation of the required flow volume for achieving the maximum of covered surface (CS) for configuration C, for all the flow conditions

8.3.5 Power spectral density of OCR-signal

Deposition patterns of the replenished material along the channel reach are visible from Figures 8.4 to 8.7. The wavelength of these bed forms is derived by the power spectral density analysis (PSD). Figure 8.12 shows the PSD for the tested cases.

Considering the constant flow case, both configurations have frequency peak at a wavelength of 1.7*w. When using a transient flow, the frequency peak for configuration B moves from 1.7 to 2.2 times the channel width w. The peak intensity is higher for H_1 and H_2, while for H_3 and H_4 the peak is much smother. For configuration C, the wavelength is constant, equal to 1.7*w independently from the performed case. The morphological bed forms are more evident for this configuration.

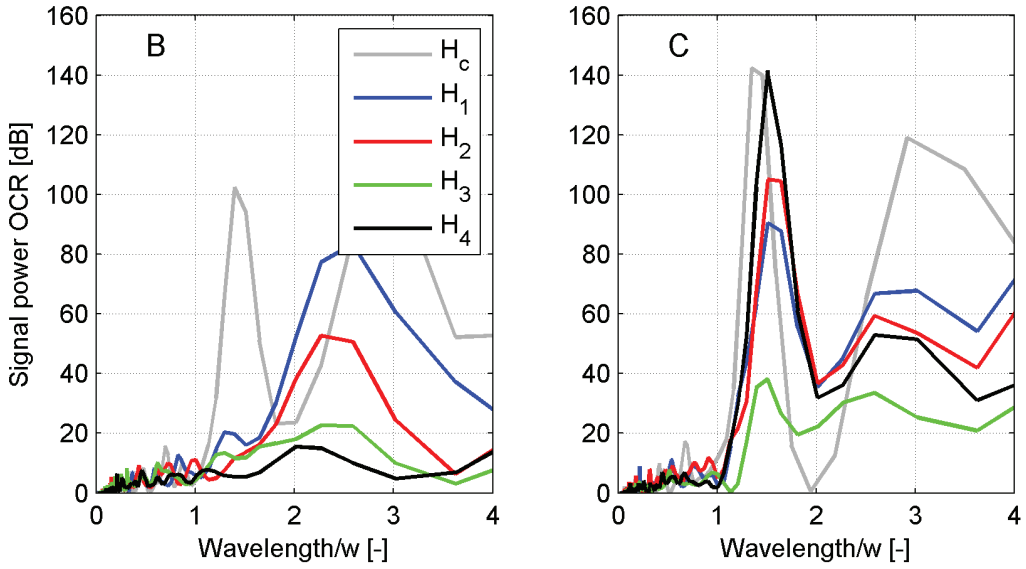

Figure 8.12 – Power spectral density of the OCR-signal for configuration B and C, for constant discharge (H_c) and transient flow (H_1, H_2, H_3 and H_4). Wavelength normalized by the channel width, w

8.3.6 Transport mechanism for transient flows and constant discharge

Figure 8.13 shows the transport mechanism for configurations B and C when subjected to a transient flows and a constant discharge. A general behaviour can be withdrawn for the proposed cases: a mixed transported develops during the initial phases of tests, then both configurations move towards a translation transport mechanism. This development is more evident for configuration C, especially for long duration rising limbs (H_3, H_4 and H_c). Thus, for these cases, the grains tend to move compacted through the channel length.

For configuration B, the movement is generally mixed, toward translation in the last phases. Thus, it can be assumed, that a general spread of material on the whole channel is occurring.

This phenomenon is related to the section narrowing effect which leads to a higher transport capacity. The latter, together with a mild hydrograph, produces a prominent translation movement of material. The continuous increase of bed shear stress in the rising limb does not allow the eroded sediment to settle and the transport lasts longer than for steep hydrographs. On the other hand, the narrowing effect is not evident for configuration C. It can be stated that the replenished material moves like a solid body toward the channel by translational-type mechanism.

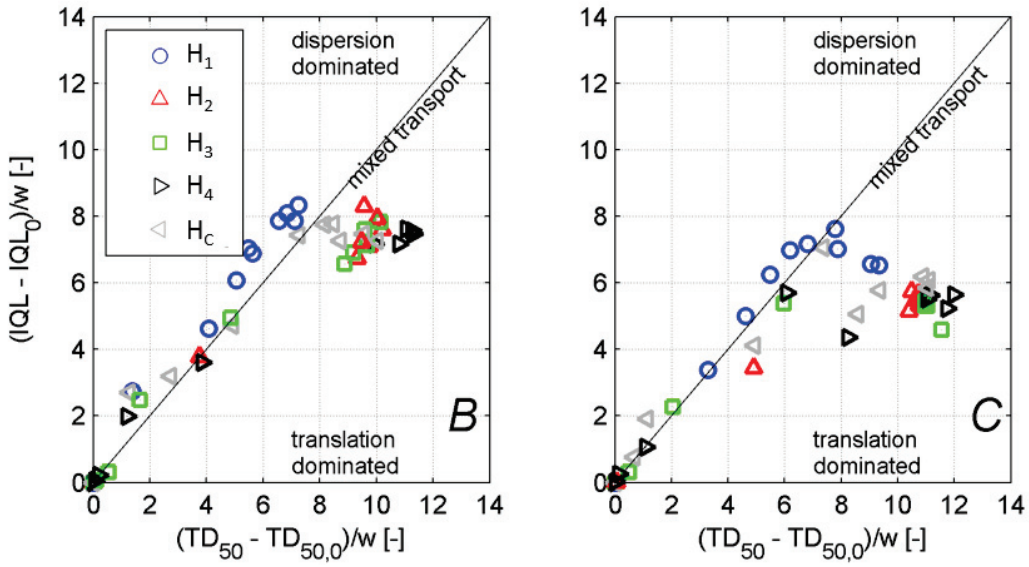

Figure 8.13 – (a) Transport mechanism for configuration B and all tested cases, (b) Transport mechanism for configuration C and all tested cases

8.4 Discussion

8.4.1 Morphological bed response to sediment replenishment and transient flow

Large deposition of material in terms of occupied surface and persistence is observed for steep hydrographs (H_1 and H_2) on the channel bed before the discharge peak. On the other hand, for mild hydrographs, most of the replenished grains have already left the channel at the discharge peak. The deposition of material on channel reach is thus lower, in agreement with Humphries et al. (2012). A counterclockwise hysteresis effect between discharge and sediment transport is thus occurring.

Counterclockwise and clockwise hysteresis are well know mechanism for sediment transport (Kuhnle, 1992; Humphries et al., 2012; Mao, 2012) and they were observed for both hydrographs and constant discharge tests. In particular, these patterns are considered releated to delay in sediment supply by Habersack et al. (2001), or consolidation of supplied material by Reid et al. (1985) or passage of bed forms by Bell and Sutherland (1983). Kuhnle (1992) linked the

development of hysteresis effect with the choice of the discharge peak. As observed by him, the hysteresis is counterclockwise when the peak discharge of the hydrograph is not enough for eroding the armour layer. Otherwise, clockwise hysteresis is observed for high flow. The here applied discharge for both transient and constant flow is settled low enough to mobilize only the replenished material, whereas bad and banks are considered immobile. In detail, the performed hydrographs have a dimensionless bed shear stress 2.5 times above the threshold of movement considered equal to 0.047. The constant discharge, for a complete submergence of the deposits, is set with a dimensionless bed shear stress of 2 times the threshold of movement. Thus, both belong to the low flow stage in agreement with Kuhnle (1992) and Humphries et al. (2012). The experiments performed by the above mentioned authors were run on a moveable bed with sediment supply from upstream. These conditions may not be well representative of the reach downstream of dams where the sediment replenishment is normally applied. This justifies the lack in positive and negative lags linked to sediment supply and observed in others studies (Kuhnle, 1992).

Nevertheless, the use of a steep hydrograph leads to a wide bed fining which is almost stable in time after the occurrence of the discharge peak. The equilibrium state is assessed in terms of stability of the bed surface occupied by replenished material. By bed fining, the bed roughness is increased and the bed shear stress decreased. The armoured bed layer,of reaches downstream of dams, can be re-mobilized by the addition of finer material. A long rising limb does not affect the channel bed immediately downstream the replenishment location, where almost no bed fining is observed. In the latter case, most of the replenished material went out from the observation reach. This reduction of replenishment material is related to the geometrical configuration. For configuration B the deposits are shift half the replenishment length downstream and the flow is constrained in one third of the channel bed. Therefore, the flow transport capacity is much higher.

In agreement with Sklar et al. (2009); Lisle et al. (1997); Sear et al. (2008); Cui et al. (2003), sediment replenishment deposits move by a combination of dispersion and translation, where translation is dominant. For a submergence ratio of 100%, the transport mechanism evolves from a dispersion dominated type to translation type in the last time steps. In partial agreement with Lisle et al. (2001); Cui et al. (2003); Sklar et al. (2009), the translation occurs when the replenishment sediments are finer than the pre-existing bed and the replenishment has a narrow grain size distribution. In agreement with Sklar et al. (2009) and Humphries et al. (2012), translation is enhanced when sediment supply is lacking from upstream and for higher discharges. Steep hydrographs, such as H_1 and H_2, tend to privilege a mixed mechanism while large rising limbs tend more to translation. Steep hydrograph leads to a longer and higher persistence of material in the reach immediately downstream the deposits initial location. Thus, this configuration may be suggested for local effect of the replenishment downstream a dam. For a longer distance impact, longer rising limbs are suggested. Thus, the choice of the hydrograph shape seems of key importance in relation to the sediment replenishment final purpose.

As for the constant flow, hydrographs released on sediment replenishment volume create downstream morphological pattern, as highlighted in Chapter 4. For configuration C with volumes shifted one length downstream, the wavelength of such bed forms equal the constant flow case, independently from the hydrograph shape. For configuration B, with deposits shifted half the length, the wavelength is increased at 2.2 times the channel width. However, the amplitude of the latter is less intense due to the reduced availability of replenished material especially for mild rising limbs.

8.4.2 Suggestions for field applications

By using a hydrograph instead of a constant discharge release from the dam bottom outlet for mobilising the replenishment material, allows for better results in terms of persistence and bed form development. Configuration B shows an average increase of 30% in terms of covered surface CS when releasing a hydrograph in the channel. In particular, steep hydrographs (steeper rising than falling limb) allows to economize 70% of the released water compared to a constant flow case.

The artificial flood is normally created by a water release from the bottom outlets of dams. Therefore, the economic advantage in preferring the hydrograph is clear. Nevertheless, it is worth to mention that ecological issues can still occur by using a triangular shape hydrograph. Artificial releases from dams flood dry areas, where the river fauna can temporarily accommodate. A rapid closure of the bottom outlets may not leave the fauna enough time to join the main reach again. Thus, fish population mortality can locally increase.

8.5 Conclusions

The response of sediment replenishment volumes to transient flows is evaluated by a series of channel experiments and compared with the constant discharge tests. Four triangular shape hydrographs, with same discharge peak but different rising limb slopes, are released on a channel where alternated replenishment volumes are placed. The hydrographs and the constant submergence case are comparable in terms of induced bed shear stress for the entire test duration.

The ringing limb slope plays a key role in determining the channel morphological response in terms of replenished material remaining close to the initial placement and robustness of bed forms. A steep limb leads to a rapid erosion and spread of replenished material. In this context, the maximum occupation of channel by replenishment grains occurs right after the discharge peak. On the contrary, when a low rising limb is applied, the maximum channel occupation is achieved before the discharge peak. Nevertheless, most of the replenished material has run more the channel length distance while the discharge peak impacts. The configuration with volume shifted half replenishment length downstream (configuration B) leads to a more intense spread of replenished material, and longer distances are travelled.

Replenished volumes shifted one length downstream (configuration C) create a more robust channel bed pattern with a wavelength corresponding to the constant discharge case. The replenished material, independently from the geometrical configuration, are transported by a mixed mechanism in the initial phases of test, while a clear translation mechanism takes over in the final states.

Steep hydrographs generate bed fining on the whole channel bed that can be estimated by the standard deviation of channel topography changes. The average grain size is almost halved when a steep hydrograph is released on the channel. Thus, a decrease roughness is produced on flume. On the other hand, no improvement of bed fining is provided by low rising limbs. It can be observed that the channel bed, after the sediment replenishment, goes back to the initial roughness state since most of the replenished material exited the channel.

Steep hydrographs allow to restore a morphological variability in the downstream reach of the deposit location. This morphological variability is defined in terms of distribution of the replenished material on the channel bed. A reduction of more than 70% of released water volume can be obtained by applying a short hydrograph lasting until the peak discharge.

9 Design of sediment replenishment for field application

9.1 Introduction

It is challenging to provide general guidelines, since each reach downstream of a dam has peculiarities and the singular river characteristics should be taken into account. Therefore, a field application of sediment replenishment helps clarifying the processes that are simplified in laboratory conditions. A field application of sediment replenishment has be designed following the results provided by this research.

9.2 Application of sediment replenishment on the Sarine river

It was observed that the residual reach between the Rossens dam and the mouth of the Gérine river suffered from a lack in sediment supply since the dam construction. Furthermore, this reach consists on a residual flow affected by hydropeaking. Figure 9.1 show the temporal evolution of this river reach from the 1929 (before the dam construction in 1948) until nowadays. It is evident that a considerable morphological change took place during these years. In particular, the vegetation grown over the floodplain areas and the river has moved from braided to single stretch.

An artificial flood was released along this affected residual reach of the Sarine river (Switzerland) in order to mobilise the armoured bed and to clean the channel bed from the growing vegetation. A triangular-shaped hydrograph was defined, with a total duration of 28 hours. The discharge increased from the actual residual flow of 2.5 m^3/s to almost 255 m^3/s. The peak discharge lasted for five hours. The flood was released from the bottom outlets of the Rossens dam (Figure 9.2).

This artificial flood gave the opportunity to experience the results of this research on the field. Four deposits, for a total amount of 1000 m^3 were placed in alternating configuration about 8 km downstream the dam (Figure 9.3a). The four deposits have a length of about 20 m, a width of 10 m (corresponding to one third of the river width) and a height of 1.5 m (Figure 9.3b). The material required for creating the deposits was excavated by the floodplain near by the deposition areas. The deposits were thus build with a wide grain size distribution with a high component of fine material (Figure 9.4).

In each deposit 250 RFID tracers were placed in respectively numbered gravels (Figure 9.5). The tracers were placed at three different height inside the deposits: bottom, middle and top. The RFID tag can be track when passing trough an electromagnetic field. Therefore, two antennas were installed on the channel bed. The antennas create the appropriate frequency able to catch the RFID signal. Being eroded and transported, and passing through the antennas placed along the reach, it would be possible to track the movement of the stones and their timing.

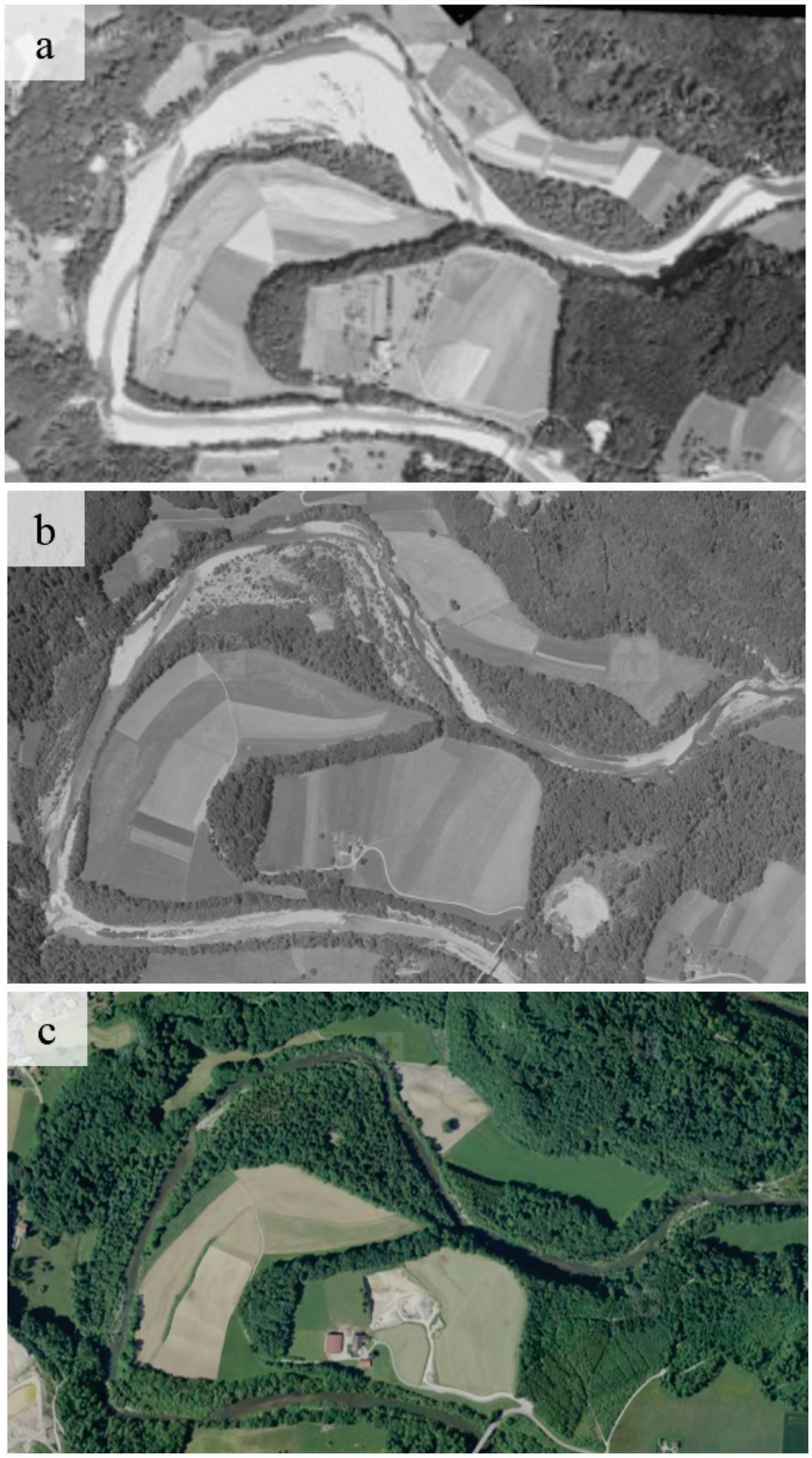

Figure 9.1 – Evidence of morphological changes from aerial photos of Sarine river (Fribourg, Switzerland), (a) 1929, (b) 1943, (c) 1972 and (d) 2016. Source https://map.geo.admin.ch

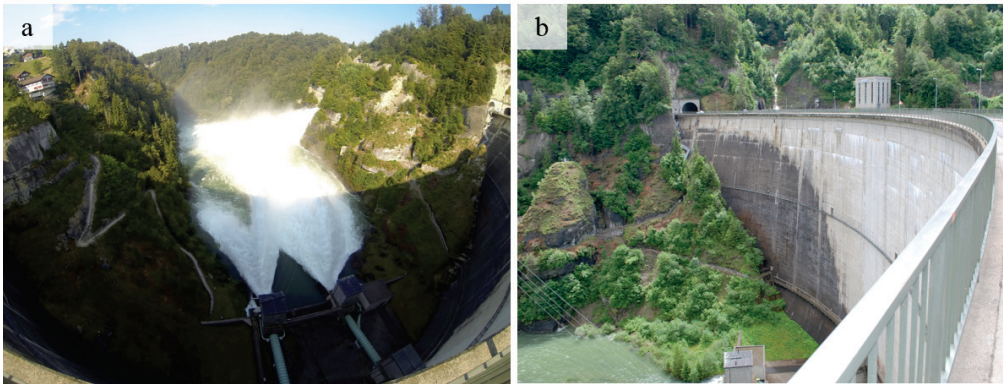

Figure 9.2 – (a) Water released from the bottom outlets of the Rossens dam, (b) Rossens arch dam

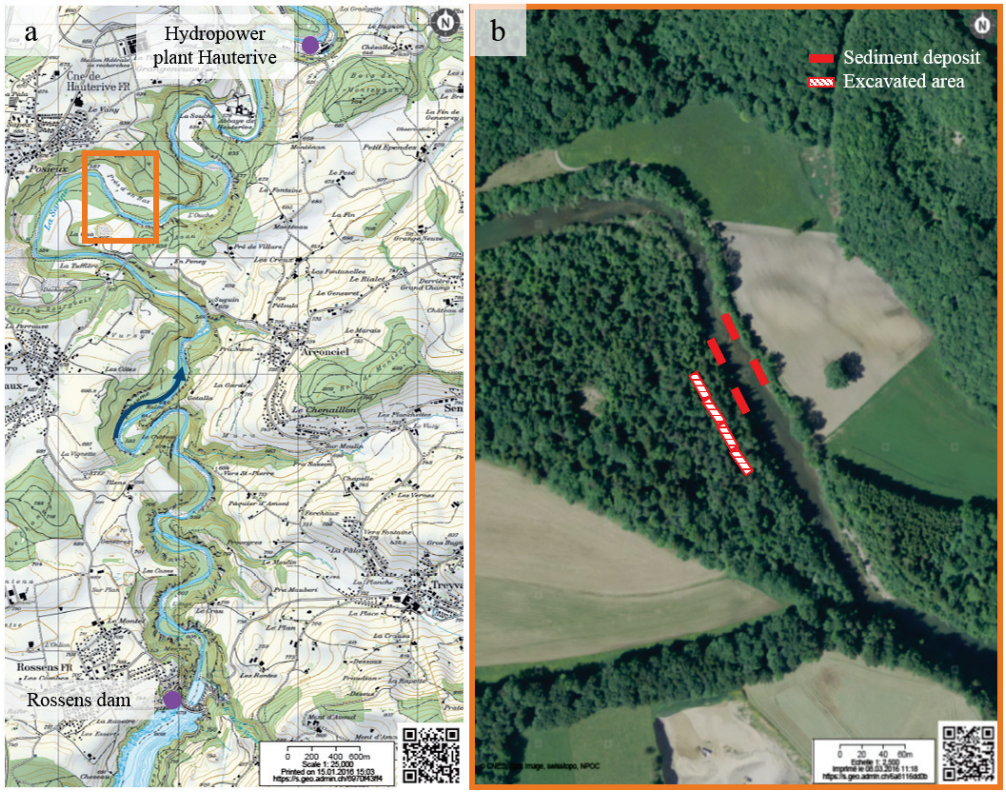

Figure 9.3 – (a) Residual reach along the Sarine river (source from https://map.geo.admin.ch/), (b) sketch of the geometrical placement of replenished deposits

Figure 9.4 – (a) View on the most upstream deposit placed on the left bank, (b) third and fourth deposits placed on the banks, (c) first and third deposits viewed from downstream, (d) machine operating the sediment replenishment placement

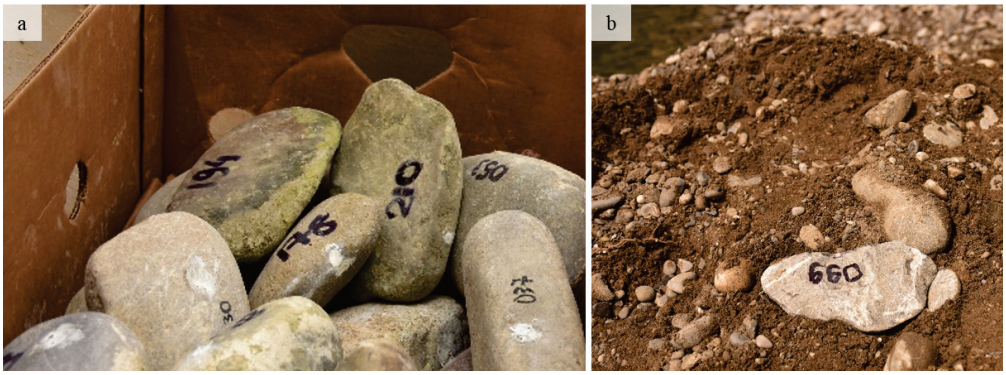

Figure 9.5 – (a) Traced gravels and (b) numbered stone with RFID tag placed on one deposit

10 Conclusions and future works

10.1 Conclusions

10.1.1 Which geometry of sediment deposits are suitable for recreating morphological variability at the water reaches downstream sediment-retaining structures?

The geometrical configuration play a key role in the success of a sediment replenishment, since it leads to different hydraulic conditions which are able to divert the flow and facilitate deposit erosion. By placing the sediment replenishment only along one bank the flow erodes the deposit toe and the main effect is mass failure. In these circumstances, the transport capacity is not enough for transporting the material along the channel and the eroded grains tend to accumulate nearby the original positions. The occupation of both the channel banks by sediment replenishment provides increase both flow velocity and transport capacity without compromising the natural water flow and leaving enough space on the channel bed. By cross section narrowing, a backwater effect is induced that leads to a higher deposit erosion. When placing four deposits on the channel, the backwater effect acts eroding the most downstream and creating an initial deposition zone between the two upstream and the following. Furthermore, the transport capacity is increased and the eroded grains travel longer distances downstream the laboratory reach. The occupation of maximum two third of channel width by placing the replenished material on both banks seems appropriate for achieving a complete erosion and the transportation of the eroded material. The above mentioned hydraulic effects are amplified in terms of achieved erosion and run distances by the grains when using longer replenishment. The study demonstrated that long replenishment placed on both banks create a long cross sectional narrowing, which drastically change both flow velocity and transport capacity. Thus, the replenished material is transported for longer distances, but no clear bed morphological patterns are created. For a ratio of about 1, bed forms are re-establish for a distance of twenty times the channel width. Nevertheless, the depositions heights are not enough in terms of providing an ecological river improvement. For two reasons these configurations proofed to be suboptimal: not enough replenishment material is left for creating morphological bed forms (ratio length to width equals to 1.25), only bed fining is obtained in the channel without the creation of morphological patterns (ratio length to width equals to 1.25). When the ratio between deposit length and channel width is lower than 2.5, higher persistence of replenished material is achieved. An optimum ratio is found equal to 1.87 which leads to a complete volume erosion and to the creation of morphological variability downstream.

10.1.2 Where and how have replenishment deposits to be placed in order to be mobilized and conveyed in order to recreate bed morphological forms?

This research revealed that bed morphological variations are sensitive to the initial geometrical configurations of sediment replenishment deposits. Both parallel and alternating configurations were tested. Sediment replenishment configurations are considered parallel when the

downstream shift of the deposits varies between zero and one quarter of the deposit length. Alternating configuration of deposits include downstream shift between half to three quarter of volume length. The parallel configurations lead to a wide spread of the replenished material on the whole channel bed. Thus, a general bed fining is obtained. Most of the replenished material reaches the channel downstream end leading to the conclusion that long distances may be travelled by the eroded grains. On the other hand, alternating configurations create a bed morphological pattern in channel. The morphological patterns is regular and repetitive with a wavelength equal about to the replenishment length. The deposition heights are almost five times the median grain diameter of the replenishment, therefore they can be considered as profitable spawning habitats for alpine fish species. These configurations may help in light of sediment replenishment as a tool to restore morphological variability and recover the ecological issues downstream of dams.

10.1.3 Which controlled discharges are necessary for mobilizing the deposits downstream of the retaining structure? Which transport mechanism is related to the different cases?

The laboratory tests included seven discharge conditions, among which three were constant discharges and four transient flows. A complete submergence of the replenishment deposit is required for obtaining complete erosion and transportation of the material. When the water depth is lower than the deposit height, the transport capacity is not enough and most of the placed material do not suffer from any erosion. This is the case of a river reach downstream a dam, where generally only a residual flow is released. Therefore, an artificial flood is required for obtaining replenishment deposit erosion. In these flow conditions, the deposits are laterally eroded at the beginning, then the erosion process finds a new equilibrium. This new condition is achieved with the reduction of the cross sectional narrowing effect. With over submerged ratio, both flow velocity and transport capacity are increased and the replenished material is quickly eroded. The overtopping of the deposits leads to a wider erosion. The transport distance is longer compared to the above tested cases. This discharge requires bigger consumption of water and reduced the creation of morphological variation downstream. Nevertheless, the application of an over submerged condition may help in overtaking site access limitations since sediment replenishment can reach longer distances.

The application of a constant discharge seems to be not directly applied to field application where the water is released from a dam. The limits are related to the dam operations timing and also to ecological implications. When the released discharge from a dam increases, the fauna may find other places where to settle with different velocity and lower water depth. With a quasi instantaneous closure of the bottom outlet of the dam, the same areas will be quickly dry again leaving almost no time to the fauna to move back to the main channel. In these context, the mortality of river inhabitants may be high. Therefore, triangular shaped hydrograph were also performed on two alternating configuration and compared with the corresponding complete submergence cases. Both steep and mild hydrograph were tested.

The hydrograph was defined steep for a rising limb slope steeper than the falling one, whereas the other way around describes the mild hydrograph.

The same results in terms of covered surface and persistence of replenished material obtained at the test end for the constant discharge case are achieved immediately after the flow peak when applying a steep rising hydrograph. The greatest improvement achieved by the use of steep hydrograph is the drastic reduction of released water. Almost the 70% of the constant discharge water volume may be economised without affecting the quality of the morphological results. Mild rising limbs of the hydrograph lead to a progressive increase of transport capacity which erodes all the replenished deposits. These grains are transported beyond the observation reach, thus it can be assumed that longer distances can be run. Due to the high flow transport capacity, the persistence is really low in the reach close to the initial deposit location. Transient flows instead of a constant discharge do not affect the development of a bed morphological pattern. Both the tested geometrical configurations create bed clusters with a certain periodicity. For the more compact configuration (*B*, deposit shifted downstream half the length), the wavelength of these bed forms is larger than for the constant discharge. For complete alternating configuration (*C*), constant discharge and transient flows have the same wavelength. These observations indicate that transient flow should be preferred to constant discharge in order to limit the water consumption, performing a high persistence of replenished material.

The role of the released discharge is studied in terms of frequency of the operation by testing consecutive replenishment on several geometrical configurations. A second replenishment affects the downstream portion of channel where the first replenishment had slight impact. The eroded material from the second replenishment follows the deposition patterns created by the first replenishment. Therefore, it can be concluded that the deposition height can be increased by consecutive replenishment. Nevertheless, the change in bed roughness should be taken into account while performing consecutive replenishment. Sediment replenishment of fine material leads to bed roughness smoothing and fining. The fine grains of the replenished percolate through the armoured bed enhancing the transport capacity close to bed surface. Therefore, the released discharge should be also decreased accounting for the new bed roughness. The replenished deposits are mainly transported by a dispersive mechanism for a complete submergence of the volumes, while a translation mechanism is evident for higher submergence conditions. The latter does not contribute in the creation of stable morphological patterns. Thus, spawning habitats and morphology cannot be properly restored while these flow conditions occur. Two velocities of movement for the replenished material can be observed. The higher velocity is responsible of the initial volume erosion, while the lower one contribute to deplete the more upstream bed forms to increase the thickness of those downstream during the entire test duration.

10.2 Future work

This research provides a contribution to the understanding of the sediment replenishment method. Nevertheless, further work is needed in order to provide a complete guideline for sediment replenishment application.

In particular, the role of the grain size distribution of the replenished material should be investigated. The present research has investigated only a narrow grain size that accounts for spawning ground needs, thus different distributions can be tested. The replenishment of fine material has demonstrated to participate in bed fining and construction of bed forms. Nevertheless, this behaviour may change for grains which size is much smaller than the existing bed. Furthermore, the role played by the longitudinal slope should be tested. The stability and the shape of bed forms are related also to the channel slope. Therefore, a steeper or milder reach will probably establish a different bed pattern.

The fixed armoured bed was necessary to initially study the channel response to the replenishment of multiple volumes and to clearly follow erosion and deposition processes. Further investigations may consider a non-fixed armoured bed which allows for estimating the possibility of the replenishment to partially break it. Moreover, by the introduction of a non-fixed bed it would be possible to investigate the degree of percolation of fine sediments. In the above mentioned conditions, continuous test recording is recommended for studying the stability of morphological bed patterns and provide a more precise understanding on the timing for erosion.

Future study on consecutive replenishment and linked change in bed roughness are necessary. It is suggested to investigate this aspect by using a different color for each replenishment deposit for better understanding the transport dynamic and the stability of bed forms.

Bibliography

Ahmari, H. and Da Silva, A. M. (2011). Regions of bars, meandering and braiding in da Silva and Yalin's plan. *Journal of Hydraulic Research*, 49(6):718–727.

Babaeyan-Koopaei, K. (2012). Discussion of "Regions of bars, meandering and braiding in da Silva and Yalin's plan". *Journal of Hydraulic Research*, 50(5):541–542.

Balland, P. (2004). Impacts des barrages sur les milieux physiques et biologiques. *Ingénieries, Supplément*, 38:23–32.

Barlaup, B. T., Gabrielsen, S. E., Skoglund, H., and Wiers, T. (2008). Addition of spawning gravel: a means to restore spawning habitat of Atlantic salmon (Salmo Salar L.), and Anadromous and resident brown trout (Salmo Trutta L.) in regulated rivers. *River Research and Applications*, 24(5):543–550.

Batalla, R. J., Gomez, C. M., and Kondolf, G. M. (2004). Reservoir-induced hydrological changes in the Ebro River basin (NE Spain). *Journal of Hydrology*, 290(1):117–136.

Batalla, R. J., Vericat, D., and Martínez, T. I. (2006). River-channel changes downstream from dams in the lower Ebro River. *Zeitschrift für Geomorphologie, Suppl. B*, 143:1–14.

Battisacco, E., Franca, M. J., and Schleiss, A. J. (2016). Sediment replenishment: Influence of the geometrical configuration on the morphological evolution of channel-bed. *Water Resources Research*. DOI: 10.1002/2016WR019157.

Bell, R. G. and Sutherland, A. J. (1983). Nonequilibrium bedload transport by steady flows. *Journal of Hydraulic Engineering*, 109(3):351–367.

Bösch, L., Battisacco, E., Franca, M. J., and Schleiss, A. J. (2016). Influence of consecutive sediment replenishment on channel bed morphology. In *Proceedings of the River Flow 2016 St. Louis, USA, 11-14 July 2016. Eds. Constantinescu, G., Garcia, M., and Hanes, D.*, pages 1147–1155. Taylor & Francis, London, UK.

Brandt, S. A. (2000). Prediction of downstream geomorphological changes after dam construction: a stream power approach. *International Journal of Water Resources Development*, 16(3):343–367.

Bribiesca, E. (1997). Measuring 2-D shape compactness using the contact perimeter. *Computers & Mathematics with Applications*, 33(11):1–9.

Buffington, J. M., Dietrich, W. E., and Kirchner, J. W. (1992). Friction angle measurements on a naturally formed gravel streambed: Implications for critical boundary shear stress. *Water Resources Research*, 28(2):411–425.

Buffington, J. M. and Montgomery, D. R. (1999). Effects of sediment supply on surface textures of gravel-bed rivers. *Water Resources Research*, 35(11):3523–3530.

Buffington, J. M. and Montgomery, D. R. (2013). Geomorphic classification of rivers. *Fluvial Geomorphology*, 9:730–767.

Bunte, K. (2004). Gravel mitigation and augmentation below hydroelectric dams: a geomorphological perspective. Technical report, U.S. Department of Agriculture, Forest Service, Rocky Mountain Research Station. Report submitted to the Stream Systems Technology Center, Fort Collins, USA.

Chapman, D. W. (1988). Critical review of variables used to define effects of fines in redds of large salmonids. *Transactions of the American Fisheries Society*, 117(1):1–21.

Church, M. (1995). Geomorphic response to river flow regulation: Case studies and time-scales. *Regulated Rivers: Research & Management*, 11(1):3–22.

Church, M. (2006). Bed material transport and the morphology of alluvial river channels. *Annual Review of Earth and Planetary Sciences*, 34:325–354.

Coleman, S. E., Nikora, V. I., and Aberle, J. (2011). Interpretation of alluvial beds through bed elevation distribution moments. *Water Resources Research*, 47(11):1–14.

Cui, Y., Parker, G., Pizzuto, J., and Lisle, T. E. (2003). Sediment pulses in mountain rivers: 2. Comparison between experiments and numerical predictions. *Water Resources Research*, 39(9):1240.

DETEC (2012). Development of Swiss water protection legislation and its implementation. Technical report, Swiss Federal Office for the Environment.

Dey, S. (2011). Experimental Methods in Hydraulic Research, pages 29-48. Springer, Berlin, Germany.

Dietrich, W. E., Kirchner, J. W., Ikeda, H., and Iseya, F. (1989). Sediment supply and the development of the coarse surface layer in gravel-bedded rivers. *Nature*, 340(6230):215–217.

Fan, J. and Morris, G. L. (1992). Reservoir Sedimentation. II: Reservoir desiltation and long-term storage capacity. *Journal of Hydraulic Engineering*, 118(3):370–384.

Ferguson, R. I., Church, M., Rennie, C. D., and Venditti, J. G. (2015). Reconstructing a sediment pulse: Modeling the effect of placer mining on Fraser River, Canada. *Journal of Geophysical Research: Earth Surface*, 120:1436–1454.

Florsheim, J. L., Mount, J. F., and Chin, A. (2008). Bank erosion as a desirable attribute of rivers. *BioScience*, 58(6):519–529.

Frey, P. and Church, M. (2009). How river beds move. *Science*, 325(5947):1509–1510.

Fuselier, L. and Edds, D. (1995). Management briefs: An artificial riffle as restored habitat for the threatened Neosho Madtom. *North American Journal of Fisheries Management*, 15(2):499–503.

Gaeuman, D. (2008). Recommended quantities and gradation for long-term coarse sediment augmentation downstream from Lewiston Dam. Technical report, TRRP, Trinity River Restoration Program, Weaverville, California.

Gaeuman, D. (2012). Mitigating downstream effects of dams. In *Gravel-Bed Rivers: Processes, Tools, Environments. Eds. Church, M., Biron, P. M. and Roy, A. G.*, pages 182–189. John Wiley & Sons, Ltd, Chichester, UK.

Gaeuman, D. and Krause, A. (2013). Assessment of pool depth changes in the Trinity River between Lewiston Dam and the North Fork Trinity River. Technical report, TRRP, Trinity River Restoration Program, Weaverville, California.

Geist, R. D. and Dauble, D. D. (1998). Redd site selection and spawning habitat use by Fall Chinook Salmon: The importance of geomorphic features in large rivers. *Environmental Management*, 22(5):655–669.

Gore, J. A., Crawford, D. J., and Addison, D. S. (1998). An analysis of artificial riffles and enhancement of benthic community diversity by physical habitat simulation (PHABSIM) and direct observation. *Regulated Rivers: Research & Management*, 14(1):69–77.

Gore, J. A., Layzer, J. B., and Mead, J. (2001). Macroinvertebrate instream flow studies after 20 years: a role in stream management and restoration. *Regulated Rivers: Research & Management*, 17(4-5):527–542.

Graf, W. H. (1984). Storage losses in reservoirs. *International Water Power & Dam Construction*, 36(4):37–40.

Grams, P. E. and Schmidt, J. C. (2005). Equilibrium or indeterminate? Where sediment budgets fail: Sediment mass balance and adjustment of channel form, Green River downstream from Flaming Gorge Dam, Utah and Colorado. *Geomorphology*, 71(1):156–181.

Grant, G. E., Schmidt, J. C., and Lewis, S. L. (2003). A geological framework for interpreting downstream effects of dams on rivers. Eds. O'Connor, J. E. and Grant, G. E. *A peculiar river. Water Science and Application*, 7:203–219.

Habersack, H. M., Nachtnebel, H. P., and Laronne, J. B. (2001). The continuous measurement of bedload discharge in a large alpine gravel bed river. *Journal of Hydraulic Research*, 39(2):125–133.

Heller, V. (2011). Scale effects in physical hydraulic engineering models. *Journal of Hydraulic Research*, 49(3):293–306.

Hersberger, D. S., Franca, M. J., and Schleiss, A. J. (2015). Wall roughness effects on flow and scouring in curved channels with gravel beds. *Journal of Hydraulic Engineering*, 142(1):04015032.

Hill, M. T., Platts, W. S., and Beschta, R. L. (1991). Ecological and geomorphological concepts for instream and out-of-channel flow requirements. *Rivers*, 2(3):198–210.

Humphries, R., Venditti, J. G., Sklar, L. S., and Wooster, J. K. (2012). Experimental evidence for the effect of hydrographs on sediment pulse dynamics in gravel-bedded rivers. *Water Resources Research*, 48(1).

Ikeda, H. (1983). Experiments on bedload transport, bed forms, and sedimentary structures using fine gravel in the 4-meter-wide flume. *Environmental Research Center Papers*, 2:1–78.

Jäggi, M. (1984). Formation and effects of alternate bars. *Journal of Hydraulic Engineering*, 110(2):142–156.

Juez, C., Battisacco, E., Schleiss, A. J., and Franca, M. J. (2016). Assessment of the performance of numerical modeling in reproducing a replenishment of sediments in a water-worked channel. *Advances in Water Resources*, 92:10–22.

Kalliola, R. and Puhakka, M. (1988). River dynamics and vegetation mosaicism: a case study of the River Kamajohka, northernmost Finland. *Journal of Biogeography*, 15:703–719.

Kantoush, S. A. and Sumi, T. (2010). River morphology and sediment management strategies for sustainable reservoir in Japan and European Alps. In *Annuals of Disaster Prevention Research Institute, Kyoto University*, volume 53B, pages 821–839.

Kantoush, S. A., Sumi, T., and Kubota, A. (2010a). Geomorphic response of rivers below dams by sediment replenishment technique. In *Proceedings of the River Flow 2010 Conference, Braunschweig, Germany, 8-10 September 2010. Eds. Dittrich, Koll and Aeberle & Geisenhainer*, pages 1155–1163. Bundesanstalt für Wasserbau, Karlsruhe, Germany.

Kantoush, S. A., Sumi, T., Kutoba, A., and Suzuki, T. (2010b). Impacts of sediment replenishment below dams on flow and bed morphology of rivers. In *First International Conference on Coastal Zone Management of River Deltas and Low Land Coastlines, Alexandria, Egypt, 6-10 March*, pages 285–303.

Karrenberg, S., Blaser, S., Kollmann, J., Speck, T., and Edwards, P. (2003). Root anchorage of saplings and cuttings of woody pioneer species in a riparian environment. *Functional Ecology*, 17(2):170–177.

Kondolf, G. M. (1997). Hungry water: Effects of dams and gravel mining on river channels. *Environmental Management*, 21(4):533–551.

Kondolf, G. M. and Matthews, W. V. (1991). Management of coarse sediment in regulated rivers of California. Technical report, University of California Water Resources Center, Berkeley, USA.

Kondolf, G. M. and Minear, J. T. (2004). Gravel augmentation below dams: California experiences. In *AGU Fall Meeting Abstracts, San Francisco, California, USA*.

Kondolf, G. M. and Wolman, M. G. (1993). The sizes of salmonid spawning gravels. *Water Resources Research*, 29(7):2275–2285.

Kuhnle, R. A. (1992). Bed load transport during rising and falling stages on two small streams. *Earth Surface Processes and Landforms*, 17(2):191–197.

Li, W., Goodchild, M. F., and Church, R. (2013). An efficient measure of compactness for two-dimensional shapes and its application in regionalization problems. *International Journal of Geographical Information Science*, 27(6):1227–1250.

Ligon, F. K., Dietrich, W. E., and Trush, W. J. (1995). Downstream ecological effects of dams. *BioScience*, 45(3):183–192.

Lisle, T. E., Cui, Y., Parker, G., Pizzuto, J. E., and Dodd, A. M. (2001). The dominance of dispersion in the evolution of bed material waves in gravel bed rivers. *Earth Surface Processes and Landforms*, 26(13):1409–1420.

Lisle, T. E. and Hilton, S. (1992). The volume of fine sediment in pools: an index of sediment supply in gravel-bed streams. *Journal of the American Water Resources Association*, 28(2):371–383.

Lisle, T. E., Pizzuto, J. E., Ikeda, H., Iseya, F., and Kodama, Y. (1997). Evolution of a sediment wave in an experimental channel. *Water Resources Research*, 8:1971–1981.

Madej, M. (2001). Development of channel organization and roughness following sediment pulses in single-thread, gravel bed rivers. *Water Resources Research*, 37(8):2259–2272.

Mao, L. (2012). The effect of hydrographs on bed load transport and bed sediment spatial arrangement. *Journal of Geophysical Research: Earth Surface*, 117(F3).

McCartney, M. (2009). Living with dams: managing the environmental impacts. *Water Policy*, 11(S1):121–139.

McManamay, R. A., Orth, D. J., Dolloff, C. A., and Cantrell, M. A. (2010). Gravel addition as a habitat restoration technique for tailwaters. *North American Journal of Fisheries Management*, 30(5):1238–1257.

Merz, J. E. and Ochikubo Chan, L. K. (2005). Effects of gravel augmentation on macroinvertebrate assemblages in a regulated California river. *River Research and Applications*, 21(1):61–74.

Meyer-Peter, E. and Müller, R. (1948). Formulas for bed-load transport. In *Second Meeting of the International Association for Hydraulic Structures Research, Stockholm*, pages 39–65.

Morris, G. L. (1994). Reservoirs and integrated management. In *Reservoir Sedimentation, Proceedings of the St Petersburg Workshop. Eds. Bruk, S and Zebidi, H. Technical Documents in Hydrology no. 2, UNESCO, Paris, 1996*, pages 135–148.

Naot, D. (1984). Response of channel flow to roughness heterogeneity. *Journal of Hydraulic Engineering*, 110(11):1568–1587.

Nelson, P. A., Brew, A. K., and Morgan, J. A. (2015). Morphodynamic response of a variable-width channel to changes in sediment supply. *Water Resources Research*, 51(7):5717–5734.

Ock, G., Sumi, T., and Takemon, Y. (2013). Sediment replenishment to downstream reaches below dams: implementation perspectives. *Hydrological Research Letters*, 7(3):54–59.

Okano, M., Kikui, M., Ishida, H., and Sumi, T. (2004). Reservoir sedimentation management by coarse sediment replenishment below dams. In *Proceedings of the 9th International Symposium on River Sedimentation, Yichang China*.

Otsu, N. (1979). Thresholds selection method form grey-level histograms. *IEEE Transactions on Systems, Man, and Cybernetics*, 9(1).

Parker, G. and Toro Escobar, C. M. (2002). Equal mobility of gravel in streams: The remains of the day. *Water Resources Research*, 38(11):46–4.

Pasternack, G. B., Morford, S. L., and Fulton, A. A. (2010). Yuba River analysis aims to aid spring-run Chinook Salmon habitat rehabilitation. *California Agriculture*, 64(2):69–77.

Pasternack, G. B., Wang, C. L., and Merz, J. E. (2004). Application of a 2D hydrodynamic model to design of reach-scale spawning gravel replenishment on the Mokelumne River, California. *River Research and Applications*, 20(2):205–225.

Pedroli, B. and Dijkman, J. (1998). River restoration in European lowland river systems. In *Restoration of degraded rivers: challenges, issues and experiences*, pages 211–227. Kluwer Academic Publishers, Dordrecht, The Netherlands.

Petts, G. E. and Gurnell, A. M. (2005). Dams and geomorphology: Research progress and future directions. *Geomorphology*, 70(1-2):27–47.

Plummer, C., McGeary, D., and Carlson, D. H. (1988). Physical Geology, 4th edition, page 535. WCB McGrawHil, Boston, USA.

Power, M. E., Dietrich, W. E., and Finlay, J. C. (1996). Dams and downstream aquatic biodiversity: potential food web consequences of hydrologic and geomorphic change. *Environmental Management*, 20(6):887–895.

Pulg, U., Barlaup, B. T., Sternecker, K., Trepl, L., and Unfer, G. (2013). Restoration of spawning habitats of brown trout (Salmo Trutta) in a regulated chalk stream. *River Research and Applications*, 29(2):172–182.

Reid, I., Frostick, L. E., and Layman, J. T. (1985). The incidence and nature of bedload transport during flood flows in coarse-grained alluvial channels. *Earth Surface Processes and Landforms*, 10(1):33–44.

Reiser, D. W., Ramey, M. P., Beck, S., Lambert, T. R., and Geary, R. E. (1989). Flushing flow recommendations for maintenance of salmonid spawning gravels in a steep, regulated stream. *Regulated Rivers: Research & Management*, 3(1):267–275.

Rickenmann, D. (1997). Sediment transport in Swiss rivers. *Earth Surface Processes and Landforms*, 22:937–951.

Rollet, A. J., Piégay, H., Dufour, S., Bornette, G., and Persat, H. (2014). Assessment of consequences of sediment deficit on a gravel river bed downstream of dams in restoration perspectives: application of a multicriteria, hierarchical and spatially explicit diagnosis. *River Research and Applications*, 30(8):939–953.

Rosgen, D. L. (1994). A classification of natural rivers. *Catena*, 22(3):169–199.

Rosgen, D. L., Silvey, H. L., and Potyondy, J. P. (1986). The use of channel maintenance flow concepts in the forest service. *Hydrological Science and Technology*, 2(1):19–26.

Salo, J., Kalliola, R., Häkkinen, I., Mäkinen, Y., Niemelä, P., Puhakka, M., and Coley, P. D. (1986). River dynamics and the diversity of Amazon lowland forest. *Nature*, 322(6076):254–258.

Schleiss, A. J., Boes, R., Brodersen, J., Doering, M., Franca, M., Nadyeina, O., Pfister, M., Robinson, C., Scheidegger, C., Vetsch, D., et al. (2014). Geschiebe-und Habitatsdynamik–Forschungsprogramm «Wasserbau und Ökologie». *Wasser Energie Luft*, 106(2):117–122.

Schleiss, A. J., Feuz, B., Aemmer, M., and Zünd, B. (1996). Verlandungsprobleme im Stausee Mauvoisin. Ausmass, Auswirkungen und mögliche Massnahmen. In *Mitteilung Nr. 142 der Versuchsanstalt für Wasserbau, Hydrologie und Glaziologie an der Eidgenössischen Technischen Hochschule Zürich*, pages 37–58. Eidgenössische Technische Hochschule Zürich.

Schleiss, A. J., Franca, M. J., Juez, C., and De Cesare, G. (2016). Reservoir sedimentation. *Journal of Hydraulic Research*, 54(6):595–614.

Schmidt, J. C. and Wilcock, P. R. (2008). Metrics for assessing the downstream effects of dams. *Water Resources Research*, 44(4).

Schumm, S. A. (1977). The fluvial system, page 338. Wiley, New York, USA.

Sear, D. A. (1995). Morphological and sedimentological changes in a gravel-bed river following 12 years of flow regulation for hydropower. *Regulated Rivers: Research & Management*, 10(2-4):247–264.

Sear, D. A., Frostick, L. B., Rollinson, G., and Lisle, T. E. (2008). The significance and mechanics of fine-sediment infiltration and accumulation in gravel spawning beds. In *Salmonid Spawning Habitat in Rivers: Physical Controls, Biological Responses, and Approaches to Remediation. Eds. Sear, David A. and DeVries, Paul*, pages 149–174. American Fisheries Society, Bethesda, USA.

Sherrard, J. J. and Erskine, W. D. (1991). Complex response of a sand-bed stream to upstream impoundment. *Regulated Rivers: Research & Management*, 6(1):53–70.

Shields, A. (1936). Anwendung der Aehnlichkeitsmechanik und der Turbulenzforschung auf die Geschiebebewegung. Technical report, Preussischen Versuchsanstalt für Wasserbau und Schiffbau, Berlin, Germany.

Sklar, L. S., Fadde, J., Venditti, J. G., Nelson, P., Wydzga, M. A., Cui, Y., and Dietrich, W. E. (2009). Translation and dispersion of sediment pulses in flume experiments simulating gravel augmentation below dams. *Water Resources Research*, 45:W08439.

Smart, G. M. and Jäggi, M. (1983). Sediment transport on steep slopes. In *Mitteilung Nr. 64 der Versuchsanstalt für Wasserbau, Hydrologie und Glaziologie an der Eidgenössischen Technischen Hochschule Zürich*. Eidgenössische Technische Hochschule Zürich.

Stoica, P. and Moses, R. L. (2005). Spectral analysis of signals, pages 285-293. Pearson Prentice Hall, Upper Saddle River, New Jersey, USA.

Sumi, T. and Kantoush, S. A. (2010). Integrated management of reservoir sediment routing by flushing, replenishing, and bypassing sediments in Japanese river basins. In *Proceedings of the 8th International Symposium on Ecohydraulics, Seoul, Korea*, pages 831–838.

Sumi, T. and Kantoush, S. A. (2011). Sediment management strategies for sustainable reservoir. In *Proceedings of the International Symposium on Dams and Reservoirs under Changing Challenges. Eds. Schleiss, A. J. and Boes, R. 79th Annual Meeting of ICOLD*, pages 353–362.

Sumi, T., Kobayshi, K., Yamaguchi, K., and Takata, Y. (2009). Study on the applicability of the asset management for reservoir sediment management. In *23th International Congress on Large Dams, Brasilia, Q.89 R.4*.

Venditti, J. G., Dietrich, W. E., Nelson, P. A., Wydzga, M. A., Fadde, J., and Sklar, L. S. (2010). Effect of sediment pulse grain size on sediment transport rates and bed mobility in gravel bed rivers. *Journal of Geophysical Research*, 115(3):1–19.

Venditti, J. G., Nelson, P. A., Minear, J. T., Wooster, J. K., and Dietrich, W. E. (2012). Alternate bar response to sediment supply termination. *Journal of Geophysical Research*, 117(2):1–18.

Vericat, D., Batalla, R. J., and Garcia, C. (2006). Breakup and reestablishment of the armour layer in a large gravel-bed river below dams: The lower Ebro. *Geomorphology*, 76(1):122–136.

Weichert, R. (2006). Bed morphology and stability of steep open channels. In *Mitteilung Nr. 192 der Versuchsanstalt für Wasserbau, Hydrologie und Glaziologie an der Eidgenössischen Technischen Hochschule Zürich*. Eidgenössische Technische Hochschule Zürich.

Wheaton, J. M., Pasternack, G. B., and Merz, J. E. (2004). Spawning habitat rehabilitation-II. Using hypothesis development and testing in design, Mokelumne River, California, USA. *International Journal of River Basin Management*, 2(1):21–37.

Whiting, P. J. and Dietrich, W. E. (1993). Experimental constraints on bar migration through bends: Implications for meander wavelength selection. *Water Resources Research*, 29(4):1091–1102.

Wilcock, P. R. (2004). Sediment transport in the restoration of gravel-bed rivers. In *Proceedings, EWRI Congress 2004, ASCE, Salt Lake City, Utah*, pages 1–11.

Williams, G. P. and Wolman, M. G. (1984). Downstream effects of dams on alluvial rivers. Technical report, US Government Printing Office Washington DC, USA.

Yalin, M. S. and Da Silva, A. M. (2001). Fluvial Processes. IAHR Monograph, IAHR Delft, The Netherlands.

Yoon, Y. N. (1992). The state and the perspective of the direct sediment removal methods from reservoirs. *International Journal of Sediment Research*, 7(20):99–115.

Zeh, M. and Dönni, W. (1994). Restoration of spawning grounds for trout and grayling in the river High-Rhine. *Aquatic Sciences*, 56(1):59–69.

A Appendix: Experiments with constant discharges

A.1 Experiment 1, Configuration A, 100% submergence

Parameters

Conf	Sub %	Shift m	L m	w m	Vol m^3	Weight kg	Q m^3/s	Duration h	Time steps
A	100	0	0.75	0.13	0.027	27.0	0.019	3	10

Configuration states

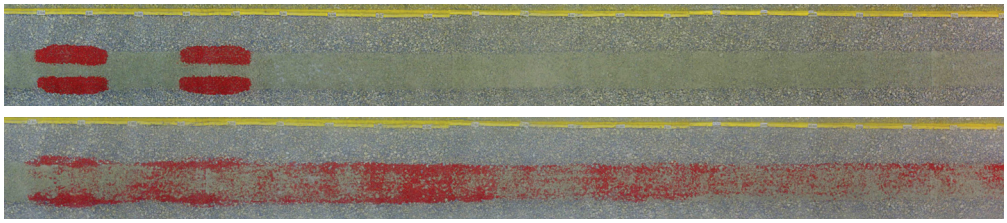

(Top) Initial state, (Bottom) final state after 3 hours testing. Flow direction from left to right

Assessed parameters

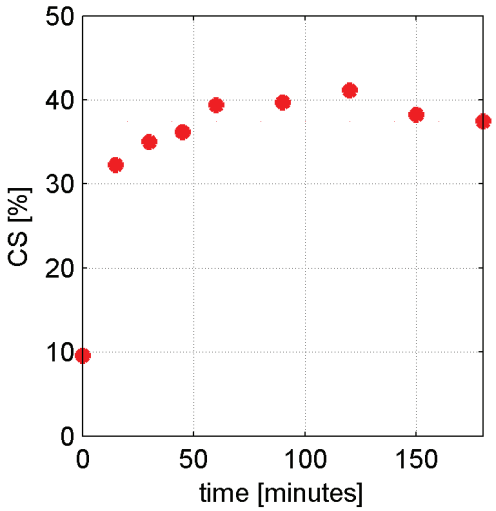

(a) Covered surface CS

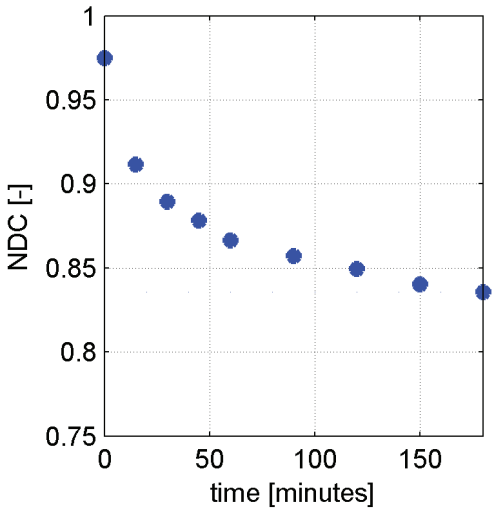

(b) Compactness NDC

(a) Temporal evolution of covered surface CS and (b) compactness NDC for the tested configuration

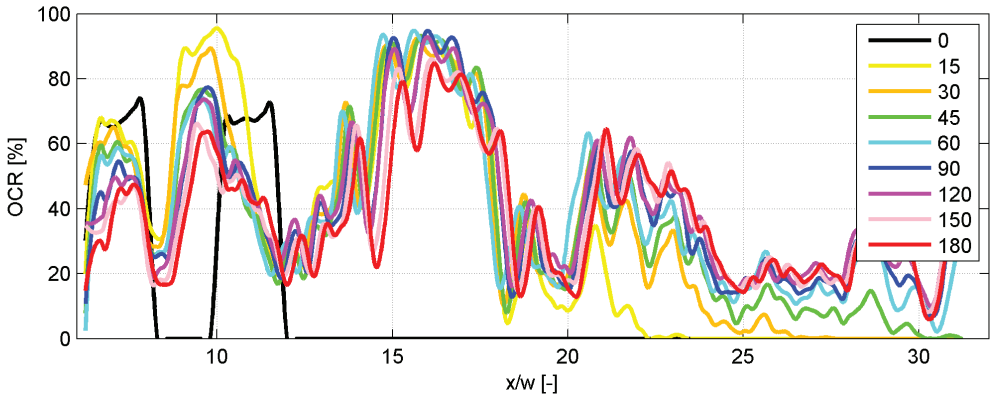

Temporal evolution of the occupation ratio distribution OCR. Time steps in minutes
Temporal evolution of the occupation ratio distribution OCR. Time steps in minutes

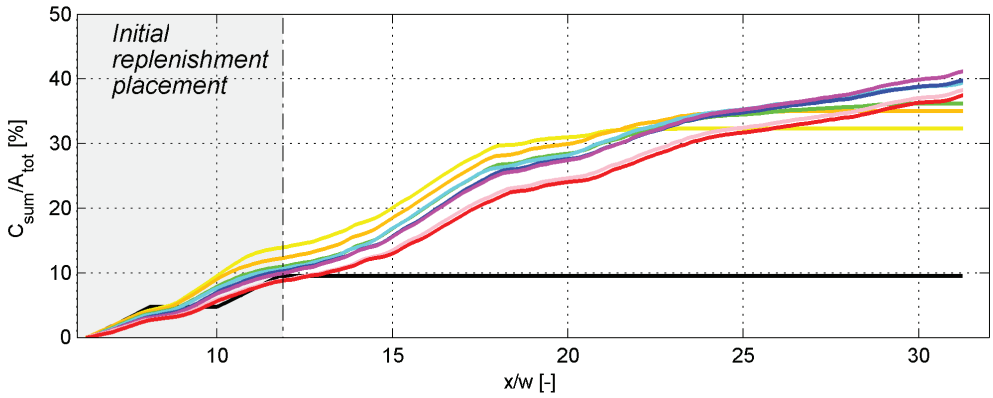

Cumulative sum of the OCR-distribution. Area initially occupied by the replenished deposits in gray. Time steps with same color map as above

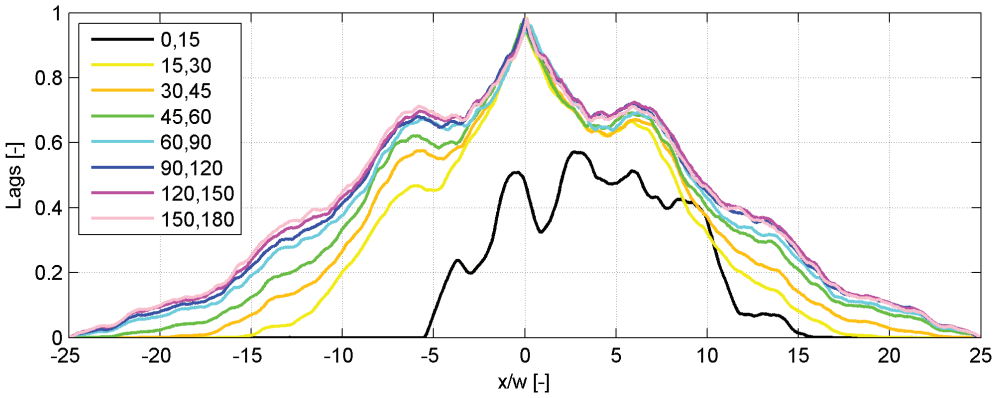

Temporal distribution of the OCR-distribution correlations

A.2 Experiment 2, Configuration B, 100% submergence

Parameters

Conf	Sub %	Shift m	L m	w m	Vol m^3	Weight kg	Q m^3/s	Duration h	Time steps
B	100	1/2	0.75	0.13	0.027	27.0	0.019	3	10

Configuration states

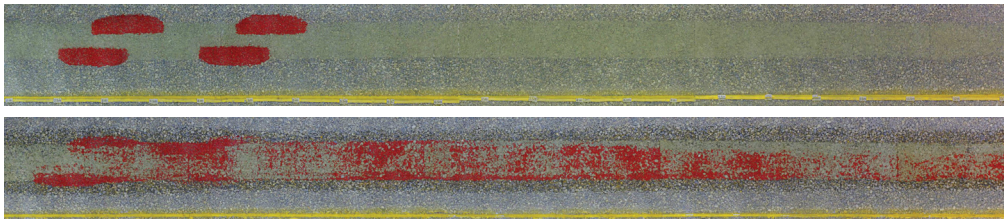

(Top) Initial state, (Bottom) final state after 3 hours testing. Flow direction from left to right

Assessed parameters

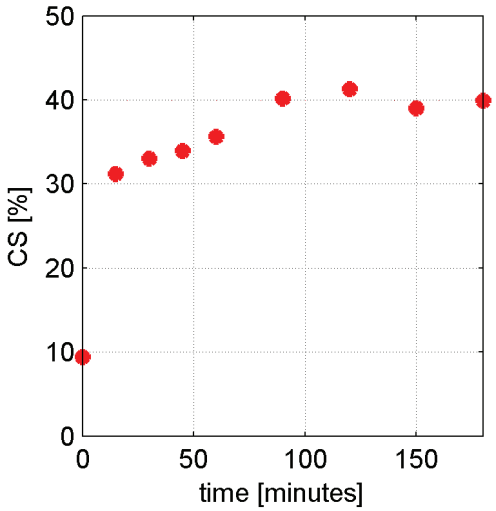

(a) Covered surface CS

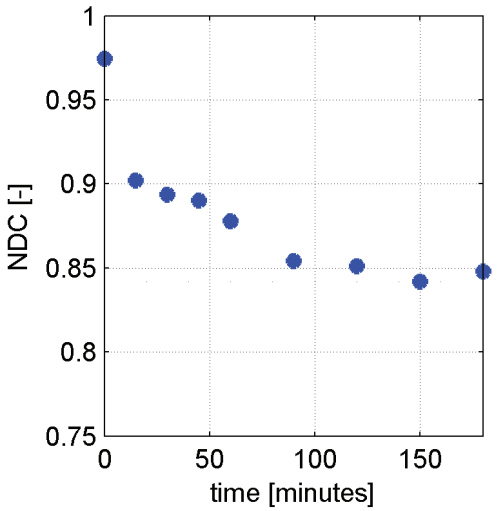

(b) Compactness NDC

(a) Temporal evolution of covered surface CS and (b) compactness NDC for the tested configuration

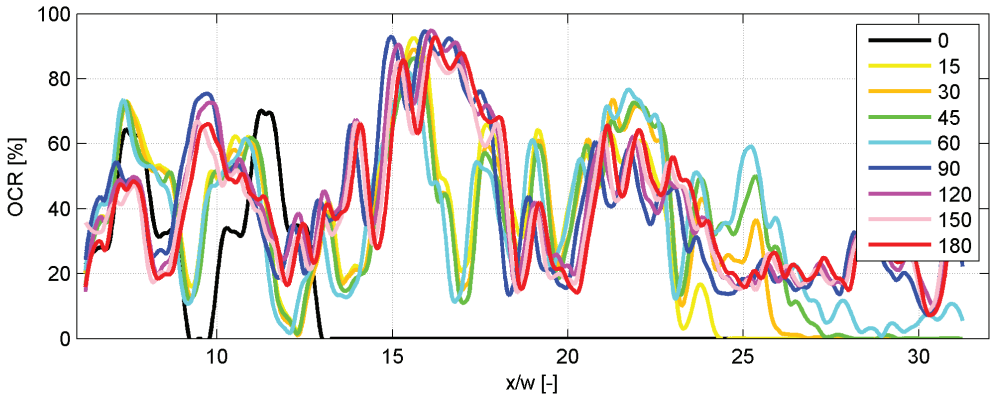

Temporal evolution of the occupation ratio distribution OCR. Time steps in minutes

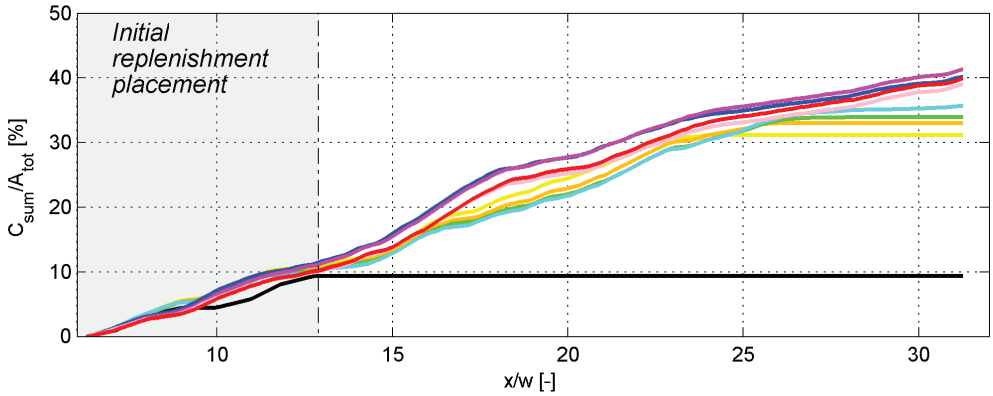

Cumulative sum of the OCR-distribution. Area initially occupied by the replenished deposits in gray. Time steps with same color map as above

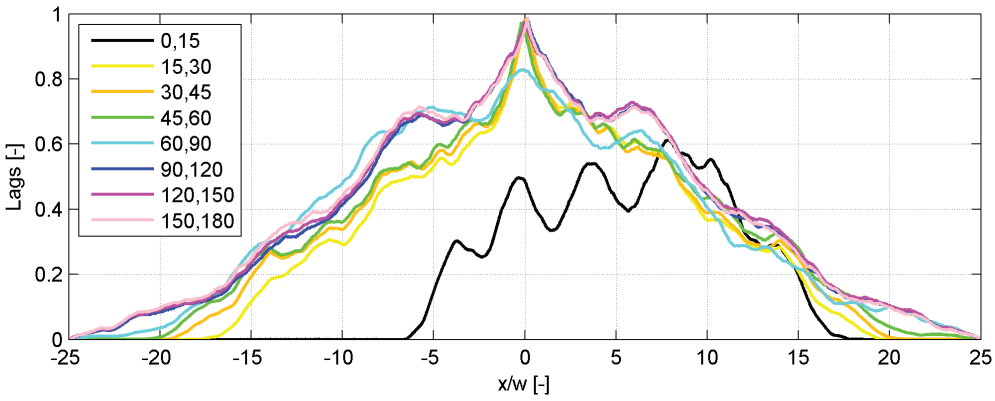

Temporal distribution of the OCR-distribution correlations

A.3 Experiment 3, Configuration A, 100% submergence

Parameters

Conf	Sub %	Shift m	L m	w m	Vol m^3	Weight kg	Q m^3/s	Duration h	Time steps
A	100	0	0.75	0.13	0.027	27.0	0.019	3	10

Configuration states

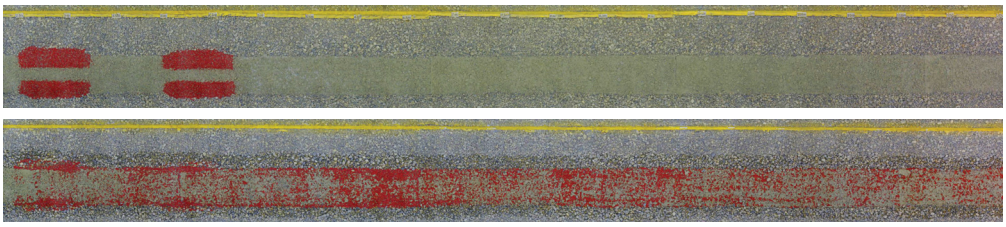

(Top) Initial state, (Bottom) final state after 3 hours testing. Flow direction from left to right

Assessed parameters

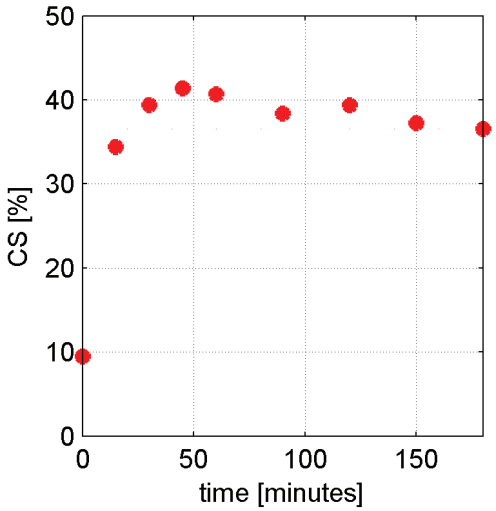

(a) Covered surface CS

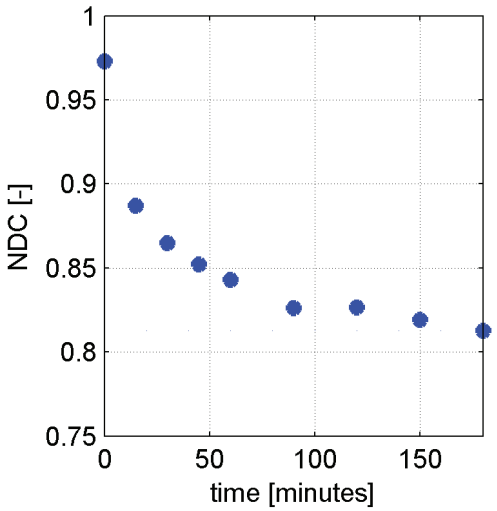

(b) Compactness NDC

(a) Temporal evolution of covered surface CS and (b) compactness NDC for the tested configuration

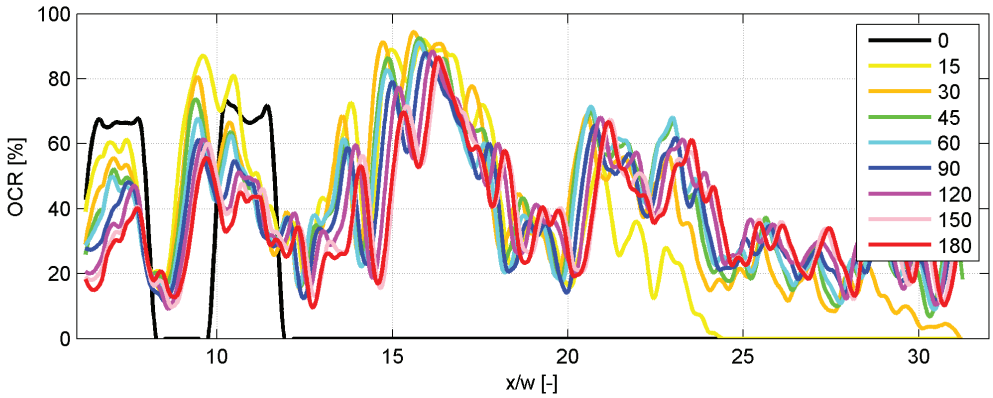

Temporal evolution of the occupation ratio distribution OCR. Time steps in minutes

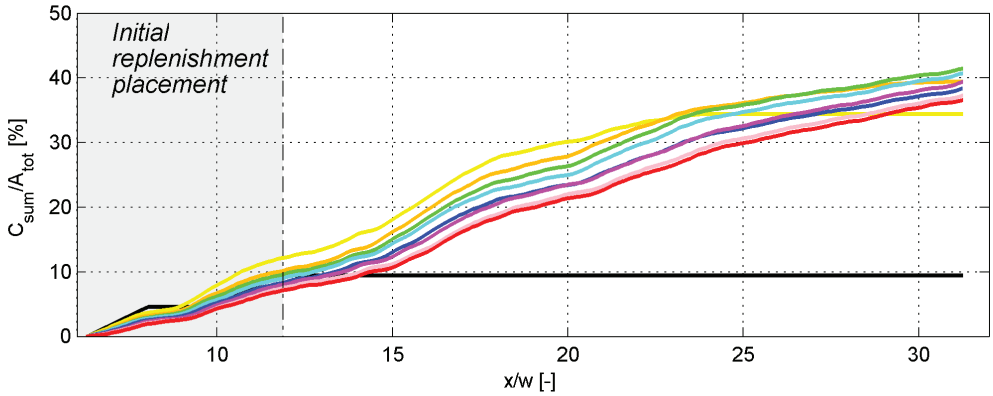

Cumulative sum of the OCR-distribution. Area initially occupied by the replenished deposits in gray. Time steps with same color map as above

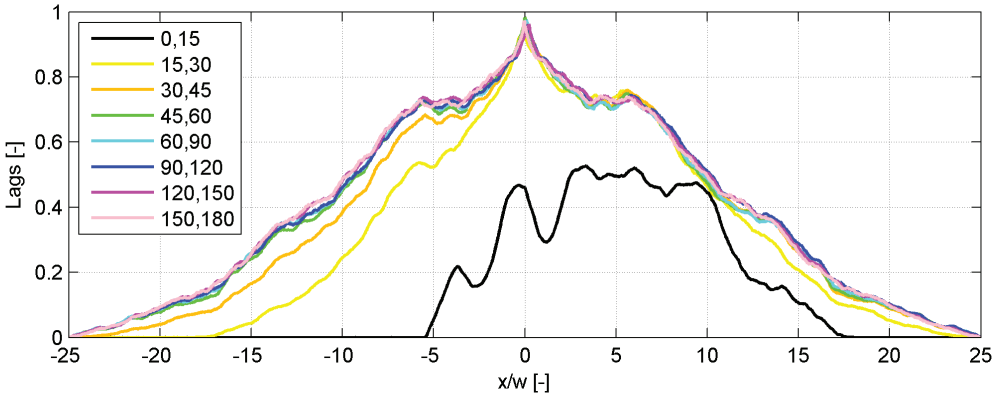

Temporal distribution of the OCR-distribution correlations

A.4 Experiment 4, Configuration B, 100% submergence

Parameters

Conf	Sub %	Shift m	L m	w m	Vol m^3	Weight kg	Q m^3/s	Duration h	Time steps
B	100	1/2	0.75	0.13	0.027	27.0	0.019	3	10

Configuration states

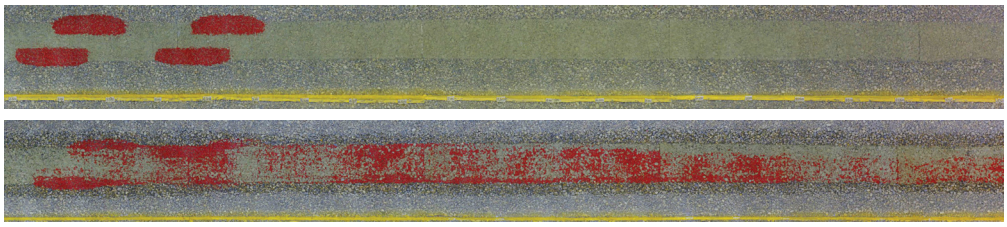

(Top) Initial state, (Bottom) final state after 3 hours testing. Flow direction from left to right

Assessed parameters

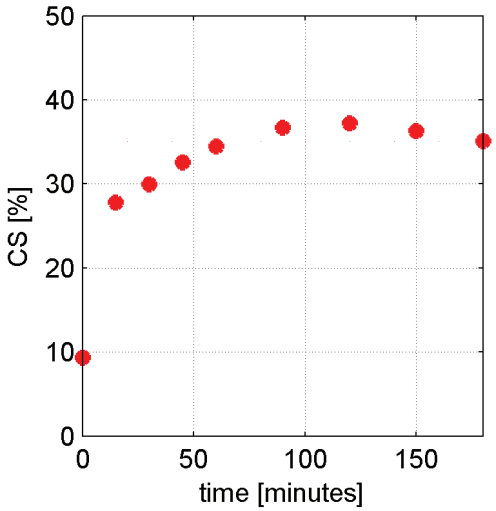

(a) Covered surface CS

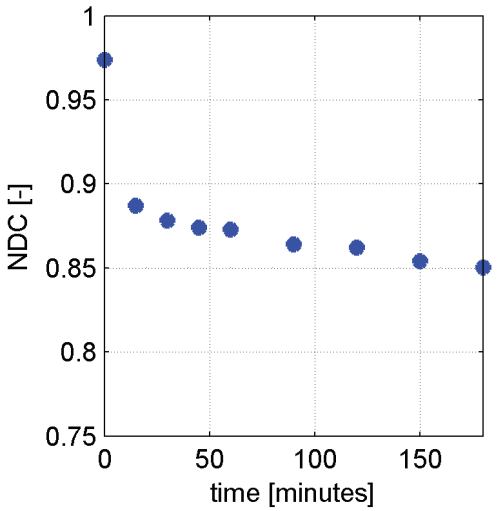

(b) Compactness NDC

(a) Temporal evolution of covered surface CS and (b) compactness NDC for the tested configuration

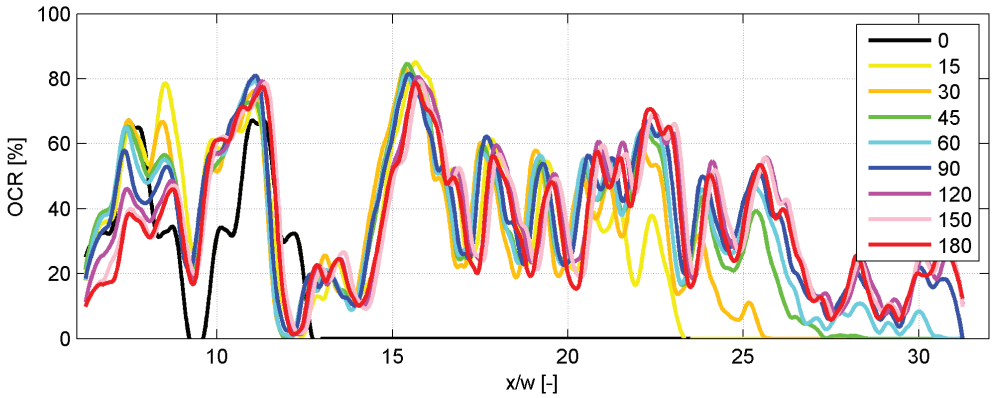

Temporal evolution of the occupation ratio distribution OCR. Time steps in minutes

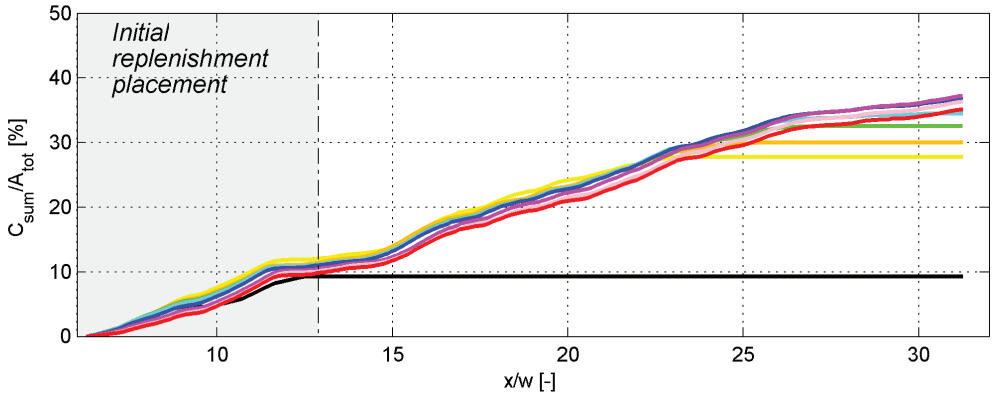

Cumulative sum of the OCR-distribution. Area initially occupied by the replenished deposits in gray. Time steps with same color map as above

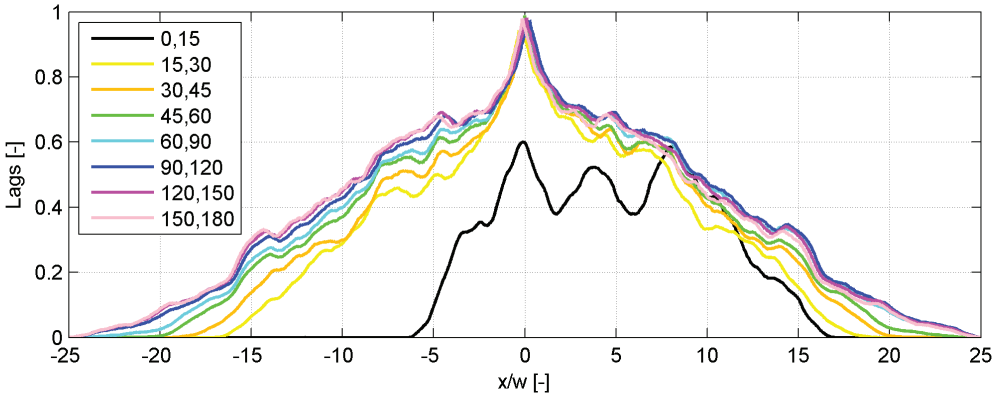

Temporal distribution of the OCR-distribution correlations

A.5 Experiment 5, Configuration A, 130% submergence

Parameters

Conf	Sub %	Shift m	L m	w m	Vol m^3	Weight kg	Q m^3/s	Duration h	Time steps
A	130	0	0.75	0.13	0.027	27.0	0.031	3	10

Configuration states

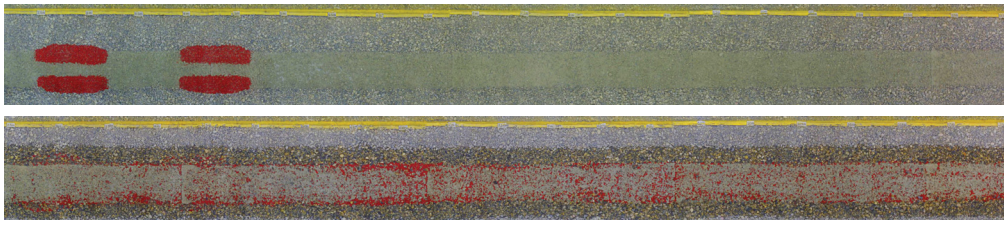

(Top) Initial state, (Bottom) final state after 3 hours testing. Flow direction from left to right

Assessed parameters

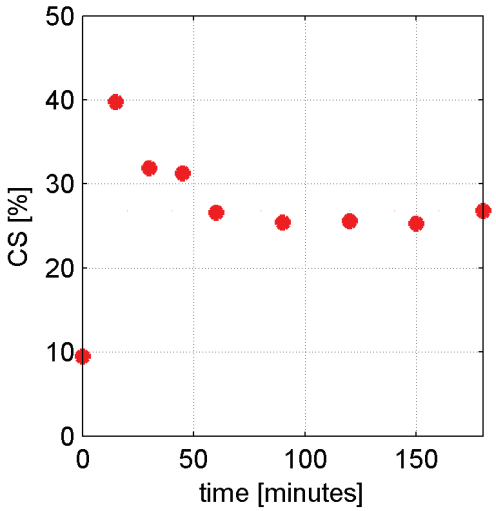

(a) Covered surface CS

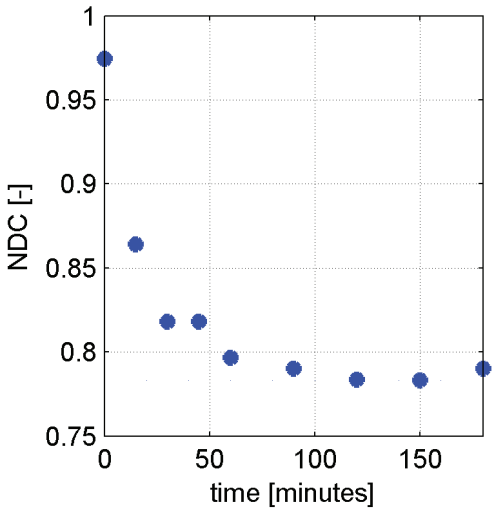

(b) Compactness NDC

(a) Temporal evolution of covered surface CS and (b) compactness NDC for the tested configuration

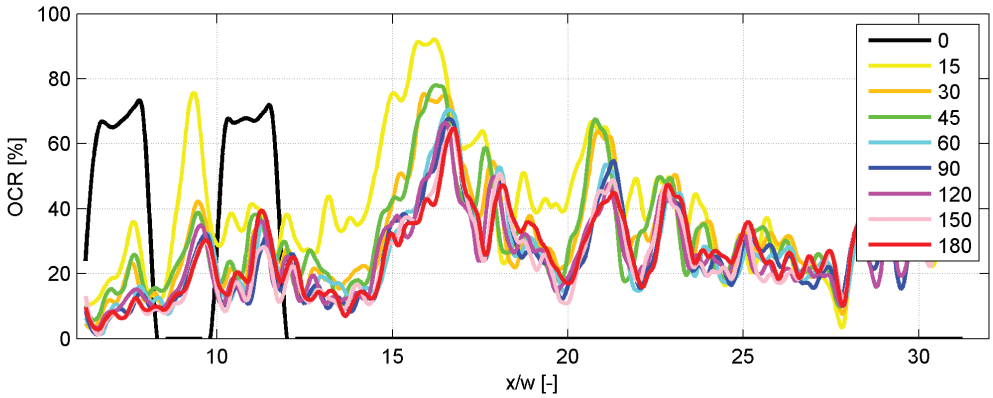

Temporal evolution of the occupation ratio distribution OCR. Time steps in minutes

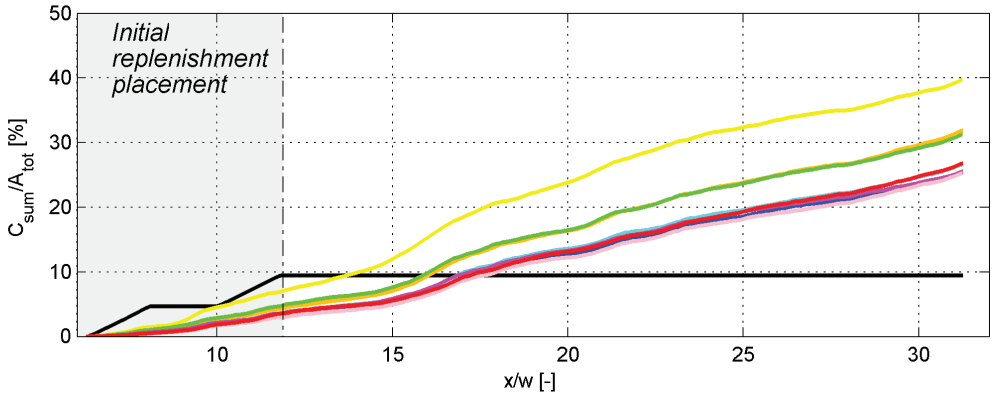

Cumulative sum of the OCR-distribution. Area initially occupied by the replenished deposits in gray. Time steps with same color map as above

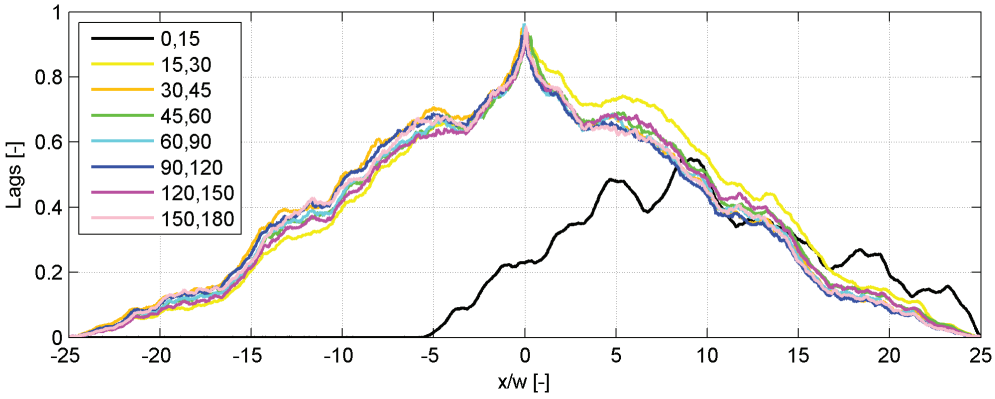

Temporal distribution of the OCR-distribution correlations

A.6 Experiment 6, Configuration B, 130% submergence

Parameters

Conf	Sub %	Shift m	L m	w m	Vol m^3	Weight kg	Q m^3/s	Duration h	Time steps
B	130	1/2	0.75	0.13	0.027	27.0	0.031	3	10

Configuration states

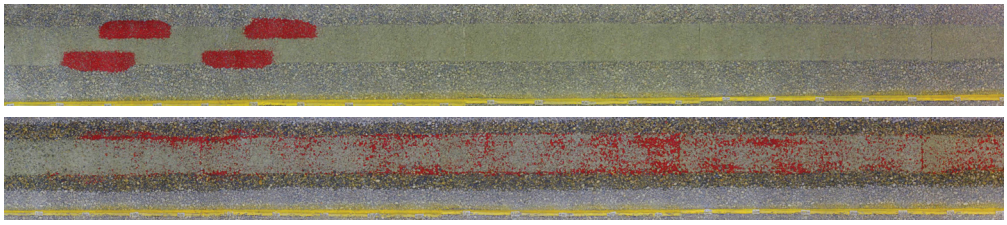

(Top) Initial state, (Bottom) final state after 3 hours testing. Flow direction from left to right

Assessed parameters

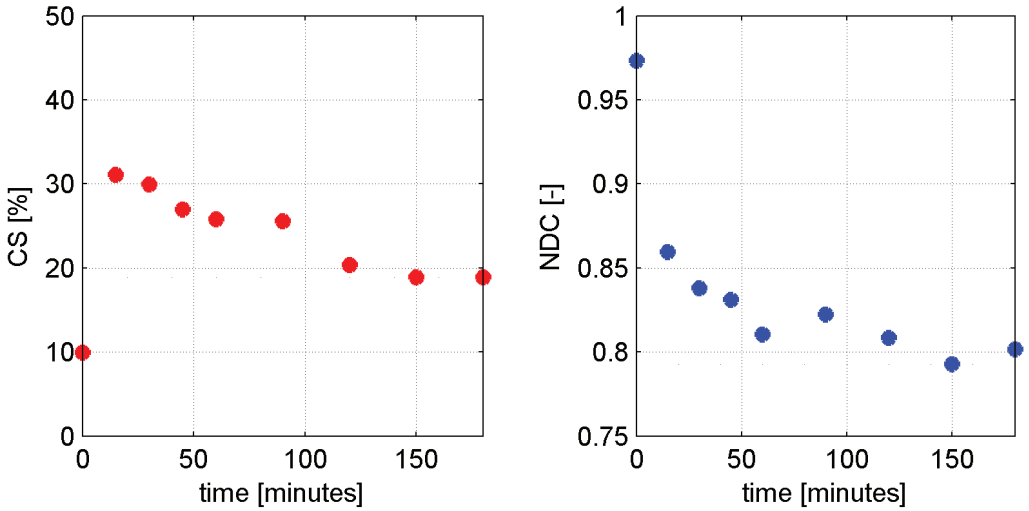

(a) Covered surface CS (b) Compactness NDC

(a) Temporal evolution of covered surface CS and (b) compactness NDC for the tested configuration

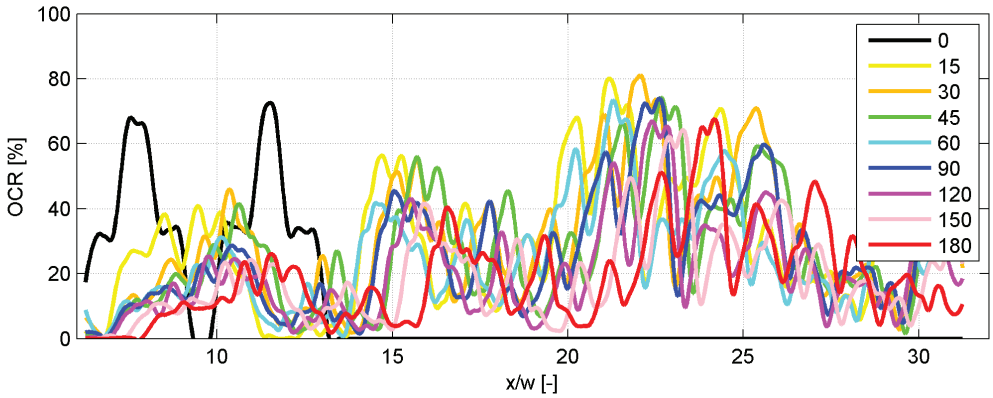

Temporal evolution of the occupation ratio distribution OCR. Time steps in minutes

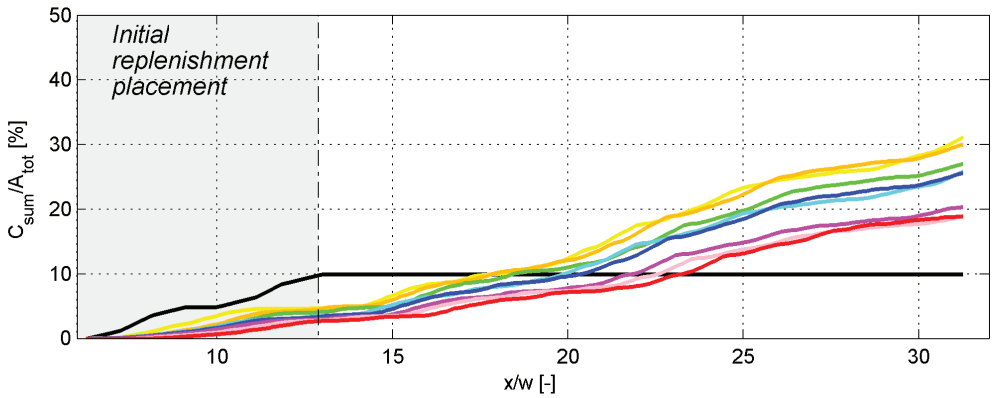

Cumulative sum of the OCR-distribution. Area initially occupied by the replenished deposits in gray. Time steps with same color map as above

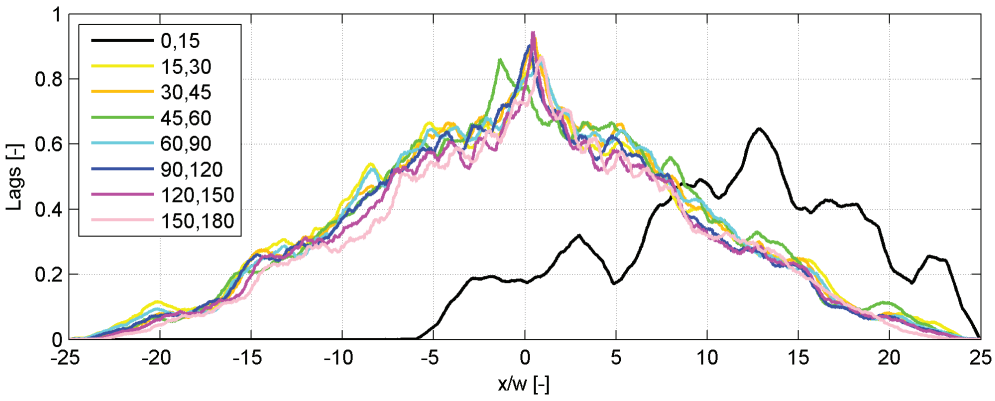

Temporal distribution of the OCR-distribution correlations

A.7 Experiment 7, Configuration C, 100% submergence

Parameters

Conf	Sub %	Shift m	L m	w m	Vol m^3	Weight kg	Q m^3/s	Duration h	Time steps
C	70	1	0.75	0.13	0.027	27.0	0.019	3	10

Configuration states

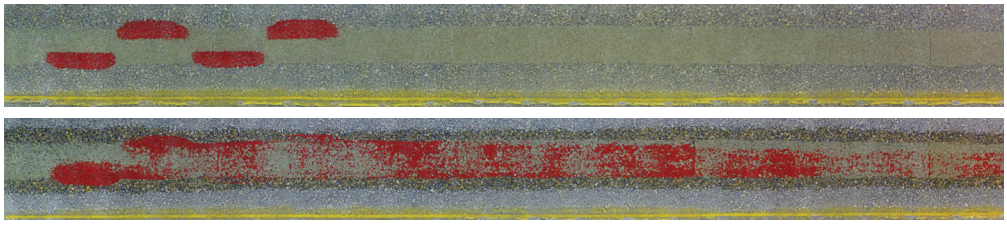

(Top) Initial state, (Bottom) final state after 3 hours testing. Flow direction from left to right

Assessed parameters

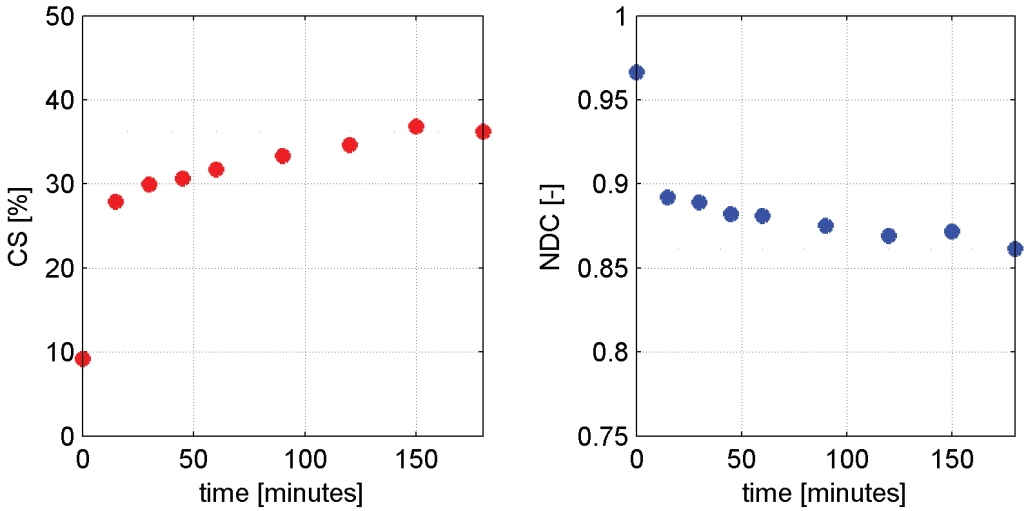

(a) Covered surface CS

(b) Compactness NDC

(a) Temporal evolution of covered surface CS and (b) compactness NDC for the tested configuration

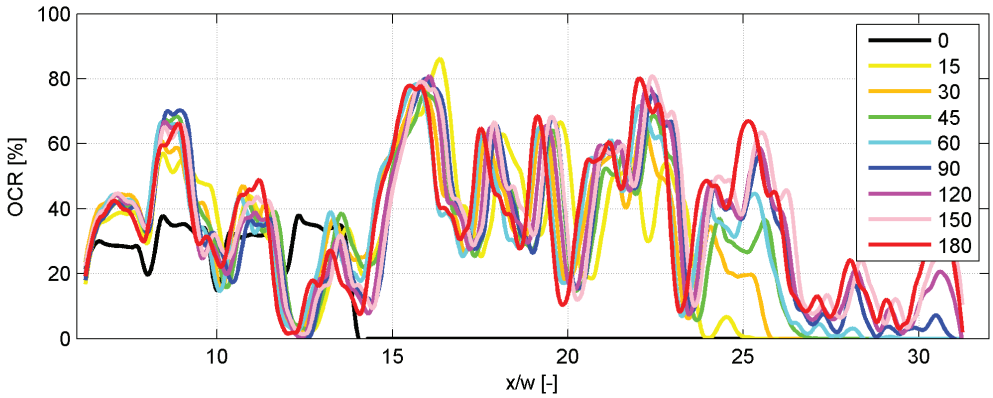

Temporal evolution of the occupation ratio distribution OCR. Time steps in minutes

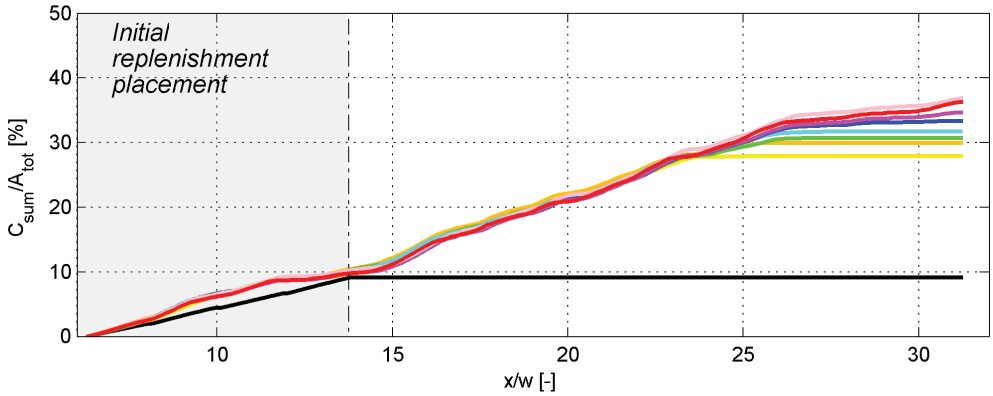

Cumulative sum of the OCR-distribution. Area initially occupied by the replenished deposits in gray. Time steps with same color map as above

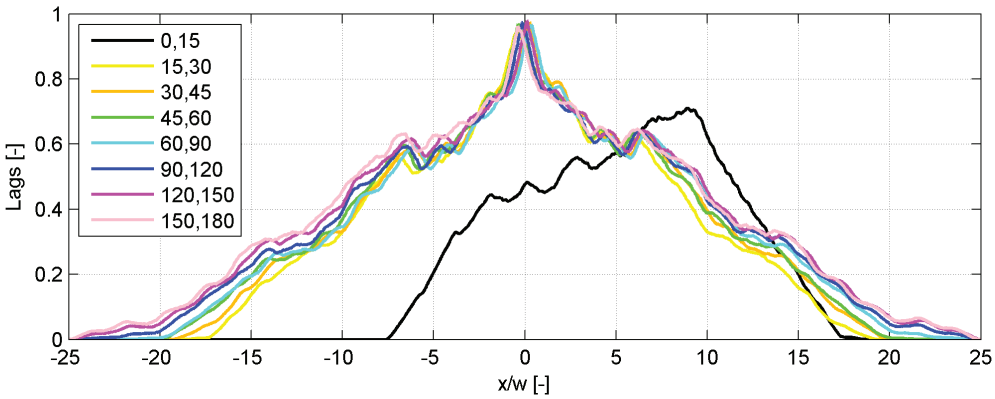

Temporal distribution of the OCR-distribution correlations

A.8 Experiment 8, Configuration D, 100% submergence

Parameters

Conf	Sub %	Shift m	L m	w m	Vol m^3	Weight kg	Q m^3/s	Duration h	Time steps
D	100	2	0.75	0.13	0.027	27.0	0.019	3	10

Configuration states

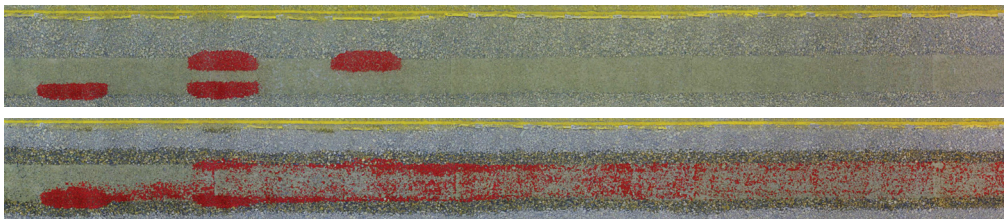

(Top) Initial state, (Bottom) final state after 3 hours testing. Flow direction from left to right

Assessed parameters

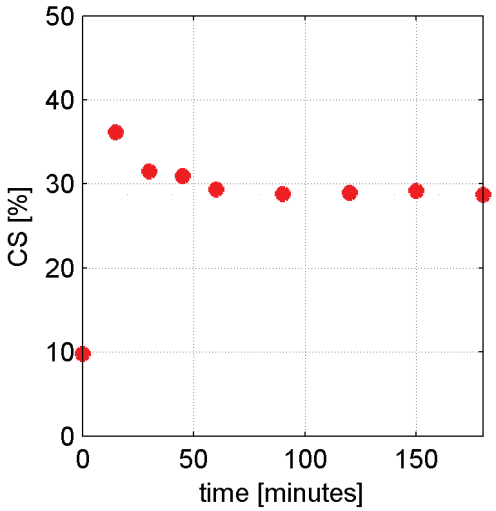

(a) Covered surface CS

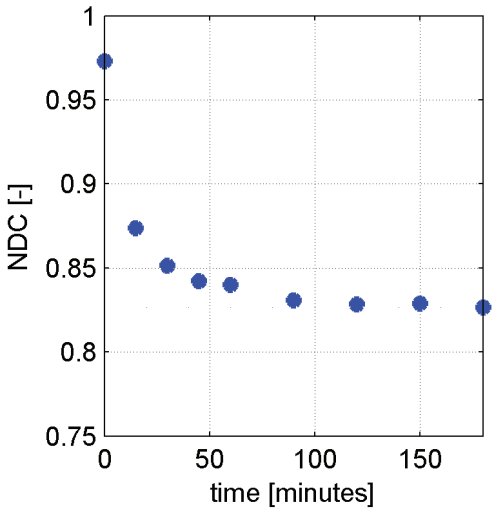

(b) Compactness NDC

(a) Temporal evolution of covered surface CS and (b) compactness NDC for the tested configuration

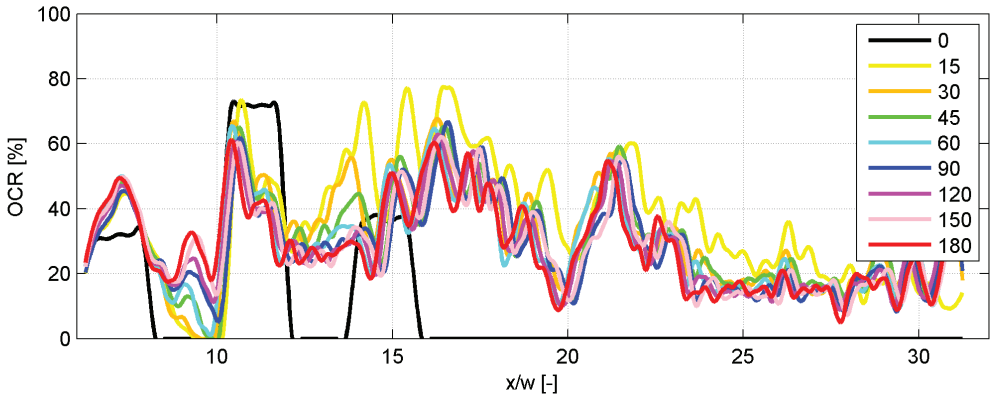

Temporal evolution of the occupation ratio distribution OCR. Time steps in minutes

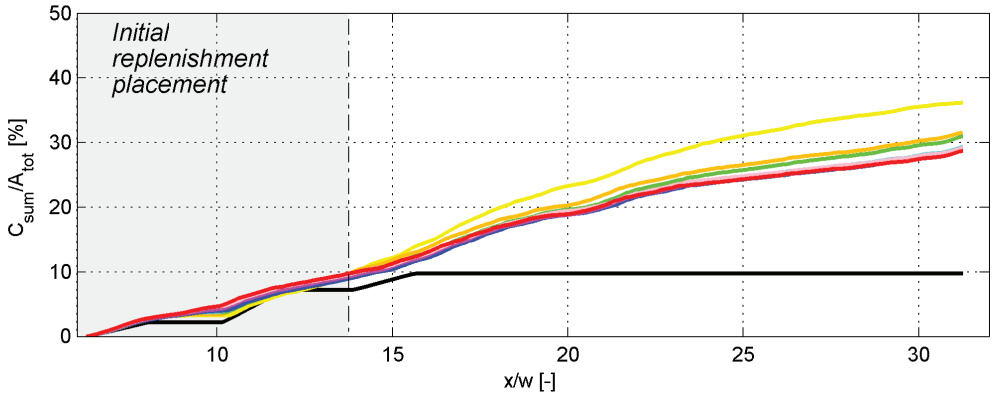

Cumulative sum of the OCR-distribution. Area initially occupied by the replenished deposits in gray. Time steps with same color map as above

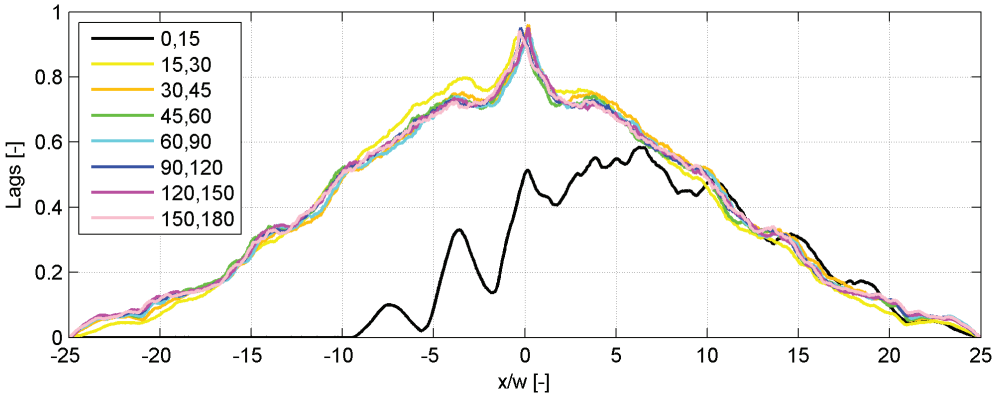

Temporal distribution of the OCR-distribution correlations

A.9 Experiment 9, Configuration C, 130% submergence

Parameters

Conf	Sub %	Shift m	L m	w m	Vol m^3	Weight kg	Q m^3/s	Duration h	Time steps
C	130	1	0.75	0.13	0.027	27.0	0.031	3	10

Configuration states

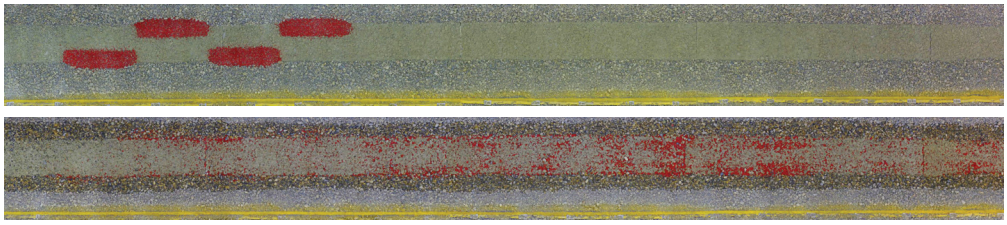

(Top) Initial state, (Bottom) final state after 3 hours testing. Flow direction from left to right

Assessed parameters

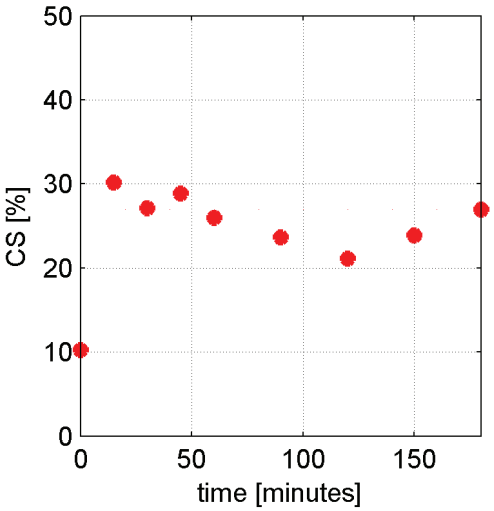

(a) Covered surface CS

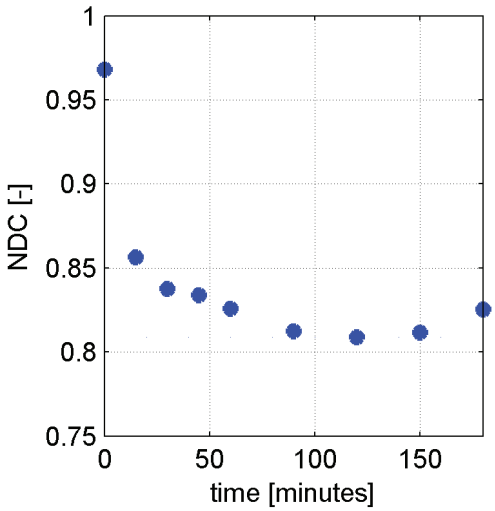

(b) Compactness NDC

(a) Temporal evolution of covered surface CS and (b) compactness NDC for the tested configuration

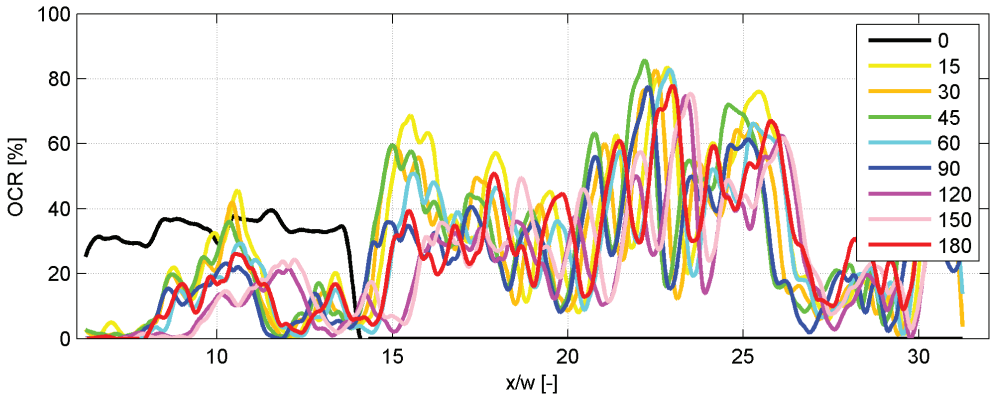

Temporal evolution of the occupation ratio distribution OCR. Time steps in minutes

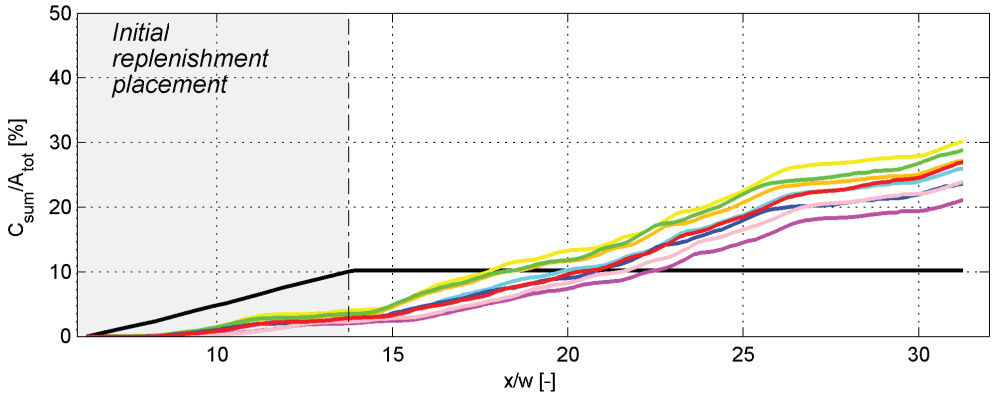

Cumulative sum of the OCR-distribution. Area initially occupied by the replenished deposits in gray. Time steps with same color map as above

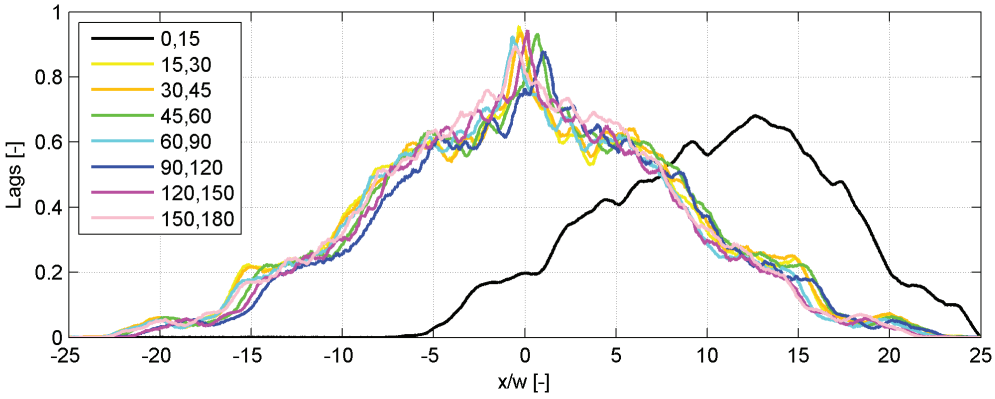

Temporal distribution of the OCR-distribution correlations

A.10 Experiment 10, Configuration D, 130% submergence

Parameters

Conf	Sub %	Shift m	L m	w m	Vol m^3	Weight kg	Q m^3/s	Duration h	Time steps
D	130	2	0.75	0.13	0.027	27.0	0.031	3	10

Configuration states

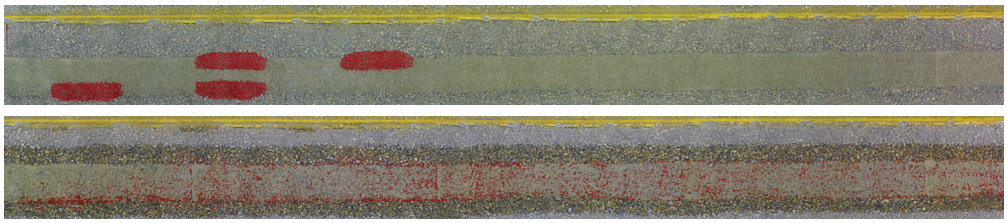

(Top) Initial state, (Bottom) final state after 3 hours testing. Flow direction from left to right

Assessed parameters

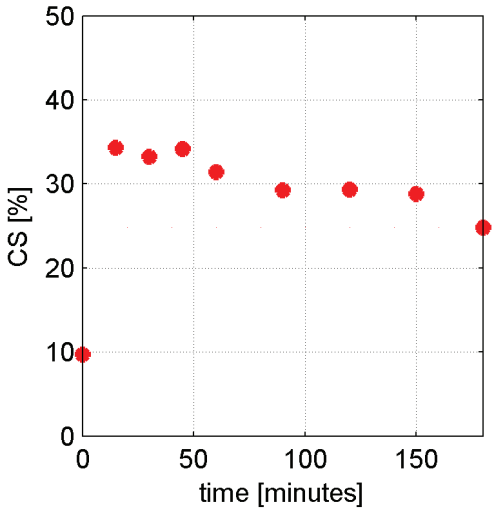

(a) Covered surface CS

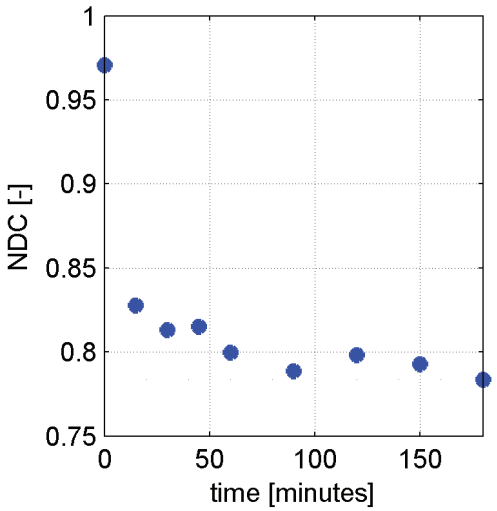

(b) Compactness NDC

(a) Temporal evolution of covered surface CS and (b) compactness NDC for the tested configuration

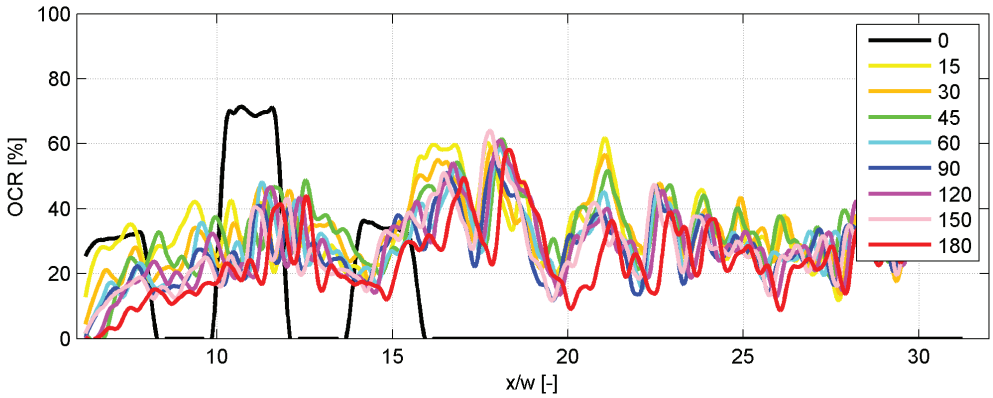

Temporal evolution of the occupation ratio distribution OCR. Time steps in minutes

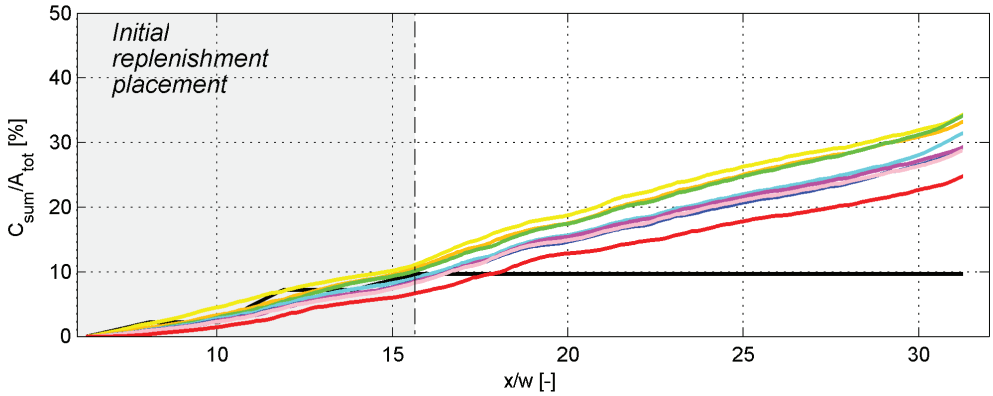

Cumulative sum of the OCR-distribution. Area initially occupied by the replenished deposits in gray. Time steps with same color map as above

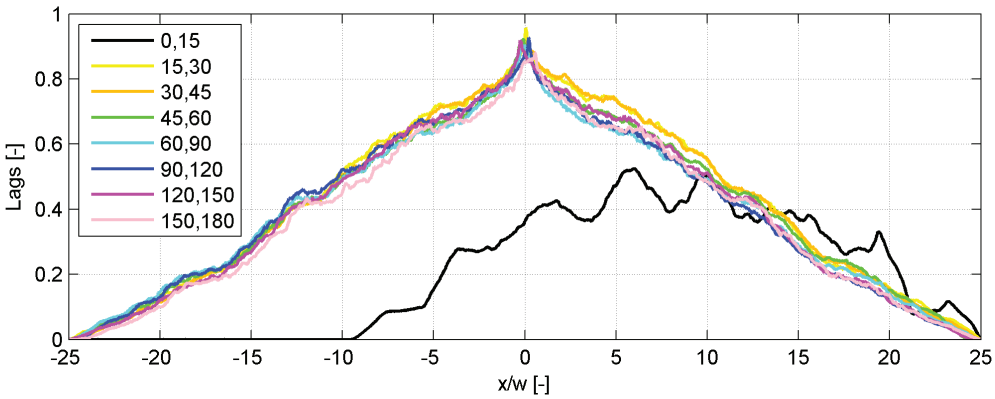

Temporal distribution of the OCR-distribution correlations

A.11 Experiment 11, Configuration C, 70% submergence

Parameters

Conf	Sub %	Shift m	L m	w m	Vol m^3	Weight kg	Q m^3/s	Duration h	Time steps
C	70	1	0.75	0.13	0.027	27.3	0.008	3	11

Configuration states

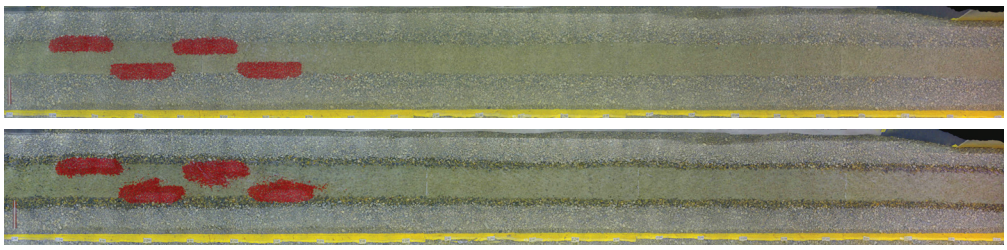

(Top) Initial state, (Bottom) final state after 3 hours testing. Flow direction from left to right

Assessed parameters

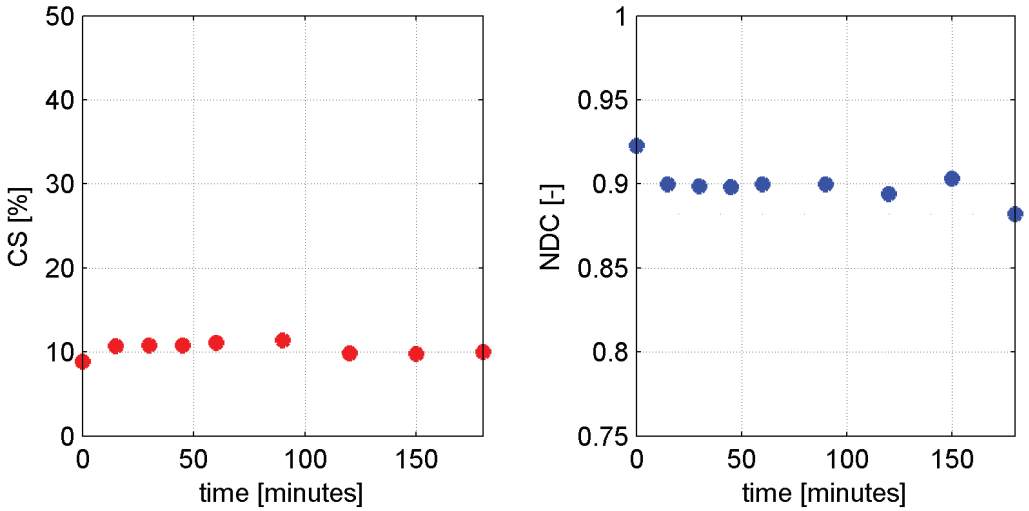

(a) Covered surface CS (b) Compactness NDC

(a) Temporal evolution of covered surface CS and (b) compactness NDC for the tested configuration

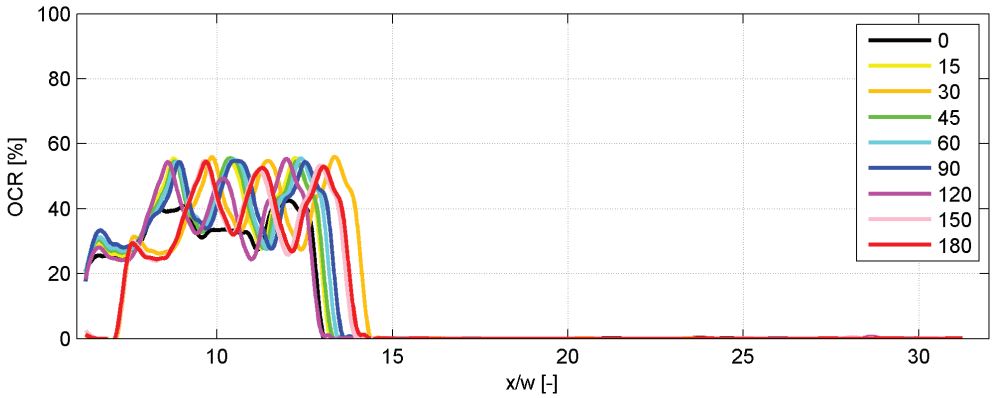

Temporal evolution of the occupation ratio distribution OCR. Time steps in minutes

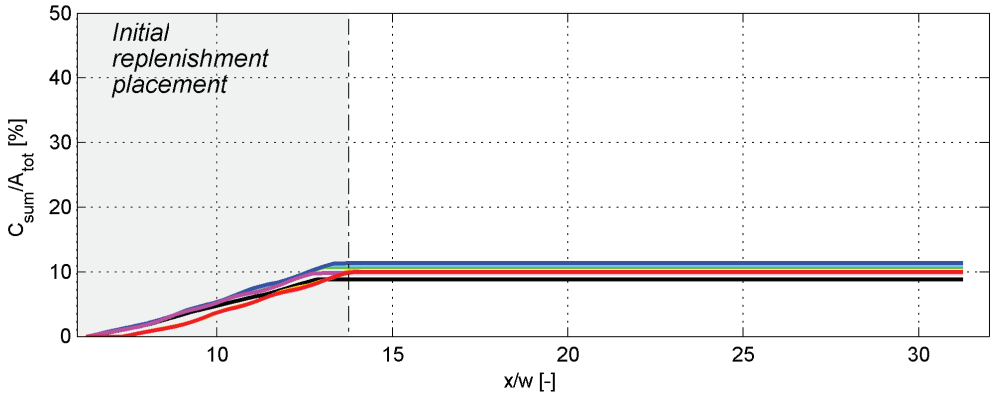

Cumulative sum of the OCR-distribution. Area initially occupied by the replenished deposits in gray. Time steps with same color map as above

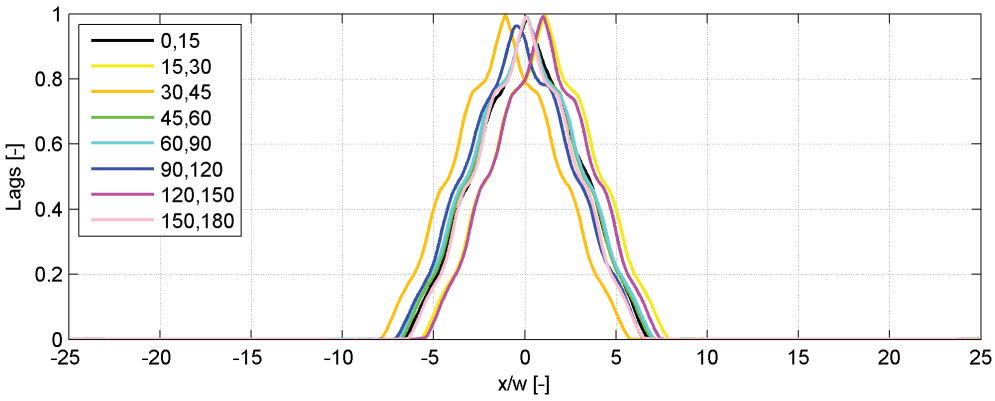

Temporal distribution of the OCR-distribution correlations

A.12 Experiment 12, Configuration D, 70% submergence

Parameters

Conf	Sub %	Shift m	L m	w m	Vol m^3	Weight kg	Q m^3/s	Duration h	Time steps
D	70	2	0.75	0.13	0.027	28.5	0.008	3	11

Configuration states

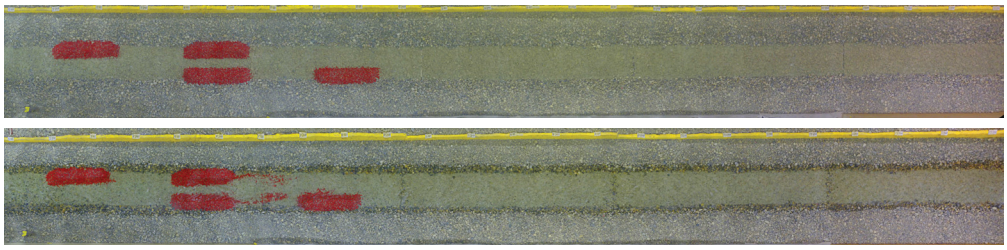

(Top) Initial state, (Bottom) final state after 3 hours testing. Flow direction from left to right

Assessed parameters

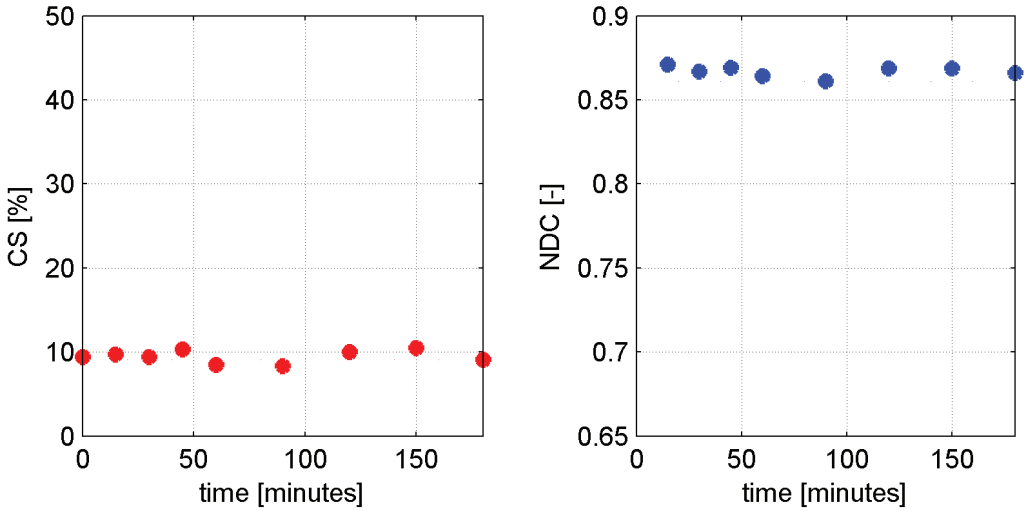

(a) Covered surface CS (b) Compactness NDC

(a) Temporal evolution of covered surface CS and (b) compactness NDC for the tested configuration

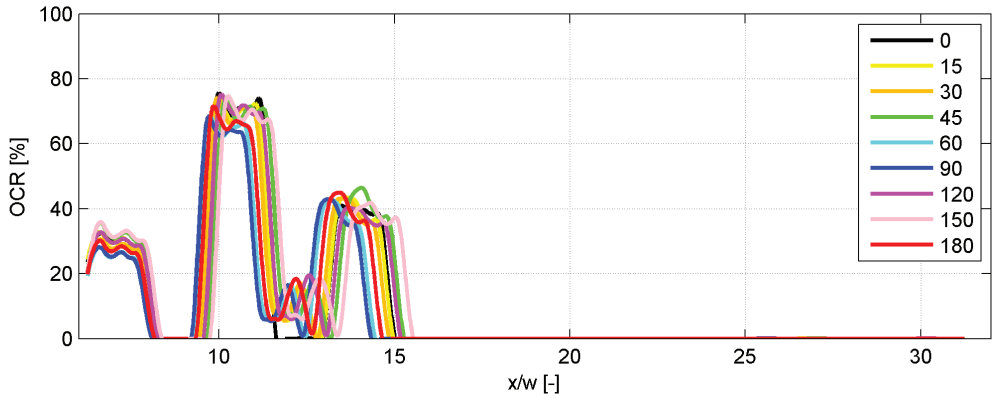

Temporal evolution of the occupation ratio distribution OCR. Time steps in minutes

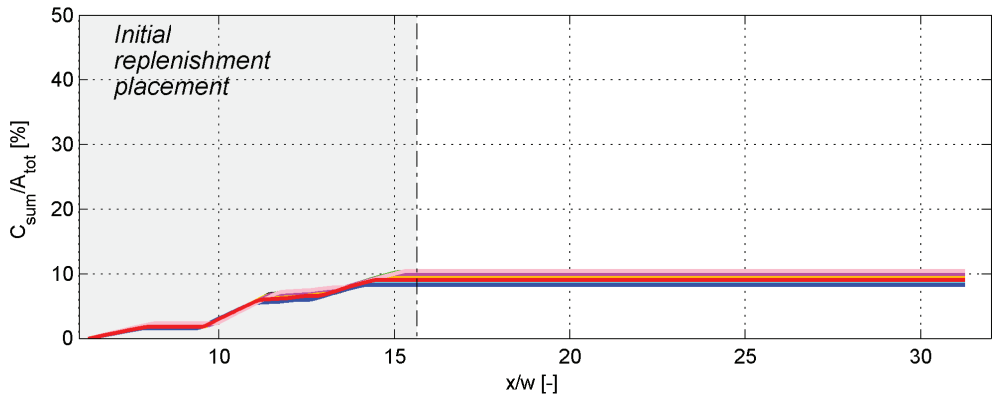

Cumulative sum of the OCR-distribution. Area initially occupied by the replenished deposits in gray. Time steps with same color map as above

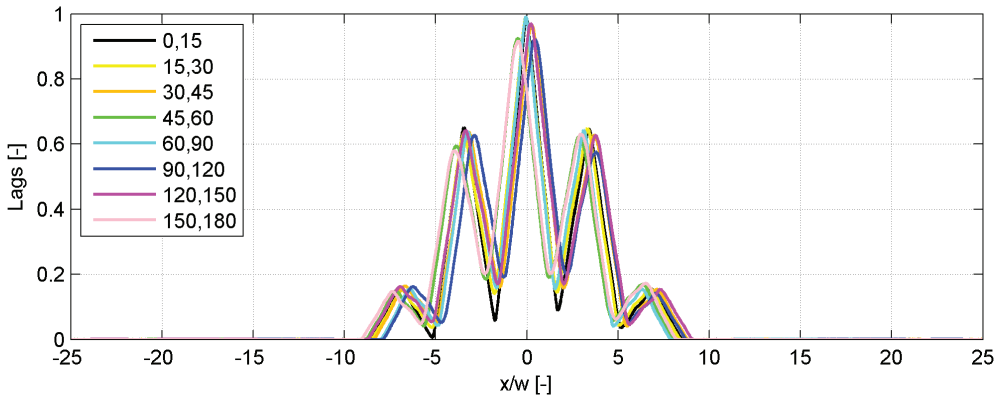

Temporal distribution of the OCR-distribution correlations

A.13 Experiment 13, Configuration A, 100% submergence

Parameters

Conf	Sub %	Shift m	L m	w m	Vol m^3	Weight kg	Q m^3/s	Duration h	Time steps
A	100	0	0.75	0.13	0.027	30.0	0.019	3	11

Configuration states

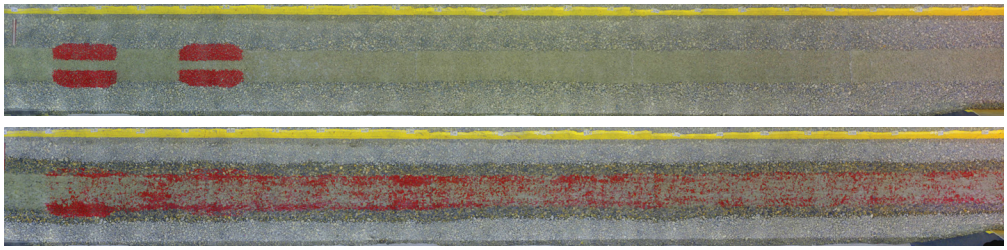

(Top) Initial state, (Bottom) final state after 3 hours testing. Flow direction from left to right

Assessed parameters

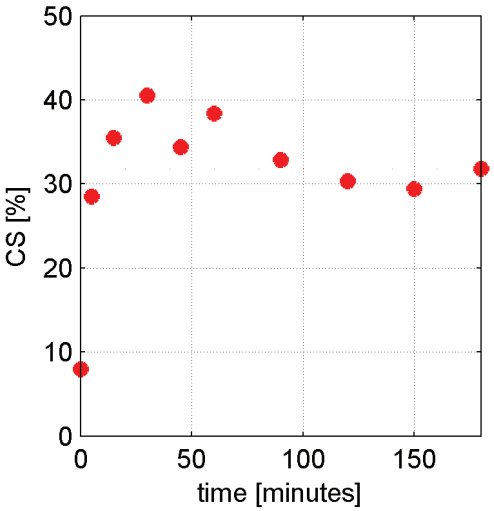

(a) Covered surface CS

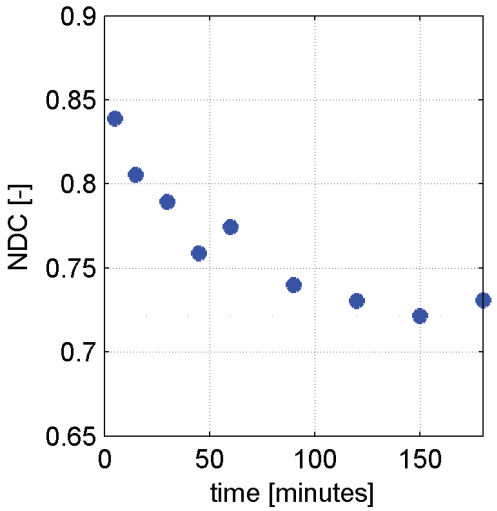

(b) Compactness NDC

(a) Temporal evolution of covered surface CS and (b) compactness NDC for the tested configuration

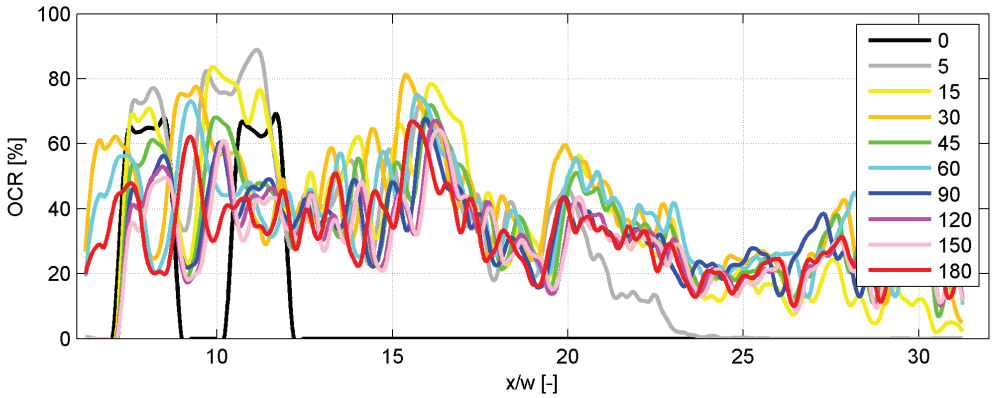

Temporal evolution of the occupation ratio distribution OCR. Time steps in minutes

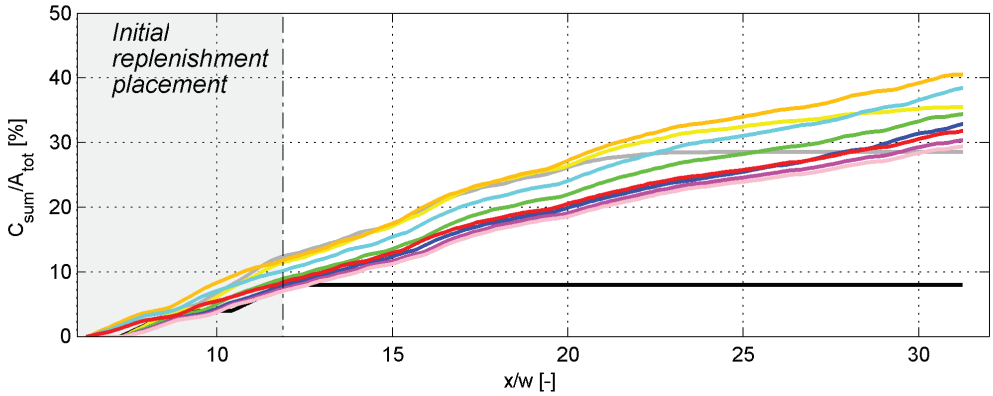

Cumulative sum of the OCR-distribution. Area initially occupied by the replenished deposits in gray. Time steps with same color map as above

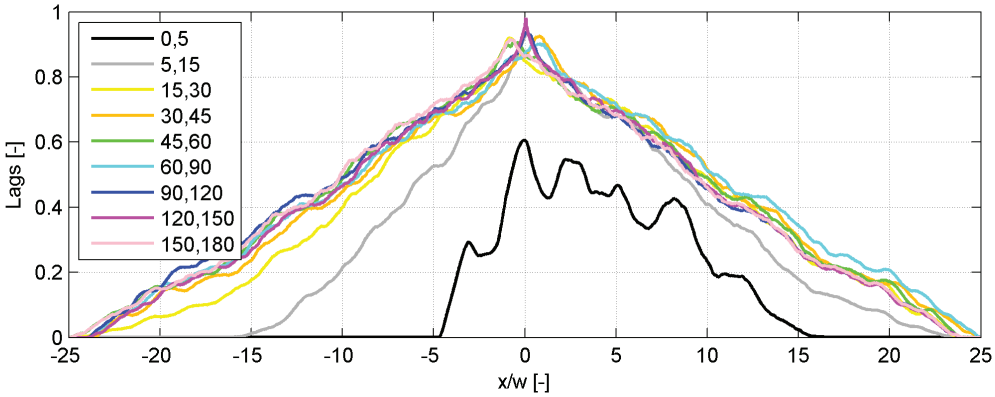

Temporal distribution of the OCR-distribution correlations

A.14 Experiment 14, Configuration B, 100% submergence

Parameters

Conf	Sub %	Shift m	L m	w m	Vol m^3	Weight kg	Q m^3/s	Duration h	Time steps
B	100	1/2	0.75	0.13	0.027	29.7	0.019	3	11

Configuration states

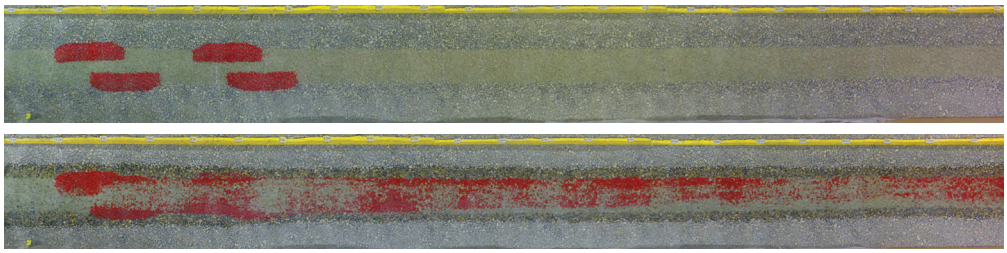

(Top) Initial state, (Bottom) final state after 3 hours testing. Flow direction from left to right

Assessed parameters

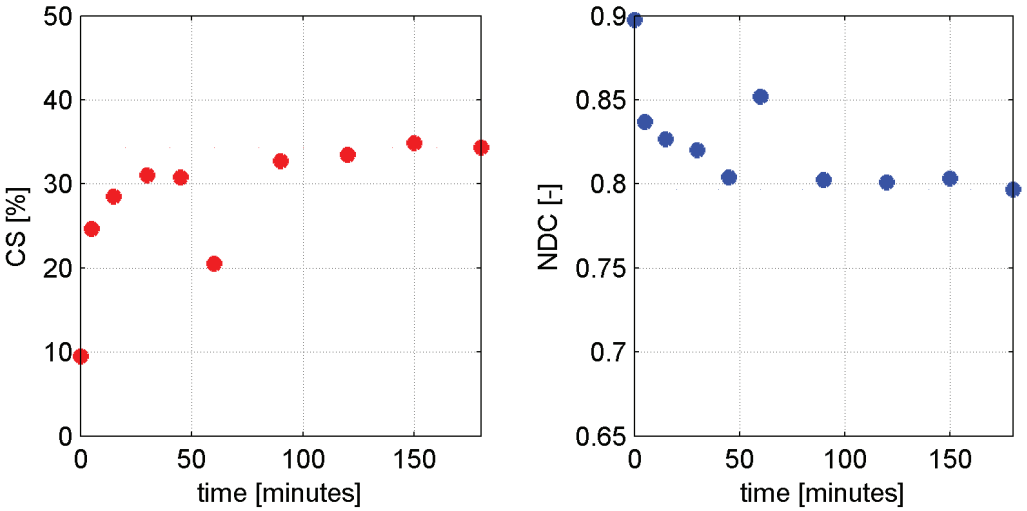

(a) Covered surface CS (b) Compactness NDC

(a) Temporal evolution of covered surface CS and (b) compactness NDC for the tested configuration

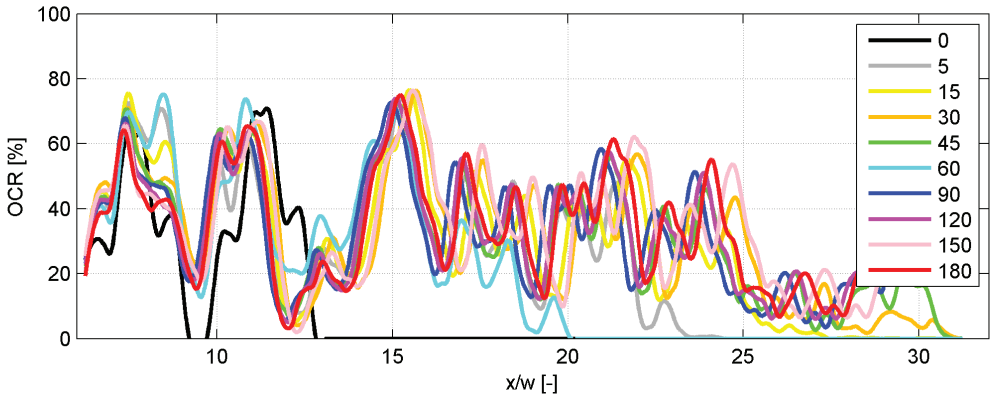

Temporal evolution of the occupation ratio distribution OCR. Time steps in minutes

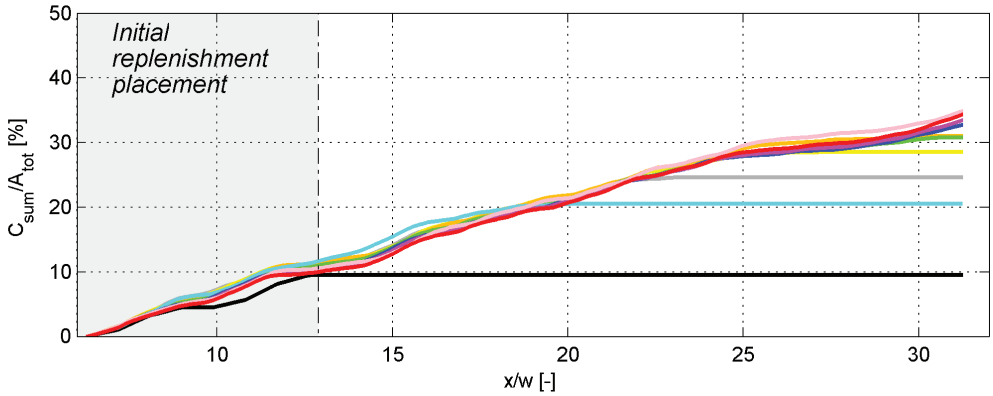

Cumulative sum of the OCR-distribution. Area initially occupied by the replenished deposits in gray. Time steps with same color map as above

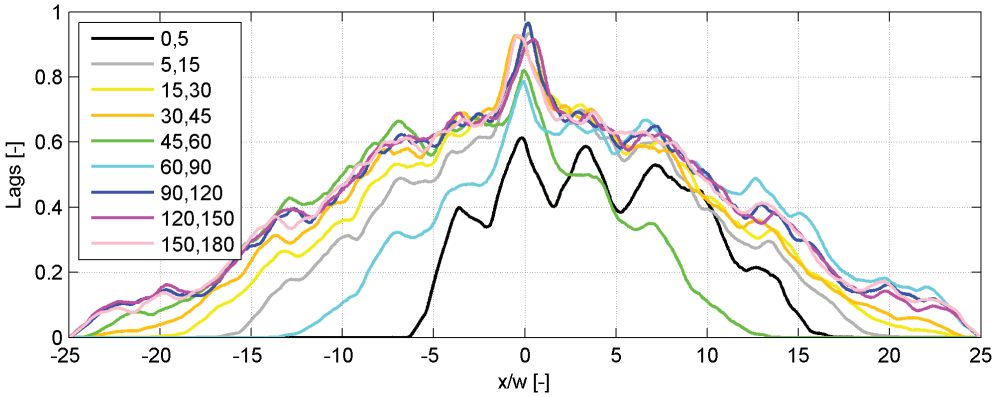

Temporal distribution of the OCR-distribution correlations

A.15 Experiment 15, Configuration C, 100% submergence

Parameters

Conf	Sub %	Shift m	L m	w m	Vol m^3	Weight kg	Q m^3/s	Duration h	Time steps
C	100	1	0.75	0.13	0.027	25.9	0.019	3	11

Configuration states

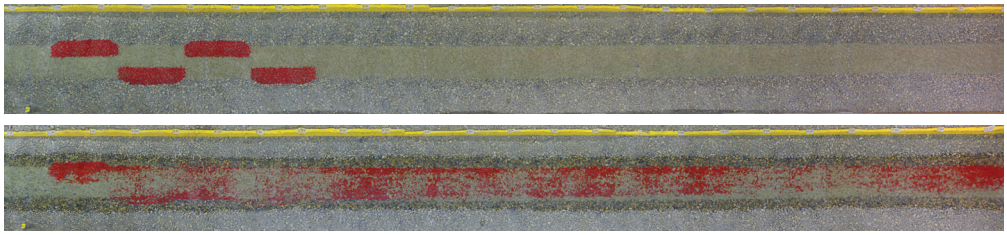

(Top) Initial state, (Bottom) final state after 3 hours testing. Flow direction from left to right

Assessed parameters

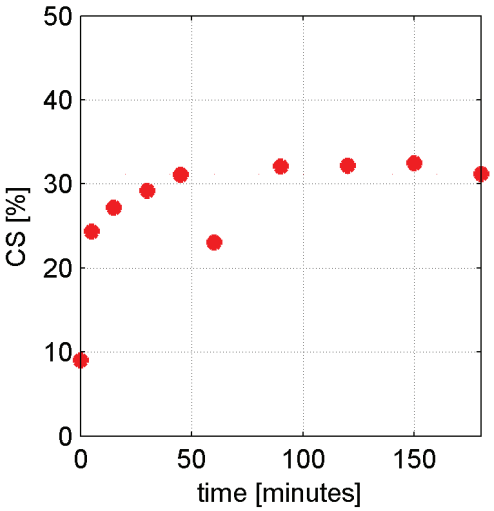

(a) Covered surface CS

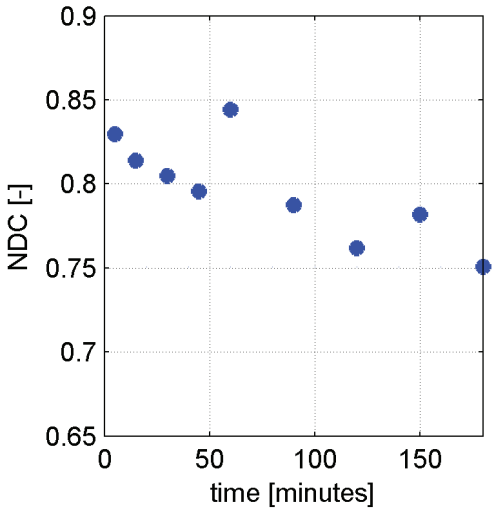

(b) Compactness NDC

(a) Temporal evolution of covered surface CS and (b) compactness NDC for the tested configuration

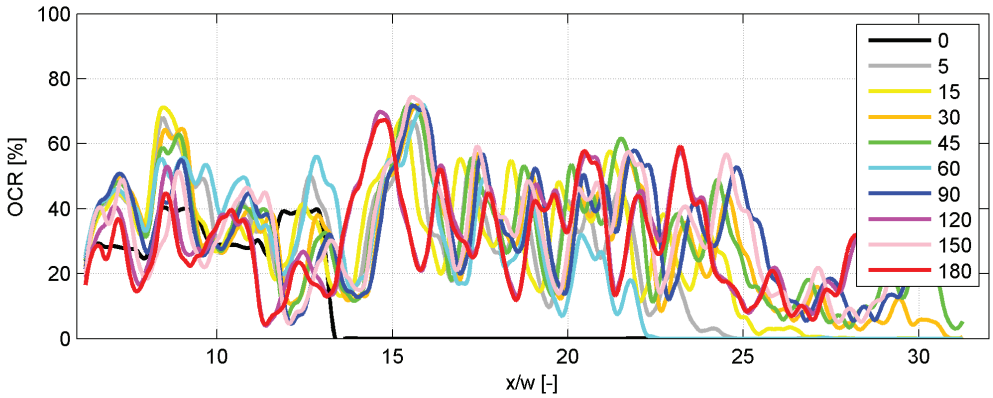

Temporal evolution of the occupation ratio distribution OCR. Time steps in minutes

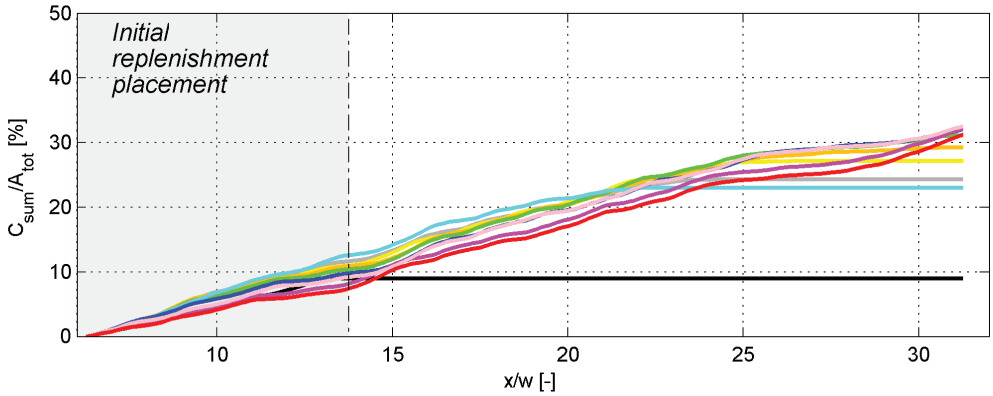

Cumulative sum of the OCR-distribution. Area initially occupied by the replenished deposits in gray. Time steps with same color map as above

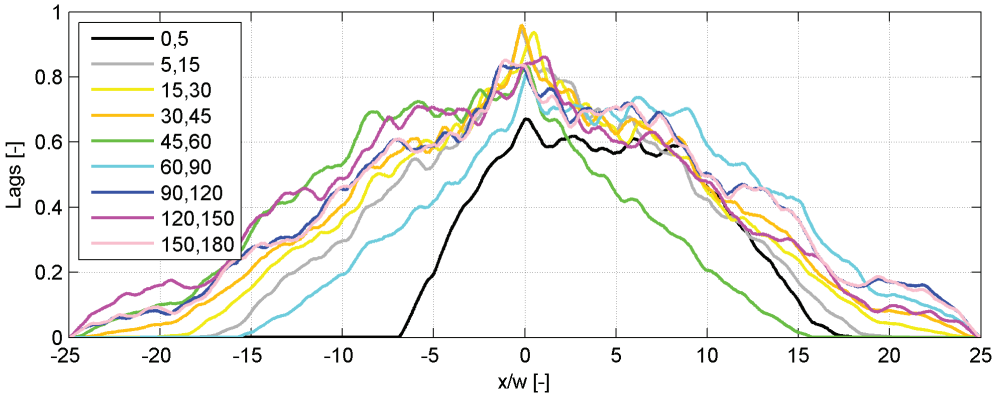

Temporal distribution of the OCR-distribution correlations

A.16 Experiment 16, Configuration D, 100% submergence

Parameters

Conf	Sub %	Shift m	L m	w m	Vol m^3	Weight kg	Q m^3/s	Duration h	Time steps
D	100	2	0.75	0.13	0.027	27.9	0.019	3	11

Configuration states

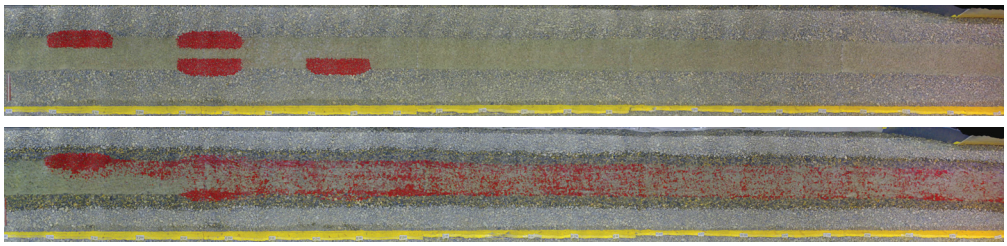

(Top) Initial state, (Bottom) final state after 3 hours testing. Flow direction from left to right

Assessed parameters

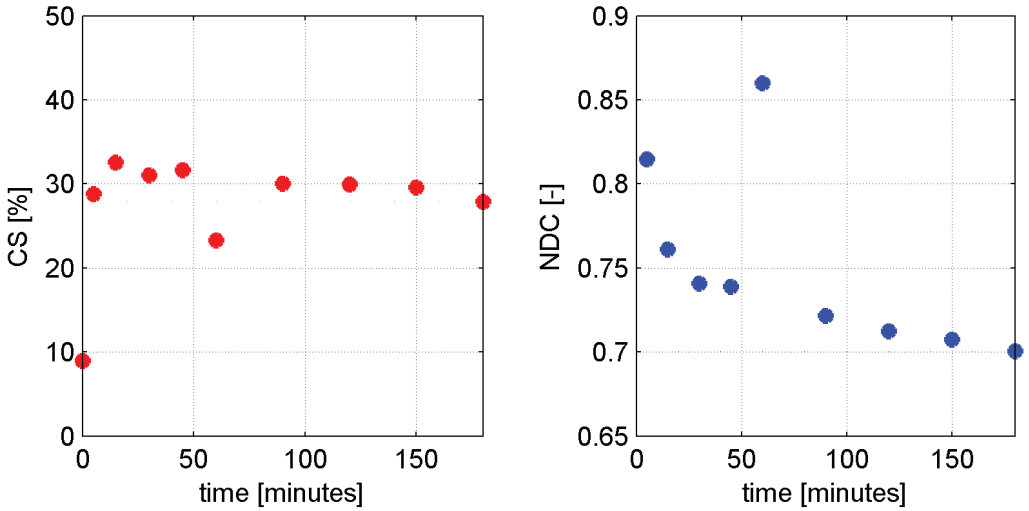

(a) Covered surface CS

(b) Compactness NDC

(a) Temporal evolution of covered surface CS and (b) compactness NDC for the tested configuration

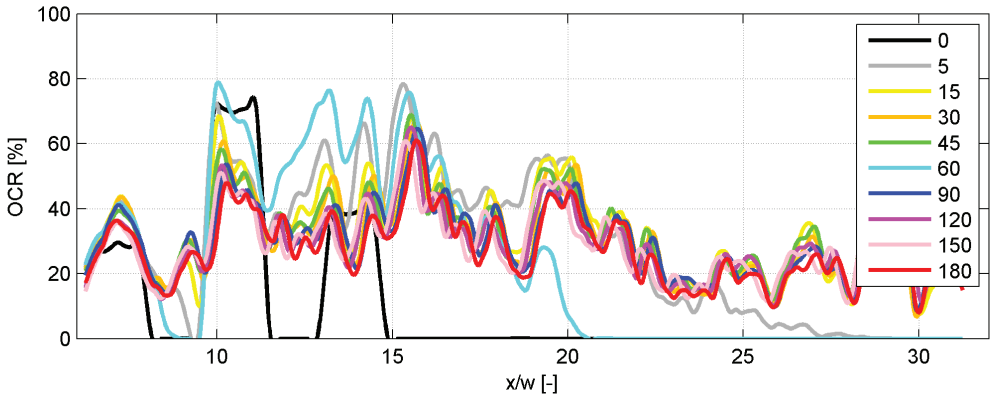

Temporal evolution of the occupation ratio distribution OCR. Time steps in minutes

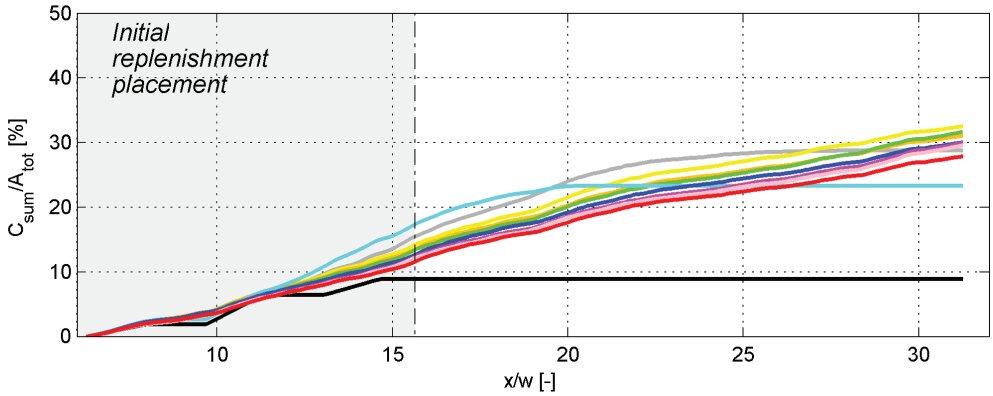

Cumulative sum of the OCR-distribution. Area initially occupied by the replenished deposits in gray. Time steps with same color map as above

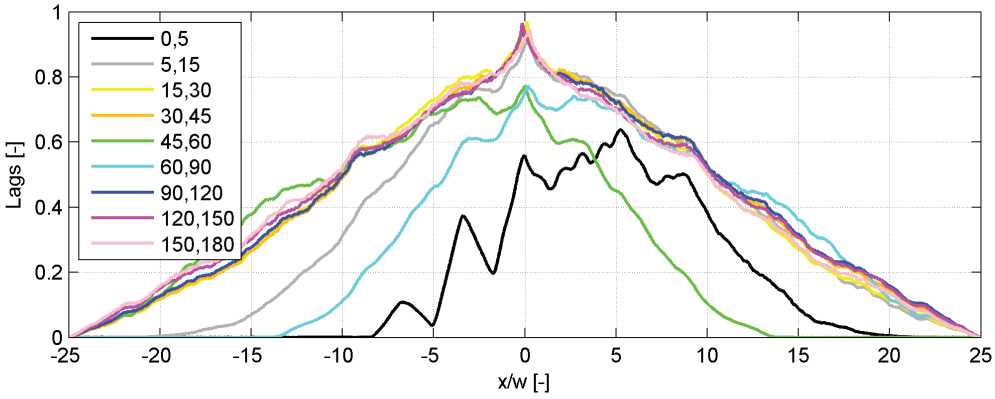

Temporal distribution of the OCR-distribution correlations

A.17 Experiment 19, Configuration C, 100% submergence

Parameters

Conf	Sub %	Shift m	L m	w m	Vol m^3	Weight kg	Q m^3/s	Duration h	Time steps
C	100	1	0.75	0.13	0.027	26.2	0.020	3	11

Configuration states

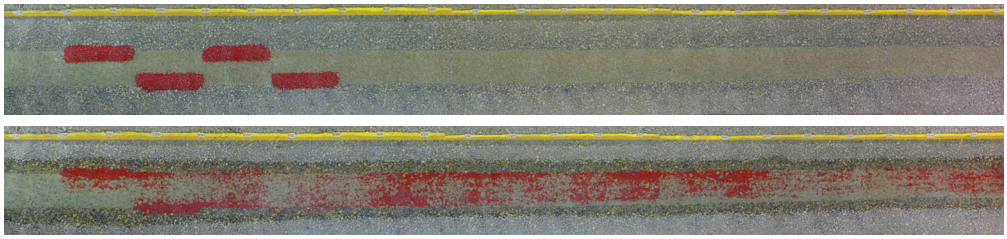

(Top) Initial state, (Bottom) final state after 3 hours testing. Flow direction from left to right

Assessed parameters

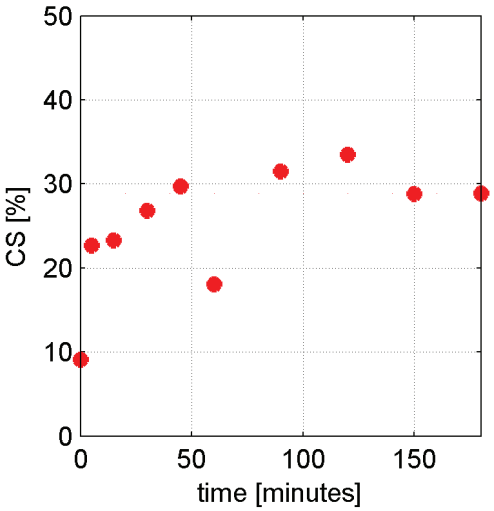

(a) Covered surface CS

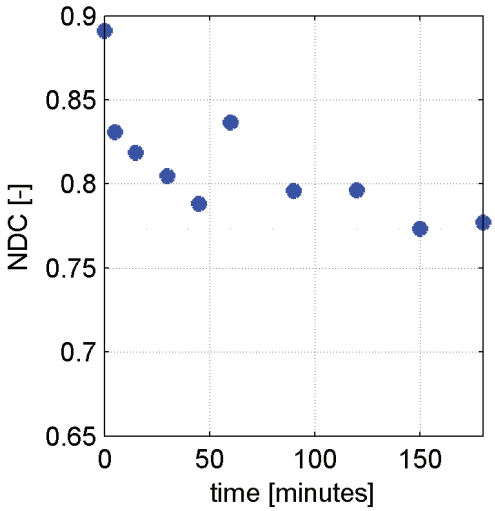

(b) Compactness NDC

(a) Temporal evolution of covered surface CS and (b) compactness NDC for the tested configuration

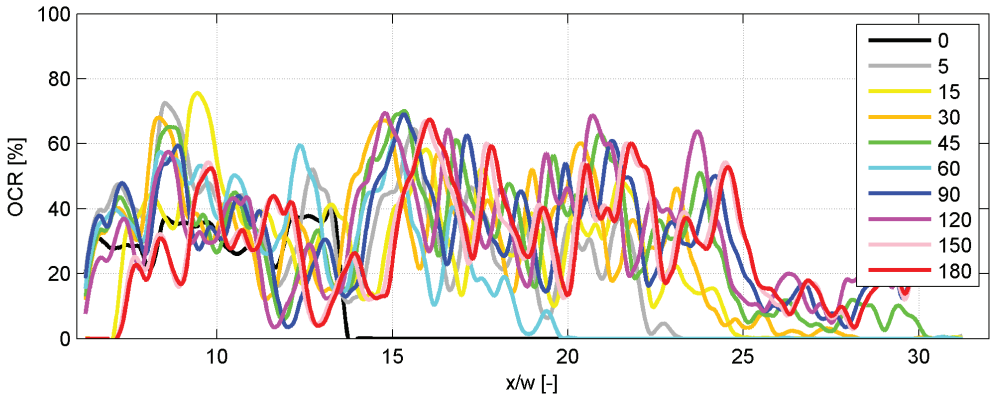

Temporal evolution of the occupation ratio distribution OCR. Time steps in minutes

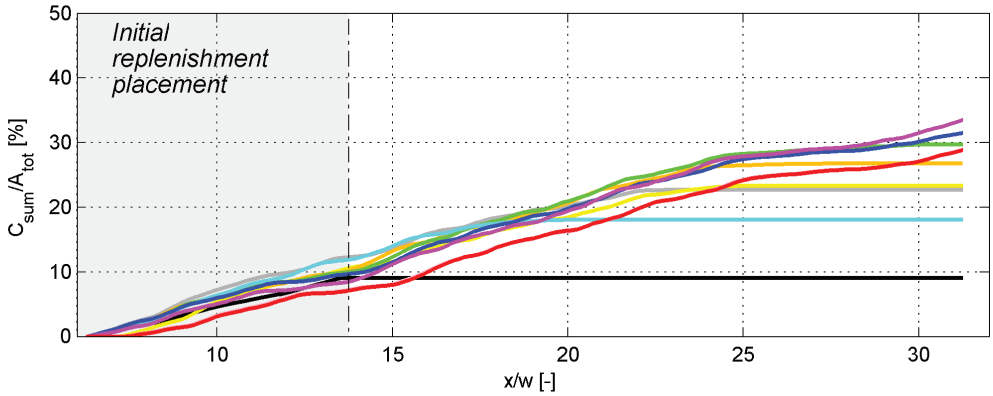

Cumulative sum of the OCR-distribution. Area initially occupied by the replenished deposits in gray. Time steps with same color map as above

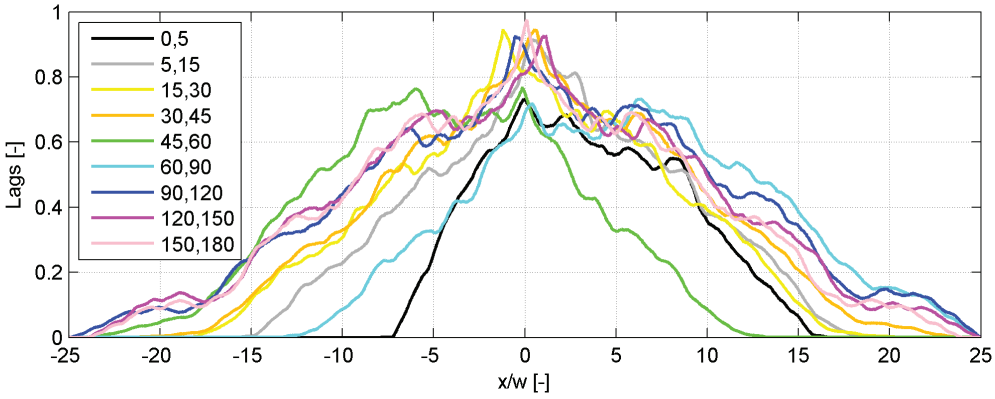

Temporal distribution of the OCR-distribution correlations

A.18 Experiment 20, Configuration D, 100% submergence

Parameters

Conf	Sub %	Shift m	L m	w m	Vol m^3	Weight kg	Q m^3/s	Duration h	Time steps
D	100	1	0.75	0.13	0.027	29.4	0.020	3	11

Configuration states

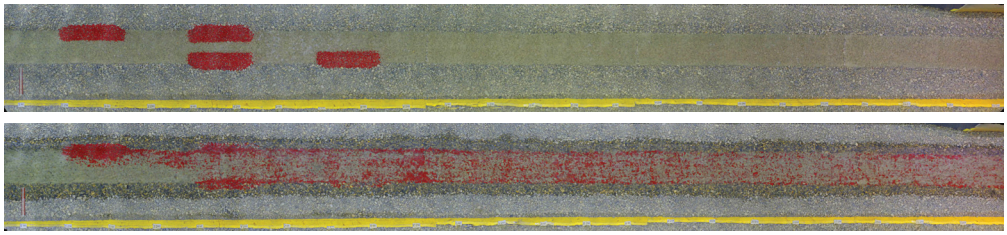

(Top) Initial state, (Bottom) final state after 3 hours testing. Flow direction from left to right

Assessed parameters

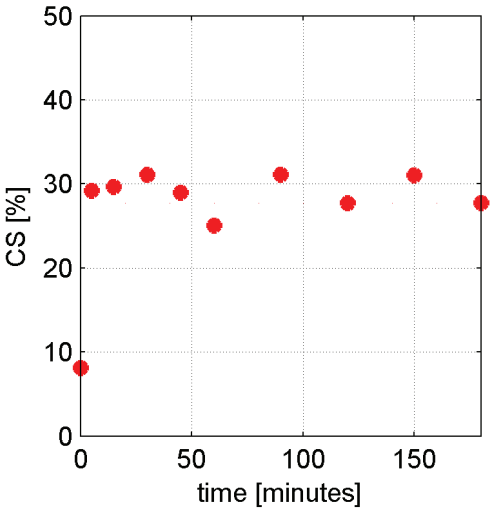

(a) Covered surface CS

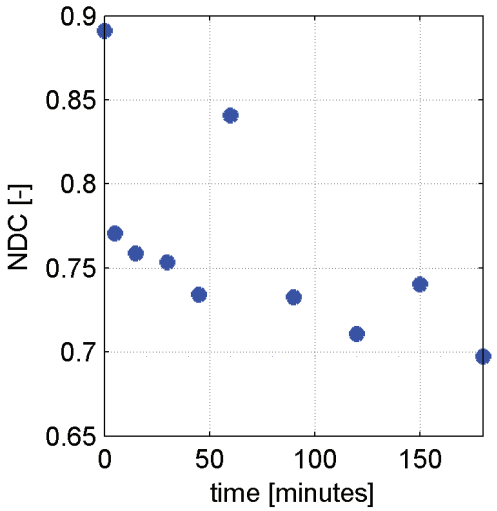

(b) Compactness NDC

(a) Temporal evolution of covered surface CS and (b) compactness NDC for the tested configuration

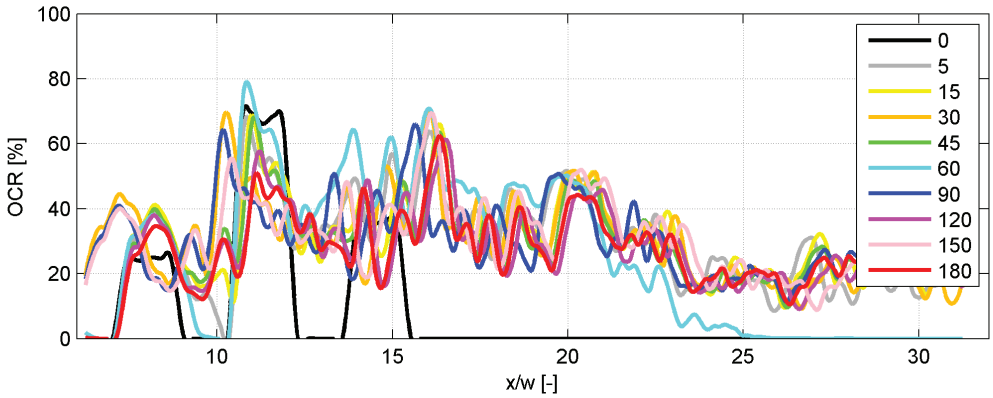

Temporal evolution of the occupation ratio distribution OCR. Time steps in minutes

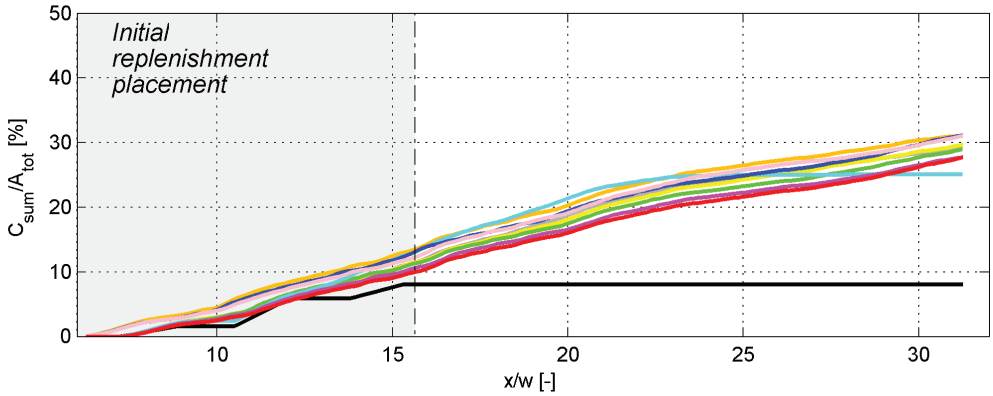

Cumulative sum of the OCR-distribution. Area initially occupied by the replenished deposits in gray. Time steps with same color map as above

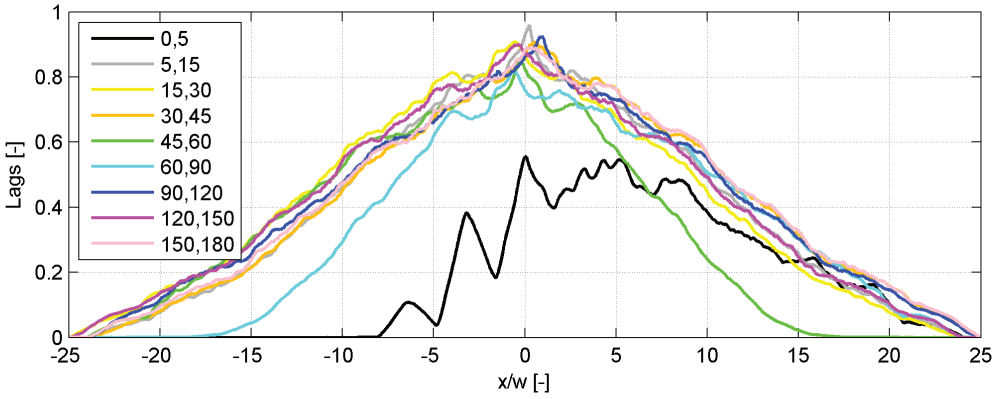

Temporal distribution of the OCR-distribution correlations

A.19 Experiment 23, Configuration C, 100% submergence

Parameters

Conf	Sub %	Shift m	L m	w m	Vol m^3	Weight kg	Q m^3/s	Duration h	Time steps
C	100	1	0.75	0.13	0.027	23.7	0.020	3	11

Configuration states

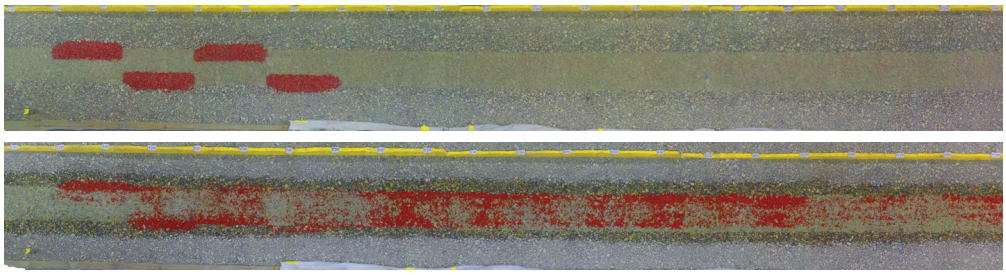

Figure A.1 – (Top) Initial state, (Bottom) final state after 3 hours testing. Flow direction from left to right

Assessed parameters

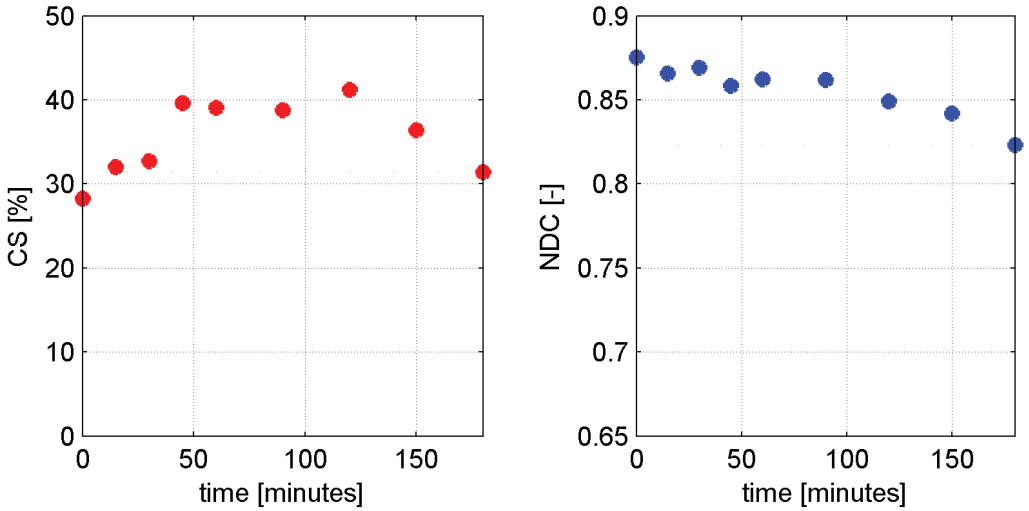

(a) Covered surface CS (b) Compactness NDC

Figure A.2 – Temporal evolution of covered surface CS and compactness NDC for the tested configuration

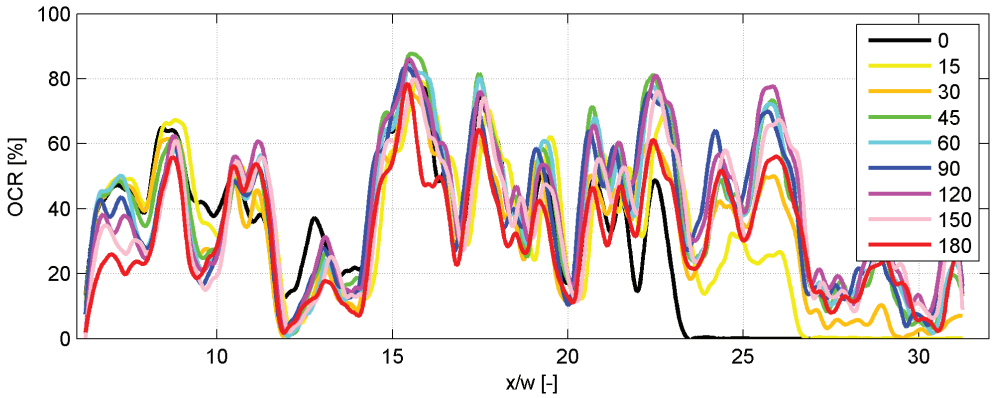

Figure A.3 – Temporal evolution of the occupation ratio distribution *OCR*. Time steps in minutes

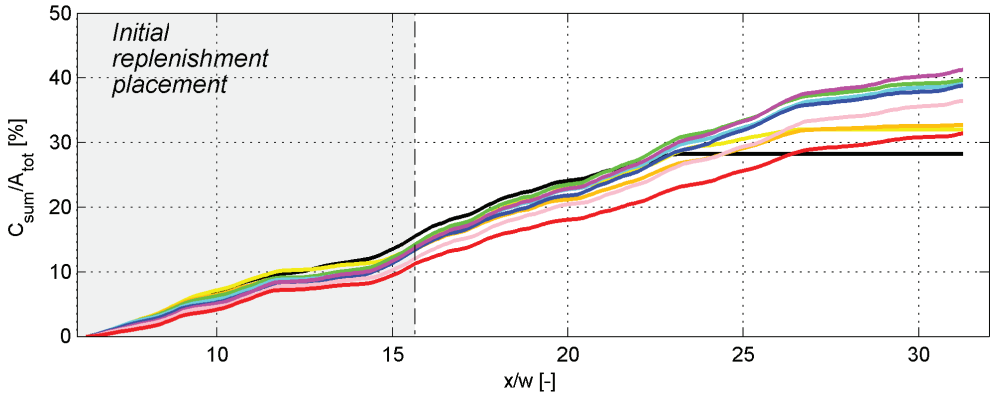

Figure A.4 – Cumulative sum of the OCR-distribution. Area initially occupied by the replenished deposits in gray. Time steps with same color map as above

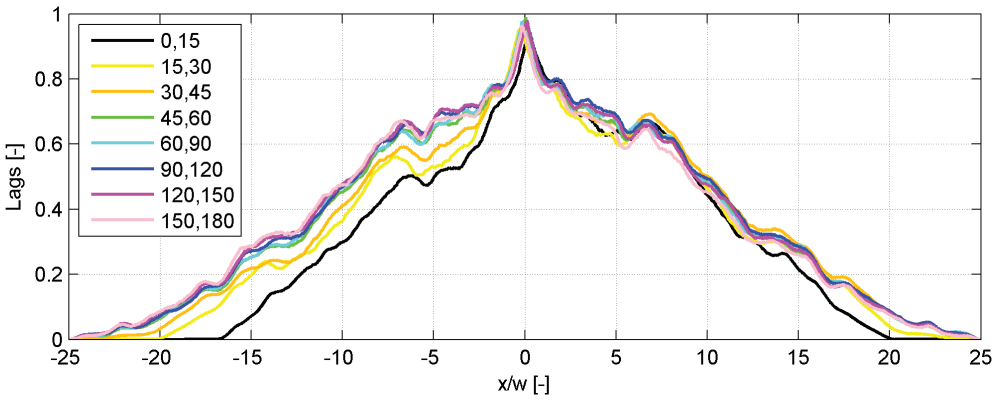

Figure A.5 – Temporal distribution of the OCR-distribution correlations

A.20 Experiment 24, Configuration D, 100% submergence

Parameters

Conf	Sub %	Shift m	L m	w m	Vol m^3	Weight kg	Q m^3/s	Duration h	Time steps
D	100	2	0.75	0.13	0.027	23.2	0.020	3	11

Configuration states

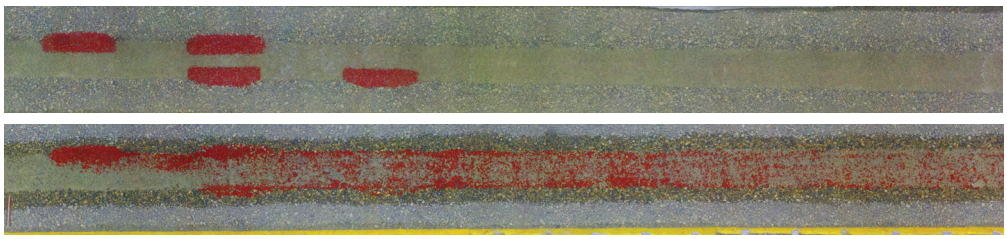

Figure A.6 – (Top) Initial state, (Bottom) final state after 3 hours testing. Flow direction from left to right

Assessed parameters

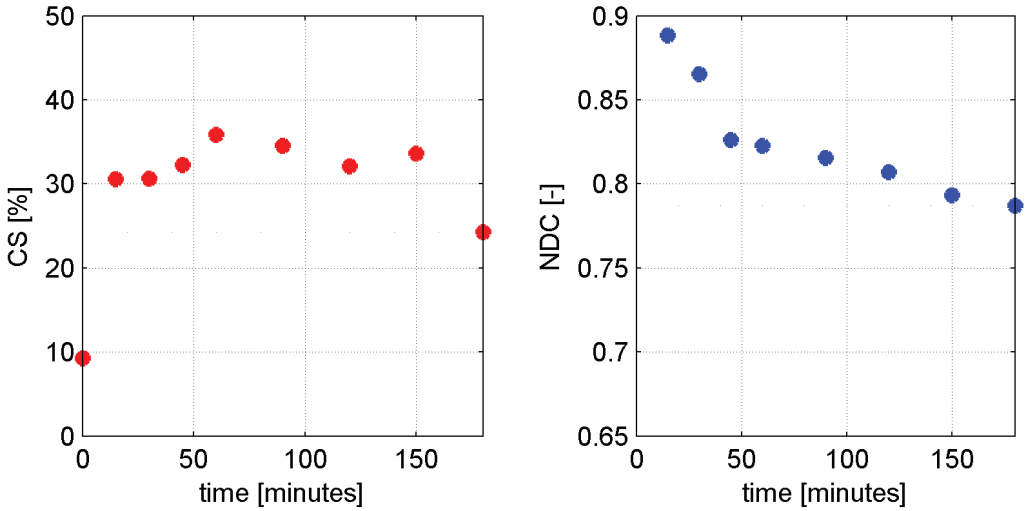

(a) Covered surface CS (b) Compactness NDC

Figure A.7 – Temporal evolution of covered surface CS and compactness NDC for the tested configuration

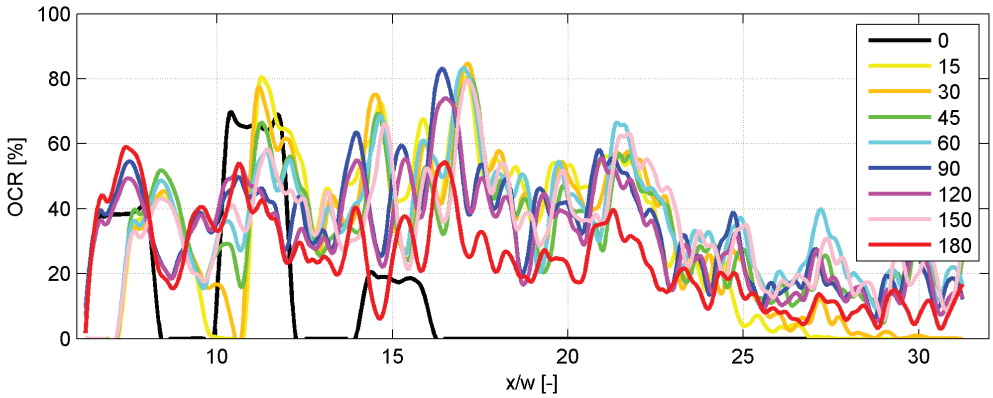

Temporal evolution of the occupation ratio distribution OCR. Time steps in minutes

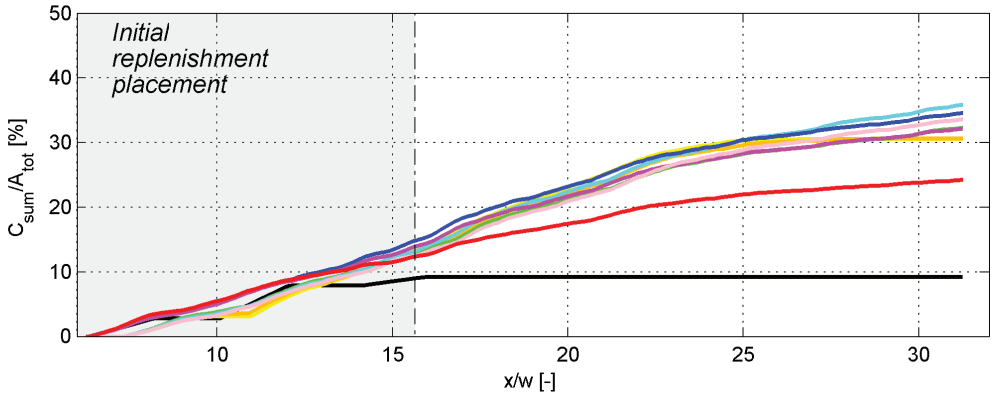

Cumulative sum of the OCR-distribution. Area initially occupied by the replenished deposits in gray. Time steps with same color map as above

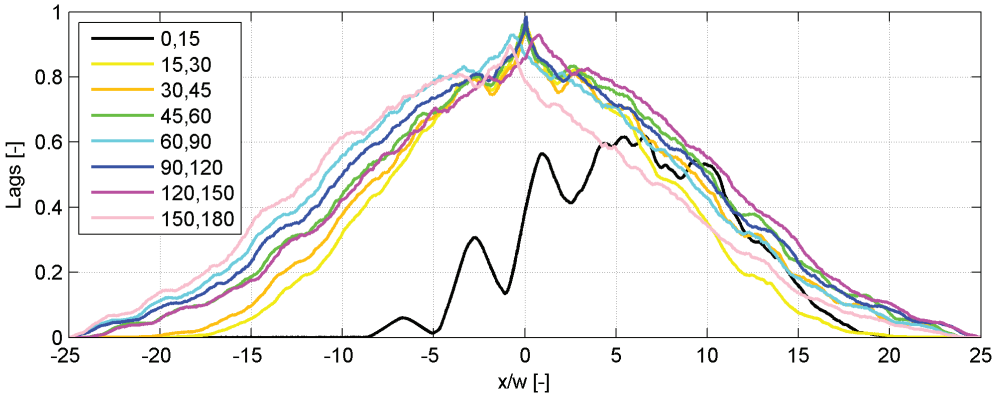

Temporal distribution of the OCR-distribution correlations

A.21 Experiment 27, Configuration E, 100% submergence

Parameters

Conf	Sub %	Shift m	L m	w m	Vol m^3	Weight kg	Q m^3/s	Duration h	Time steps
E	100	3/4	0.75	0.13	0.027	24.4	0.020 3	11	

Configuration states

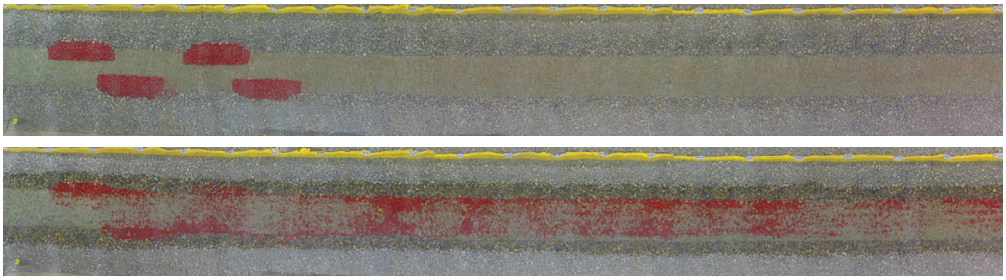

(Top) Initial state, (Bottom) final state after 3 hours testing. Flow direction from left to right

Assessed parameters

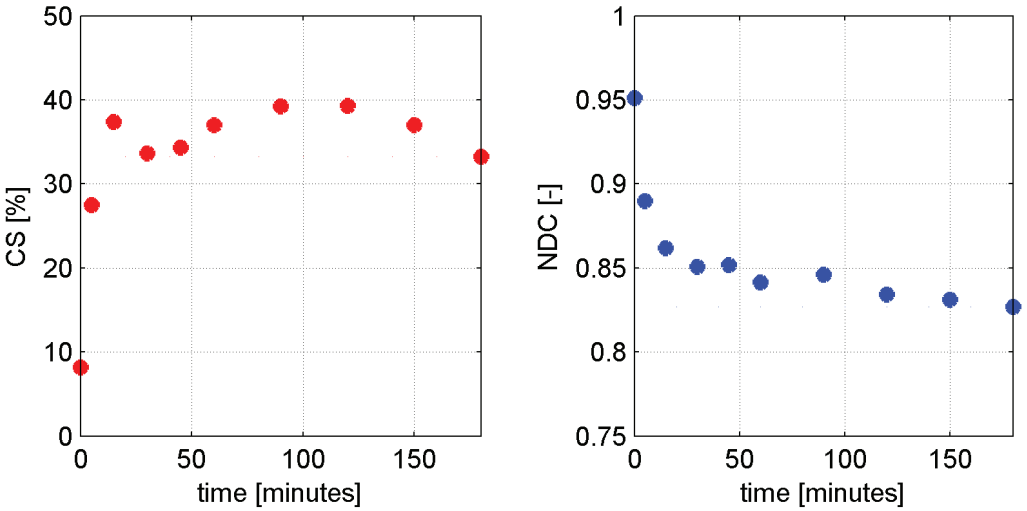

(a) Covered surface CS

(b) Compactness NDC

(a) Temporal evolution of covered surface CS and (b) compactness NDC for the tested configuration

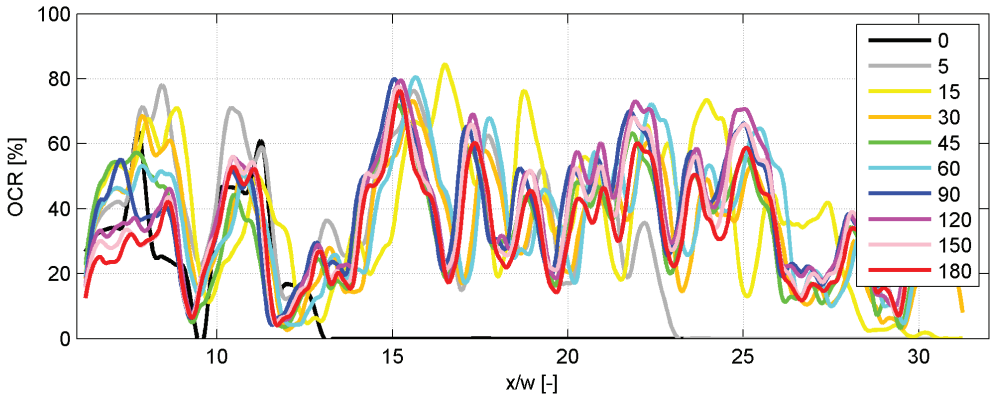

Temporal evolution of the occupation ratio distribution OCR. Time steps in minutes

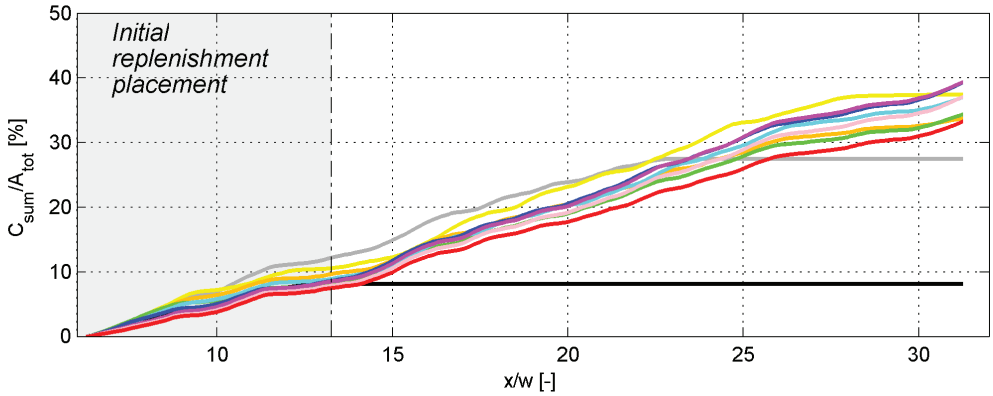

Cumulative sum of the OCR-distribution. Area initially occupied by the replenished deposits in gray. Time steps with same color map as above

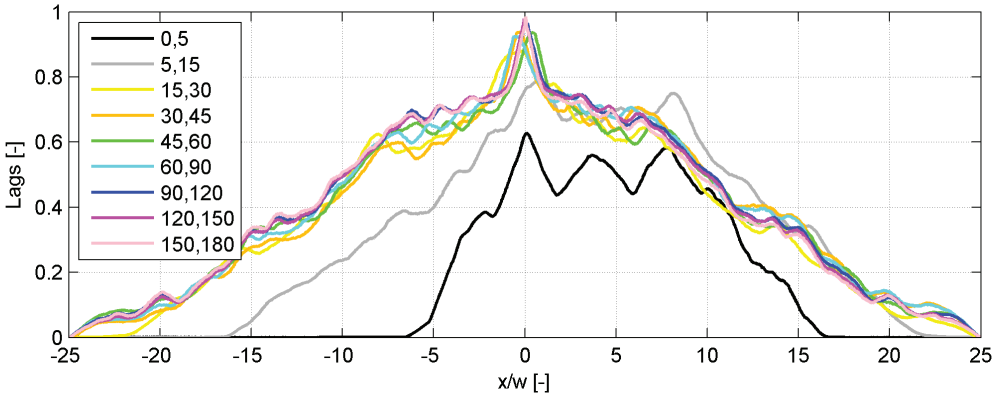

Temporal distribution of the OCR-distribution correlations

A.22 Experiment 28, Configuration F, 100% submergence

Parameters

Conf	Sub %	Shift m	L m	w m	Vol m^3	Weight kg	Q m^3/s	Duration h	Time steps
F	100	1/4	0.75	0.13	0.027	24.6	0.020	3	11

Configuration states

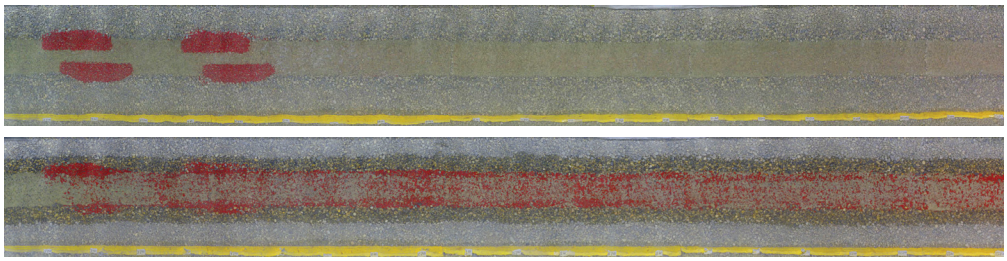

(Top) Initial state, (Bottom) final state after 3 hours testing. Flow direction from left to right

Assessed parameters

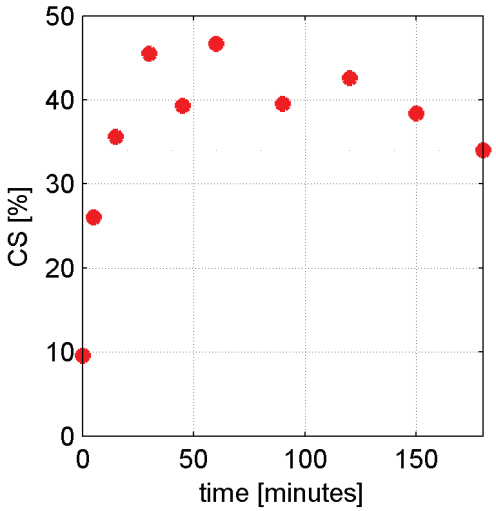

(a) Covered surface CS

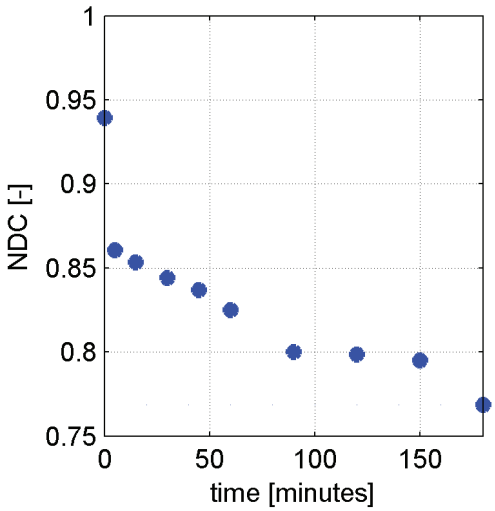

(b) Compactness NDC

(a) Temporal evolution of covered surface CS and (b) compactness NDC for the tested configuration

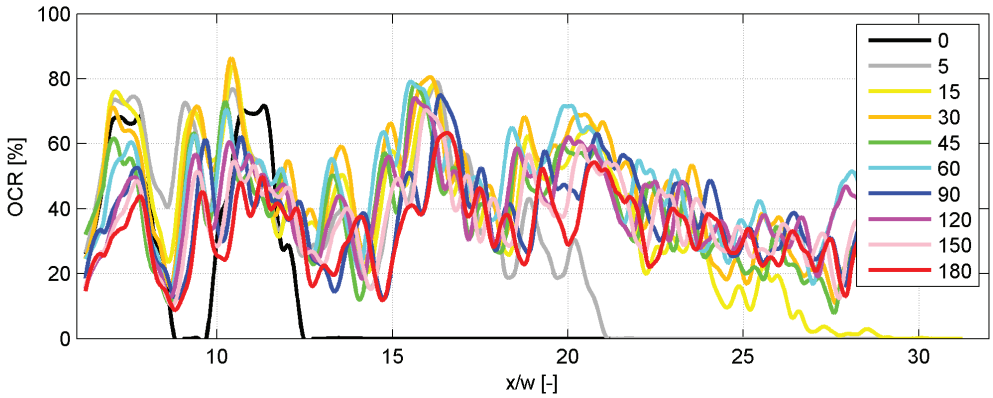

Temporal evolution of the occupation ratio distribution OCR. Time steps in minutes

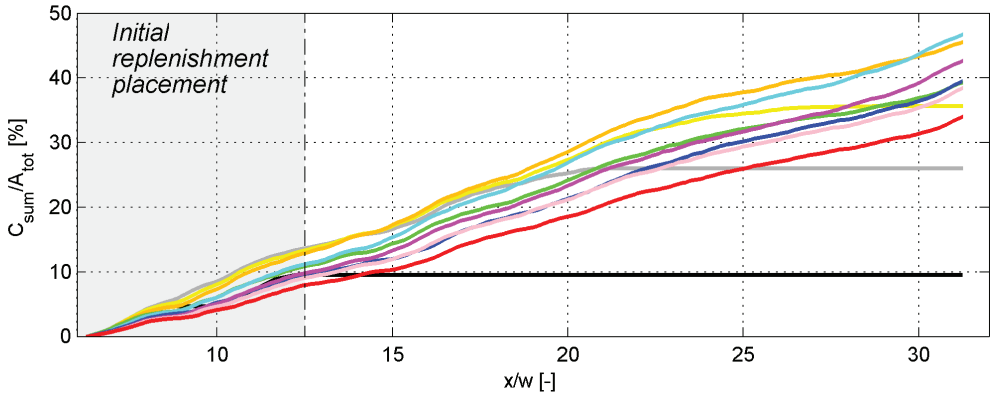

Cumulative sum of the OCR-distribution. Area initially occupied by the replenished deposits in gray. Time steps with same color map as above

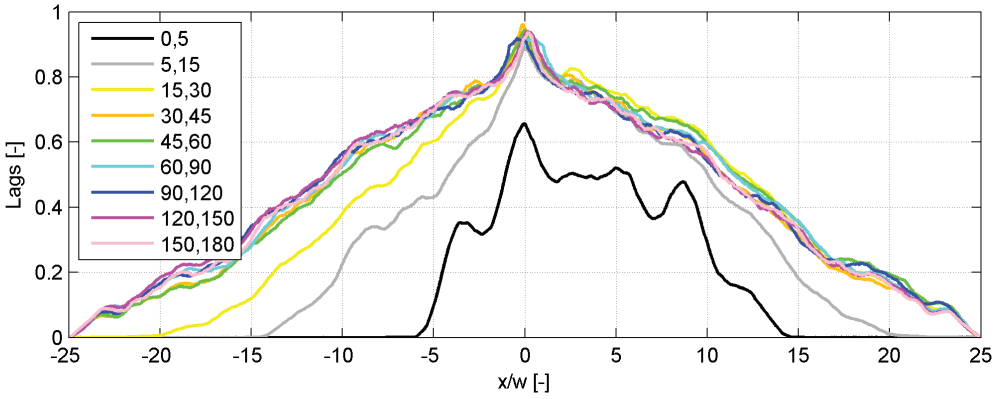

Temporal distribution of the OCR-distribution correlations

A.23 Experiment 31, Configuration E, 130% submergence

Parameters

Conf	Sub %	Shift *m*	L *m*	w *m*	Vol m^3	Weight kg	Q m^3/s	Duration *h*	Time steps
E	130	3/4	0.75	0.13	0.027	21.4	0.031 3	11	

Configuration states

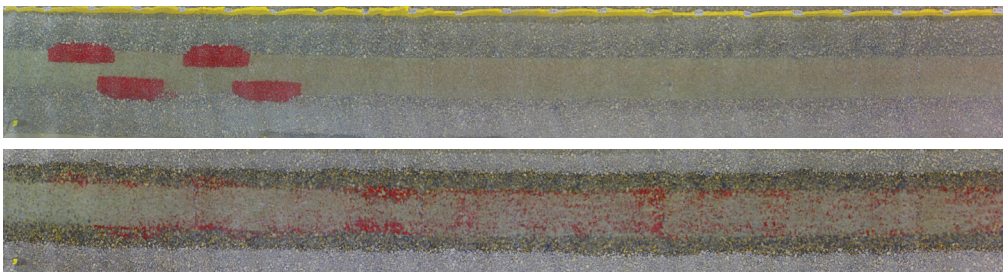

(Top) Initial state, (Bottom) final state after 3 hours testing. Flow direction from left to right

Assessed parameters

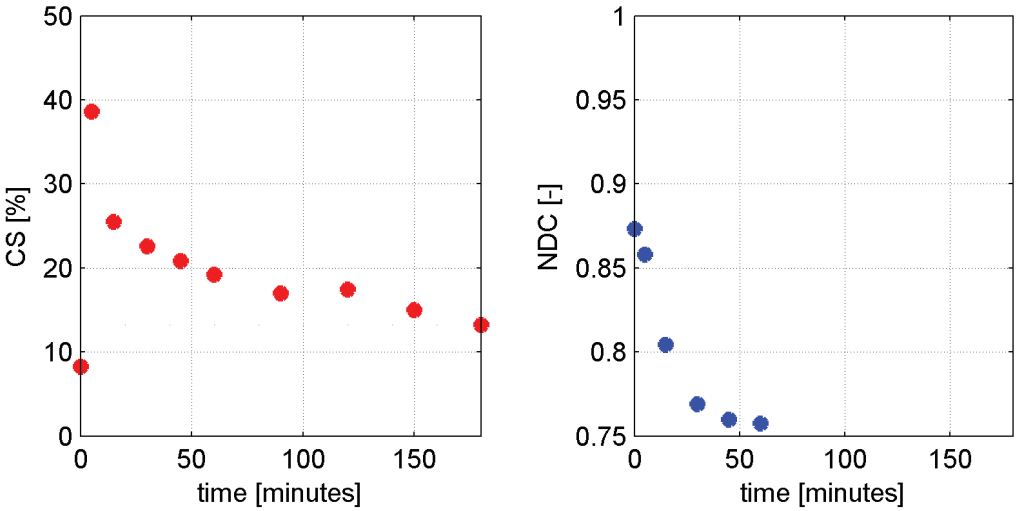

(a) Covered surface *CS* (b) Compactness *NDC*

(a) Temporal evolution of covered surface *CS* and (b) compactness *NDC* for the tested configuration

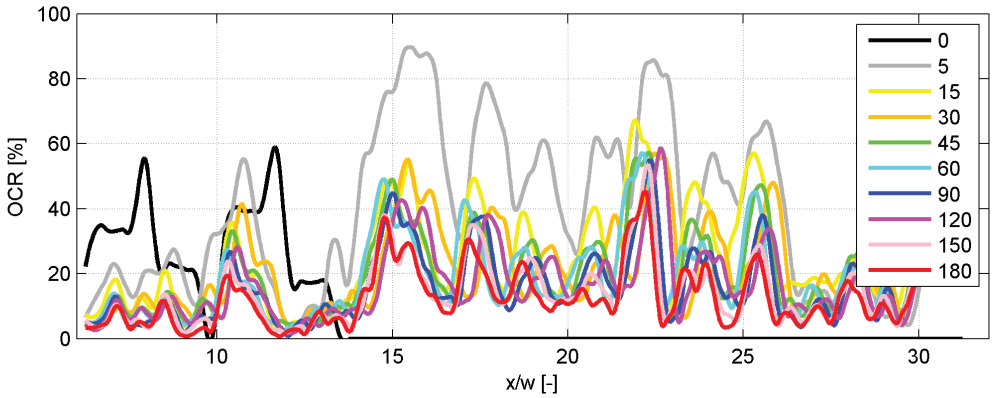

Temporal evolution of the occupation ratio distribution OCR. Time steps in minutes

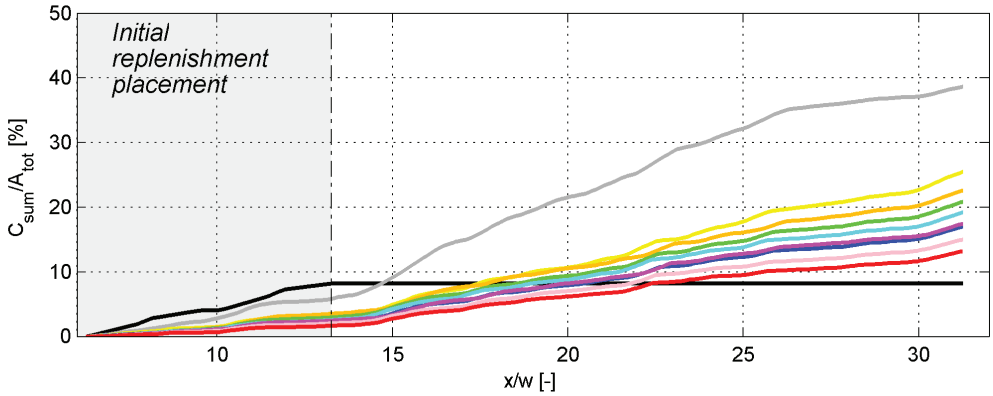

Cumulative sum of the OCR-distribution. Area initially occupied by the replenished deposits in gray. Time steps with same color map as above

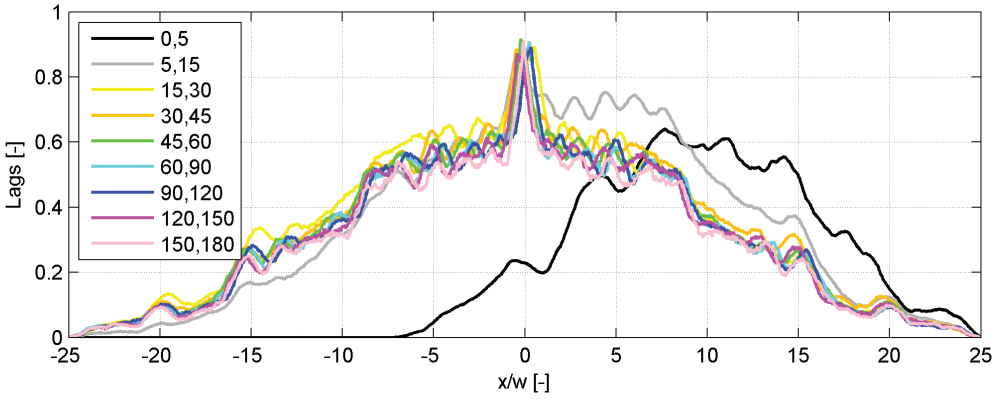

Temporal distribution of the OCR-distribution correlations

A.24 Experiment 32, Configuration F, 130% submergence

Parameters

Conf	Sub %	Shift *m*	L *m*	w *m*	Vol m^3	Weight kg	Q m^3/s	Duration *h*	Time steps
F	130	1/4	0.75	0.13	0.027	22.9	0.031	3	11

Configuration states

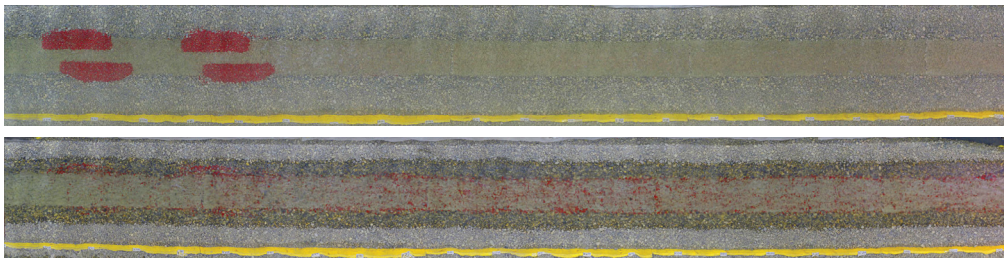

(Top) Initial state, (Bottom) final state after 3 hours testing. Flow direction from left to right

Assessed parameters

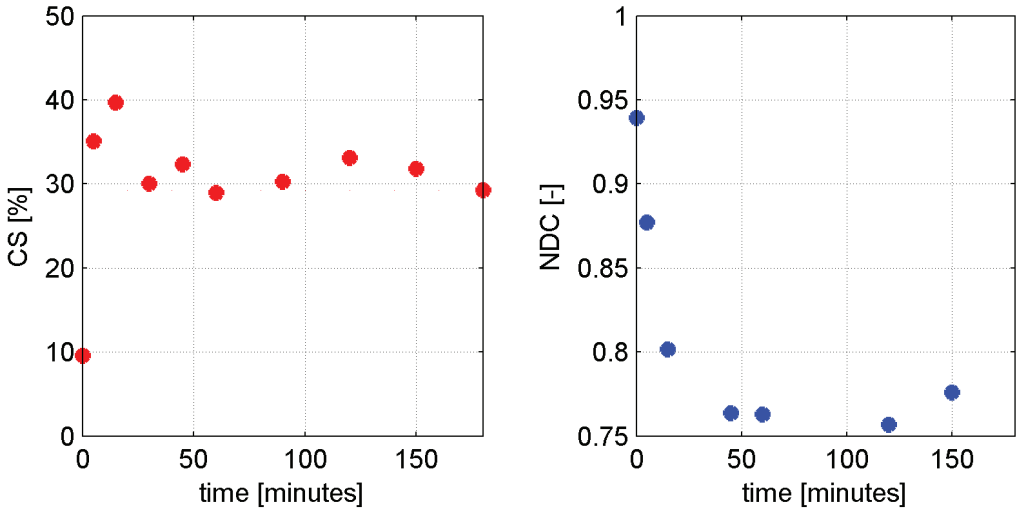

(a) Covered surface *CS* (b) Compactness *NDC*

(a) Temporal evolution of covered surface *CS* and (b) compactness *NDC* for the tested configuration

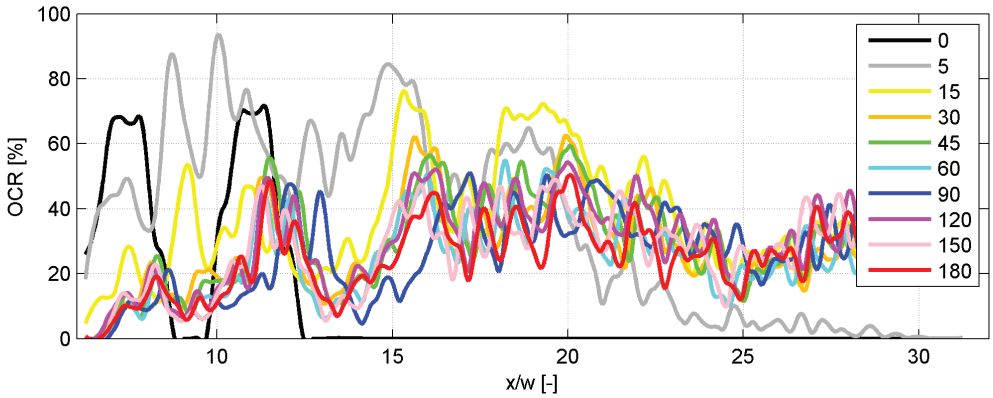

Temporal evolution of the occupation ratio distribution OCR. Time steps in minutes

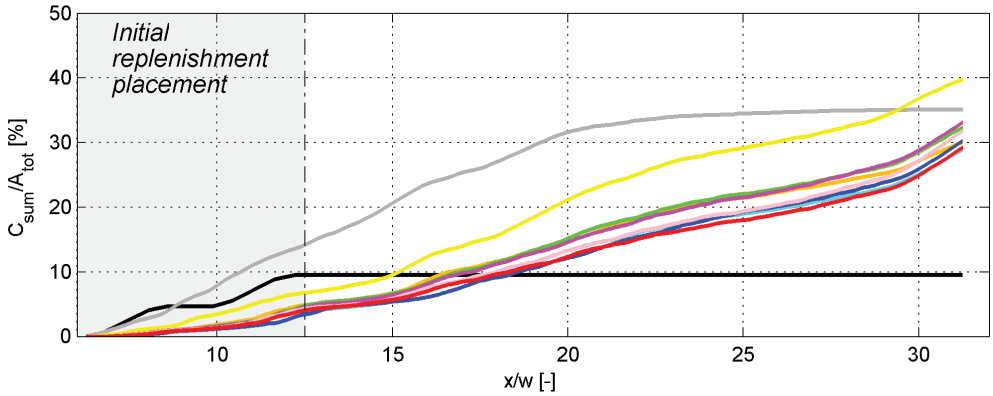

Cumulative sum of the OCR-distribution. Area initially occupied by the replenished deposits in gray. Time steps with same color map as above

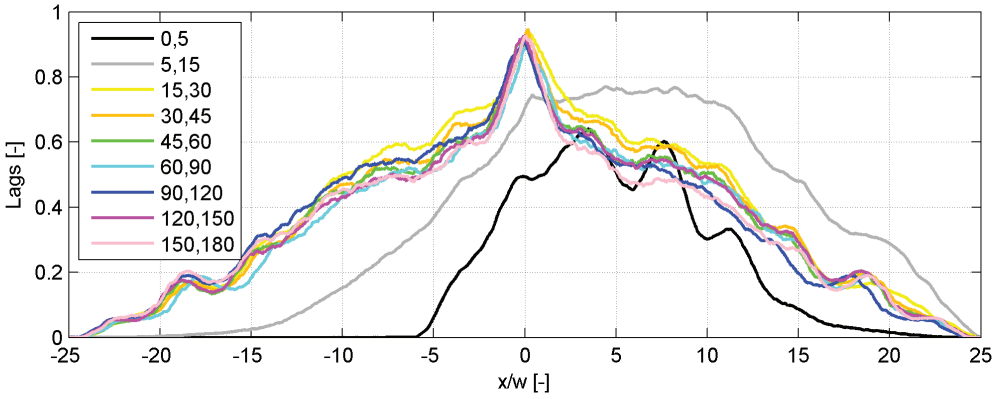

Temporal distribution of the OCR-distribution correlations

A.25 Experiment 33, Configuration B, 100% submergence

Parameters

Conf	Sub %	Shift m	L m	w m	Vol m^3	Weight kg	Q m^3/s	Duration h	Time steps
B	100	1/2	0.50	0.13	0.027	13.4	0.020	3	11

Configuration states

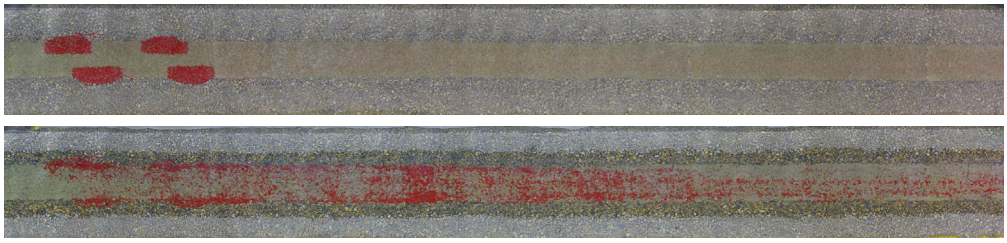

(Top) Initial state, (Bottom) final state after 3 hours testing. Flow direction from left to right

Assessed parameters

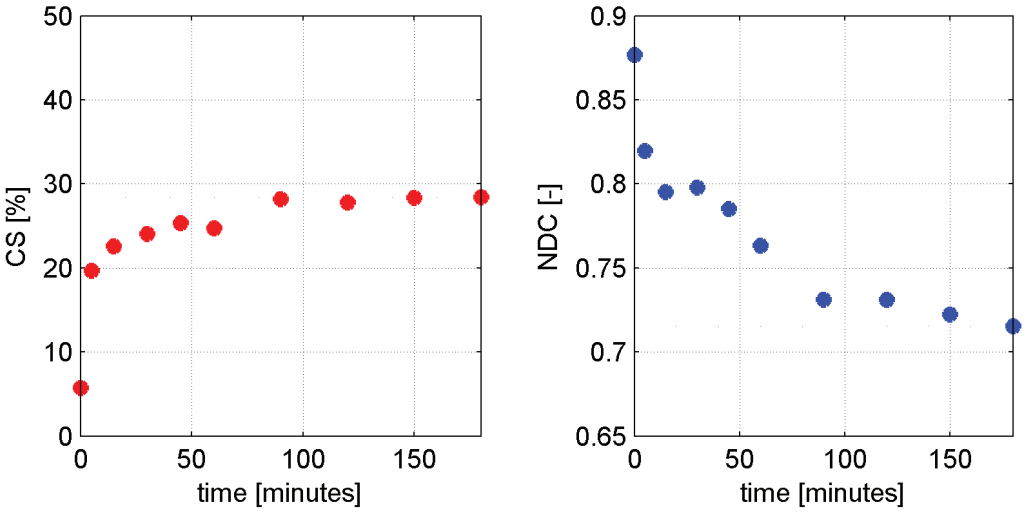

(a) Covered surface CS (b) Compactness NDC

Temporal evolution of covered surface CS and compactness NDC for the tested configuration

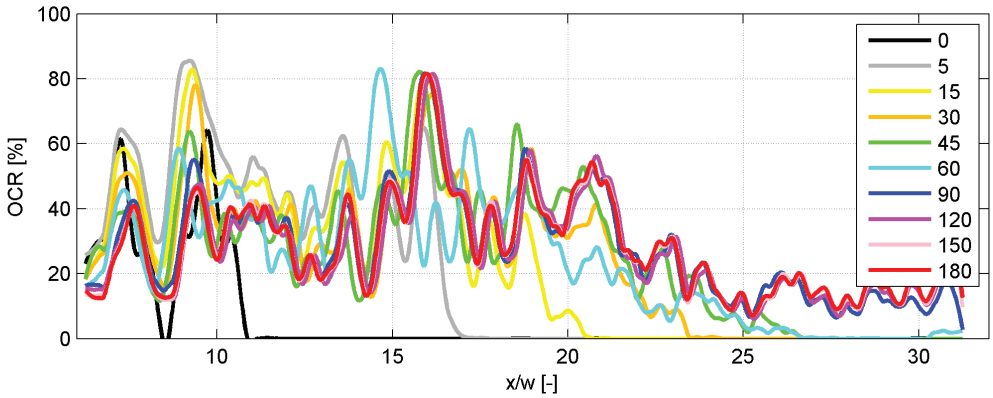

Temporal evolution of the occupation ratio distribution OCR. Time steps in minutes

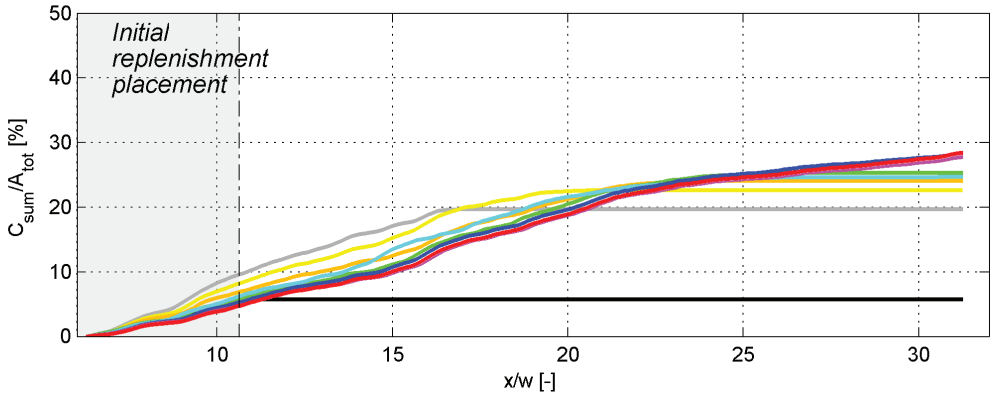

Cumulative sum of the OCR-distribution. Area initially occupied by the replenished deposits in gray. Time steps with same color map as above

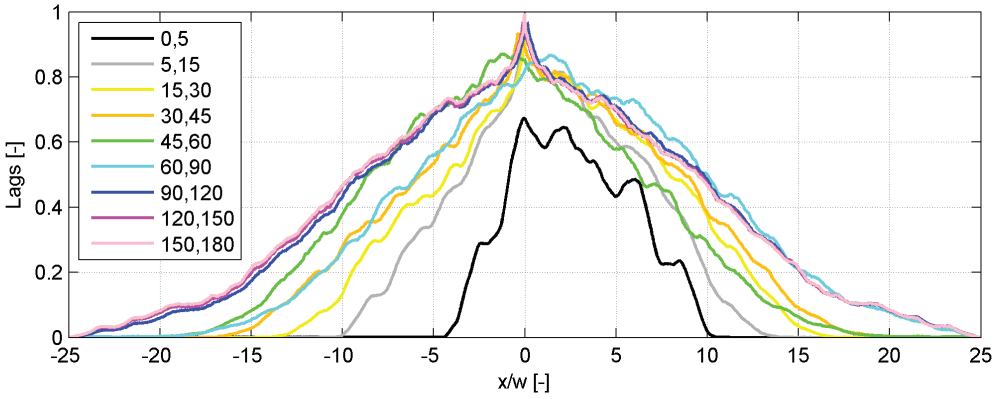

Temporal distribution of the OCR-distribution correlations

A.26 Experiment 34, Configuration C, 100% submergence

Parameters

Conf	Sub %	Shift m	L m	w m	Vol m^3	Weight kg	Q m^3/s	Duration h	Time steps
C	100	1	0.50	0.13	0.027	14.0	0.019	3	11

Configuration states

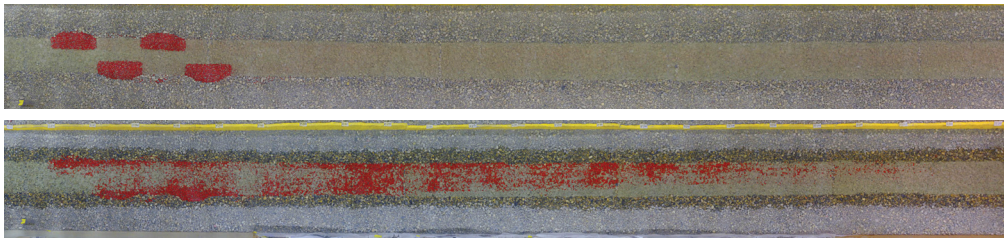

(Top) Initial state, (Bottom) final state after 3 hours testing. Flow direction from left to right

Assessed parameters

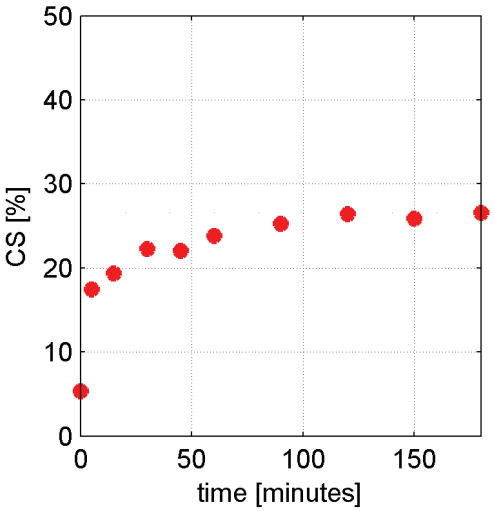

(a) Covered surface CS

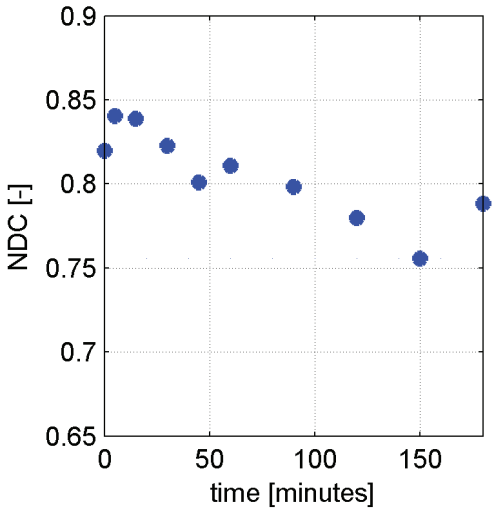

(b) Compactness NDC

(a) Temporal evolution of covered surface CS and (b) compactness NDC for the tested configuration

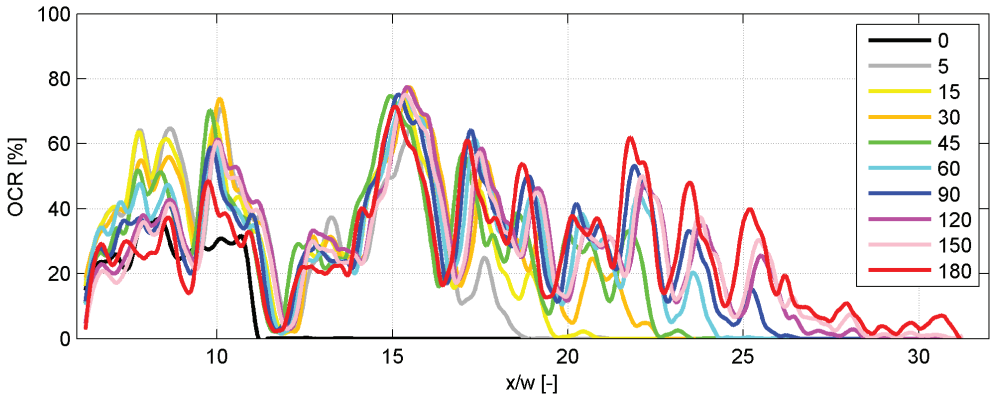

Temporal evolution of the occupation ratio distribution OCR. Time steps in minutes

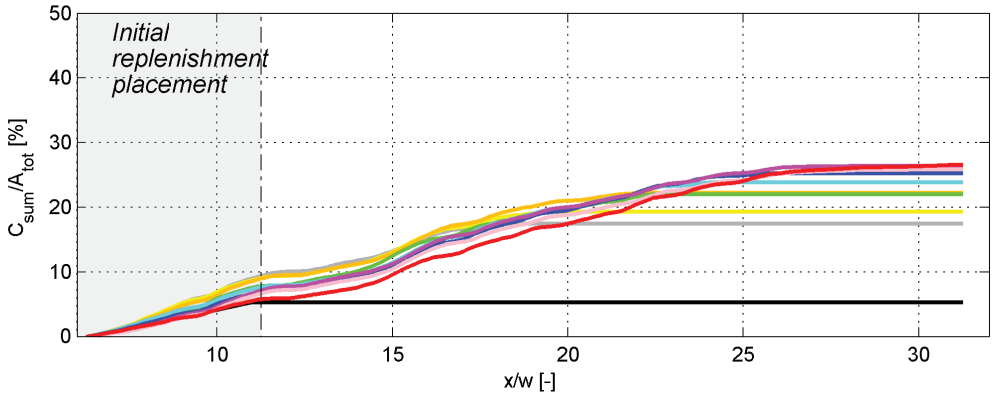

Cumulative sum of the OCR-distribution. Area initially occupied by the replenished deposits in gray. Time steps with same color map as above

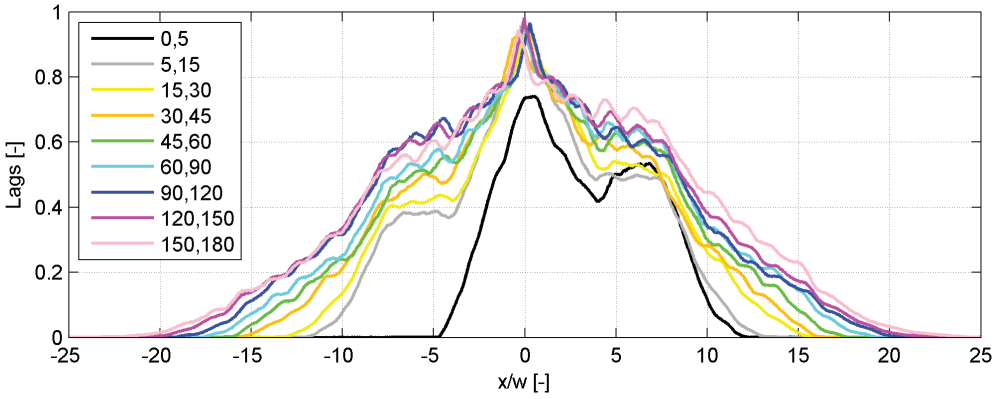

Temporal distribution of the OCR-distribution correlations

A.27 Experiment 35, Configuration B, 100% submergence

Parameters

Conf	Sub %	Shift m	L m	w m	Vol m^3	Weight kg	Q m^3/s	Duration h	Time steps
B	100	1/2	1.00	0.13	0.027	31.0	0.020	3	11

Configuration states

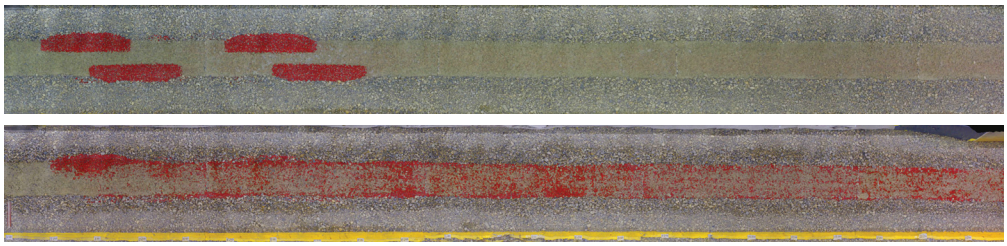

(Top) Initial state, (Bottom) final state after 3 hours testing. Flow direction from left to right

Assessed parameters

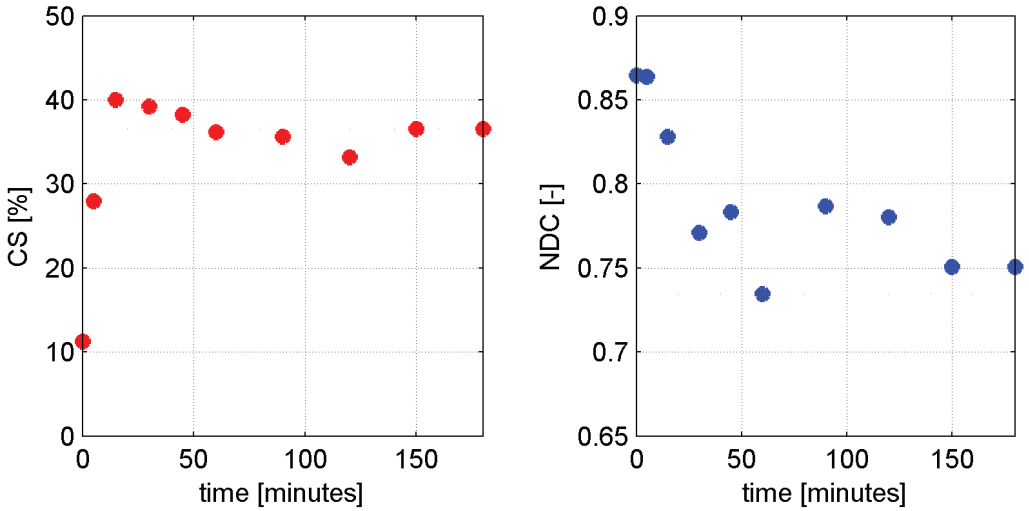

(a) Covered surface CS

(b) Compactness NDC

(a)Temporal evolution of covered surface CS and (b) compactness NDC for the tested configuration

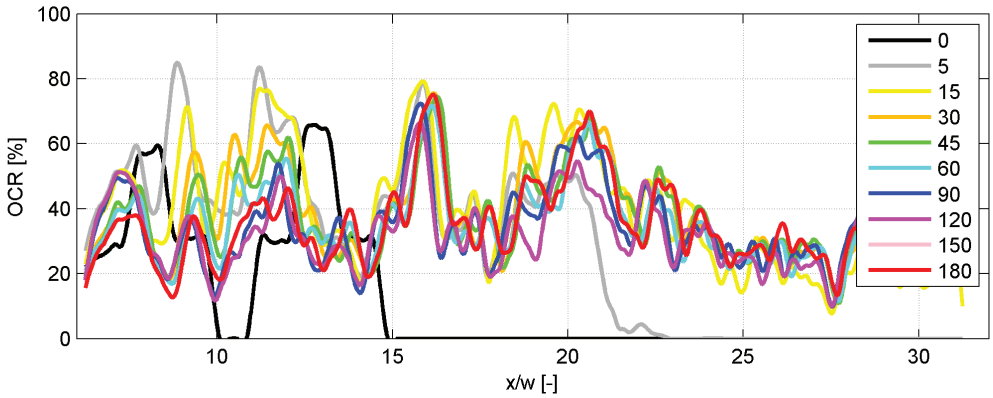

Temporal evolution of the occupation ratio distribution OCR. Time steps in minutes

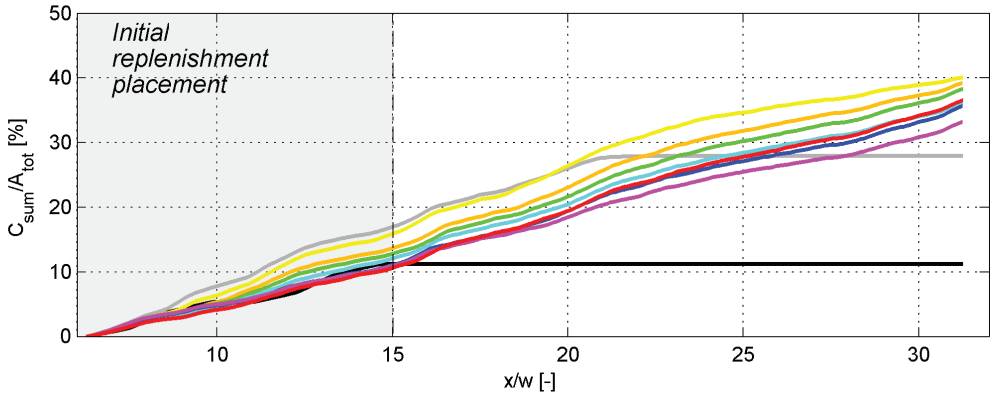

Cumulative sum of the OCR-distribution. Area initially occupied by the replenished deposits in gray. Time steps with same color map as above

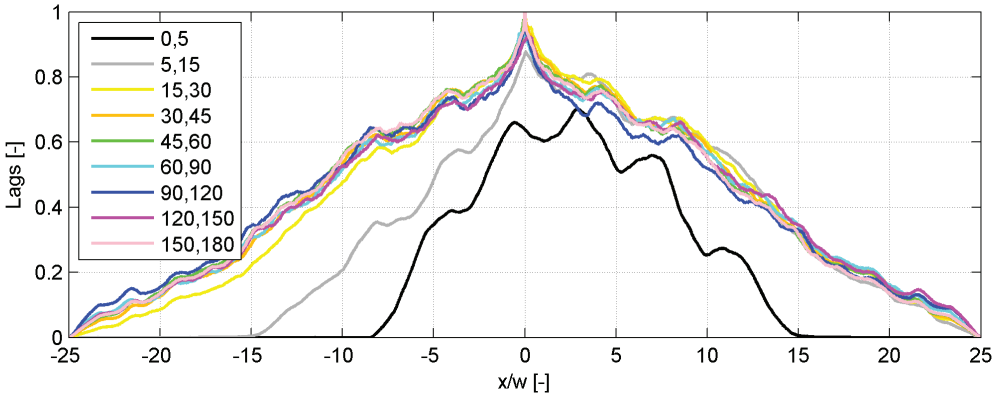

Temporal distribution of the OCR-distribution correlations

A.28 Experiment 36, Configuration C, 100% submergence

Parameters

Conf	Sub %	Shift m	L m	w m	Vol m^3	Weight kg	Q m^3/s	Duration h	Time steps
C	100	1	1.00	0.13	0.027	32.9	0.020	3	11

Configuration states

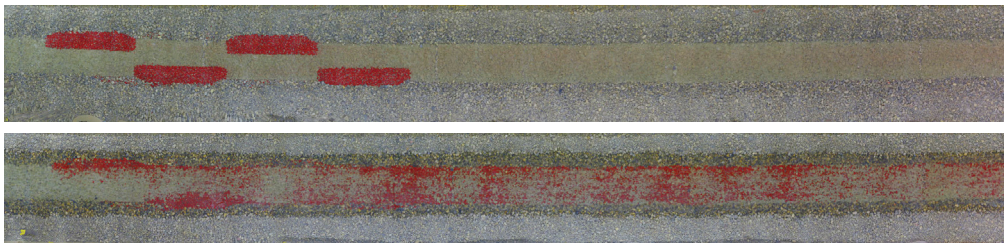

(Top) Initial state, (Bottom) final state after 3 hours testing. Flow direction from left to right

Assessed parameters

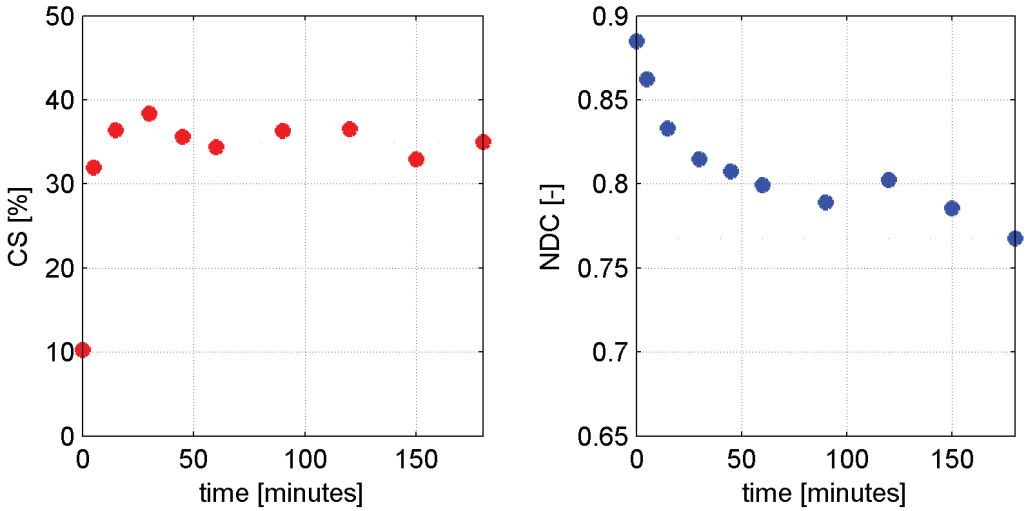

(a) Covered surface CS

(b) Compactness NDC

(a) Temporal evolution of covered surface CS and (b) compactness NDC for the tested configuration

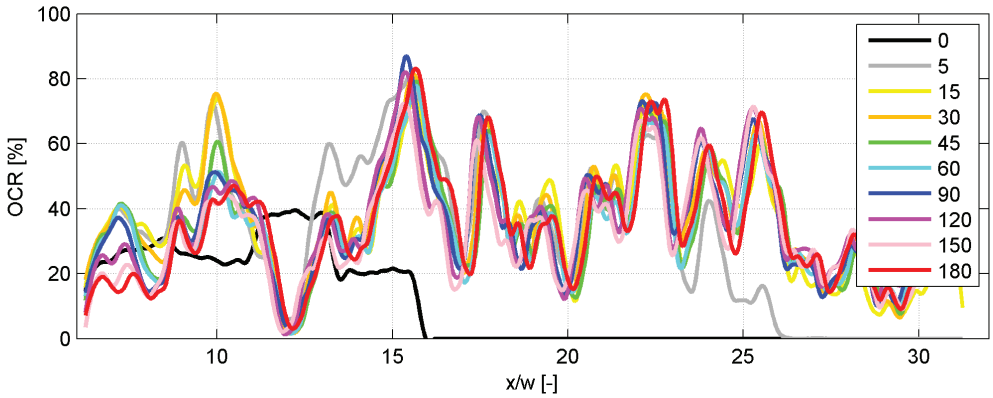

Temporal evolution of the occupation ratio distribution OCR. Time steps in minutes

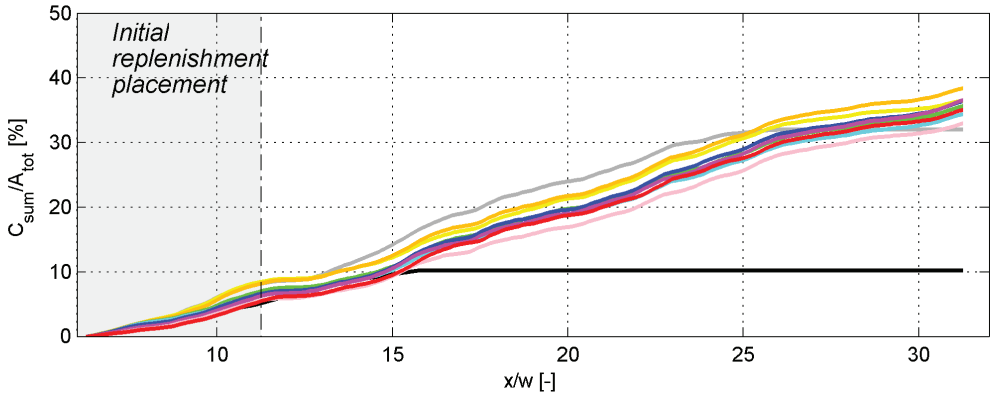

Cumulative sum of the OCR-distribution. Area initially occupied by the replenished deposits in gray. Time steps with same color map as above

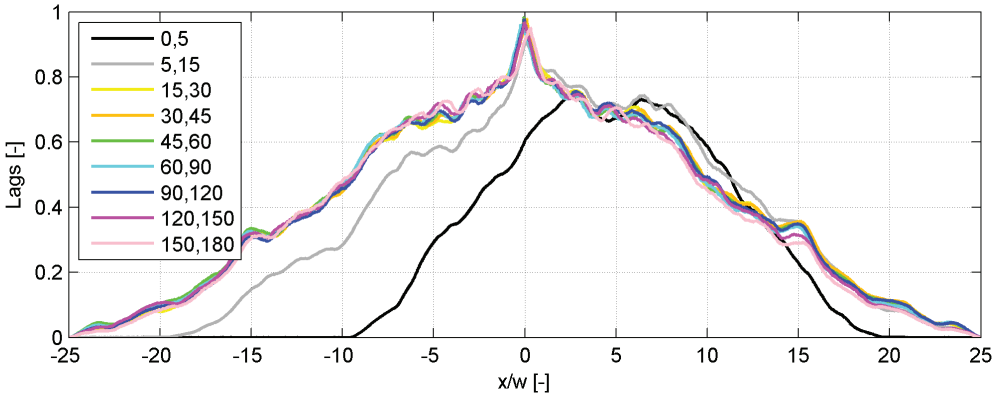

Temporal distribution of the OCR-distribution correlations

B Appendix: Experiments with consecutive replenishment deposits

B.1 Experiment 17, Configuration A 2^{ND}, 100% submergence

Parameters

Conf	Sub %	Shift m	L m	w m	Vol m^3	Weight kg	Q m^3/s	Duration h	Time steps
A	100	0	0.75	0.13	0.027	27.0	0.019	3-6	10

Configuration states

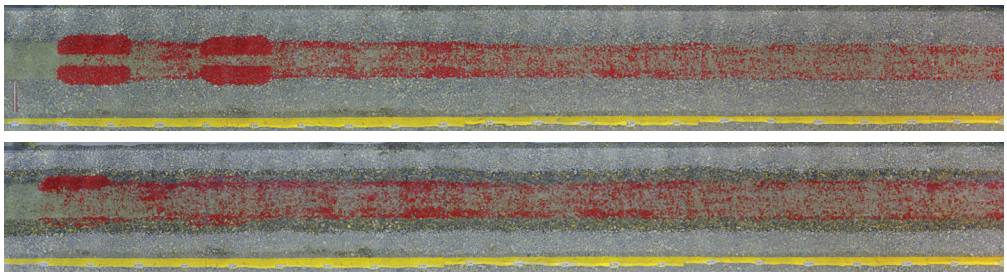

(Top) Initial state, (Bottom) final state after 3 hours testing. Flow direction from left to right

Assessed parameters

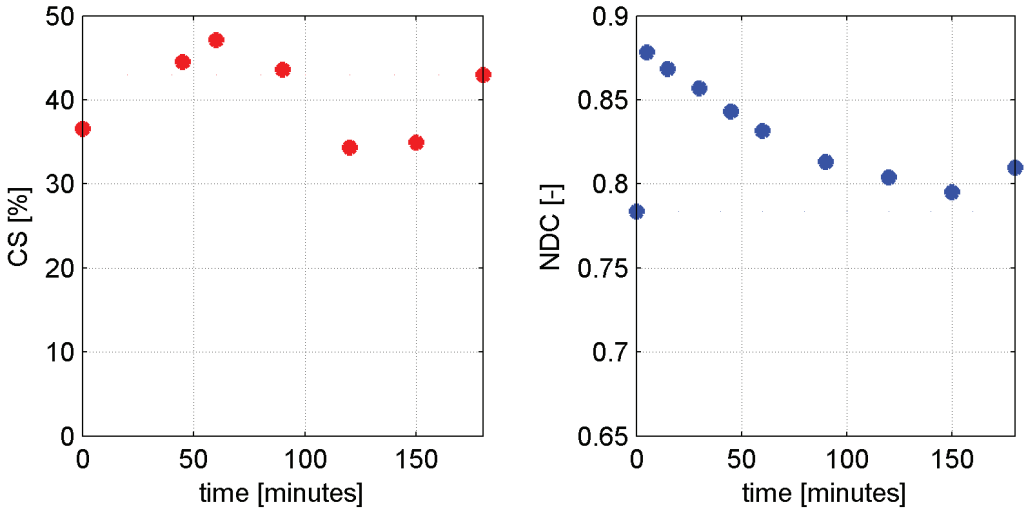

(a) Covered surface CS

(b) Compactness NDC

(a) Temporal evolution of covered surface CS and (b) compactness NDC for the tested configuration

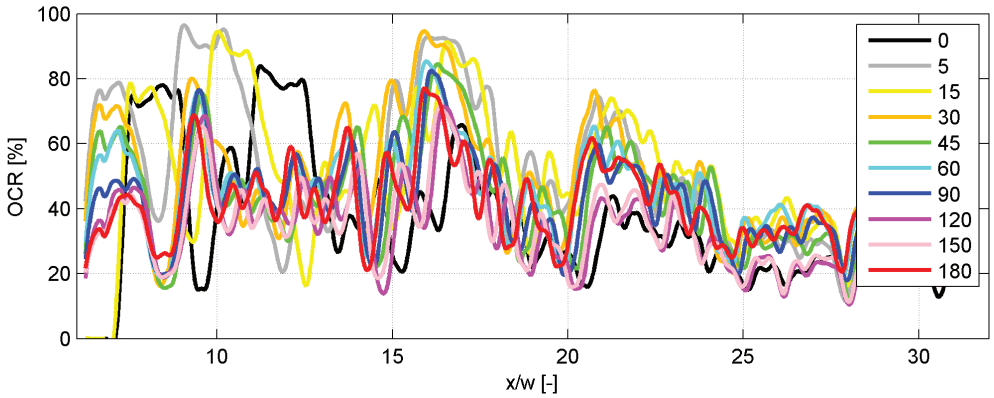

Temporal evolution of the occupation ratio distribution OCR. Time steps in minutes

Temporal evolution of the occupation ratio distribution OCR. Time steps in minutes

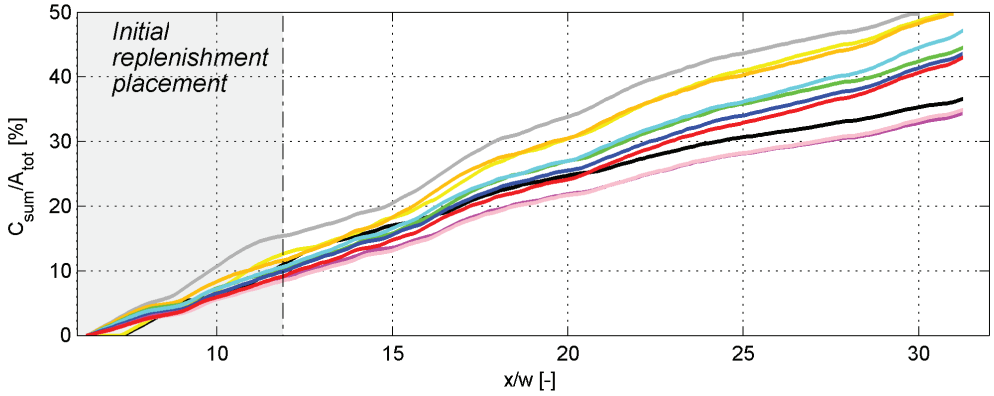

Cumulative sum of the OCR-distribution. Area initially occupied by the replenished deposits in gray. Time steps with same color map as above

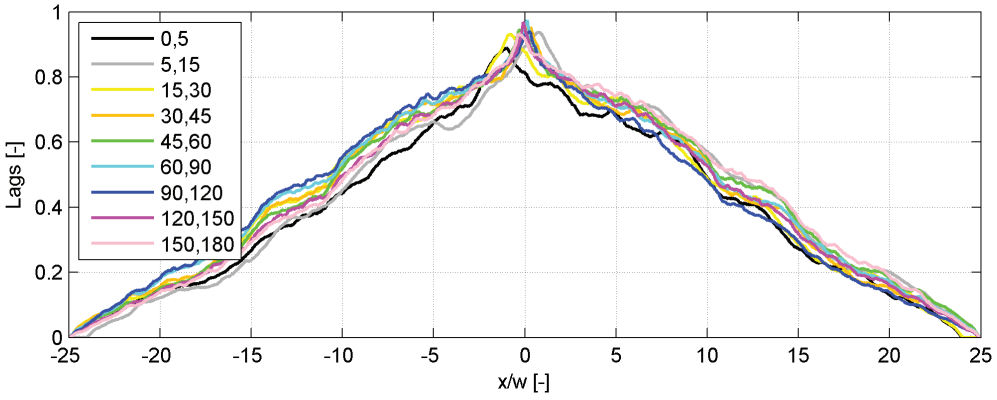

Temporal distribution of the OCR-distribution correlations

B.2 Experiment 18, Configuration B 2^{ND}, 100% submergence

Parameters

Conf	Sub %	Shift m	L m	w m	Vol m^3	Weight kg	Q m^3/s	Duration h	Time steps
B	100	1/2	0.75	0.13	0.027	27.0	0.019	3-6	10

Configuration states

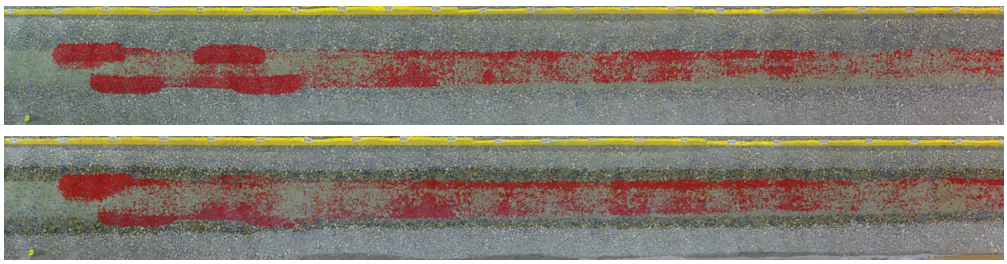

(Top) Initial state, (Bottom) final state after 3 hours testing. Flow direction from left to right

Assessed parameters

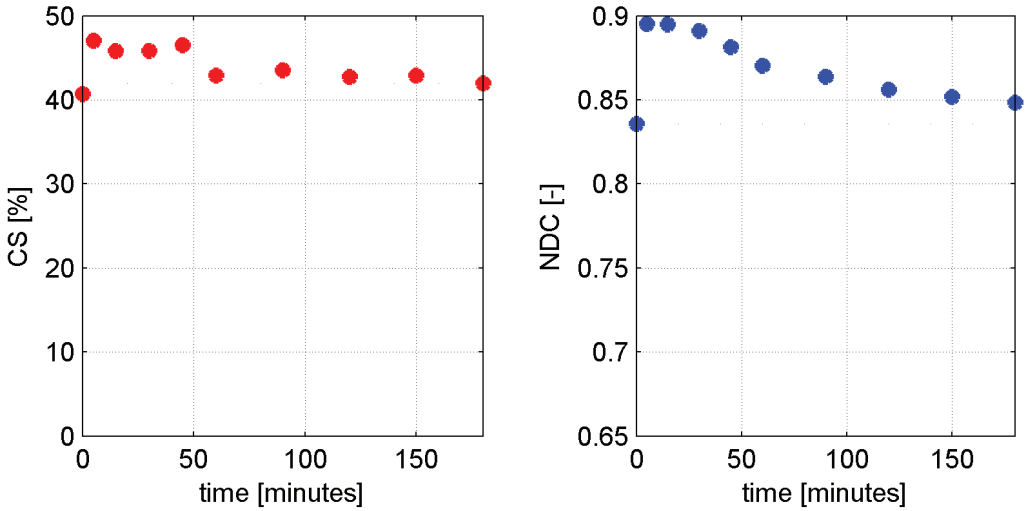

(a) Covered surface CS

(b) Compactness NDC

(a) Temporal evolution of covered surface CS and (b) compactness NDC for the tested configuration

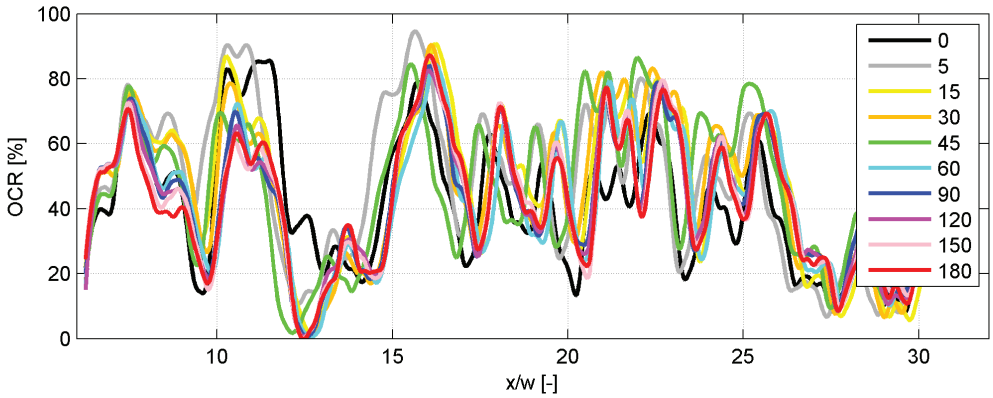

Temporal evolution of the occupation ratio distribution OCR. Time steps in minutes

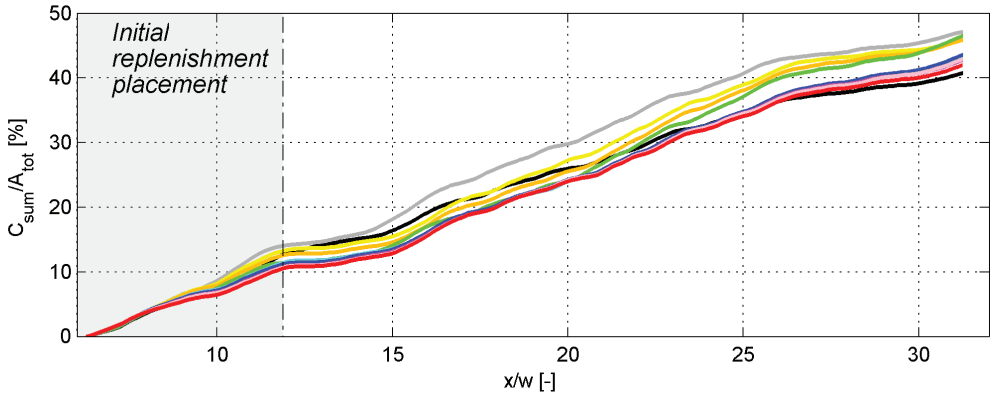

Cumulative sum of the OCR-distribution. Area initially occupied by the replenished deposits in gray. Time steps with same color map as above

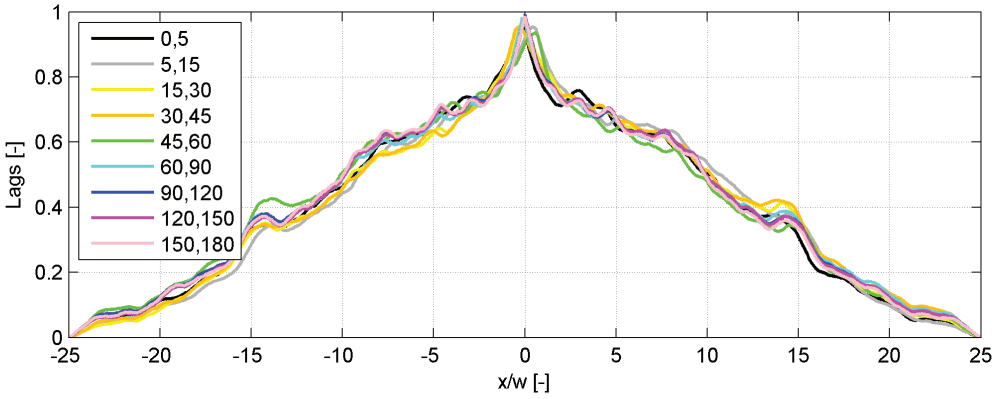

Temporal distribution of the OCR-distribution correlations

B.3 Experiment 21, Configuration C 2^{ND}, 100% submergence

Parameters

Conf	Sub %	Shift m	L m	w m	Vol m^3	Weight kg	Q m^3/s	Duration h	Time steps
C	100	1	0.75	0.13	0.027	27.0	0.019	3-4.5	10

Configuration states

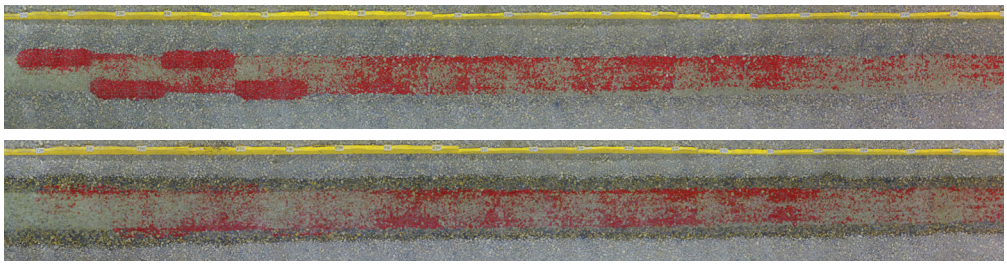

(Top) Initial state, (Bottom) final state after 1.5 hours testing. Flow direction from left to right

Assessed parameters

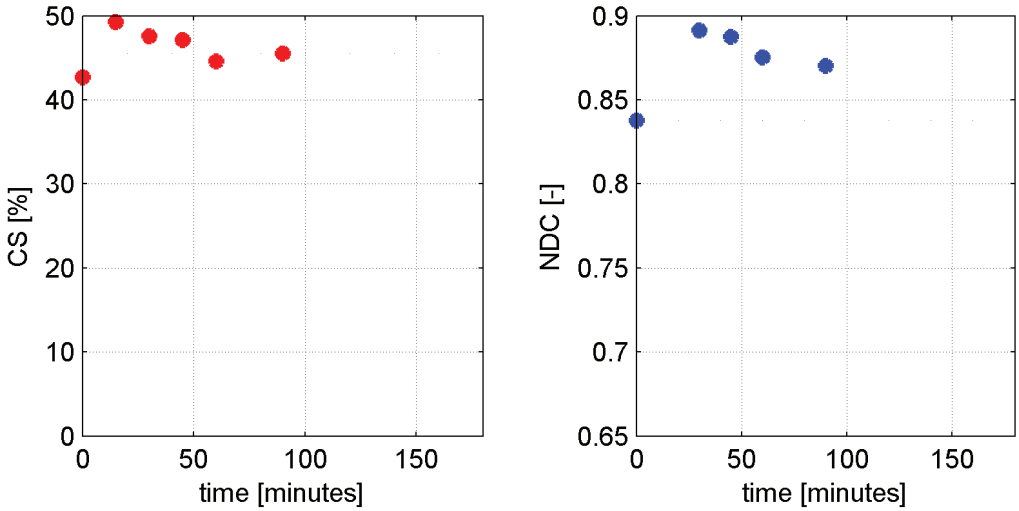

(a) Covered surface CS

(b) Compactness NDC

(a) Temporal evolution of covered surface CS and (b) compactness NDC for the tested configuration

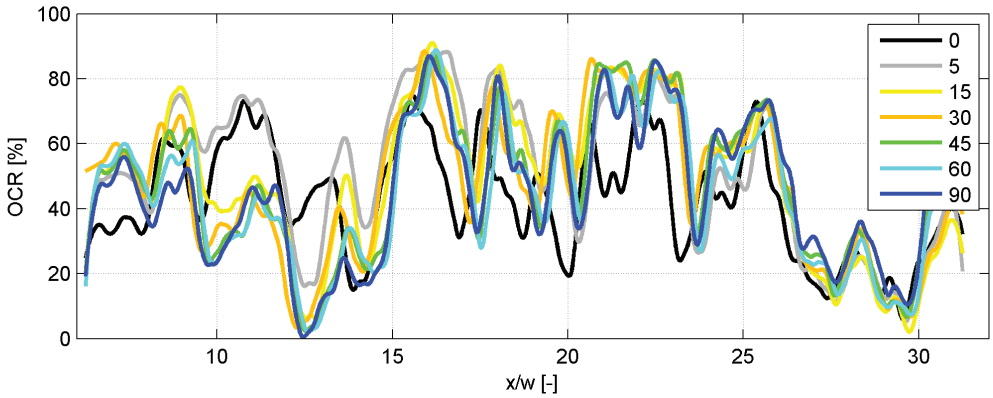

Temporal evolution of the occupation ratio distribution OCR. Time steps in minutes

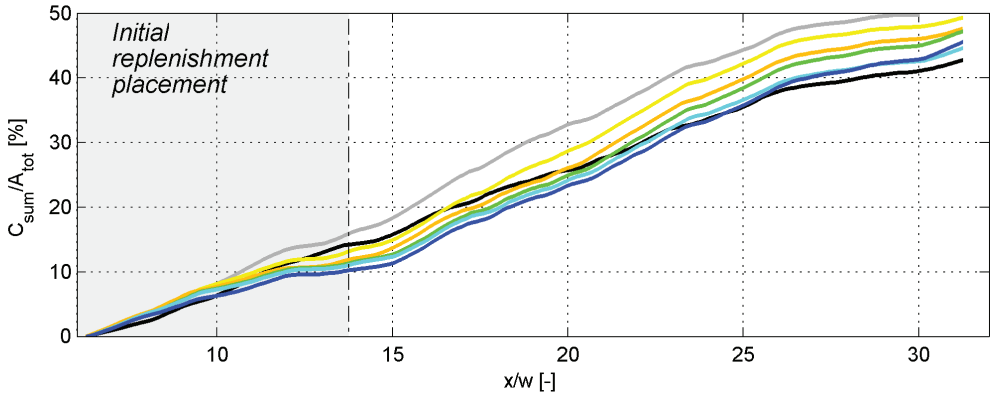

Cumulative sum of the OCR-distribution. Area initially occupied by the replenished deposits in gray. Time steps with same color map as above

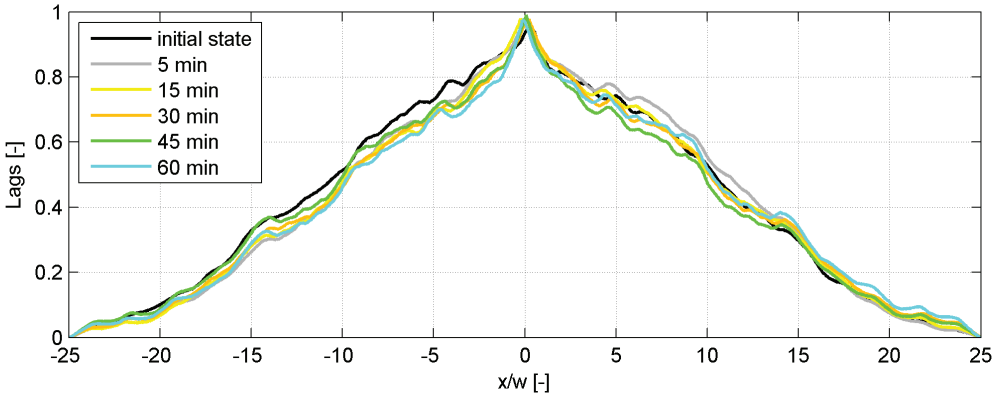

Temporal distribution of the OCR-distribution correlations

B.4 Experiment 22, Configuration D 2^{ND}, 100% submergence

Parameters

Conf	Sub %	Shift m	L m	w m	Vol m^3	Weight kg	Q m^3/s	Duration h	Time steps
D	100	2	0.75	0.13	0.027	27.0	0.019	3-4.5	10

Configuration states

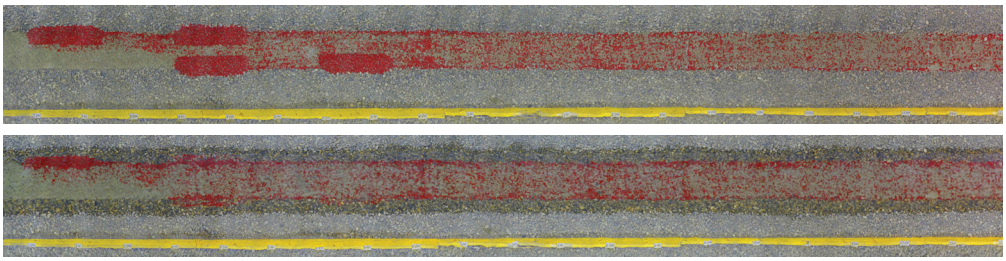

(Top) Initial state, (Bottom) final state after 1.5 hours testing. Flow direction from left to right

Assessed parameters

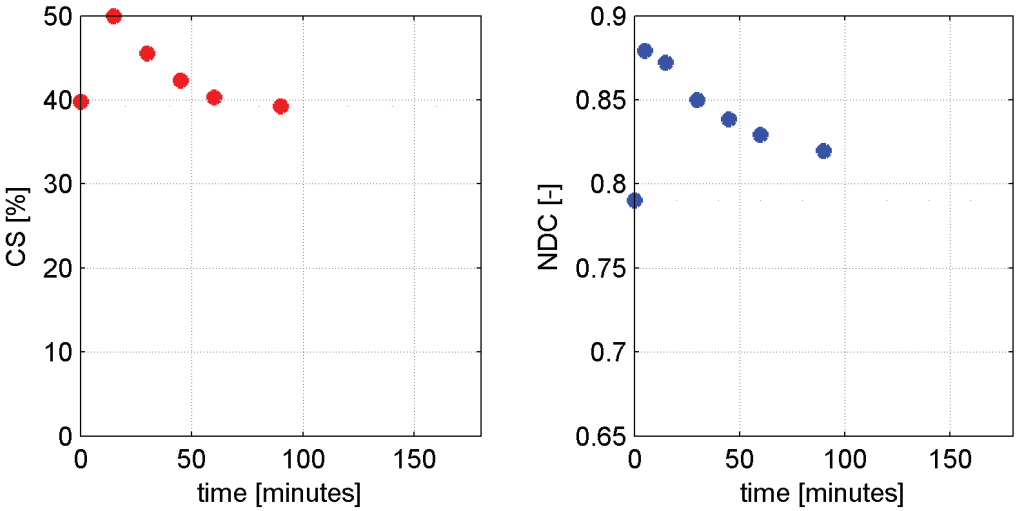

(a) Covered surface CS

(b) Compactness NDC

(a) Temporal evolution of covered surface CS and (b) compactness NDC for the tested configuration

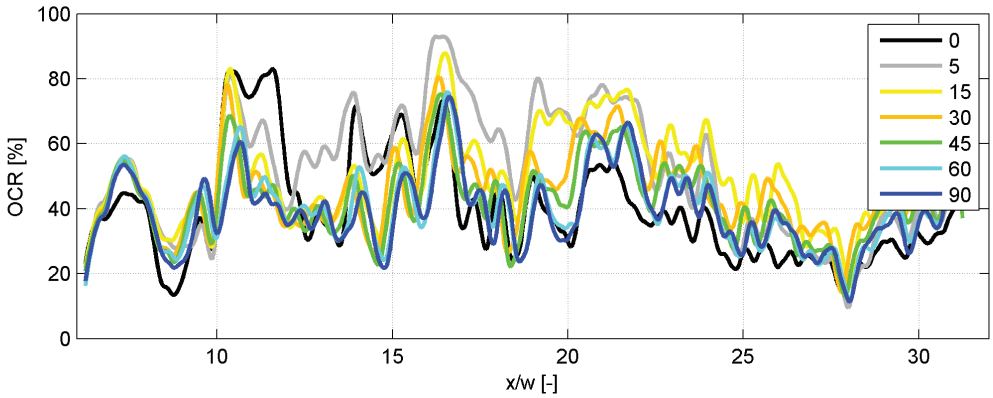

Temporal evolution of the occupation ratio distribution OCR. Time steps in minutes

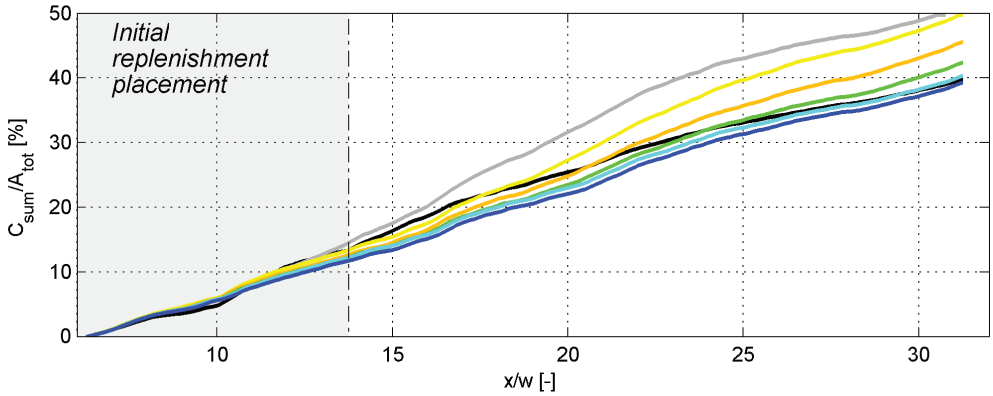

Cumulative sum of the OCR-distribution. Area initially occupied by the replenished deposits in gray. Time steps with same color map as above

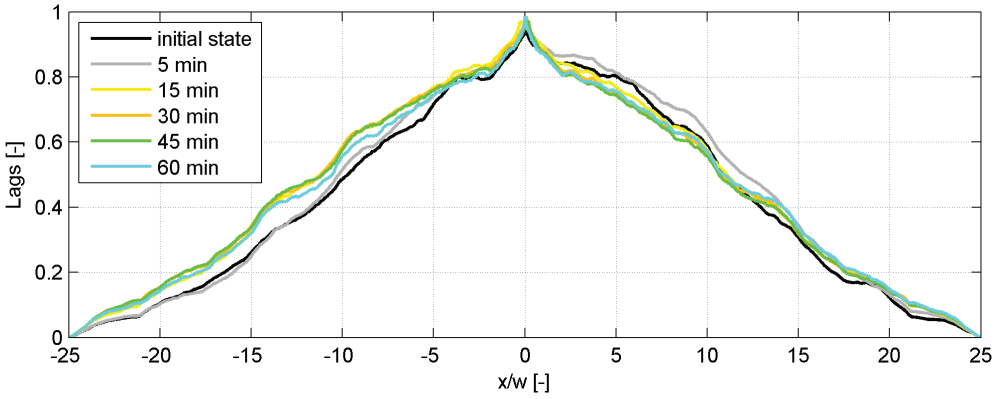

Temporal distribution of the OCR-distribution correlations

B.5 Experiment 25, Configuration C 2^{ND}, 100% submergence

Parameters

Conf	Sub %	Shift m	L m	w m	Vol m^3	Weight kg	Q m^3/s	Duration h	Time steps
C	100	1	0.75	0.13	0.027	27.0	0.019	3-6	10

Configuration states

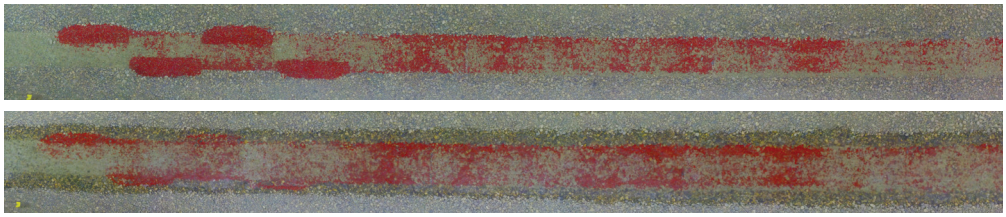

(Top) Initial state, (Bottom) final state after 3 hours testing. Flow direction from left to right

Assessed parameters

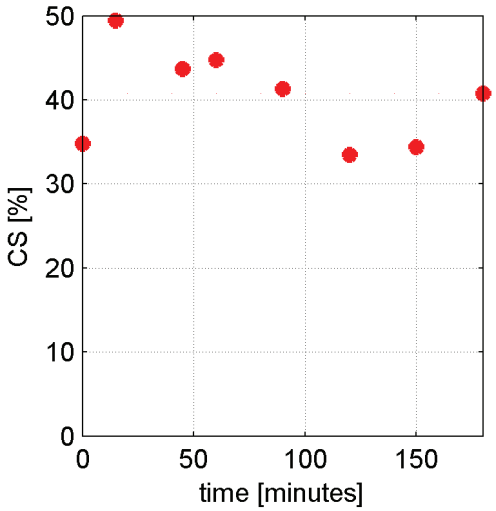

(a) Covered surface CS

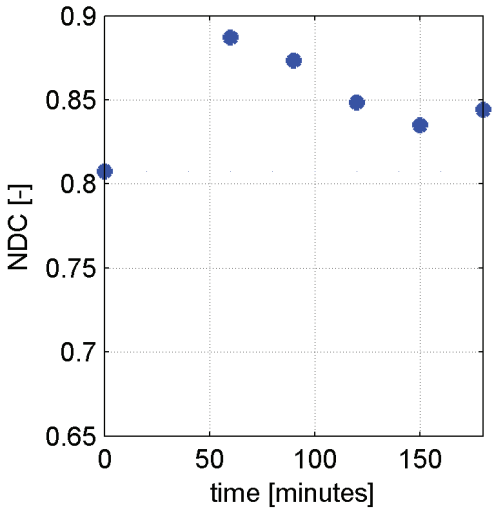

(b) Compactness NDC

(a) Temporal evolution of covered surface CS and (b) compactness NDC for the tested configuration

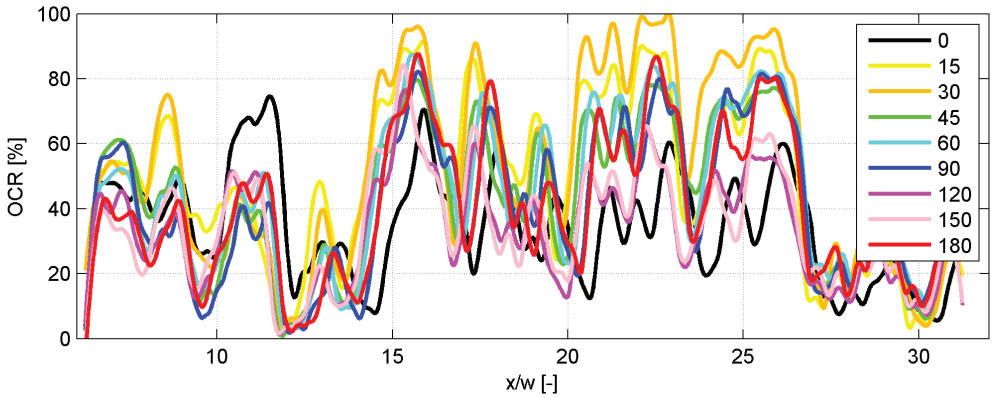

Temporal evolution of the occupation ratio distribution OCR. Time steps in minutes

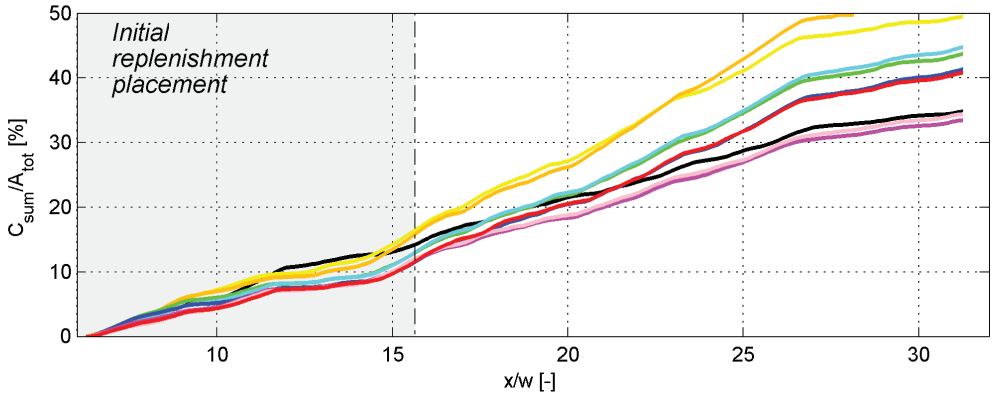

Cumulative sum of the OCR-distribution. Area initially occupied by the replenished deposits in gray. Time steps with same color map as above

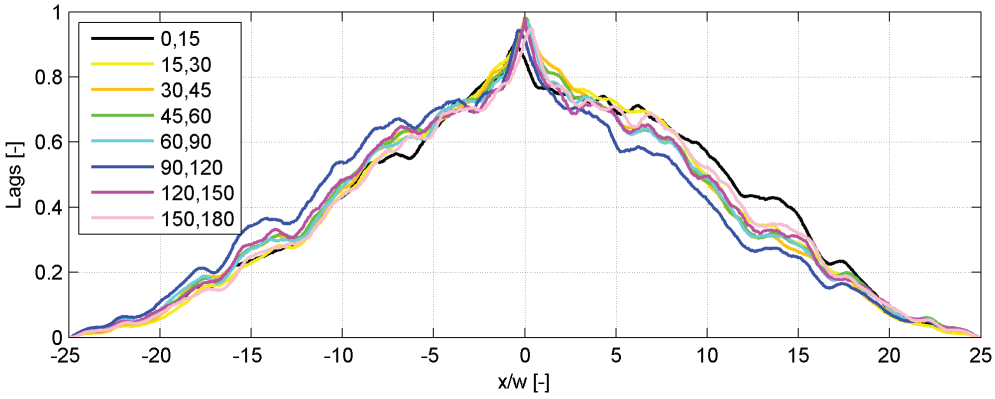

Temporal distribution of the OCR-distribution correlations

B.6 Experiment 26, Configuration D 2^{ND}, 100% submergence

Parameters

Conf	Sub %	Shift m	L m	w m	Vol m^3	Weight kg	Q m^3/s	Duration h	Time steps
D	100	2	0.75	0.13	0.027	27.0	0.019	3-6	10

Configuration states

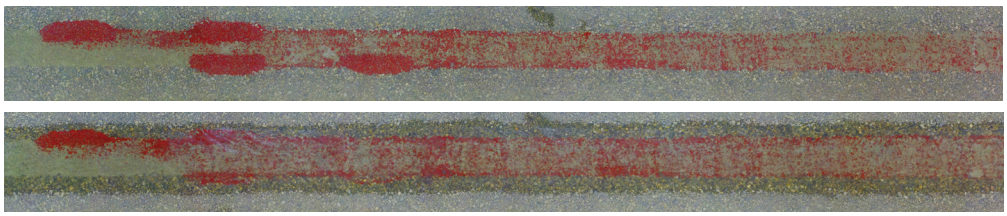

(Top) Initial state, (Bottom) final state after 3 hours testing. Flow direction from left to right

Assessed parameters

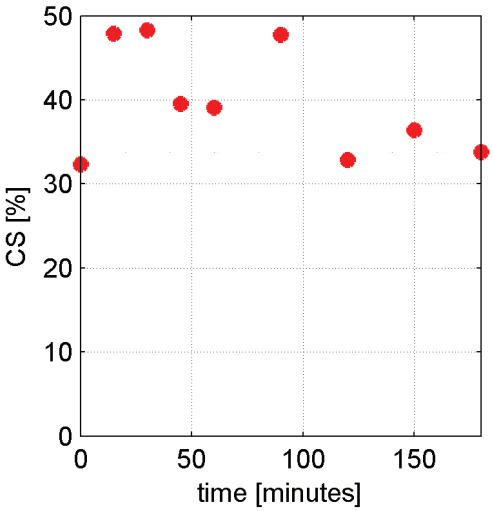

(a) Covered surface CS

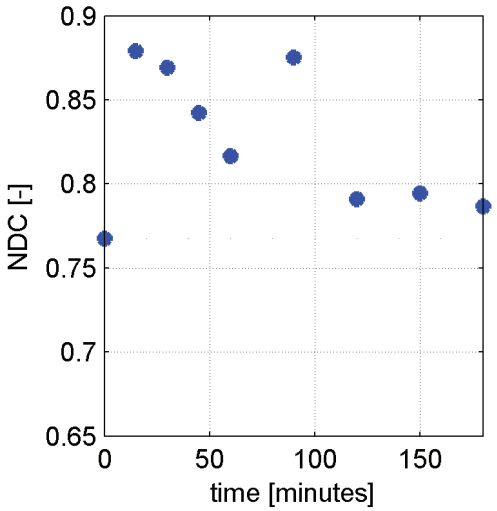

(b) Compactness NDC

(a) Temporal evolution of covered surface CS and (b) compactness NDC for the tested configuration

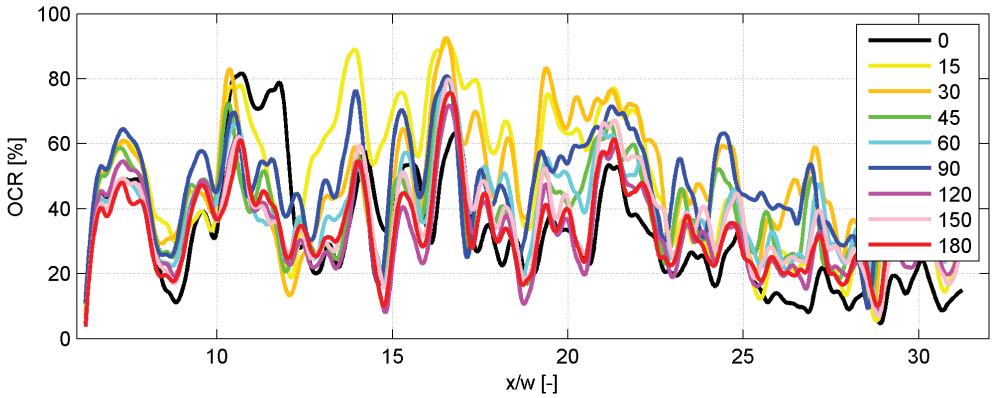

Temporal evolution of the occupation ratio distribution OCR. Time steps in minutes

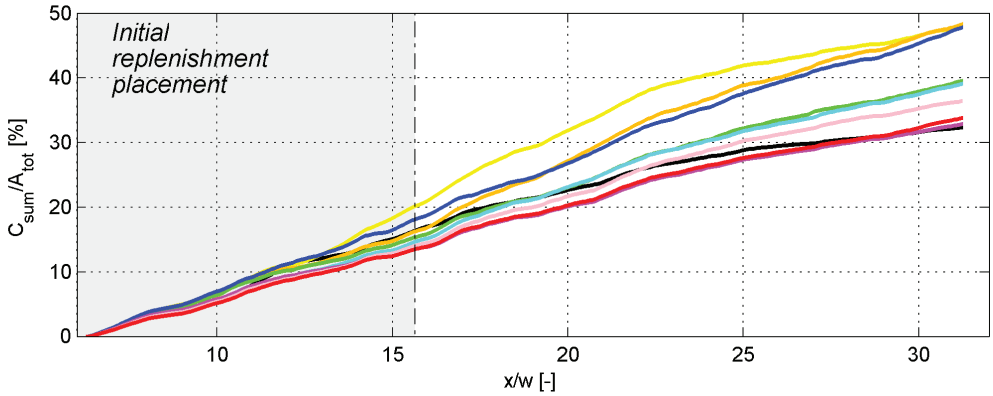

Cumulative sum of the OCR-distribution. Area initially occupied by the replenished deposits in gray. Time steps with same color map as above

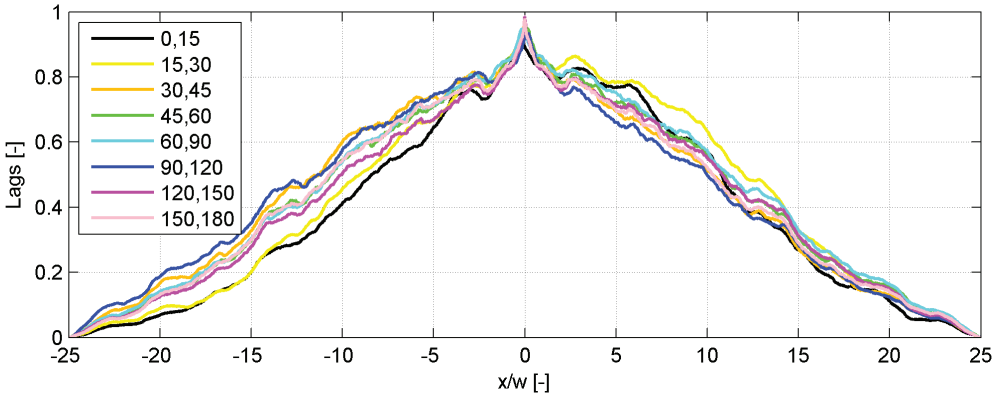

Temporal distribution of the OCR-distribution correlations

B.7 Effect of second replenishment on Configurations C and D

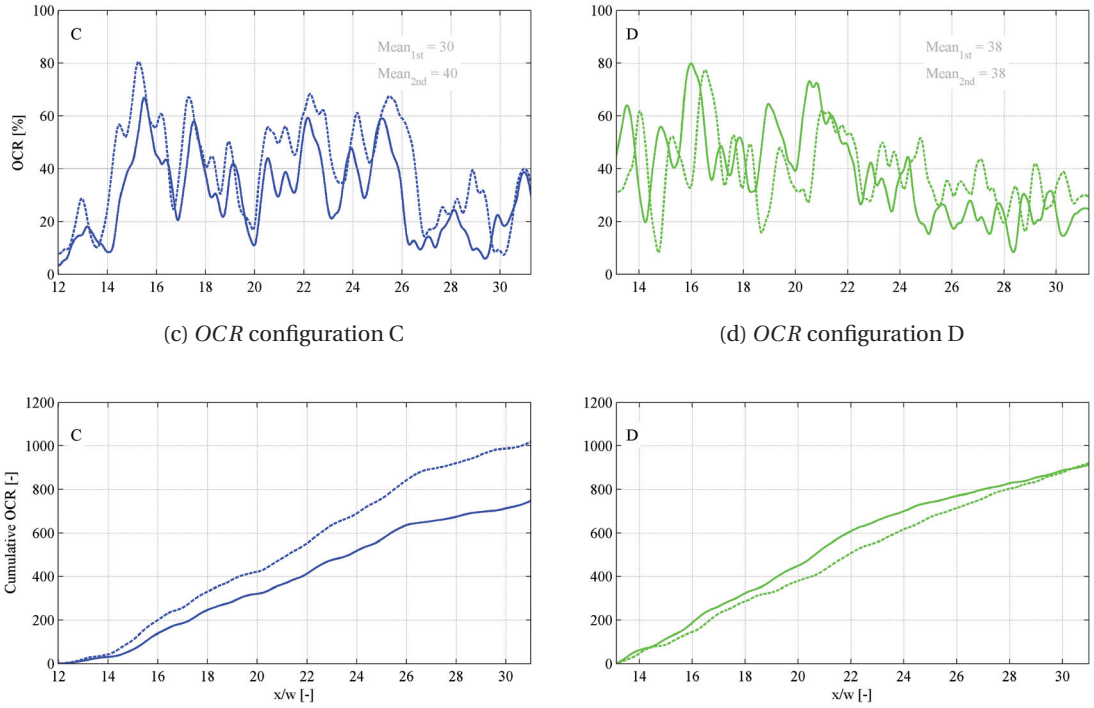

(c) *OCR* configuration C

(d) *OCR* configuration D

(e) Cumulative sum of *OCR*, for configuration C

(f) Cumulative sum of *OCR*, for configuration D

Figure B.1 – Occupational rate (OCR) along channel reach downstream of the replenishments and their cumulative sum for configuration C and D. First replenishment=solid line, second replenishment=dashed line

C Appendix: Experiments with transient flows

C.1 Experiment 39, Configuration B, hydrograph H_1

Parameters

Conf	Peak min	Shift m	L m	w m	Vol m^3	Weight kg	Q_p m^3/s	Duration h	Time steps
B	20	1/2	0.75	0.13	0.027	27.0	0.031	3	11

Configuration states

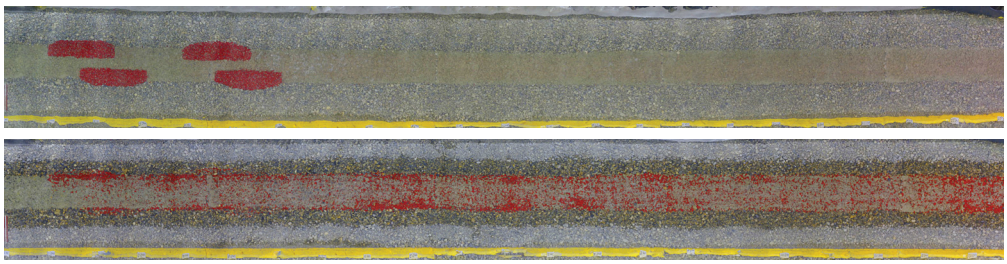

(Top) Initial state, (Bottom) final state after 3 hours testing. Flow direction from left to right

Assessed parameters

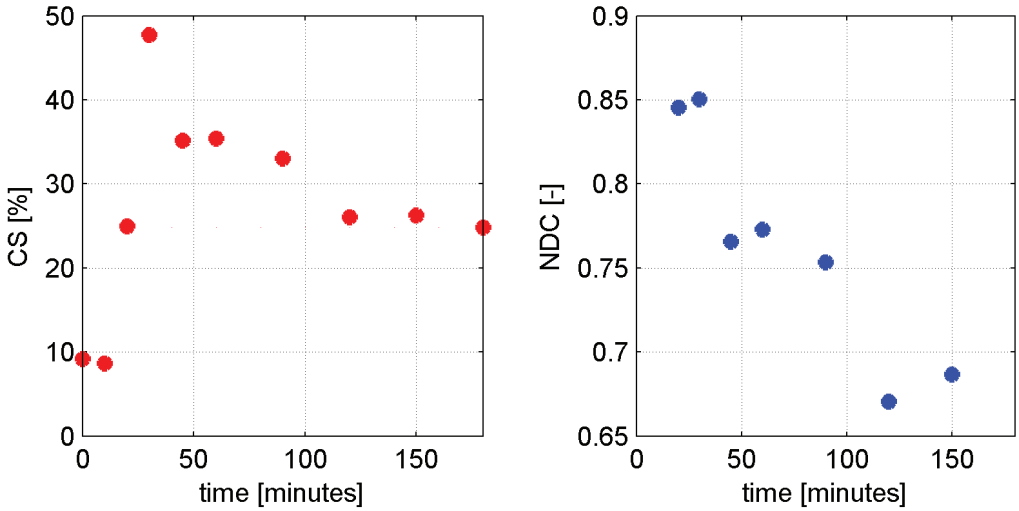

(a) Covered surface CS

(b) Compactness NDC

(a) Temporal evolution of covered surface CS and (b) compactness NDC for the tested configuration

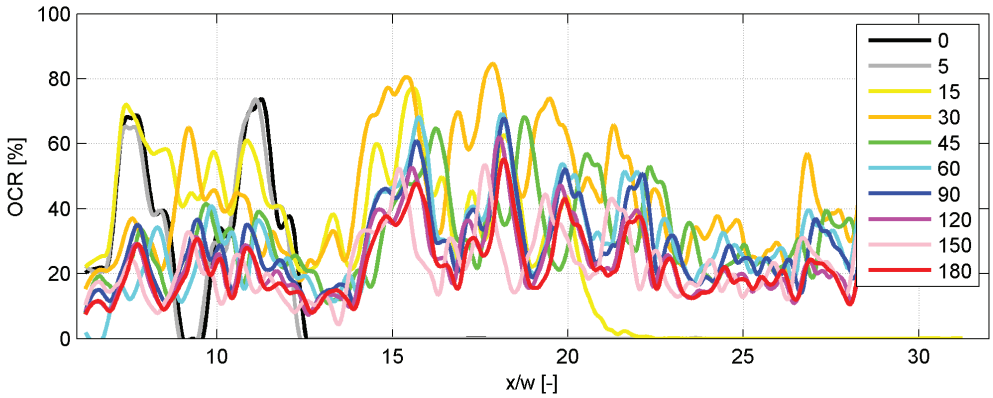

Temporal evolution of the occupation ratio distribution OCR. Time steps in minutes

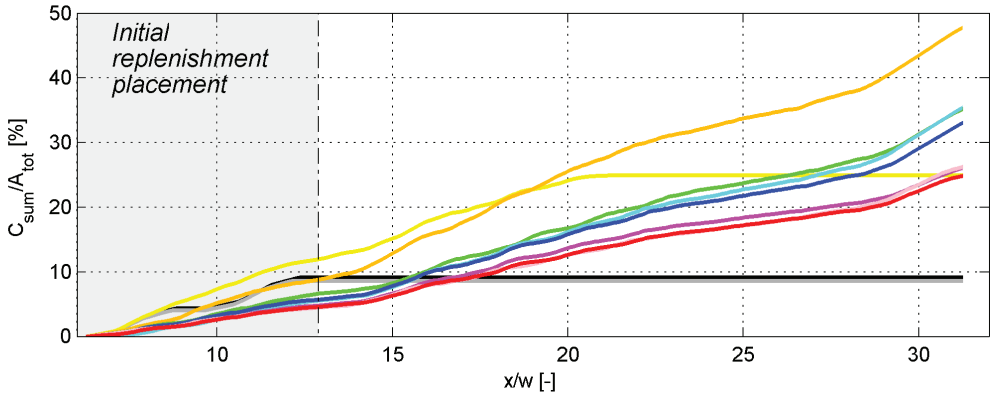

Cumulative sum of the OCR-distribution. Area initially occupied by the replenished deposits in gray. Time steps with same color map as above

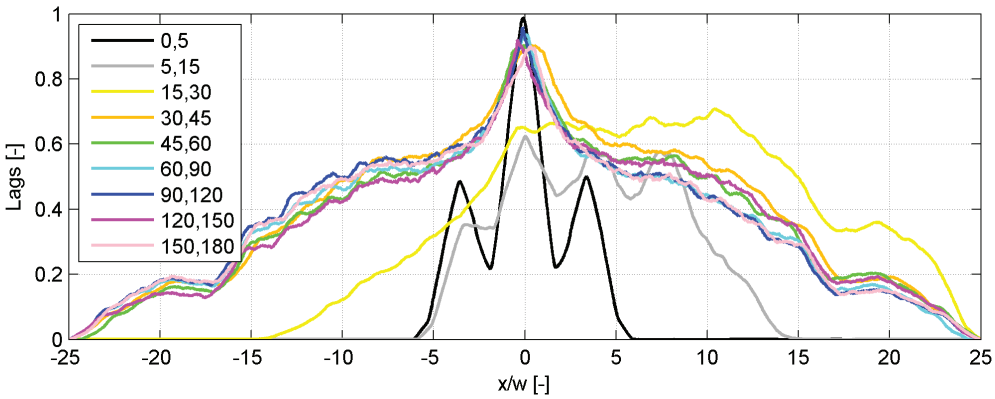

Temporal distribution of the OCR-distribution correlations

C.2 Experiment 40, Configuration C, hydrograph H_1

Parameters

Conf	Peak min	Shift m	L m	w m	Vol m^3	Weight kg	Q_p m^3/s	Duration h	Time steps
C	20	1	0.75	0.13	0.027	27.0	0.031	3	11

Configuration states

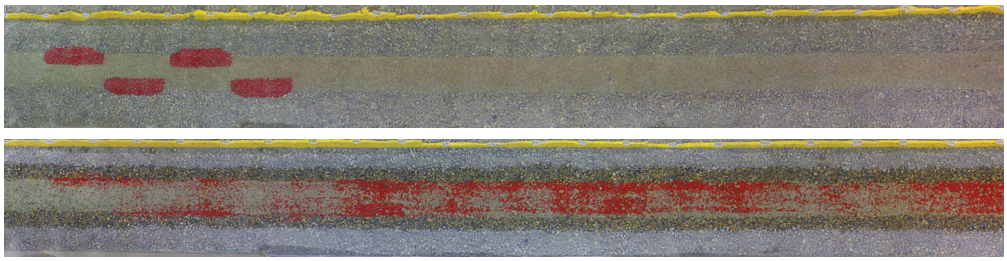

(Top) Initial state, (Bottom) final state after 3 hours testing. Flow direction from left to right

Assessed parameters

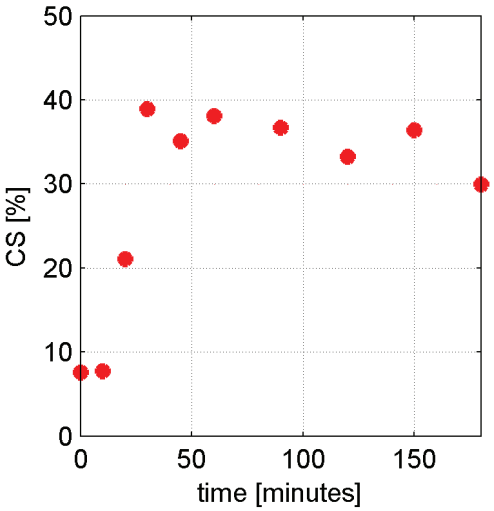

(a) Covered surface CS

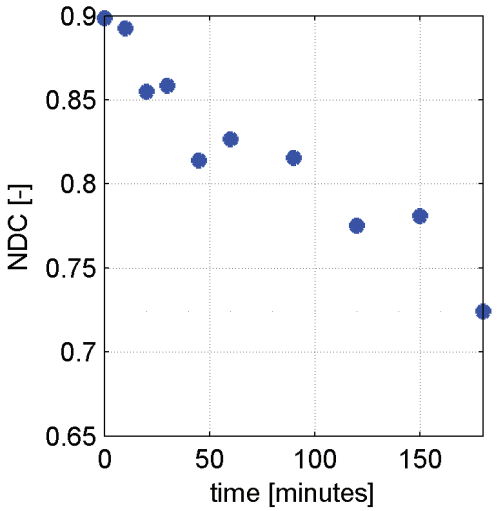

(b) Compactness NDC

(a) Temporal evolution of covered surface CS and (b) compactness NDC for the tested configuration

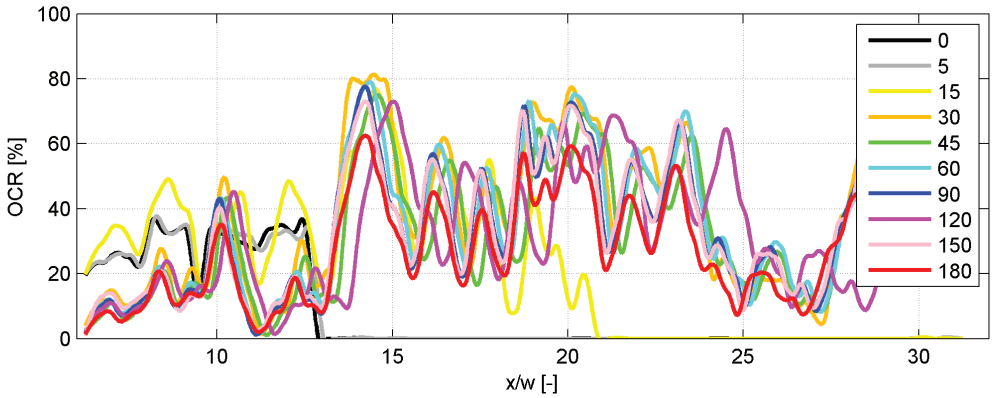

Temporal evolution of the occupation ratio distribution OCR. Time steps in minutes

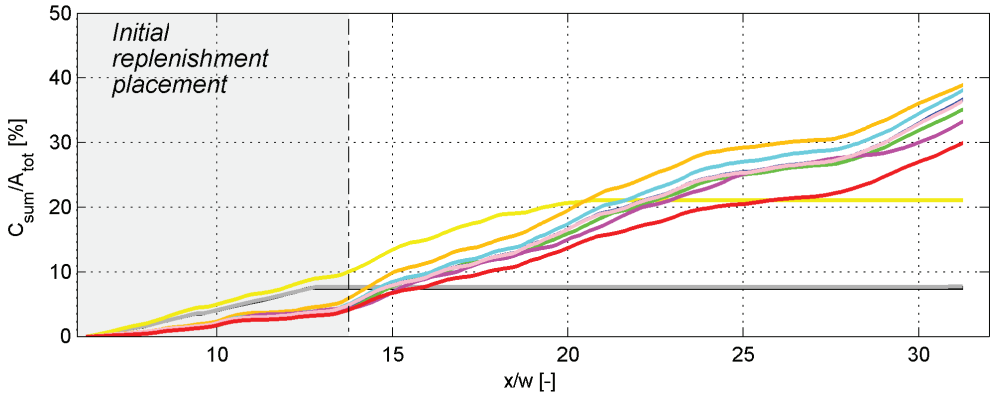

Cumulative sum of the OCR-distribution. Area initially occupied by the replenished deposits in gray. Time steps with same color map as above

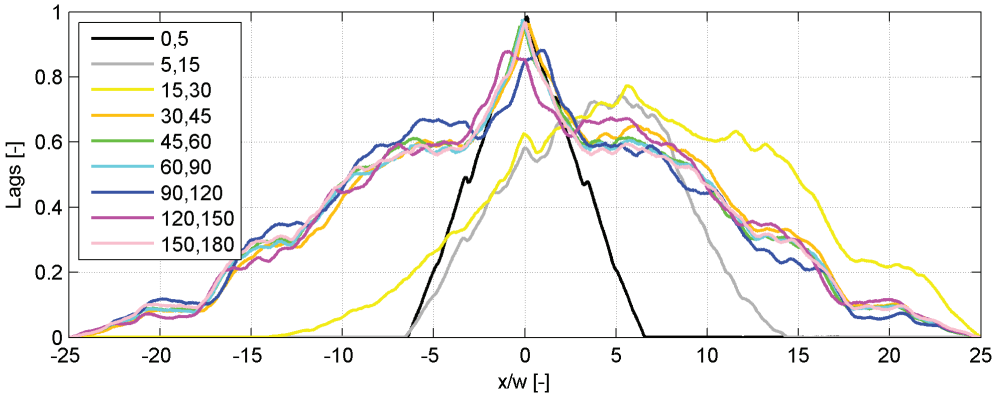

Temporal distribution of the OCR-distribution correlations

C.3 Experiment 41, Configuration B, hydrograph H_2

Parameters

Conf	Peak min	Shift m	L m	w m	Vol m^3	Weight kg	Q_p m^3/s	Duration h	Time steps
B	45	1/2	0.75	0.13	0.027	27.0	0.031	3	11

Configuration states

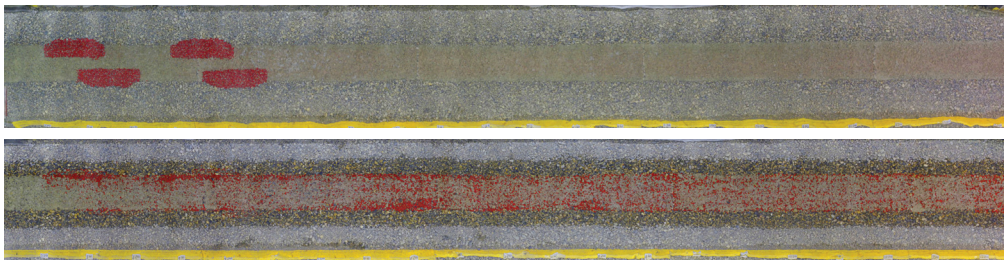

(Top) Initial state, (Bottom) final state after 3 hours testing. Flow direction from left to right

Assessed parameters

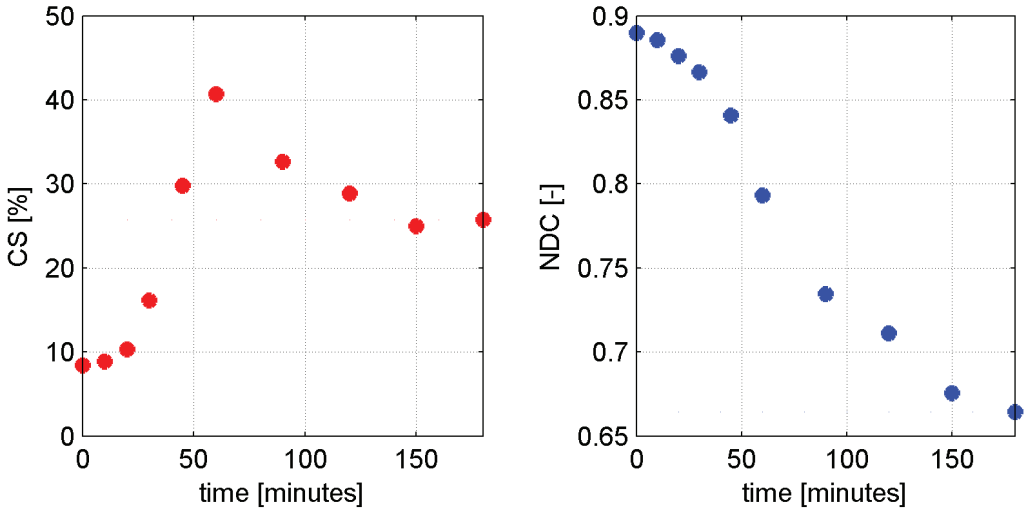

(a) Covered surface CS

(b) Compactness NDC

(a) Temporal evolution of covered surface CS and (b) compactness NDC for the tested configuration

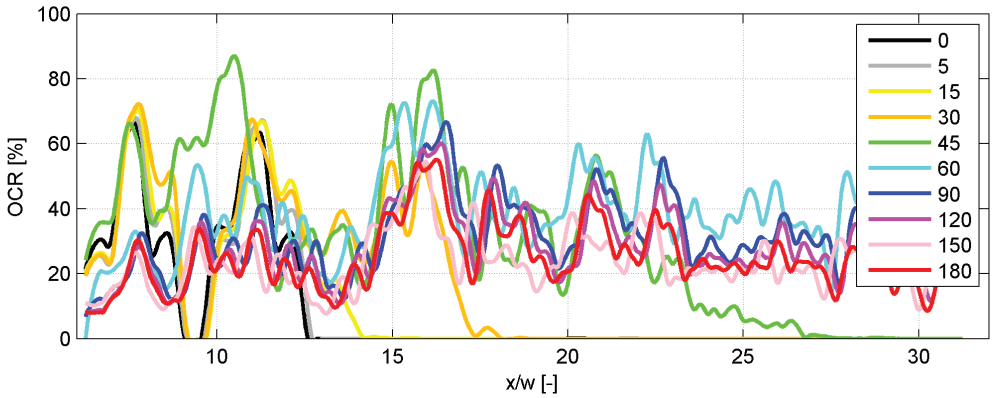

Temporal evolution of the occupation ratio distribution OCR. Time steps in minutes

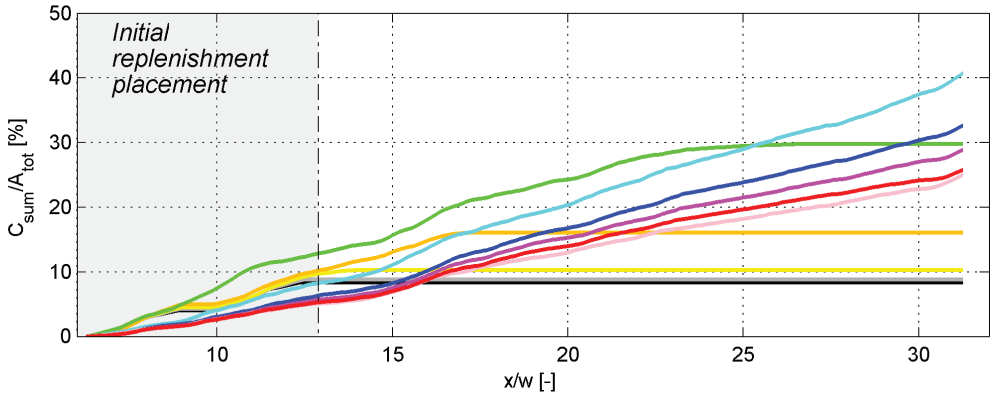

Cumulative sum of the OCR-distribution. Area initially occupied by the replenished deposits in gray. Time steps with same color map as above

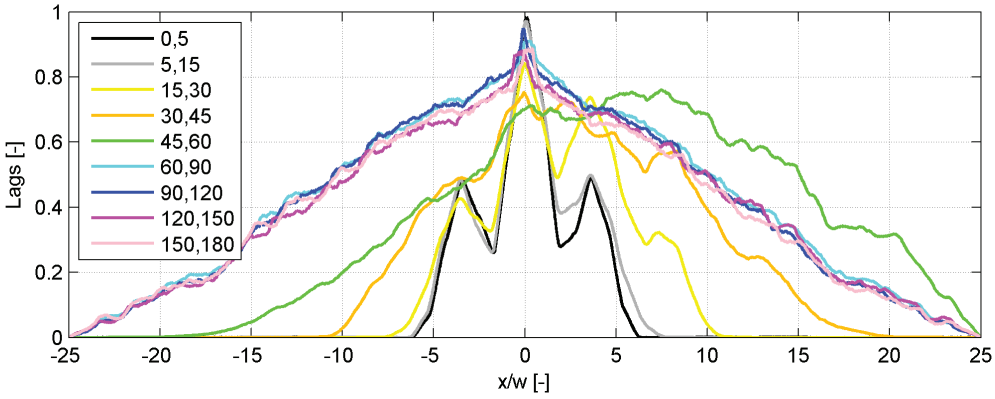

Temporal distribution of the OCR-distribution correlations

C.4 Experiment 42, Configuration C, hydrograph H_2

Parameters

Conf	Peak min	Shift m	L m	w m	Vol m^3	Weight kg	Q_p m^3/s	Duration h	Time steps
B	45	1	0.75	0.13	0.027	27.0	0.031	3	11

Configuration states

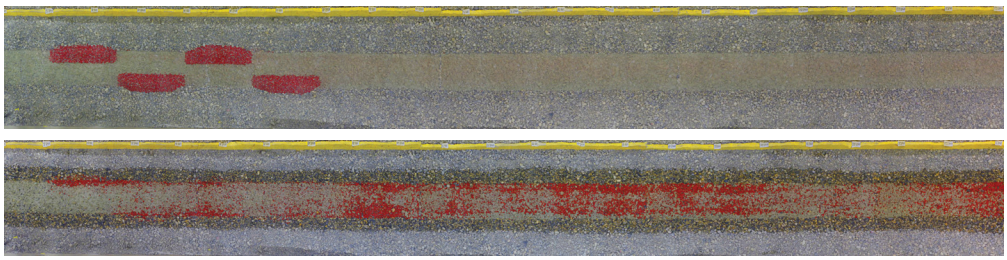

(Top) Initial state, (Bottom) final state after 3 hours testing. Flow direction from left to right

Assessed parameters

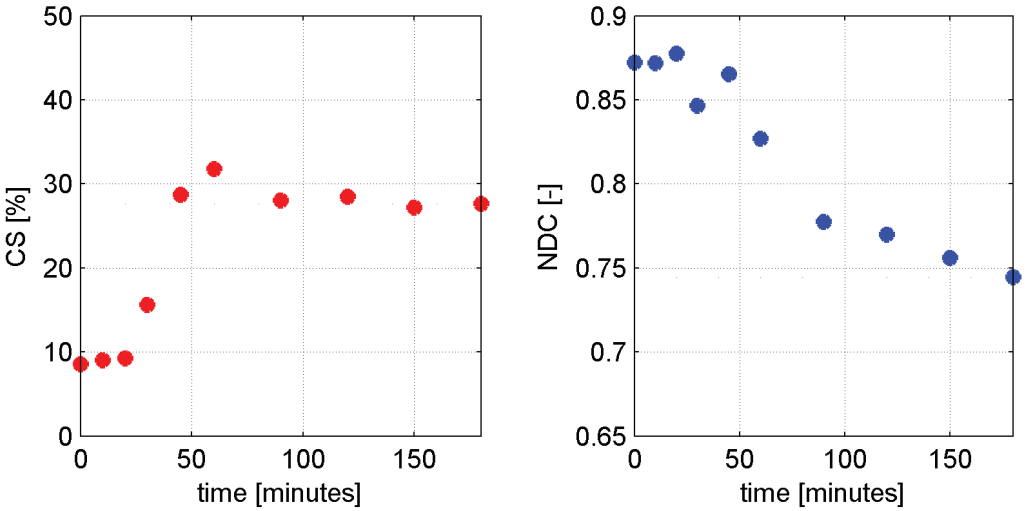

(a) Covered surface CS

(b) Compactness NDC

(a) Temporal evolution of covered surface CS and (b) compactness NDC for the tested configuration

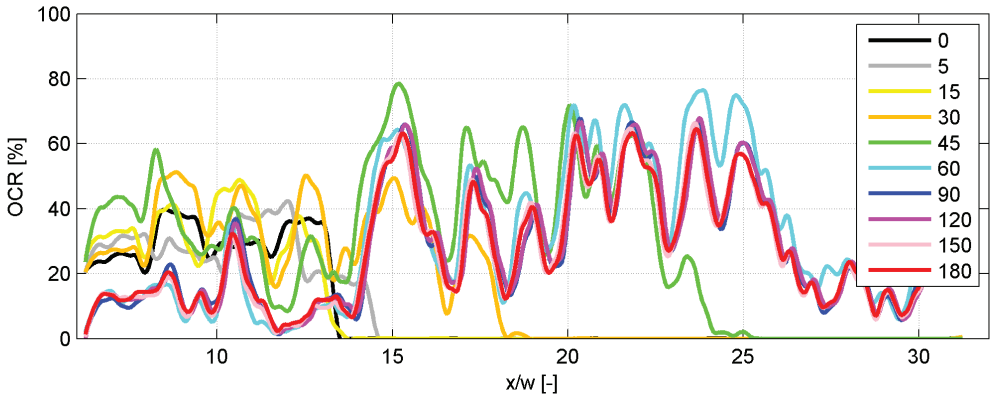

Temporal evolution of the occupation ratio distribution OCR. Time steps in minutes

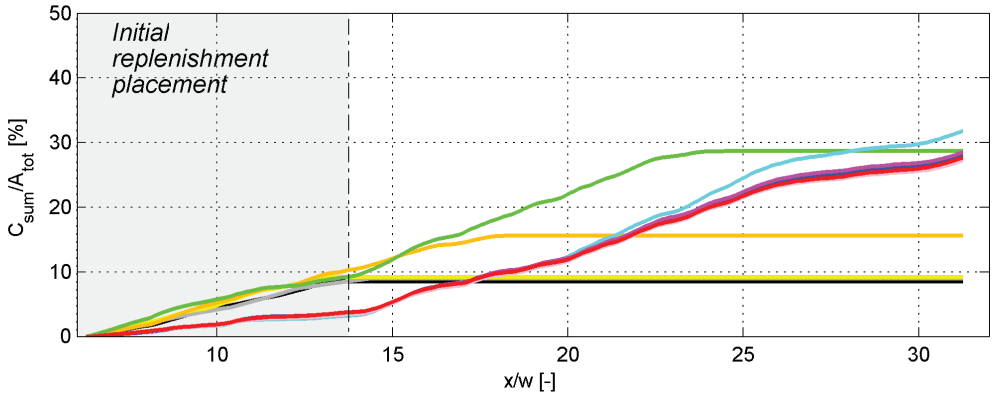

Cumulative sum of the OCR-distribution. Area initially occupied by the replenished deposits in gray. Time steps with same color map as above

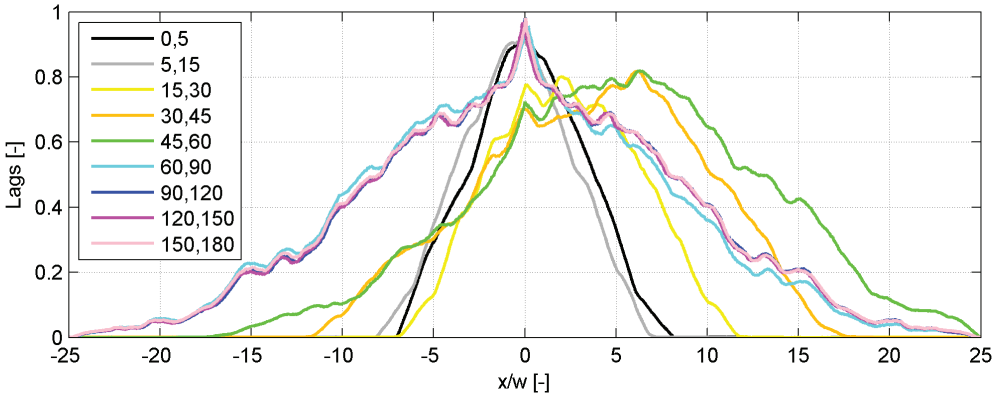

Temporal distribution of the OCR-distribution correlations

C.5 Experiment 43, Configuration B, hydrograph H_3

Parameters

Conf	Peak min	Shift m	L m	w m	Vol m^3	Weight kg	Q_p m^3/s	Duration h	Time steps
B	90	1/2	0.75	0.13	0.027	27.0	0.031	3	11

Configuration states

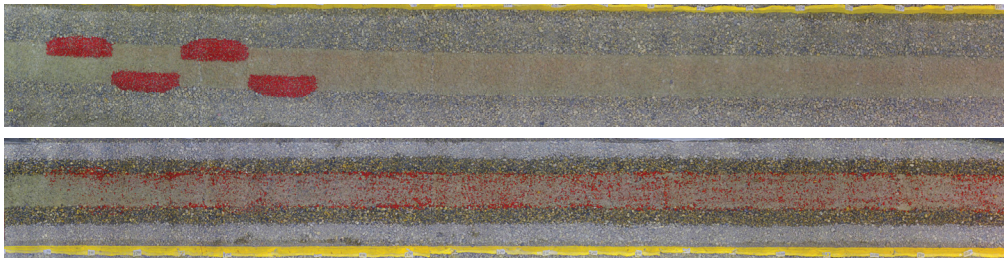

(Top) Initial state, (Bottom) final state after 3 hours testing. Flow direction from left to right

Assessed parameters

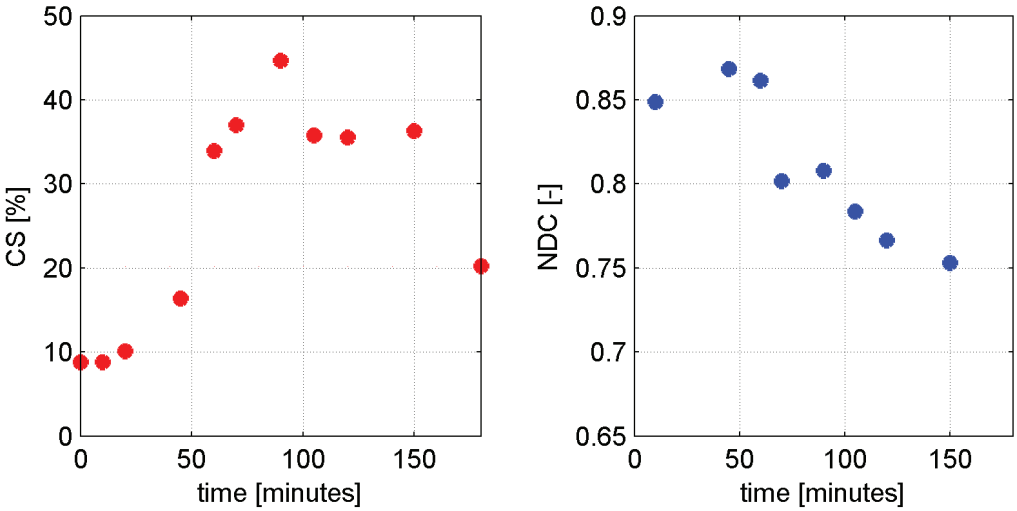

(a) Covered surface CS

(b) Compactness NDC

(a) Temporal evolution of covered surface CS and (b) compactness NDC for the tested configuration

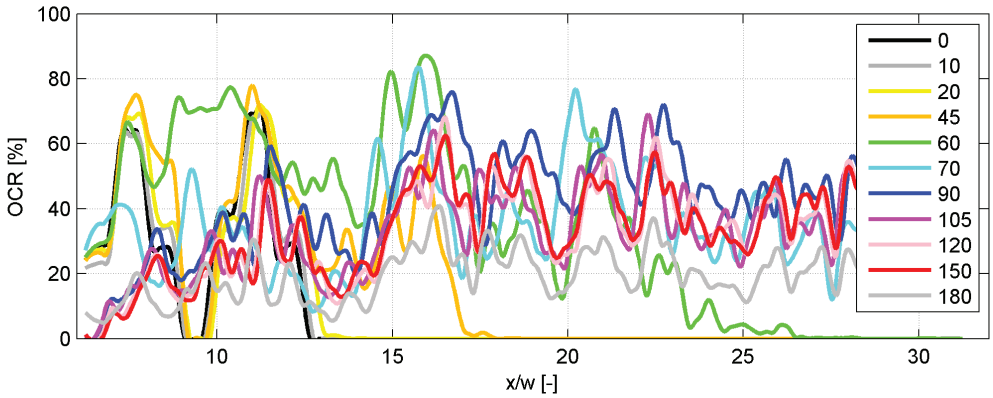

Temporal evolution of the occupation ratio distribution OCR. Time steps in minutes

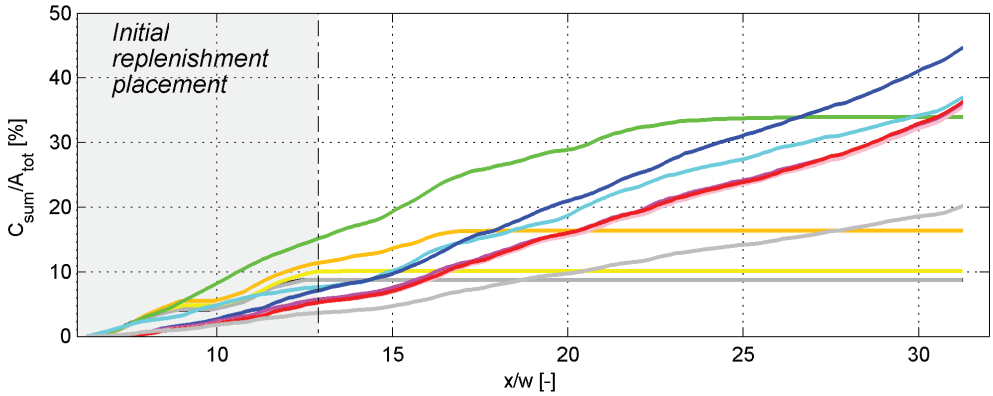

Cumulative sum of the OCR-distribution. Area initially occupied by the replenished deposits in gray. Time steps with same color map as above

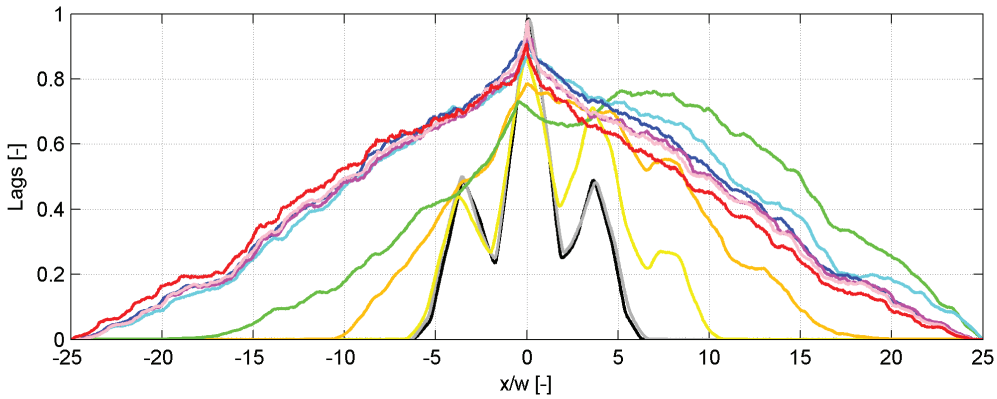

Temporal distribution of the OCR-distribution correlations

C.6 Experiment 44, Configuration C, hydrograph H_3

Parameters

Conf	Peak min	Shift m	L m	w m	Vol m^3	Weight kg	Q_p m^3/s	Duration h	Time steps
C	90	1	0.75	0.13	0.027	27.0	0.031	3	11

Configuration states

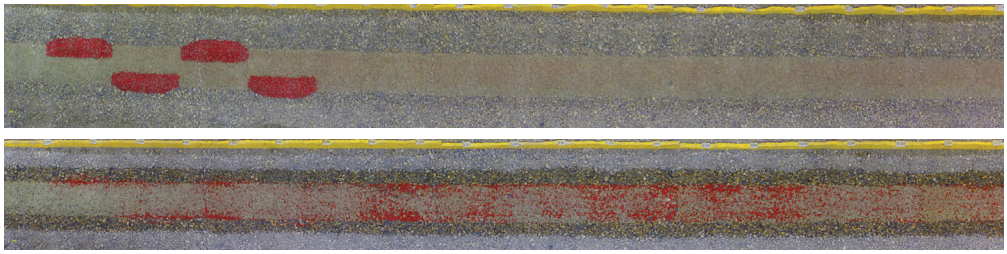

(Top) Initial state, (Bottom) final state after 3 hours testing. Flow direction from left to right

Assessed parameters

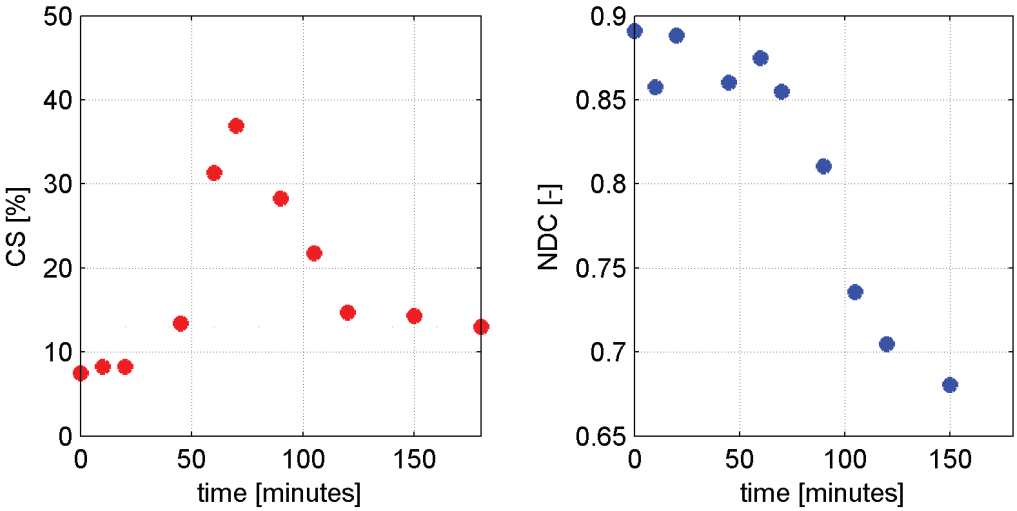

(a) Covered surface CS

(b) Compactness NDC

(a) Temporal evolution of covered surface CS and (b) compactness NDC for the tested configuration

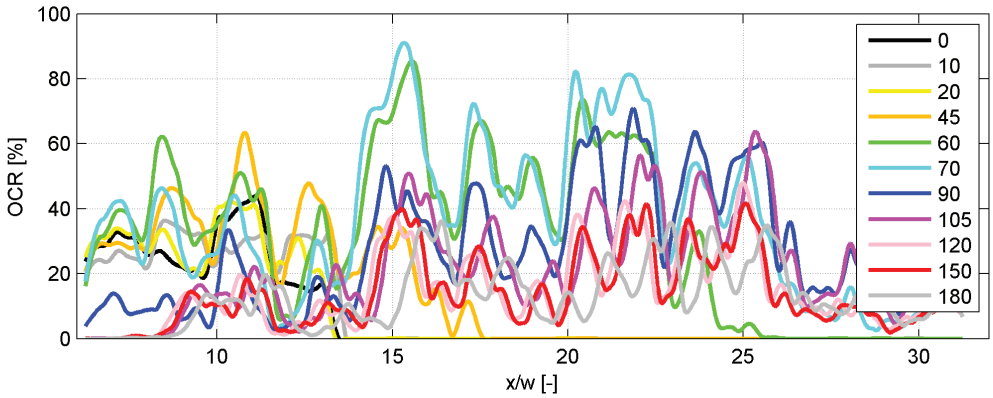

Temporal evolution of the occupation ratio distribution OCR. Time steps in minutes

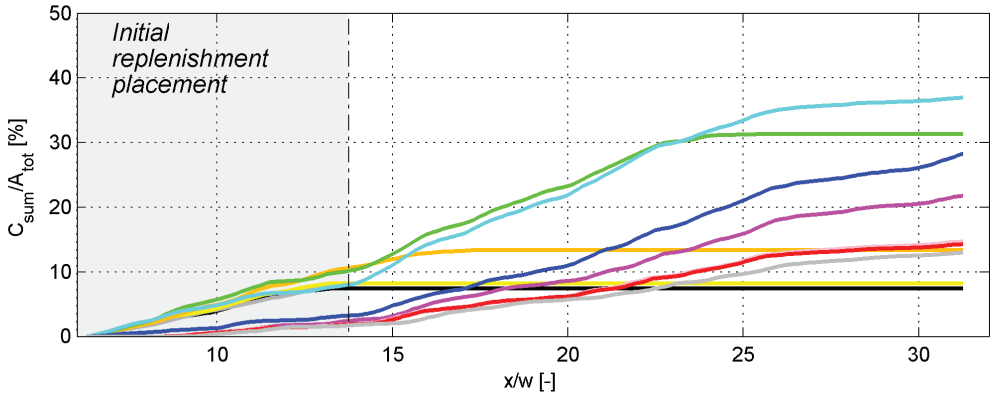

Cumulative sum of the OCR-distribution. Area initially occupied by the replenished deposits in gray. Time steps with same color map as above

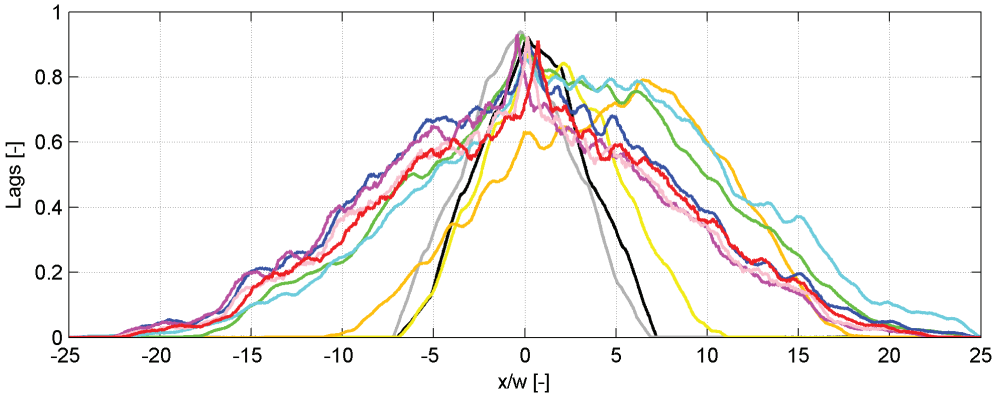

Temporal distribution of the OCR-distribution correlations

C.7 Experiment 45, Configuration B, hydrograph H_4

Parameters

Conf	Peak min	Shift m	L m	w m	Vol m^3	Weight kg	Q_p m^3/s	Duration h	Time steps
B	160	1/2	0.75	0.13	0.027	27.0	0.031	3	11

Configuration states

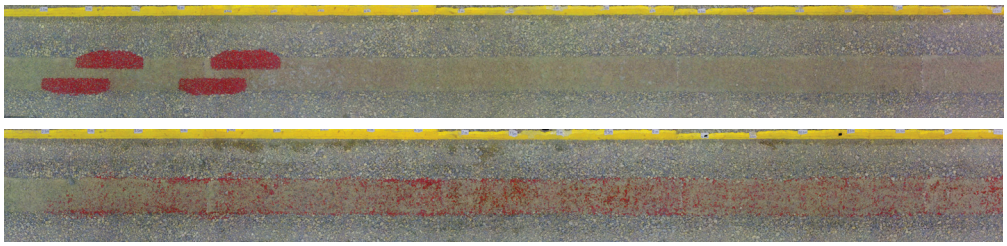

(Top) Initial state, (Bottom) final state after 3 hours testing. Flow direction from left to right

Assessed parameters

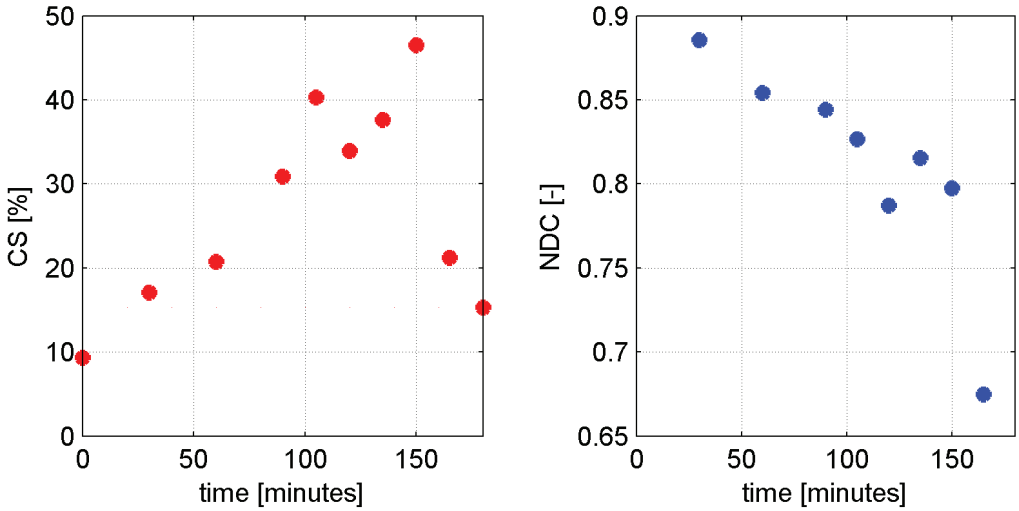

(a) Covered surface CS

(b) Compactness NDC

(a) Temporal evolution of covered surface CS and (b) compactness NDC for the tested configuration

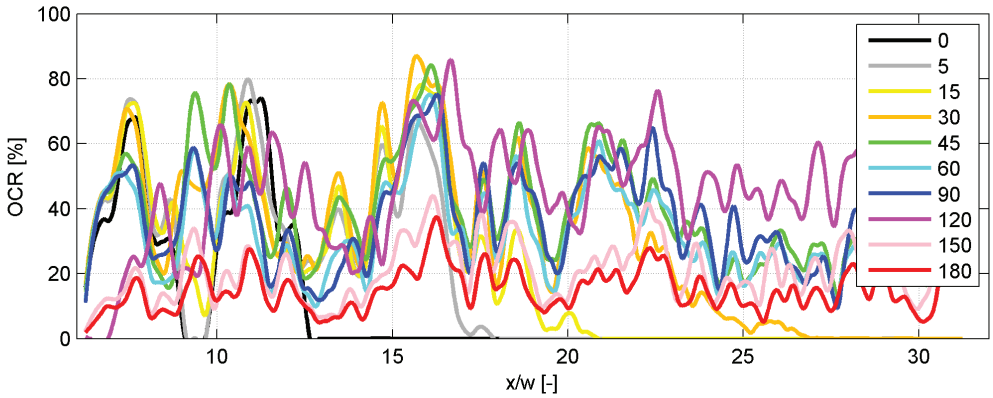

Temporal evolution of the occupation ratio distribution OCR. Time steps in minutes

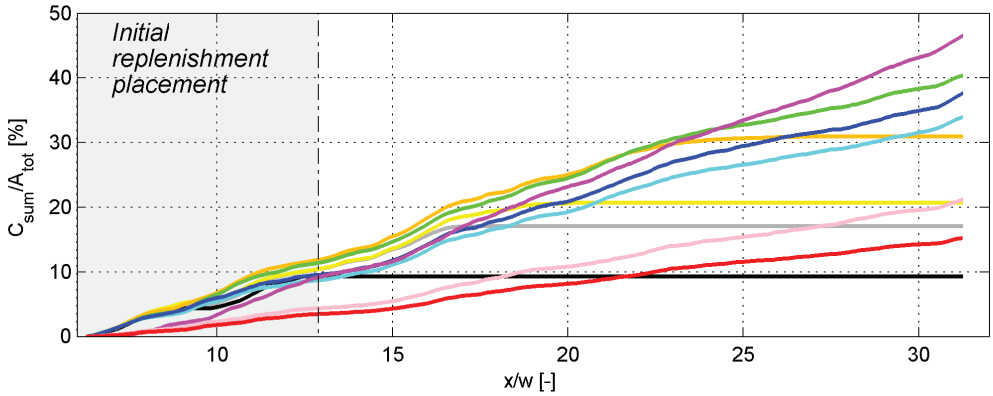

Cumulative sum of the OCR-distribution. Area initially occupied by the replenished deposits in gray. Time steps with same color map as above

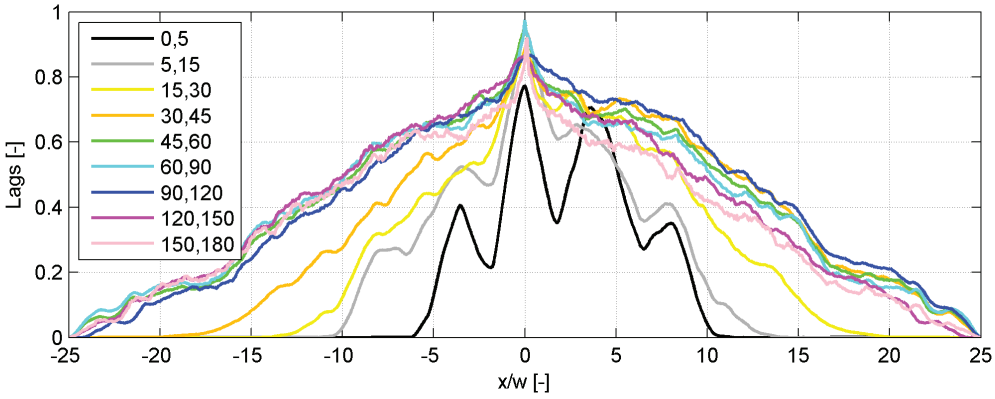

Temporal distribution of the OCR-distribution correlations

C.8 Experiment 46, Configuration C, hydrograph H_4

Parameters

Conf	Peak min	Shift m	L m	w m	Vol m^3	Weight kg	Q_p m^3/s	Duration h	Time steps
C	160	1	0.75	0.13	0.027	27.0	0.031	3	11

Configuration states

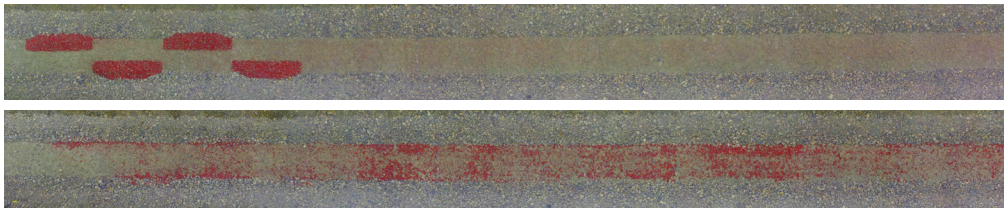

(Top) Initial state, (Bottom) final state after 3 hours testing. Flow direction from left to right

Assessed parameters

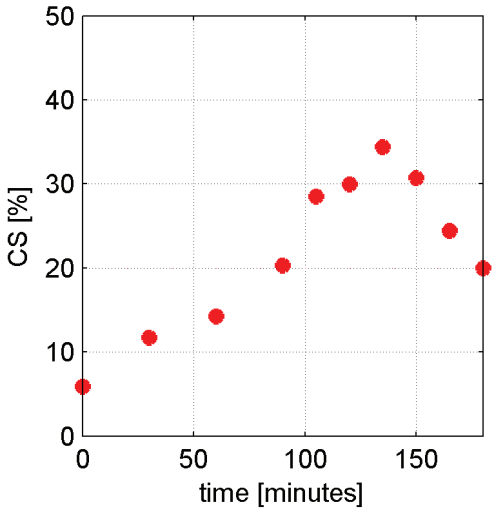

(a) Covered surface CS

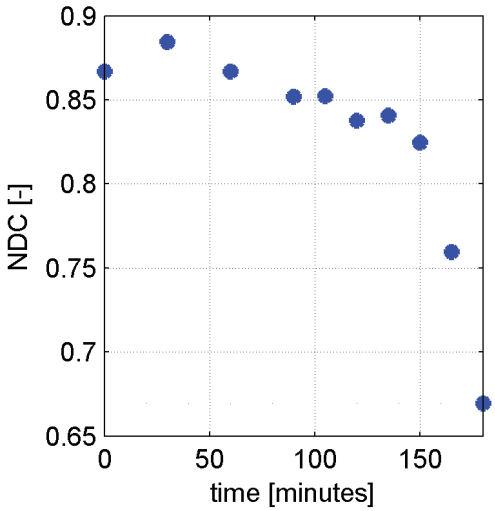

(b) Compactness NDC

(a) Temporal evolution of covered surface CS and (b) compactness NDC for the tested configuration

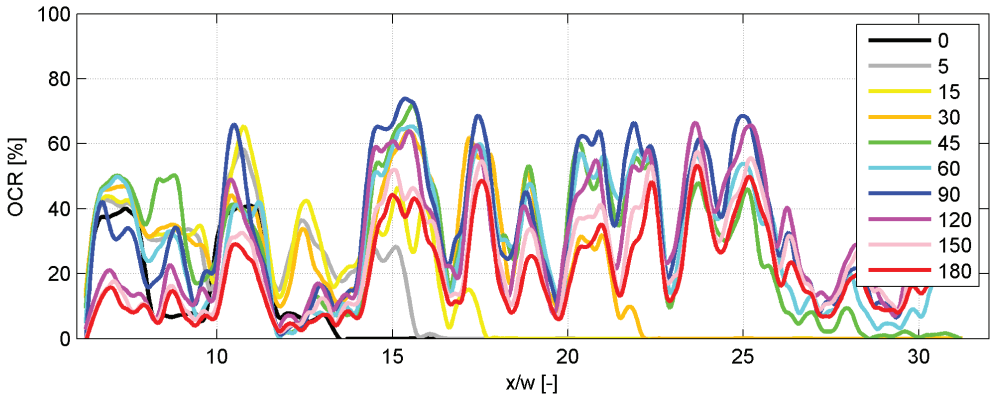

Temporal evolution of the occupation ratio distribution OCR. Time steps in minutes

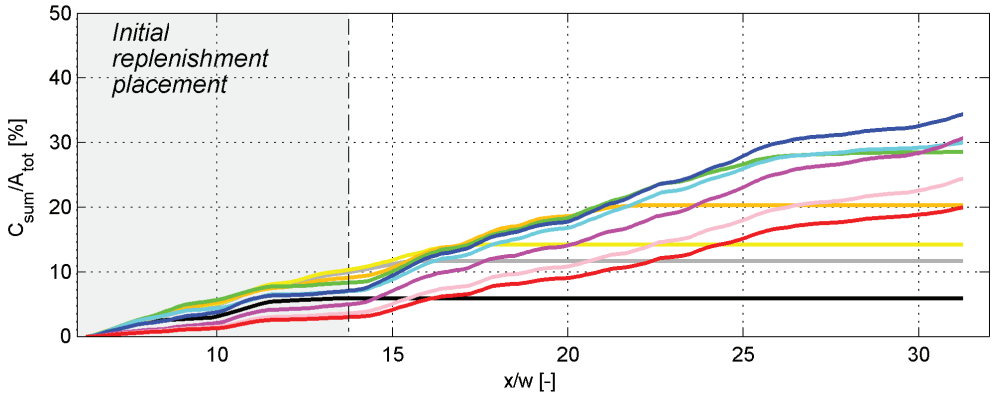

Cumulative sum of the OCR-distribution. Area initially occupied by the replenished deposits in gray. Time steps with same color map as above

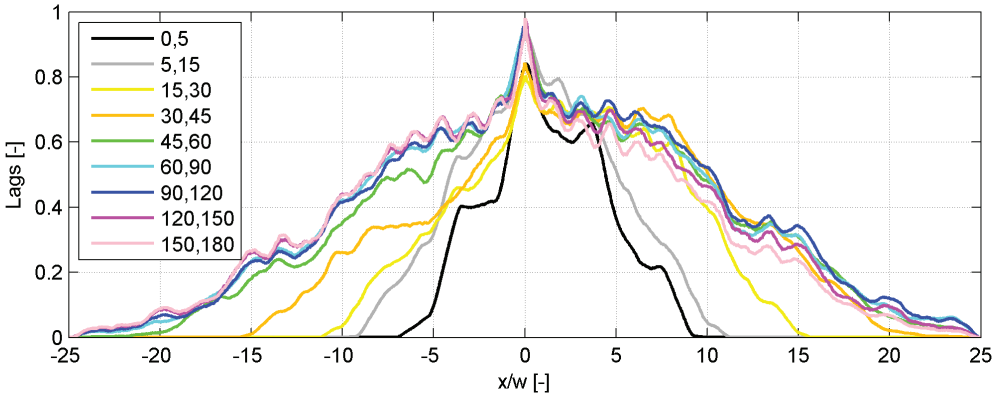

Temporal distribution of the OCR-distribution correlations

Curriculum vitae
Elena Battisacco

Dr.in Civil Engineer

- Nationality: Italian
- Date of birth: 03/10/85
- E-mail: elena.battisacco@gmail.com

EDUCATION

- 1999 – 2004 High School: Liceo Scientifico XXV Aprile, Portogruaro (Venezia, Italy) (Finished with degree of 90/100).
- 2008– 2011 MSc in Civil Engineering: Università degli Studi di Trieste, Trieste (Italy) (Finished with degree of 110/110 cum lode).
- 2012– 2016 PhD in Civil Engineering: École Polytechnique Fédérale de Lausanne (EPFL), Lausanne.

EMPLOYMENT HISTORY

- 2009 – 2009: Servizio idrico integrato della città di Udine, CAFC s.p.a. (CAFC) - Lignano Sabbiadoro (Udine, Italy)
- 2012 – 2016 Research assistant at Laboratory of Hydraulic Constructions (LCH-EPFL).

Participation on commissioned studies on several topics during the PhD, following listed:

- Impact sur le ballast des eaux de ruissellement : analyzing the relationship water depth-flow velocity that causes ballast instabilities on aphysical scaled model. Use of numerical simulations to optimize the drainage.
- Projet FontEN, Fontaine Monumentale du Musée Olympique à Ouchy: applied research on the optimisation of the spillway shape in the scope of the reduction of the energy consumption by numerical simulations.
- Concept de sécurité du torrent des Bossons – Protection contre les laves torrentielles: study on phisical model on security measures against debris floods
- Fischzucht Valperca SA: numerical simulations on the optimum shape pipe for retention basins for fish.

Participation as assistant on supervision of master projects. Among others the following can be highlighted:

- Influence of multiple volumes on the replenishment of sediment technique *(Student: Giovanni Massazza)*
- Consecutive sediment replenishment in alpine rivers: Quantitative assessment and reproducibility of morphological response *(Student: Lena Bösch)*
- Undular wave in transcritical flow *(Student: Théo Cormor)*
- Projet d'un barrage au Honduras, avec ouvrages annexes *(Student : Pierre-Yves Adant)*
- Design of the Balintingon Multipurpose Project (MPP) *(Student: Marc-André Berchtold)*
- Vorprojekt zur Revitalisierung der Mündung des Baltschiederbachs in die Rhone *(Student: Yasmin Dressler)*

Teaching assistant for master courses on hydraulic structures and dams at École Polytechnique Fédérale de Lausanne, Lausanne.

Member of the organising committee of the Summer School on Fluivial Geomorphology, Losone (Switerland) 27/06 –1/07/2016.

LANGUAGES

Native language : Italian
Fluent in English and French.

COMPUTER SKILLS

- Autodesk AutoCAD and Inventor
- Basement and basegrain
- Flow 3D
- Matlab

PUBLICATIONS

Pfister, M., Battisacco, E., De Cesare, G., Schleiss, A., (2013) "Scale effects related to the rating curve of cylindrically crested Piano Key weirs", Proceedings of the 2nd International Workshop on Labyrinth and Piano Key Weirs - PKW 2013, Paris, France, 20-22 novembre 2013, Erpicum et al. (Eds), CRC Press, Boca Raton 73-82

Battisacco E., Maire A., Franca M.J. , Schleiss A.J. (2015). "Physical modelling of artificial river replenishment techniques to restore morphological conditions downstream of dams", Proc. of Int. Congress IAHR 2015 (on-line version). The Hague (The Netherlands), 19.6-3.7.2015, http://app.iahr2015.info/programma_details/2798

Amblard, J., Pams Capoccioni, C., Nivon, D., Mellal, L., De Cesare, G., Ghilardi, T., Jafarnejad, M., Battisacco, E. (2015), "Analysis of Ballast Transport in the Event of Overflowing of the Drainage System on High Speed Lines", International Journal of Railway Technology, 4(2), 19-43, DOI:10.4203/ijrt.4.2.2

Elena Battisacco, Giovanni De Cesare & Anton J. Schleiss (2016): "Reestablishment of a uniform discharge on the Olympic fountain in Lausanne", Journal of Applied Water Engineering and Research, DOI: 10.1080/23249676.2016.1163648

Bösch, L., Battisacco, E., Franca, M.J., and Schleiss, A.J. (2016). "Influence of consecutive sediment replenishment on channel bed morphology." Proc. of River Flow 2016, St. Louis, USA, 11-14 July 2016; Eds. Constantinescu, G., Garcia, M., and Hanes, D., 1147-1155

Juez, C., Battisacco, E., Franca, M.J., and Schleiss, A.J. (2016) "Modeling sediment pulses on an armored channel." Proc. of River Flow 2016, St. Louis, USA, 11-14 July 2016; Eds. Constantinescu, G., Garcia, M., and Hanes, D., 1314-1320

Juez, C.; Battisacco, E.; Schleiss, A. J.; Franca, M. J., (2016). "Assessment of the performance of numerical modeling in reproducing a replenishment of sediments in a water-worked channel". in Advances In Water Resources, 92:10-22, doi:10.1016/j.advwatres.2016.03.010

Battisacco, E.; Franca, M. J., Schleiss, A. J (2016). "Laboratory experiments on the influence of the length of a replenishment volume applied with alternated geometrical configuration". Proc. of ISRS 2016, Stuttgart, Germany, 19-22 September 2016, Eds. Wieprecht, S., Haun, S., Weber, C., Noack, M., Terheinden, K., 121

Battisacco, E.; Franca, M. J., Schleiss, A. J (2016). "Sediment replenishment: influence of the geometrical configuration on the morphological evolution of channel-bed", Water Resources Research, DOI: 10.1002/2016WR019157

CONFERENCE POSTERS

Battisacco, E.; Franca, M. J., Schleiss, A. J (2014). "Preliminary experimental results on the technique of artificial river replenishment to mitigate sediment loss downstream dams", AGU, Fall meeting, California, USA.

Battisacco, E.; Franca, M. J., Schleiss, A. J (2015). "Physical modeling of artificial river replenishment techniques to restore morphological conditions downstream of dams", EGU 2015, General Assembly, Vienna, Austria

Battisacco, E.; Franca, M. J., Schleiss, A. J (2016). "Effect of geometrical configuration of sediment replenishment on the development of bed form patterns in a gravel bed channel", EGU 2016, General Assembly, Vienna, Austria